

Synthesis and characterization of polymer based Cu(I)-mechanocatalysts

Dissertation

zur Erlangung des
Doktorgrades der Naturwissenschaften (Dr. rer. nat.)

der

Naturwissenschaftlichen Fakultät II
Chemie, Physik und Mathematik

der Martin-Luther-Universität
Halle-Wittenberg

vorgelegt

von Herrn Philipp Michael
geb. am 02.09.1986 in Halle (Saale)

Gutachter

1. Prof. Dr. Wolfgang H. Binder
2. Prof. Dr. Holger Frey

Verteidigung: 16.11.2016

Halle (Saale), 13.07.2016

Danksagung

An dieser Stelle möchte ich mich bei allen Mitarbeitern des Instituts für Makromolekulare und Technische Chemie der Martin-Luther-Universität Halle-Wittenberg für die gewährte Unterstützung und gute Zusammenarbeit bedanken. Mein besonderer Dank gilt Herrn Prof. Dr. Wolfgang H. Binder für die Bereitstellung des interessanten Themas und der stets sehr guten Betreuung, sowie der vielen individuellen Ausgestaltungsmöglichkeiten während der Durchführung der Dissertation und den Möglichkeiten der Mitarbeit in nationalen und internationalen Projekten.

Weiterhin möchte ich mich bei der gesamten Arbeitsgruppe Binder und ihren ehemaligen Mitgliedern für das angenehme Arbeitsklima, sowie für die gute Zusammenarbeit und die entgegengebrachte Unterstützung bedanken. Mein besonderer Dank geht hierbei an Susanne Tanner, Norman Diedrich und Julia Weichhold für durchgeführte GPC-, ESI- und MALDI-TOF-MS Messungen und für die Bestellung und Bereitstellung von Chemikalien und Arbeitsmitteln, sowie an Anke Hassi für ihre Unterstützung bei allen administrativen Angelegenheiten und ein offenes Ohr für alle kleinen und großen Probleme. Weiterhin möchte ich mich im Besonderen bei meiner langjährigen Büro- und Laborkollegin Diana Döhler für die fachlichen Diskussionen, die permanente Hilfsbereitschaft und die immer gute und unterhaltsame Zusammenarbeit bedanken.

Des Weiteren möchte ich den Arbeitsgruppen von Prof. Blume/ Prof. Hinderberger und insbesondere Dr. Andreas Kerth für die Bereitstellung des Fluoreszenz- und UV-vis-Spektrometers, sowie die Hilfestellung bei Fragen hinsichtlich der optischen Spektroskopie danken. Dr. Ströhl und seinem Team danke ich für die Anfertigung aller NMR-Spektren.

Abschließend möchte ich mich bei meiner Familie und meinen Freunden für ihre ständige Motivation und für die Unterstützung bedanken. Insbesondere danke ich meiner Mutter für den Rückhalt während meiner gesamten Studienzzeit.

Abstract

Mechanochemistry is a versatile tool to trigger chemical reactions and are of growing interest for a wide range of applications in material science. Especially in the field of polymer science a variety of potential mechanophores was developed able to transmit applied external force directly to a labile chemical bond via the attached polymer chains culminating thus the force and cleave the most labile bond close to the midpoint of the polymer.

In the scope of this thesis latent poly(isobutylene)- (PIB) as well as poly(styrene)- (PS) based copper(I) bis(*N*-heterocyclic carbene) (NHC) catalysts were developed which can be activated through mechanical force applied e.g. by ultrasound in solution or by compression in the solid state. The synthesis of the mechanocatalysts was accomplished preparing the bromo-telechelic polymers via living polymerization techniques, namely the living carbocationic polymerization (LCCP) for PIB as well as the atom transfer radical polymerization (ATRP) for PS allowing to tune the molecular weight and thus the applied force to the centrally placed catalyst. A subsequent quaternization with *N*-methylimidazol generated the corresponding *N*-methylimidazolium-telechelic polymers. Their deprotonation through a strong base yielded the free NHCs which were used to coordinate to a copper(I) salt forming thus the final PIB- respectively PS-based bis(*N*-methylimidazol-2-ylidene) copper(I)X complexes.

GPC as well as ¹H-NMR spectroscopic investigations proved the initial latency and subsequent activation of the designed mechanophores by cleaving one of the shielding polymeric NHC-ligands generating thus a catalytic active monocarbene copper(I) moiety which is able to trigger the copper(I)-catalyzed alkyne/azide “click” cycloaddition (CuAAC) reaction. It could be shown, that up to 80% of the more rigid PS-based (*T_g* ~ 373 K) and 84% of the more flexible PIB-based mechanocatalysts (*T_g* ~ 193 K) could be cleaved in solution by applied ultrasound. Moreover, an increased cleavage efficiency with increased initial molecular weight of the attached polymer chains could be shown enabling a more efficient transmission of force. However, a slow decomposition of the active monocarbene copper(I)X complex was observed applying ultrasound over a longer period of time.

Furthermore, the catalytic activity of the initially latent and later by mechanical force activated mechanocatalysts was successfully demonstrated in solution as well as in bulk state. A model CuAAC reaction of benzyl azide and phenylacetylene was chosen to investigate the catalytic activity in solution revealing up to 52% “click” conversion for the PS-based biscarbene copper(I)X mechanophores after activation by ultrasound, while in case of the PIB-based mechanocatalysts only 28% “click” conversion could be observed indicating thus a higher catalytic activity of the PS-based biscarbene catalysts. Probing the mechanochemical activation in bulk polymer matrices was accomplished via a fluorogenic “click” reaction of non-fluorescent 3-azido-7-hydroxy-coumarin with phenylacetylene generating the highly fluorescent 7-hydroxy-3-(4-phenyl-1*H*-[1,2,3]triazole-1-yl)-coumarin in yields up to 8% using PIB- as well as PS-based mechanocatalysts. Thus, the potential of the designed polymeric bis(*N*-heterocyclic carbene) copper(I)X mechanocatalysts for autonomous stress-sensing applications could be demonstrated as the fluorescence reaction takes solely place when activated by applied external mechanical force.

Kurzzusammenfassung

Mechanochemie stellt ein vielseitig einsetzbares Werkzeug zum gezielten Auslösen chemischer Reaktionen dar und ist somit für viele Anwendungen vor allem im Bereich der Materialwissenschaften von wachsendem Interesse. Insbesondere im Bereich der Polymerwissenschaften wurde eine Vielzahl von Mechanophoren entwickelt, die in der Lage sind eine externe mechanische Kraft mittels der angehängten Polymerketten direkt auf eine chemisch labile Bindung nahe des Zentrum der Polymerkette zu übertragen.

Im Rahmen der vorliegenden Arbeit wurden latente, inaktive Polyisobutylene (PIB) und Polystyrol (PS) basierte Kupfer(I)-bis(*N*-heterozyklische Carben) (NHC) Katalysatoren entwickelt, welche durch die Anwendung von mechanischer Kraft durch z.B. Ultraschall in Lösung oder Kompression im festen Zustand aktiviert werden können. Die Synthese der für die Mechanokatalysatoren notwendigen bromtelechelen Präkursorpolymere wurde mittels lebender Polymerisationstechniken durchgeführt, wobei die bromtelechelen PIBs durch lebende carbokationische Polymerisation (LCCP) und die bromtelechelen PSs durch ATRP (atom transfer radical polymerization) hergestellt wurden. Die Anwendung dieser Techniken ermöglichte eine exakte Einstellung des Molekulargewichts und somit auch die Justierung der zur Aktivierung der zentral positionierten Metallkomplexe notwendigen Kraft. Die anschließende Quaternisierung der bromtelechelen Polymere mittels *N*-Methylimidazol erzeugte die entsprechenden *N*-methylimidazolium-telechelen Polymere, welche nach Deprotonierung durch eine starke Base die freien NHCs generierten die wiederum als Makroliganden für die Bildung der finalen PIB- bzw. PS-basierten Bis(*N*-methylimidazol-2-yliden)-Kupfer(I)X Komplexe dienen.

Die Latenz der hergestellten Mechanokatalysatoren im Ursprungszustand und deren Aktivierung durch die Abspaltung eines der stereoelektronisch abschirmenden NHC-Liganden mittels Ultraschall unter Bildung der katalytisch aktiven Kupfer(I)-Monocarben Komplexe konnte durch GPC und ¹H-NMR-spektroskopische Untersuchungen nachgewiesen werden. 84% der flexibleren PIB-basierten ($T_g \sim 193$ K) und 80% der weniger flexiblen PS-basierten Mechanokatalysatoren ($T_g \sim 373$ K) konnten durch Ultraschall gespalten werden. Außerdem konnte eine effektivere Spaltung mit zunehmendem anfänglichem Molekulargewicht der Mechanophore nachgewiesen werden, da längere Polymerketten eine effektivere Kraftübertragung auf die labile Kupfer-Carben-Bindung ermöglichen. Darüber hinaus konnte bei Anwendung von Ultraschall über einen längeren Zeitraum eine langsame Zersetzung der katalytisch aktiven Monocarben-Komplexe beobachtet werden.

Des Weiteren wurde die katalytische Aktivität der anfänglich inaktiven und später durch mechanische Kraft aktivierten Mechanokatalysatoren sowohl in Lösung als auch im festen Zustand nachgewiesen. Die Kupfer(I)-katalysierte Alkin/Azid „click“ (CuAAC) Reaktion von Phenylacetylen und Benzylazid zeigte in Lösung einen Umsatz von bis zu 52% für die PS-basierten Mechanophore und bis zu 28% für die PIB-basierten Mechanophore nach jeweiliger Aktivierung mit Ultraschall. Die mechanochemische Aktivierbarkeit der Katalysatoren im festen Zustand konnte mittels der fluorogenen „click“ Reaktion von nicht-fluoreszenten 3-Azido-7-hydroxy-coumarin mit Phenylacetylen in einer Polymermatrix gezeigt werden. Kompressionsexperimente und anschließende fluoreszenzspektroskopische Untersuchungen zeigten die Bildung von bis zu 8% des stark fluoreszierende 7-Hydroxy-3-(4-phenyl-1*H*-[1,2,3]triazole-1-yl)-coumarin Farbstoffes für die PIB- und PS-basierten Mechanokatalysatoren einzig durch die Anwendung von Druck. Somit konnte das Potential der polymeren Bis(*N*-heterozyklische Carben)-Kupfer(I)X Mechanokatalysatoren für die autonome Detektion von externen mechanischen Belastungen bzw. Beschädigungen nachgewiesen werden.

Table of Contents

Danksagung	1
Abstract	2
Kurzzusammenfassung	3
List of abbreviations	7
1 Introduction	11
1.1 Polymer mechanochemistry	11
1.2 Mechanochemical activation methods	12
1.2.1 Mechanochemical activation by ultrasound	12
1.2.2 Mechanochemical activation in bulk material	14
1.3 Mechanochemical self-healing approaches	16
1.3.1 Mechanocatalysts	17
1.3.1.1 Pd/Pt-phosphane coordinated mechanocatalysts	18
1.3.1.2 Ag/Ru <i>N</i> -heterocyclic carbene mechanocatalysts	19
1.3.1.3 Ru <i>N</i> -heterocyclic carbene mechanocatalysts in bulk applications	21
1.3.1.4 Pincer complexes for mechanocatalysis	22
1.3.1.5 Boronium-pyridine mechanocatalysts	23
1.3.2 Generation of reactive species by cyclic mechanophores	24
1.3.2.1 <i>gem</i> -Dihalocyclopropanes	25
1.3.2.2 <i>gem</i> -Dichlorocyclopropanated indene	27
1.3.2.3 Epoxides	27
1.3.2.4 Annulated cyclobutanes	28
1.3.2.5 Dicyano-substituted cyclobutane-di-esters	30
1.3.2.6 Retro-Staudinger cycloaddition of β -lactams	31
1.3.2.7 Bergmann cyclization of enediynes	31
1.3.2.8 Cyclobutane-1,3-diones	32
1.3.3 Other mechanophores	33
1.3.3.1 Oxime sulfonates	34
1.3.3.2 Triarylsulfonium salts	34
1.3.3.3 Poly(<i>o</i> -phthalaldehyde)s	34
1.3.3.4 1,1'-Bi-2-naphthol	35
1.4 Mechanochemical damage-sensing approaches	35
1.4.1 Mechanochromophore	37
1.4.1.1 Spiropyranes	37
1.4.1.2 Spirothiopyranes	39
1.4.1.3 Coumarins	39
1.4.1.4 Anthracenes	40
1.4.2 Mechanoluminescence of dioxetanes	41
1.5 Copper(I)-catalyzed alkyne-azide cycloaddition reaction	43
2 Aim of the thesis	46
2.1 Objective and motivation	46
2.2 Concept	47
3 Results and Discussion	50
3.1 Synthesis and characterization of PIB-based bis(<i>N</i> -methylimidazol-2-ylidene) copper(I)X mechanocatalysts (6)	50
3.2 Synthesis and characterization of PS-based bis(<i>N</i> -methylimidazol-2-ylidene) copper(I)X mechanocatalysts (14)	57

3.3	Mechanochemical activation of polymeric bis(<i>N</i> -methylimidazol-2-ylidene) copper(I)X complexes 6 and 14 by external force	62
3.3.1	Ultrasound-induced scission of mechanocatalysts 6 and 14	62
3.3.1.1	GPC investigations of ultrasound-induced scission of mechanocatalysts (6 and 14)	62
3.3.1.2	¹ H-NMR spectroscopic investigations of ultrasound-induced scission of mechanocatalysts 6	66
3.3.2	Mechanochemical triggered CuAAC “click” reaction of benzyl azide (19) and phenylacetylene (17) using latent mechanocatalysts	70
3.3.3	Mechanochemical activation of latent catalysts in solid state by compression	77
4	Experimental Part	81
4.1	Materials and methods	81
4.2	Synthesis of PIB-based bis(<i>N</i> -methylimidazol-2-ylidene) copper(I)X mechanocatalysts (6)	83
4.2.1	Synthesis of TMPCl (1)	83
4.2.2	Synthesis of bromo-telechelic PIB (3)	83
4.2.3	Synthesis of <i>N</i> -methylimidazolium-telechelic PIB (5)	85
4.2.4	Synthesis of bis(<i>N</i> -methylimidazol-2-ylidene-telechelic PIB-copper(I)X complex [Cu(PIB-NHC) ₂]X (6) and PIB-monocarbene complex [Cu(PIB-NHC)]X (7)	87
4.2.4.1	Synthesis of 6 and 7 by KHMDS and [Cu(CH ₃ CN) ₄]PF ₆	87
4.2.4.2	Synthesis of 6 and 7 by KO ^t Bu and [Cu(CH ₃ CN) ₄]PF ₆	90
4.2.4.3	Synthesis of 6 by Cu ₂ O	90
4.3	Synthesis of [Cu(BPB-NHC) ₂]X model complex (10)	91
4.3.1	Synthesis of 1-(3-phenoxypropyl)-3-methylimidazolium bromide (8)	91
4.3.2	Synthesis of 1-(3-phenoxypropyl)-3-methylimidazol-2-ylidene silver (I) bromide (9)	92
4.3.3	Synthesis of bis(1-(3-phenoxypropyl)-3-methylimidazol-2-ylidene) copper (I) bromide (10)	92
4.3.3.1	Synthesis of 10 from 8 by NaO ^t Bu and CuBr	93
4.3.3.2	Synthesis of 10 from 8 by Cu ₂ O	93
4.3.3.3	Synthesis of 10 from 9 by CuBr	93
4.4	Synthesis of PS-based bis(<i>N</i> -methylimidazol-2-ylidene) copper(I)X mechanocatalysts (14)	94
4.4.1	Synthesis of bromo-telechelic poly(styrene) (12)	94
4.4.2	Synthesis of <i>N</i> -methylimidazolium-telechelic PS (13)	95
4.4.3	Synthesis of bis(<i>N</i> -methylimidazol-2-ylidene-telechelic PS-copper(I)X complex [Cu(PS-NHC) ₂]X (14)	97
4.4.3.1	Synthesis of 14 by NaO ^t Bu and [Cu(CH ₃ CN) ₄]PF ₆	97
4.4.3.2	Synthesis of 14 by KHMDS and [Cu(CH ₃ CN) ₄]PF ₆	98
4.4.3.3	Synthesis of 14 by Cu ₂ O	99
4.5	Synthesis of 3-azido-7-hydroxy-coumarin (16)	99
4.6	Synthesis of 7-hydroxy-3-(4-phenyl-1 <i>H</i> -[1,2,3]triazole-1-yl)-coumarin (18)	100
4.7	Synthesis of benzyl azide (19)	101
4.8	Synthesis of high molecular weight PTHF (20)	101
4.9	Mechanochemical activation of latent catalysts in solution by ultrasonication	102
4.9.1	Concentration-RI-intensity calibration of GPC	102
4.9.2	Ultrasound-induced cleavage of mechanocatalyst in solution	103
4.9.3	Control and thermal scission experiments	104

4.9.4	Ultrasound triggered CuAAC “click” reaction of benzyl azide (19) and phenylacetylene (17) using latent mechanocatalysts	105
4.10	Mechanochemical activation of latent catalysts in solid state by compression	107
4.10.1	Fluorescence calibration for fluorogenic “click” reaction	107
4.10.2	Fluorogenic “click” reaction of 3-azido-7-hydroxy-coumarin (16) and phenylacetylene (17) in solid state	110
5	Summary	113
6	References	117
7	Appendix	127
7.1	NMR-spectra of bromo-telechelic PIB (3)	127
7.2	NMR-spectra and MALDI-TOF-MS of <i>N</i> -methylimidazolium-telechelic PIB (5)	129
7.3	GPC, NMR-spectra and MALDI-TOF-MS of bis(<i>N</i> -methylimidazol-2-ylidene-telechelic poly(isobutylene) copper(I)X [Cu(PIB-NHC) ₂]X (6)	132
7.4	NMR-spectra and ESI-TOF-MS of 1-(3-phenoxypropyl)-3-methylimidazolium bromide (8)	137
7.5	NMR-spectra of bis(1-(3-phenoxypropyl)-3-methylimidazol-2-ylidene) copper (I) bromide (10)	138
7.6	NMR-spectra of bromo-telechelic poly(styrene)s (12)	139
7.7	NMR-spectra and MALDI-TOF-MS of <i>N</i> -methylimidazolium-telechelic PS (13)	140
7.8	GPC and NMR-spectra of bis(<i>N</i> -methylimidazol-2-ylidene-telechelic poly(styrene) copper(I)X complex [Cu(PS-NHC) ₂]X (14)	141
7.9	NMR-spectra and ESI-TOF-MS of 3-azido-7-hydroxycoumarin (15)	143
7.10	NMR-spectra and ESI-TOF-MS 7-hydroxy-3-(4-phenyl- <i>1H</i> -[1,2,3]triazole-1-yl)-coumarin (17)	145
7.11	Calibration of GPC traces	147
7.12	GPC traces of ultrasound-induced cleavage of mechanocatalyst in solution	151
7.13	¹ H-NMR spectra of CuAAC “click” kinetic of 17 and 19 using mechanocatalysts	156
7.14	Mechanochemical activation of latent catalysts in solid state by compression	162
8	Curriculum Vitae	164
9	Eigenständigkeitserklärung	167

List of abbreviations

AFM	atomic force microscopy
Asc	sodium ascorbate
ATRP	atom transfer radical polymerization
BAD	bis(adamantyl)-1,2-dioxetane
BCB	benzocyclobutene
BD	1,4-butane diol
Binol	1,1'-bi-2-naphthol
BPB	3-(bromopropoxy)benzene
bpy	2,2'-bipyridine
CoGEF	Constrained Geometries simulate External Force
CuAAC	copper(I)-alkyne/azide cycloaddition
DA	Diels-Alder reaction
DBU	1,8-diazabicyclo[5.4.0]undec-7-ene
DCM	dichloromethane
DCTB	<i>trans</i> -2-[3-(4- <i>tert</i> -butylphenyl)-2-methyl-2-propenylidene]malononitrile
D_e	dissociation energy
DHA	2,3-dihaloalkene
DIPEA	<i>N,N</i> -diisopropylethylamine
Dithranol	1,8-dihydroxy-9,10-dihydroanthracen-9-one
DMA	dynamic mechanical analysis
DMF	dimethylformamide
DMSO	dimethyl sulfoxide
DN	double network
DS	damage-sensing
DSC	different-scanning-calorimetry
EDXS	Energy Dispersive X-ray Spectroscopy
err	error
ESI	electron-spray-ionization
F_{ext}	external force
<i>g</i> DBC	<i>gem</i> -dibromocyclopropane
<i>g</i> DCC	<i>gem</i> -dichlorocyclopropane
<i>g</i> DFC	<i>gem</i> -difluorocyclopropane
<i>g</i> DHC	<i>gem</i> -dihalocyclopropane
GPC	gel permeation chromatography
HDMI	hexamethylene diisocyanate
HMTETA	hexamethyltriethylenetetramine
IB	isobutylene
Ini	Initiator
IR	infrared
s	strong
m	middle
w	weak
KHMDS	potassium hexamethyldisilazide
LCCP	living carbocationic polymerization
MALDI	matrix-assisted-laser-desorption-ionization
MBPP	methyl 2-bromopropionate

MC	merocyanine
<i>m</i> CPBA	<i>meta</i> -chloroperoxybenzoic acid
Me ₆ -TREN	tris[(2-dimethylamino)ethyl]amine
M _n	number average molar mass
MS	mass spectrometry
M _w	weight average molar mass
NHC	<i>N</i> -heterocyclic carbene
NMR	nuclear magnetic resonance spectroscopy
s	singlet
bs	broad singlet
d	doublet
dd	double doublet
t	triplet
q	quartet
m	multiplet
<i>o</i> QDM	<i>ortho</i> -quinodimethide diene
PBD	poly(1,4-butadiene)
PDI	polydispersity index (PDI = M _w /M _n)
PEG	poly(ethylene glycol)
PIB	poly(isobutylene)
PMA	poly(methylacrylate)
PMDETA	<i>N,N,N',N'',N'''</i> - pentamethyl-diethylenetriamine
PMMA	poly(methylmethacrylate)
PNB	poly(norbornene)
PS	poly(styrene)
PSMS	poly(dimethylsiloxane)
PSS	Polymer Standards Service
PTHF	poly(tetrahydrofuran)
PU	poly(urethane)
PVA	poly(vinyl alcohol)
Qu	quencher
RCM	ring-closing metathesis
rDA	retro-Diels-Alder reaction
RI	refractive index
ROMP	ring opening metathesis polymerization
rpm	rounds per minute
SH	self-healing
SN	single network
SP	spiropyran
STP	spirothiopyran
STEM	Scanning Transmission Electron Microscopy
TABS	Thermally Activated Barrier to Scission
TBTA	tris[(1-benzyl-1 <i>H</i> -1,2,3-triazol-4-yl)methyl]amine
T _g	glass transition temperature
THF	tetrahydrofuran
TGA	thermogravimetric analysis
TLC	thin-layer-chromatography
TMC	thiomerocyanine
TMPCI	2-chloro-2,4,4-trimethyl-pentane

TN	triple network
TOF	time-of-flight
TPMA	tris[(2-pyridyl)-methyl]amine
tpy	2,2':6',2''-terpyridine
UPy	2-ureido-4-pyromidone
US	ultrasound
UV	ultraviolet
vis	visible
λ_{em}	emission wavelength
λ_{ex}	excitation wavelength

Parts of the results and discussion as well as of the experimental part were already published in “A Mechanochemically Triggered “Click” Catalyst” (Michael, P.; Binder, W. H. *Angew. Chem. Int. Ed.* **2015**, *54*, 13918. <http://dx.doi.org/10.1002/anie.201505678>; Michael, P.; Binder, W. H. *Angew. Chem.* **2015**, *127*, 14124. <http://dx.doi.org/10.1002/ange.201505678>) and were in parts adapted with permission from John Wiley and Sons (Copyright 2015).

1 Introduction

1.1 Polymer mechanochemistry

Mechanochemistry is a versatile tool to trigger chemical reactions solely by applied external mechanical force and are of growing interest for a wide range of applications in material science¹⁻⁵. It combines the usually destructive nature of mechanical force towards polymeric material, composites or coatings with the productive character of defined chemical reactions triggered by the activation of so called mechanophores. Mechanophores are in its initial state inactive molecules containing mechanically labile bonds or functional groups which are able to undergo chemical transformations when incorporated into polymers and are thus *in situ* activated under external mechanical force^{1-2; 4; 6-7} generating either reactive compounds⁸⁻⁵⁴ or change certain properties, like color^{1; 39; 55-80}, appearing chemiluminescence⁸¹⁻⁸⁷ or conducted isomerization⁸⁸.

Force induced changes of polymeric material properties were known anyway since the first mastication experiments of Staudinger in the 1930s⁸⁹⁻⁹¹. Due to the applied external force a homolytic chain cleavage of the polymer backbone into two radicals could be observed leading in turns to a decreased molecular weight. The rubber material was softened when the mastication was conducted under normal air trapping the free radicals by oxygen, while in the absence of oxygen, the initial material properties restore as these radicals recombine and reform thus the cross-linking bonds. In the following years it was demonstrated that certain chemical bonds, like azo- or peroxy-linkers^{1; 92-93} can be cleaved easier than other chemical bonds which enabled a selective scission on defined positions and originated thus the concept of mechanophores.

Especially in the field of polymer science a bunch of potential mechanophores was developed able to transmit applied external force directly to a labile chemical bond via the attached polymer chains culminating thus the force and cleave the most labile bond close to the midpoint of the polymer. Figure 1 shows some generalized examples for some common mechanophoric approaches within the scope of polymer mechanochemistry, such as the selective scission of labile bonds which lead to the generation of reactive species (Figure 1A) or in case of mechanocatalysts to the generation of catalytic active moieties (B). Also cyclic mechanophores are known which are able to release stress either via a ring-opening reaction elongating the polymer backbone (C) or perform a cycloreversion reaction (D), while other mechanophores are able to release small molecules (E) or perform an isomerization (F). Another kind of mechanophores are the so called mechanochromophores, which change their colour or emit light under applied external force (G, H). Some of the most vivid examples are discussed within the subsequent chapters 1.3 and 1.4.

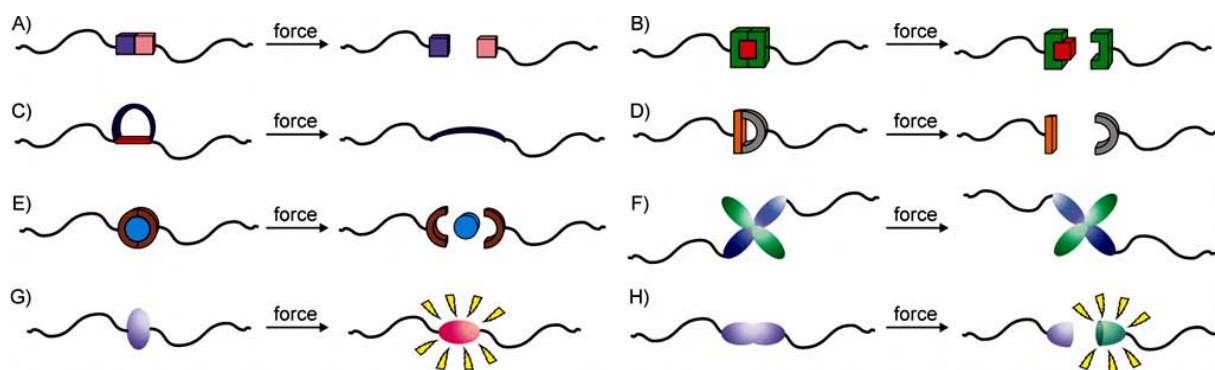


Figure 1. Generalized examples for polymer based mechanophores and their response to external mechanical force: (A) selective scission of labile bonds, (B) activation of mechanocatalysts, (C) ring-opening of cyclic mechanophores, (D) cycloreversions, (E) exclusion of small molecules, (F) isomerization, (G) colour change or chemiluminescence and (H) colour change or chemiluminescence with coincident degradation.

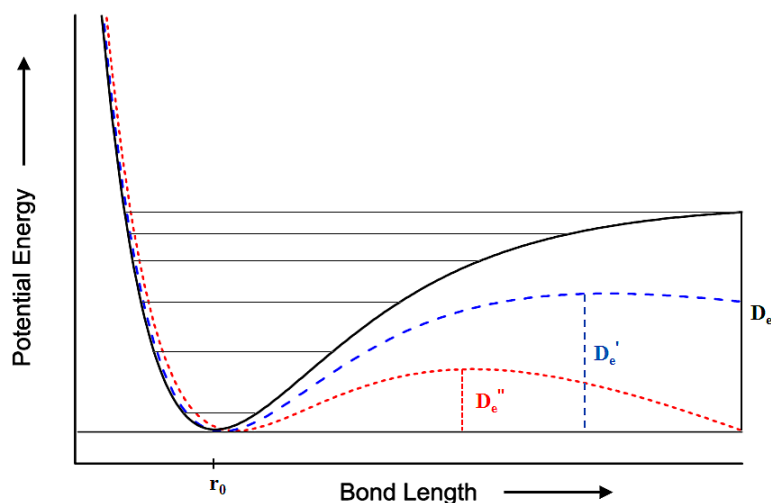


Figure 2. Lowering the dissociation energy barrier (D_e) in the Morse energy potential by the influence of an external pulling force applying the TABS theory under implementation of the CoGEF method. The solid black line represents the potential of the unaffected mechanolabile chemical bond with the thermal dissociation energy barrier D_e , while the blue dashed line as well as the red dotted line shows the decreasing of D_e by gradually increasing external force (F_{ext}) with $F_{\text{ext}}(D_e'') > F_{\text{ext}}(D_e')$.

However, before individual chemical bonds can break, the applied external force had to cause a partial uncoiling of the polymer chain, which stretch and weaken thus the labile bond leading finally to an activation of the mechanophore. This phenomenon can also be explained by the lowering of the dissociation energy barrier (D_e) in the Morse potential by applying the Thermally Activated Barrier to Scission (TABS)-theory under implementation of the so called CoGEF (Constrained Geometries simulate External Force) method^{13; 38; 94-96}. Herein, the effect of constrained geometry optimizations under the influence of an external pulling force to the thermal activation barrier within the Morse potential is investigated (Figure 2). Increased force lead to a decreasing in the dissociation barrier and thus in turns to a mechanophoric activation even at lower temperatures (represented by the horizontal vibration levels). Quantum mechanical calculations yielded typical external force for the activation of mechanophores under ambient conditions ranging from 400 – 900 pN for the cleavage of copper and silver biscarbene mechanocatalysts^{13; 97} or 1500 – 5900 pN for the scission of substituted cyclobutane rings^{38; 42; 58; 94} just to name a few.

1.2 Mechanochemical activation methods

In principle two different scenarios for the activation of mechanophores are feasible: The activation in solution or in bulk matrix materials. Most common methods for the activation in diluted media are the mechanophore chain scission by pulsed ultrasound^{4; 98-102}, turbulent and elongation (cross-)flow¹⁰²⁻¹⁰⁵ or repeated freeze-thaw cycles¹⁰⁶⁻¹⁰⁹, while the activation in solid state is usually performed by tensile testing^{39; 55-56; 58}, torsional shear force^{68; 81-82}, grinding/ball milling^{108; 110-111} or compression^{19; 28-29; 36; 58; 97; 112-113}. Investigations on single (mechanophore) molecule activation using e.g. atomic force microscopy (AFM)¹¹⁴⁻¹¹⁷ enable a deeper look into the details of the activation mechanisms of mechanophores, but are not suitable for broader applications. In the following part, the most widespread activation mechanisms will be explained in more detail.

1.2.1 Mechanochemical activation by ultrasound

The most common activation method for mechanophores in solution is the activation by pulsed ultrasound which creates shockwaves within the solvent causing so called cavitation bubbles^{4-5; 98-102; 118}. These increase periodically in size until they collapse pulling thus one end of the polymer handle faster to the created void volume than the other. That way the initially randomly coiled polymeric

mechanophore is stretched until a certain limit is reached and the most labile bond close to the midst point is cleaved (Figure 3).

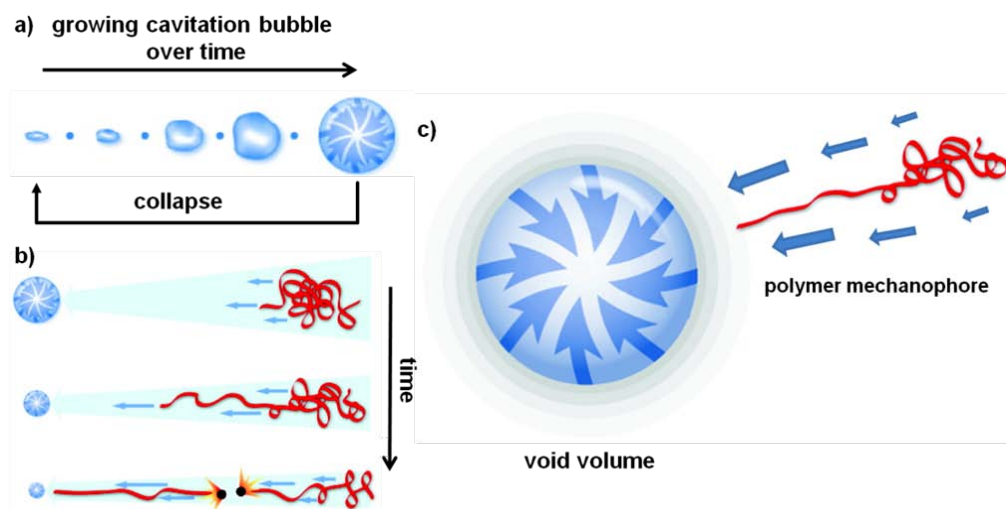


Figure 3. Schematic illustration of ultrasound induced scission of polymeric mechanophores. **a)** Ultrasound induced shockwaves caused periodically growing cavitation bubbles which collapse under formation of a void volume. **b)** The created void volume pull one end of the mechanophore faster than the other and stretch thus the initially randomly coiled polymer handle until the weakest bond break. **c)** Magnification of the collapsing cavitation bubble and subsequent stretching of the mechanophore. (Adapted with permission from literature⁴. Copyright (2009) American Chemical Society.)

Within this scenario the mechanophore scission proceeds more rapidly with an increased initial molecular weight of the attached polymer as the longer polymers favors the transmittance of force due to its longer relaxation times resulting in a higher impact of the cavitation^{4-6; 13; 34; 96; 103; 119}. If the initial molecular weight drops below a certain (polymer depending) limiting molecular weight, no efficient activation by acoustic fields will be possible. For the same reason, the midpoint positioning of the most labile bond is one of the crucial points in designing mechanophores. Only locating the weak bond in the 15% of the chain midst will ensure an efficient force transmission prohibiting otherwise possible homolytic C-C bond rupture (Figure 4)^{1-2; 4; 7}.

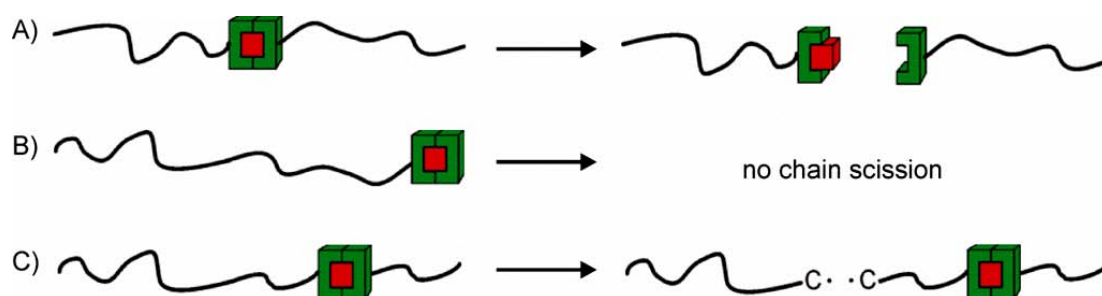


Figure 4. Schematic illustration of bisfunctional mechanophores: **a)** mechanochemical labile group placed close to the midst of the polymer chain; **b)** labile group placed at the chain end leading to no chain scission or C-C bond rupture; **c)** functional group placed far of the center of polymer chain yielding C-C bond rupture of the polymer backbone.

Moreover, the sonication intensity has a strong impact on the mechanophore activation: Higher ultrasound intensities increase the number and the size of the formed cavitation bubbles leading to a more efficient cleavage and lowering of the required limiting molecular weight^{4; 33; 99}. Additionally, the choice of solvent, the temperature as well as the mechanophore concentration have a crucial influence^{4; 33; 99; 120-122}. On the one hand, polymer-solvent interactions play an important role

influencing the conformational preferences of the polymer in solution^{4; 33; 120-121}. Strongly coiled polymers degrade much slower than linearly stretched ones. Therefore, solvents enabling a good polymer-solvent interaction and thus a fast coil-to-stretch transformation increase the mechanophore scission rate significantly. On the other hand, solvents with higher vapor pressure generate a stronger vaporization during the cavitation event within the cavitation bubbles which cushions the collapse lowering thus the mechanochemical scission rate and increase the limiting molecular weight. This effect is also the reason, while - in contrast to the majority of the chemical processes - higher temperatures affect the mechanical cleavage negatively^{4; 33; 122}. Increased temperatures lead to an increased vapor pressure which in turns buffer the cavitation collapse and damps the scission rate. Furthermore, the mechanophore concentration influences the activation behavior: high concentrations lead to higher solution viscosities which in turn increase the cavitation threshold. Due to the hindered formation of cavitation bubbles, the chain scission rate is lowered^{4; 33; 120}.

1.2.2 Mechanochemical activation in bulk material

The activation behavior of mechanophores in bulk material is of major importance for studying mechanochemistry as the most polymeric materials are applied in the solid state. In this scenario the polymer handle, attached to the labile mechanochemical active bond, act as a kind of anchor within the polymer matrix. Therefore, a sufficiently high entanglement is fundamental for an efficient activation in order to prevent the drag out of the anchoring polymers from the matrix and inhibiting thus the transfer of the applied force to the mechanophore. The anchoring of mechanophores can be ensured either by purely physical entanglement or by chemically crosslinked networks, based on supramolecular interactions^{62-65; 82} or covalent bonds^{60; 62; 68; 84; 86; 123}. Especially in case of purely physical entanglement, a sufficiently long chain length is crucial as efficient mechanochemical activation is just possible far above the critical entanglement molecular weight, which strongly depends on the nature of the attached polymer as well as of the matrix material. The basic steps of mechanophore activation are the same as for the activation by ultrasound (Figure 5): (A) initially the polymer handles are entangled within the matrix material and are continually stretched by the applied external force (B–D) until a certain limit is reached and the labile mechanophoric bond will be cleaved (E).

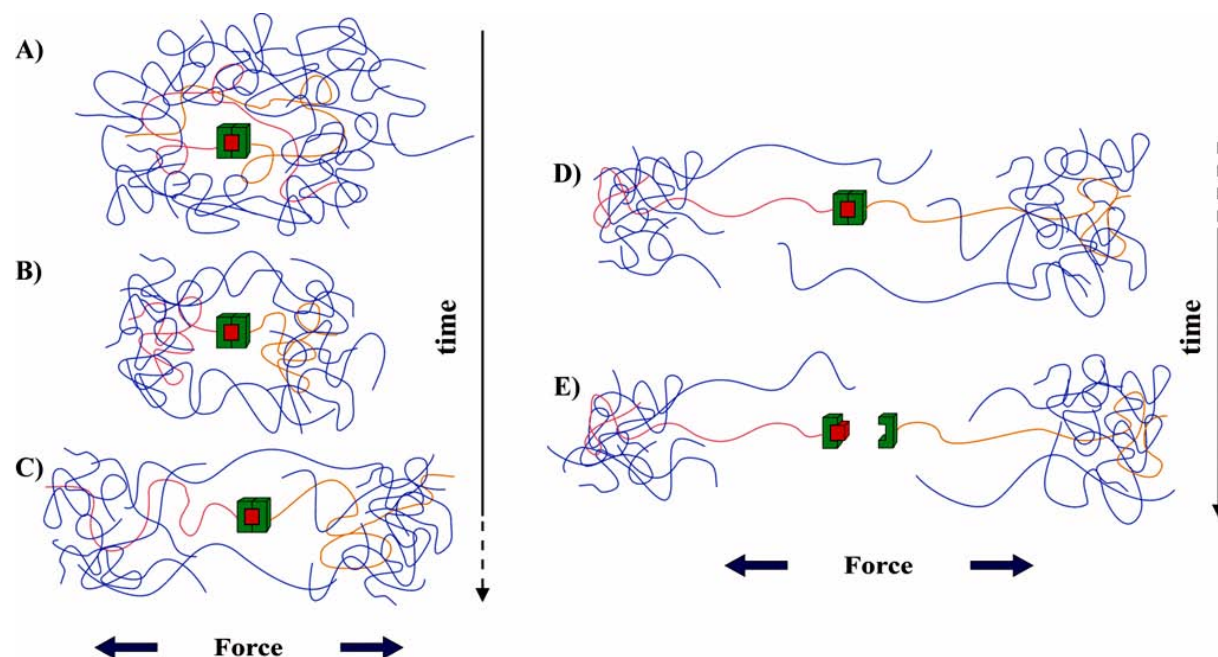


Figure 5. Solid state activation of purely physical entangled polymer mechanophores: (A) Statistic entanglement of mechanophores with the polymeric matrix; (B–D) continual stretching of polymer anchors by applied external force; (E) rupture of the most labile bond and activation of mechanophore.

However, the activation of mechanophores is more efficient embedding the anchoring polymer handles into networks^{4; 60; 62-65; 68; 82; 84; 86; 123} or co-crystallize them with the matrix material¹⁹ as the additional crosslinking points limit the polymer chain mobility and prohibit disentanglements which in turn would inhibit the force transmission (Figure 6). Moreover, experimental investigations have shown that mechanophores orientated parallel to the direction of applied force are activated most efficient⁵⁵⁻⁵⁷. Due to the additional crosslinking points, the randomly orientated mechanophores are able to “collect” the usually one directional external force and transmit also the perpendicular parts of the applied force to the mechanochemical labile groups. This effect was extensively studied e.g. in case of spiroyrans which undergo under mechanical stress a significantly more efficient ring opening reaction forming merocyanine when they are embedded into chemically crosslinked networks^{60; 62-65; 68; 123} compared to the activation in non-crosslinked environments^{55-56; 58}. Similar observations were made for bis(adamantly)-1,2-dioxetanes^{81-82; 84; 86}.

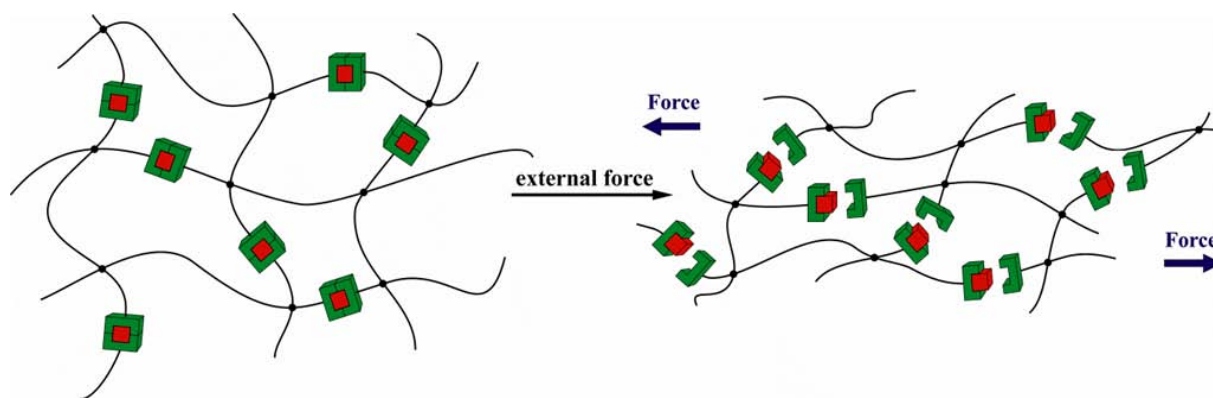


Figure 6. Solid state activation of polymeric mechanophores embedded into networks: The additional chemical crosslinking points (\times) prevent the disentanglement and enable a more efficient transmission of the applied external force to the most labile bond ensuring thus a more effective activation of mechanophores.

Theoretical considerations as well as practical investigations have shown, that the maximal applicable force in bulk state is several magnitudes higher than in diluted media, while the behavior is opposed for the applicable strain rates^{4; 102}. Due to the higher strain rates in solution, linear polymers are much easier activatable in this scenario than in solid state, while in case of the solid state scenario strongly entangled polymers with significant higher initial molecular weights or chemical crosslinked networks are required in order to transmit the applied strong force.

Another important factor for activating mechanophores in the solid state is the polymer chain mobility as it strongly influences the ability to transmit the applied force to the labile mechanophoric bond. A sufficiently high activation is only possible above or close below the glass transition temperature (T_g) of the anchoring polymer handle^{4; 55; 58}. However, also for elastomers the stress level needed to activate the mechanophore is quite high and requires a large deformation of several hundred percent of strain. Thermoplastic polymer handles show no significant chain scission far below their T_g and could only be activated close to it when plastic deformation already takes place.

In practice there is a number of different methods to activate mechanophores in bulk state, like tensile testing^{39; 55-56; 58}, torsional shear force^{68; 81-82} or compression^{19; 28-29; 36; 58; 97; 112-113}. One of the simplest and most vivid ways to activate mechanophores in solid state is the tensile testing. This can be realized either via manual stretching by hand, which is the most trivial, but least reproducible method imaginable for activating mechanophores or by specialized instrumentation, like tensile test machines or dynamic mechanical analysis (DMA) enabling the quantification of the applied elongation forces^{39; 55-56; 58; 102; 124}. Thus, using this method enables e.g. a detailed investigation of the role of mechanophore orientation in respect to the direction of the applied external force⁵⁶. However, the mechanochemical activation in bulk applied by tensile testing is less efficient compared to the activation by compression²⁹.

Compression e.g. by hydraulic press^{19; 29; 36} or pressure cells^{58; 112-113} is another well known method for activating mechanophores in the solid state enabling in comparison to all other activation methods the highest rate of force application and thus the usually most efficient mechanoactivation^{4; 29; 102}.

1.3 Mechanochemical self-healing approaches

In the last century polymers have been used in various applications and became thus ubiquitous in our daily life. They are applied in a broad diversity of technical and ordinary items which are expected to resist mechanical stress - also over a longer period of time. Common polymeric materials will fail inevitably due to mechanical, thermal or chemical stress or decomposition by UV irradiation¹²⁵. As a result, microcracks can be formed and may propagate over the time, which weaken the material and causing finally its catastrophic failure. Thus, the stability as well as usability of the polymeric material will be affected and their lifetime as well as their reliability will be reduced distinctly. The industry develops various methods to detect and repair such damage, but under certain conditions it is not or just with great technical effort possible to detect those microcracks. For that purpose, autonomous damage-sensing (DS) and self-healing (SH) approaches were developed^{3; 5; 126-130} enabling the detection and subsequent repair of microcracks during, or direct after their formation which extend the durability and safety of polymeric compounds. Thus, the initial material properties are restored without the enormous costs of active monitoring or external repair.

Truly autonomous self-healing or damage-sensing requires no external stimulus, like heat or light and is triggered only by the damage event itself¹²⁶. Following those concepts it is important to prevent premature reactions in order to avoid the consumption of reactants inhibiting the later healing or leading to false-positive indications of damage. Therefore, three principle methods can be applied: On the one hand extrinsic approaches can be followed which based on embedding reactive compounds enclosed within nano- or microreservoirs¹³¹⁻¹³⁶, such as microcapsules or microvascular networks, into matrices to protect the reactive compounds from each other and preventing thus premature reactions. On the other hand intrinsic concepts based on Diels-Alder/retro-Diels-Alder (DA/rDA) cycloaddition reactions¹³⁷⁻¹⁴⁹ or supramolecular interactions^{3; 127; 150-151}, like hydrogen bonds or metal-ligand coordinations are feasible. In that case, the whole material or at least its major part consists out of the SH agent and the reactive species is formed usually by disrupting the thermodynamic equilibrium. The SH reaction is subsequently driven by returning back to the equilibrium state consuming thus the active moieties. Another alternative for autonomous extrinsic self-healing or damage-sensing is based on mechanochemical activation of mechanophores^{1-2; 4-5; 7; 102-103}. As defined above mechanophores are in their initial state inactive molecules containing mechanically labile bonds or functional groups which are activated *in situ* by applied external force and are cleaved in a well defined manner enabling thus subsequent SH or SD reactions. Moreover, the mechanophore concept supersedes the need of protecting nano- or microreservoirs, which usually have a negative influence on the material properties^{124; 132} enabling the direct embedding of the mechanophore into the matrix.

Thus, mechanochemistry offers the potential to play an important role in the world of polymeric self-healing and damage-sensing materials as it enables to convert external mechanical stress into directed transformations of chemical structures directly on the molecular level even before macroscopic failure appears. Well suitable self-healing strategies should enable an efficient crosslinking reaction under ambient conditions, like room temperature, humidity or oxygen atmosphere, without the requirement of an additional external trigger to recover the material properties after occurred damage and act thus as a truly autonomous self-healing material^{3; 127-128}. Mechanochemical cleavage can appear in principle in two different ways - either homolytically or heterolytically. In case of homolytic chain scission commonly two radicals are generated e.g. by C-C bond rupture which are able to recombine and restore thus the mechanical properties. The development of mechanophores with selective cleavable bonds able to undergo a heterolysis in the 1980th, like peroxy- or azo-linkers⁹²⁻⁹³, enables the change

from destructive to productive mechanochemistry as they generate two different reactive species disparate from each other. The consequent extension of these concepts in the following years end up in the development of more complex mechanophoric approaches for self-healing materials, like mechanocatalysts⁸⁻²² or cyclic precursors which generate under disruption force reactive compounds^{23-47; 51}. The frequently also as mechanochemical SH approaches listed concepts like Diels-Alder/retro-Diels-Alder reactions^{137-141; 144-149} or supramolecular interactions based methods^{3-4; 127; 150} will not be discussed in particular in the following section as they founded solely on the disruption of a chemical equilibrium by the applied external force and the subsequent restoration of the same kind of chemical bond and do not generate active catalysts or reactants.

1.3.1 Mechanocatalysts

Mechanocatalysts - also referred as latent catalysts - are commonly late transition metal complexes coordinated with strongly shielding ligands, which are inactive in its initial state and can be activated *in situ* by cleaving one of the stereo-electronic hindering ligands by applying external forces² (Figure 7).

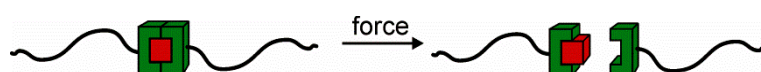


Figure 7. Generalized example for polymer embedded mechanocatalysts.

Mechanocatalysts are ideal candidates for enhanced self-healing materials as they generate active catalysts instead of reactants which allow an improving of the self-healing efficiency by repetitive turnover of the catalytic cycle. Thus, a single scission event is able to create subsequently many bonds facilitating the reduction of the mechanophore content necessary for an effective self-healing. Table 1 shows some of the most common examples for mechanocatalysts and list some characteristic benchmarks according to the previously in Chapter 1.2.1 and 1.2.2 discussed requirements. A detailed discussion of each example will be done in the subsequent chapters.

Table 1. Overview of mechanocatalysts benchmarks (mechanolabile bonds are highlighted in red).

	Mechanophore	Polymer handle (T _g [K])	Activation	Limiting molecular weight [g/mol]	Cleavage efficiency [%]	Activation force/ bond strength	Ref
1		PTHF (190) ¹⁵²	<u>Solution:</u> Ultrasound	< 7 500	quant.	141 kJ/mol ₁₁	8-11
2		PTHF (190) ¹⁵²	<u>Solution:</u> Ultrasound	< 10 000	50%; quant. (trapped by CS ₂)	450 pN ¹³ / 255 kJ/mol ₁	12-17
3		PTHF (190) ¹⁵²	<u>Solution:</u> Ultrasound <u>Bulk:</u> Compression	< 9 000 < 34 000	-	276 kJ/mol ₁	16-19
4		PMA (282) ¹⁵²	<u>Solution:</u> Ultrasound	< 132 000	quant. (replaced by MeCN)	-	20-21
5		PMA (282) ¹⁵²	<u>Solution:</u> Ultrasound	< 40 000	quant.	-	22

1.3.1.1 Pd/Pt-phosphane coordinated mechanocatalysts

Plenty of mechanochemical reactions were originally not be designed for self-healing applications, like the Bergman cyclization of enediyne macrocycles generating free radicals⁴⁵⁻⁴⁷ or the implementation of peroxy- or azolinkers within polymer chains⁹²⁻⁹³, but were applied later as such. The first systematically designed examples for mechanophores was developed in 2004 by Sijbesma *et al.* who investigate the mechanochemical activation of a palladium coordinated polymer⁸ (Figure 8) and establish thus the modern productive mechanochemistry. For that purpose, a linear multicenter coordinated, high molecular weigh $[\text{PdCl}_2(\text{PPh}_2\text{-PTHF-PPh}_2)]_m$ mechanocatalyst was synthesized. PTHF was chosen as polymeric handle to transmit the applied force to the labile metal-phosphane bond as it was known to enable in common solvents like toluene, acetonitrile or tetrahydrofurane a good polymer-solvent interaction and thus a fast coil-to-stretch transformation, which is in turn a crucial requirement for an efficient mechanochemical activation in solution (see Chapter 1.2.1).

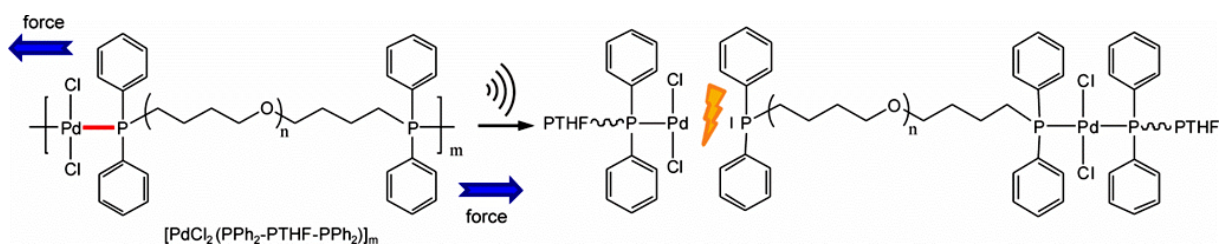


Figure 8. Mechanochemical induced selective Pd-P bond scission within $[\text{PdCl}_2(\text{PPh}_2\text{-PTHF-PPh}_2)]_m$ complexes by applied external force via ultrasound.

Subjecting the mechanocatalyst to strong ultrasound in toluene led to a selective scission of one palladium phosphane bond activating thus the catalyst (Figure 8). ³¹P-NMR as well as GPC experiments support the proposed mechanism proving the Pd-P bond scission by the presence of free phosphane ligands as well as by the reduction of molecular weight. However, the multi-Pd-centered architecture of the mechanocatalyst enables a multiple chain scission leading to a non-linear decrease in molecular weight up to an almost quantitative scission of the high molecular weight $[\text{PdCl}_2(\text{PPh}_2\text{-PTHF-PPh}_2)]_m$ compound during the sonication process⁸. The subsequent re-equilibration resulted beside the desired restoration of the initial high molecular weight compounds also in the formation of cyclic monomeric and dimeric species (Figure 8 $m = 1$ or 2), which hamper a clear prediction of the scission process. The addition of further low molecular weight monofunctional Pd-phosphane complexes to the $[\text{PdCl}_2(\text{PPh}_2\text{-PTHF-PPh}_2)]_m$ mechanocatalysts led to a permanent end capping of the Pd-P chain and thus to a complete restoration of the molecular weight in a second sonication process indicating that solely the reversible palladium-phosphorus bonds were broken and no C-C bond rupture within the PTHF backbone occurred^{10, 101}.

Moreover, the effects of the bond strength were investigated incorporating defined weak and strong metal-ligand interactions into the mechanophore. Therefore, mixed Pt/Pd complexes of the desired $([\text{PdCl}_2(\text{PPh}_2\text{-PTHF-PPh}_2)]_m\text{-}[\text{PtCl}_2(\text{PPh}_2\text{-PTHF-PPh}_2)]_p)$ mechanocatalyst were synthesized^{9, 11} and subjected to ultrasonication. It was found, that the weaker Pd-P bond (~ 141 kJ/mol) broke 3 times faster than the stronger Pt-P bond (~ 169 kJ/mol), even if the Pt-P bond scission cannot be completely suppressed. These results prove the selectivity of mechanochemical reactions, but also show their limits: differences in bond strength of ~ 28 kJ/mol between Pd-P and Pt-P enable a predominate scission, but do not prevent cross cleavage, while no C-C or C-O bond scission of the PTHF backbone ($\sim 330 - 350$ kJ/mol)¹⁵³⁻¹⁵⁴ could be observed.

Further systematic investigations of the activation behavior had shown a clear dependency of the initial molecular weight as well as of the mechanophore concentration on the efficiency of the mechanophore activation: High mechanophore concentration and increased initial polymer chain length led to a more efficient activation⁸⁻¹¹. Additionally, the authors claimed a limiting molecular weight which is necessary to cleave the mechanophores at all, albeit a detailed prove e.g. by a low molecular weight model complex is missing. This would prove that the chain scission occurs solely due to transmission of the applied force via the attached polymeric handles. Furthermore, the catalytic activity of the mechanophores e.g. for cross-coupling or hydrogenation reactions was not tested.

1.3.1.2 Ag/Ru *N*-heterocyclic carbene mechanocatalysts

Another type of mechanocatalyst based on the metal-carbene complexes which were also linked to PTHF handles in order to transmit the applied external force¹²⁻¹⁹ (Figure 9). Homogeneous organometallic complexes in general are well known examples for excellent catalyst in chemical reactions due to their good miscibility, selectivity as well as a high turnover numbers and fast reaction rates, while metal-carbenes in particular were selected as they are known as relative stable and chemical inert functionalities¹⁵⁵⁻¹⁵⁷.

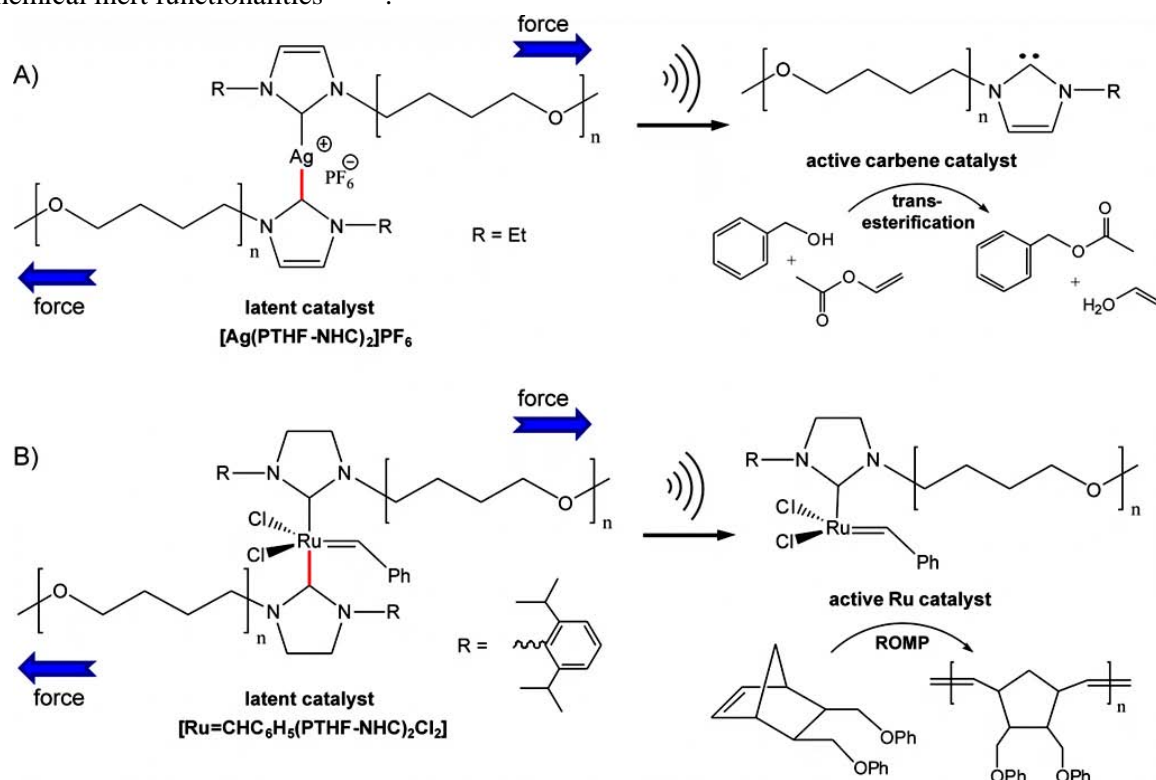


Figure 9. Mechanochemical activation of latent Ru and Ag *N*-heterocyclic carbene (NHC) coordinated polymers by applied ultrasound. (A) Subjecting the $[\text{Ag}(\text{PTHF-NHC})_2]\text{PF}_6$ mechanophore to external force led to the cleavage of one carbene ligand which in turns catalyzes a transesterification reaction of benzyl alcohol and vinyl acetate. (B) Ultrasonication led in case of $[\text{Ru}=\text{CHC}_6\text{H}_5(\text{PTHF-NHC})_2\text{Cl}_2]$ to an activation by cleaving of one ligand from the metal center generating thus a free coordination site which enables to initiate the catalytic ROMP of the norbornene monomers.

Based on the considerations of Grubbs *et al.*¹⁵⁵⁻¹⁵⁶, who developed ruthenium *N*-heterocyclic carbene (NHC) based catalysts for the ring opening metathesis polymerization (ROMP), a latent metal-NHC catalyst was developed attaching two polymeric NHC ligands to either one Ru or Ag center. Due to the strongly stereo-electronic shielding of the second NHC ligand, the catalyst was - in contrast to the commonly by thermal treatment activatable metal-carbene catalysts of Grubbs - inactive in its initial state, but can be activated selectively by cleaving of one NHC-ligand by external force, like ultrasound

or compression (Figure 9). The obtained reactive species can be distinguished into two different cases: either the free carbene or the metal center becomes the catalytic active species after mechanochemical activation¹²⁻¹⁹. In case of the $[\text{Ag}(\text{PTHF-NHC})_2]\text{X}$ mechanophore a transesterification reaction of benzyl alcohol and vinyl acetate was catalyzed by the generated highly nucleophilic free carbene, while in case of the $[\text{Ru}=\text{CHC}_6\text{H}_5(\text{PTHF-NHC})_2\text{Cl}_2]$ mechanocatalyst a free coordination site on the metal center was generated enabling thus to initiate the ROMP of the disubstituted norbornene monomers (Figure 9).

Beside the extensive investigated effects of the concentration as well as the effect of the initial molecular weight, which both increase the efficiency of the mechanochemical activation with their own increase, the influence of the solvent as well as the role of the steric hindering substituents on the activation behavior was investigated¹²⁻¹⁹. Subjecting the $[\text{Ag}(\text{PTHF-NHC})_2]\text{X}$ ($M_n = 13\,400$ g/mol) mechanophore to ultrasonication for 10 minutes in toluene led to a scission of ~30% of the mechanocatalyst, while ~50% of the mechanophores were cleaved when acetonitrile was used as solvent. Trapping the generated free carbene with CS_2 led to an almost quantitative cleavage in acetonitrile and ~90% in toluene and is thus more effective as the back reaction restoring the initial complex is prevented¹². The differences in scission efficiencies between toluene and acetonitrile can be explained by the better polymer-solvent interactions in case of acetonitrile and thus the faster coil-to-stretch transition led to a more efficient force transmission. The same effect was shown for the catalyzed transesterification reaction of benzyl alcohol and vinyl acetate yielding conversions up to 60% after 30 minutes of ultrasonication¹⁷.

However, practical investigations had shown a low activity of the $[\text{Ag}(\text{PTHF-NHC})_2]\text{X}$ mechanocatalyst towards transesterification reactions (~4%) even without applied external force^{12; 17}. In order to suppress this undesired reactivity and ensuring a completely latent mechanophore, the bulkiness of the second substituent on the NHC was increased from ethyl to diisopropylphenyl. Furthermore, the type of NHC was changed from a planar aromatic imidazolium to an angled non-aromatic imidazoline based scaffold (Figure 9), which decreased the theoretical reactivity, but increased the stability of the obtained complex¹⁵⁸⁻¹⁶¹. These modifications led in case of the ruthenium-NHC based mechanocatalyst the desired complete latency¹⁷⁻¹⁸. Subjecting this complex to ultrasonication revealed to an activation and subsequent conversion in the ring-closing metathesis (RCM) of diethyl diallylmalonate up to 35% and for the ROMP of disubstituted norbornenes up to 20%¹⁸. The obtained reactivity was thus significant lower compared to the Ag based mechanophore as expected according to the modification in the NHC structure, which stabilized the Ru-NHC complex, but lowering its activity. Further investigation on the stability of the activated $[\text{Ru}=\text{CHC}_6\text{H}_5(\text{PTHF-NHC})_2\text{Cl}_2]$ moiety were however ambiguous as the reported results for the performed “on/off” sonication experiments were inconsistent. In case of the RCM of diethyl diallylmalonate an immediate stop in RCM propagation was reported when ultrasonication was switched off indicating the fast collapse/deactivation of the active species¹⁷ and continued when ultrasound was again turned on, while a persisting of the reactive species was claimed for the ROMP of disubstituted norbornenes, which was indicated by a continuing propagation even when sonication was stopped¹⁸.

The final proof of the mechanophore activation solely due to the applied external force by ultrasound was done via a low molecular weight model compound containing the potential mechano-labile Ru-NHC group, but no polymer handles to transmit the force. Subjecting this complex to ultrasound revealed no Ru-carbene bond scission and no catalytic activity¹⁷, which prove the true mechanochemical nature of the activation process. Further investigations had shown a limiting molecular weight of ~9000 g/mol for the polymer handle which is needed to obtain an efficient mechanophore activation¹⁷.

1.3.1.3 Ru N-heterocyclic carbene mechanocatalysts in bulk applications

Studying mechanocatalysis in bulk state is of major importance for the development of suitable mechanochemical self-healing concepts as the most polymeric materials are applied in the solid state. One of the rare examples is the aforementioned latent poly(tetrahydrofuran) based Ru-NHC mechanocatalyst (34 000 g/mol) which was therefore embedded together with mono- and bifunctional norbornene monomers into a high molecular weight semi-crystalline PTHF matrix (170 000 g/mol) (Figure 10)¹⁹. The PTHF handles attached to the NHC are able to co-crystallize with the PTHF matrix which enhance the anchor effect significantly leading in turns to a better transmission of the applied mechanical force and thus to a more efficient activation of the mechanocatalysts (see Chapter 1.2.2). The additional crosslinking points, formed by the co-crystalline regions, enable to “collect” the shear force applied by repetitive compressions via a hydraulic press and transmit also its perpendicular parts to the labile metal-carbene bond increasing thus the efficiency of cleaving one polymeric NHC ligand.

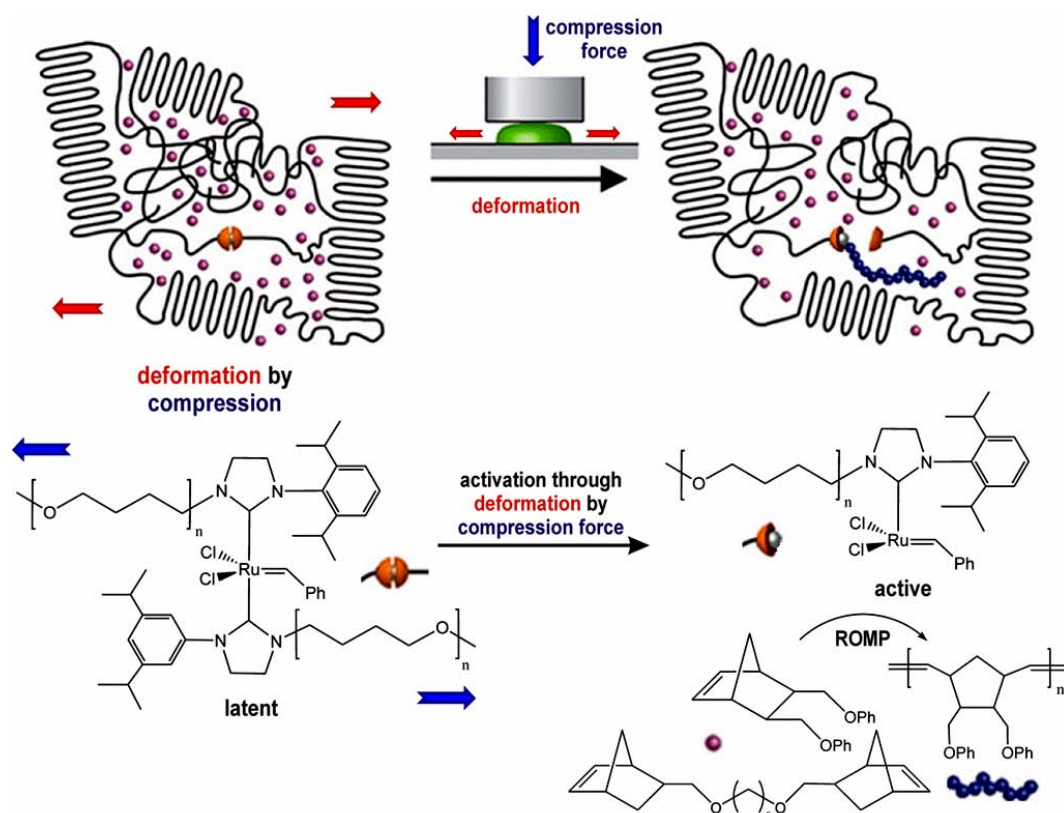


Figure 10. The bulk activation of latent Ru-carbene complex in high molecular weight PTHF matrix by applied shear force via co-compression of a hydraulic press trigger the ROMP of mono- and bifunctional norbornene monomers enabling the formation of a crosslinked network restoring the material properties and opens the opportunity to a truly autonomous self-healing material. (Adapted from literature¹⁹ with permission. Copyright 2013 American Chemical Society.)

The generated catalytic active species (Figure 10) was now able to trigger the ROMP of the two norbornene monomers yielding after five compression cycles a crosslinked poly(norbornene) with a conversion up to 25%, which reveals the potential to restore the material properties. However, the effect of the initial mechanophore molecular weight onto the activation behavior was not studied as only one molecular weight was investigated. The performed control experiment using a low molecular weight model complex without polymeric handles revealed no catalytic activity, which qualifies the demonstrated concept for truly autonomous self-healing by an *in situ* generated catalyst via applied compression force in the solid state, albeit no final proof of the self-healing behavior was accomplished.

1.3.1.4 Pincer complexes for mechanocatalysis

Pincer complexes are usually late transition metal complexes which are coordinated tridentate to a strongly chelating eponymous Pincer ligand consisting out of two donor atoms (commonly phosphorus, sulfur or nitrogen) and one σ -carbene bond (mostly phenylic) retaining an additional free coordination site on the metal which is usually blocked with another, simply removable nitrogen donor¹⁶²⁻¹⁶⁴. Therefore, Pincer complexes are well suitable in different kinds of catalytic reactions and organic synthesis as their special design enables a well understood fine tuning of their catalytic capability, e.g. by adjusting the electronic properties of the central metal or setting of the steric requirements by the choice of ligands. This knowledge offers the opportunity for further application and the implementation of well suitable functions. Thus, linear and crosslinked supramolecular polymer networks were designed using bifunctional Pd/Pt-Pincer complexes as building blocks, which are able to form reversible networks based on multiple repeatable coordination and cleavage of the metal-ligand interactions^{21; 162; 165-167}.

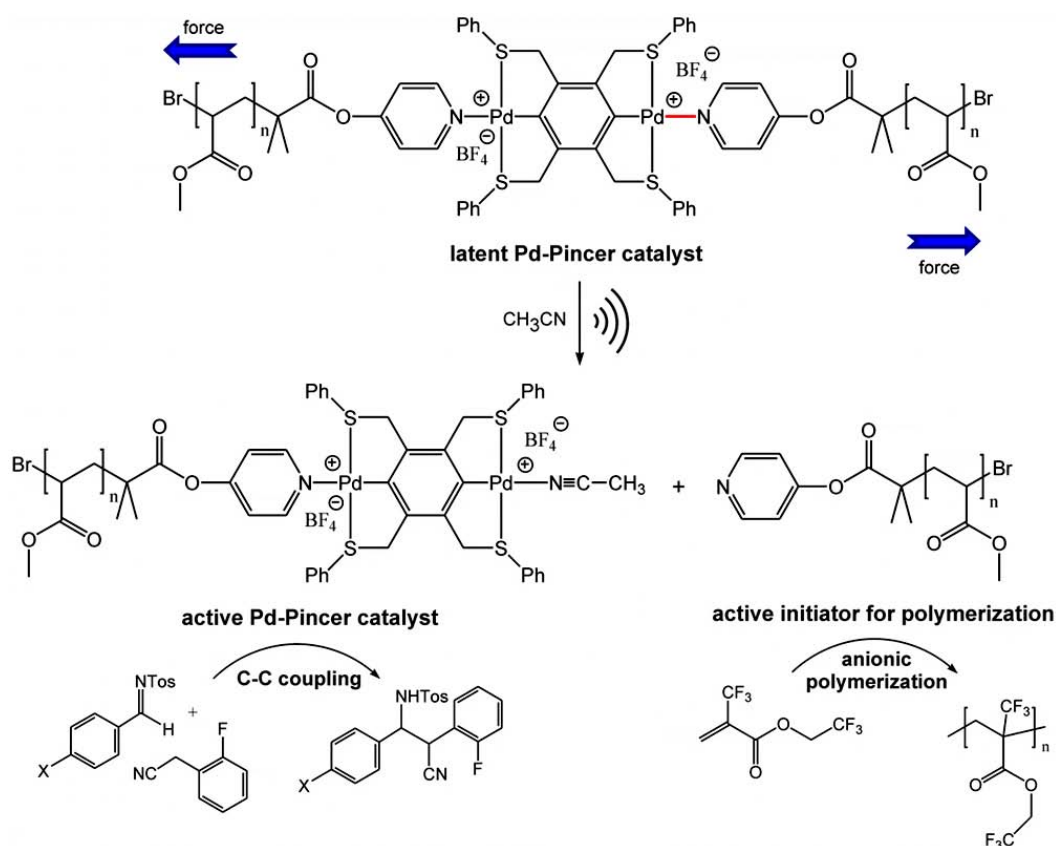


Figure 11. Mechanochemical activation of a pyridine telechelic poly(methylacrylate) (PMA) Pd-Pincer complex by applied ultrasound led to a cleavage of the labile Pd-pyridine bond and generate an activated Pd-Pincer complex able to trigger a carbon-carbon bond formation of 2-fluorobenzyl cyanide and *N*-tosylbenzylimine as well as the cleaved PMA-pyridine ligand initiating the anionic polymerization of α -trifluoromethyl-2,2,2-trifluoroethyl acrylate.

However, Pincer complexes can also be used in a more productive manner in order to design autonomous self-healing materials. For that purpose, a bifunctional Pd-based Pincer complex was centrally implemented within a polymer scaffold by coordination to two pyridine telechelic poly(methylacrylate) (PMA) chains (Figure 11)²⁰. Subjecting this complex in the presence of acetonitrile to ultrasonication for 2 hours led to an almost quantitative replacement of the shielding polymeric PMA-pyridine ligand generating two reactive species: the activated Pd-Pincer complex and the cleaved PMA-pyridine ligand. However, to ensure an efficient activation HBF_4 had to be added to block the free pyridine moiety and prevent an immediate re-coordination and thus the deactivation of

the activated moieties. Also the limiting molecular weight which was necessary for an effective activation is with 132 000 g/mol quite high. Nevertheless, the obtained activated Pd-Pincer complex was able to catalyze e.g. in a Heck type coupling the carbon–carbon bond formation of 2-fluorobenzyl cyanide and *N*-tosylbenzylimine within 2 hours with 93% conversion, while the free PMA-pyridine ligand is able to initiate an anionic polymerization of α -trifluoromethyl-2,2,2-trifluoroethyl acrylate yielding a polymer within 42% conversion (Figure 11). Control experiments applying either no ultrasonication or using low molecular weight complexes as well as monofunctional Pd-Pincer-complexes carrying only one polymer handle provided just a low catalytic activity below 3% towards the C-C bond formation of 2-fluorobenzyl cyanide and *N*-tosylbenzylimine which was in the range of thermal reaction indicating thus the true mechanochemical nature of these reactions. Moreover, the effect of the ligand replacement from pyridine to acetonitrile respectively DMSO, which was necessary to stabilize the obtained catalyst, was investigated in detail via AFM measurements²¹.

Summing-up, both types of investigated reactions, the C-C bond formation as well as the anionic polymerization offer the potential for self-healing crosslinking reactions, albeit no self-healing behavior or activation in solid state was demonstrated.

1.3.1.5 Boronium-pyridine mechanocatalysts

Similarly, a boronium-pyridine mechanocatalyst was developed by linking two pyridine telechelic PMA chains to one bis(pentafluorophenyl) substituted boronium atom (Figure 12)²². Applied ultrasound generate almost quantitatively a free pyridine ligand by selective scission of one boronium-pyridine bond, which is able to act as Brønsted bases in sol-gel processes or can trigger an anionic polymerization of α -trifluoromethyl-2,2,2-trifluoroethyl acrylate with conversions up to 49% (Figure 12). The limiting initial molecular weight for an effective mechanophore scission was found to approximately 40 000 g/mol and is thus significant lower compared to the previous discussed Pd-Pincer complex indicating a weaker boronium-pyridine bond. Control experiments using colorimetric investigations by means of azo dyes prove the activation of the boronium-pyridine complex solely by mechanical force.

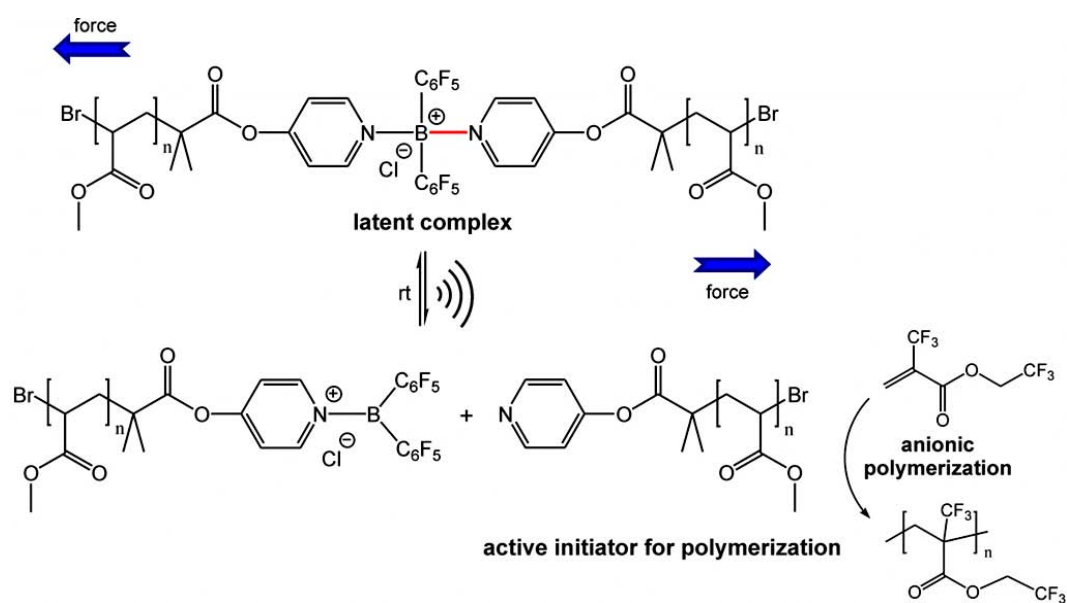


Figure 12. Ultrasound induced scission of mechanolabile boronium-pyridine bonds in solution and subsequently triggered anionic polymerization of α -trifluoromethyl-2,2,2-trifluoroethyl acrylate.

However, additional experiments investigating high concentrated solutions of the mechanophore in acetonitrile revealed an ineffective chain scission presumably due to immediate re-coordination of the liberated free pyridine ligand to the boronium center, which limits the applicability of the concept for self-healing approaches in the solid state.

1.3.2 Generation of reactive species by cyclic mechanophores

Cyclic mechanophores are often used as well suitable precursors for self-healing applications as their constrained rings enable the generation of reactive species usable for a large diversity of chemical transformations^{23-47; 85}, like pericyclic rearrangements, electrocyclic ring opening reactions or the generation of radicals (Figure 13). The inherent ring strain of such mechanophores reduces the usually high dissociation energy of C-C or C-O bonds (>300 kJ/mol) significantly and allows a bond cleavage by external mechanical force under ambient conditions^{1; 153-154}. Thus, mechanophores containing centrally positioned, activated cyclic functionalities like three membered *gem*-dihalocyclopropanes²³⁻³⁴ or epoxides³⁷ as well as four membered annulated cyclobutanes^{35; 38-41; 52}, dicyano-substituted cyclobutane-di-esters⁴²⁻⁴³, β -lactams⁴⁴ or cyclobutane-1,3-diones⁸⁵ can be activated by mechanical force. Larger rings may also be activated but they had to contain highly strained or reactive bonds, like in the Bergmann cyclization of enediyne⁴⁵⁻⁴⁷ or must offer a special driving force, like the re-aromatization of *gem*-dichlorocyclopropanated indenyls³⁶. Table 2 provides some examples for cyclic mechanophores and lists its characteristic benchmarks.

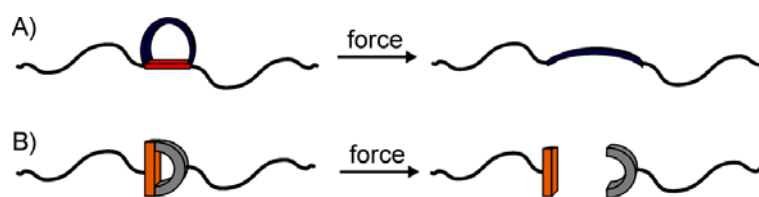


Figure 13. Generalized examples for polymer embedded cyclic mechanophores.

Table 2. Overview of benchmarks from cyclic mechanophores generating reactive species (mechanolabile bonds are highlighted in red).

Mechanophore	Polymer handle (T _g [K])	Activation	Limiting molecular weight [g/mol]	Cleavage efficiency [%]	Activation force/bond strength	Ref
<p>X = F (gDFC); Cl (gDCC); Br (gDBC)</p>	PBD (263) ²⁹	Solution: Ultrasound Bulk: Compression, Extrusion, Tension	> 40 000	Ultrasound 80% ²⁸ Compression 3% ²⁹ Extrusion 30% ²⁷ Tension not activatable ²⁹	<i>cis</i> -gDFC 1290 pN; <i>trans</i> - gDFC 1820 pN <i>cis</i> -gDCC 1300 pN; <i>trans</i> - gDCC 2290 pN	23-35; 52-54
	PMA	Bulk: Compression	network ^{a)}	20%	-	36
	PNB (308) ¹⁵²	Solution: Ultrasound	> 48 000	-	272 kJ/mol	37

	Mechanophore	Polymer handle (T _g [K])	Activation	Limiting molecular weight [g/mol]	Cleavage efficiency [%]	Activation force/ bond strength	Ref
4		PEG (232) ¹⁵²	<u>Solution:</u> Ultrasound	< 20 000	quant.	<i>cis</i> -BCB 1270 pN <i>trans</i> -BCB 1500 pN	35; 38- 39
5		PMA (282) ¹⁵²	<u>Solution:</u> Ultrasound	> 23 000	-	6010 pN	40
6		Poly-ester	<u>Solution:</u> Ultrasound	-	48%	-	41
7		PMA (282) ¹⁵²	<u>Solution:</u> Ultrasound	11 700	quant.	3300 pN; 239 kJ/mol	42- 43
8		PMA (282) ¹⁵²	<u>Solution:</u> Ultrasound	-	65%	3470 pN; 284kJ/mol	44
9		PMMA	<u>Bulk:</u> Swelling	network ^{a)}	-	5000 pN	45- 47

^{a)}prepared by free radical polymerization of the corresponding monomer using the mechanophore as crosslinking points

1.3.2.1 *gem*-Dihalocyclopropanes

Some of the most thoroughly investigated cyclic mechanophores are the *gem*-dihalocyclopropanes (gDHC) incorporated randomly within the widely used poly(1,4-butadiene) (PBD) by treating commercially available PBDs with *in situ* generated dihalocarbenes^{23-35; 52-54}. The obtained dichloro as well as dibromo gDHC-PBD copolymers show typically functionalization over 90% of the double bonds. Subjecting these copolymers to mechanical force resulted in an electrocyclic ring opening reaction of the gDHC moieties generating 2,3-dihaloalkenes (DHA) (Figure 14)²³⁻³⁴.

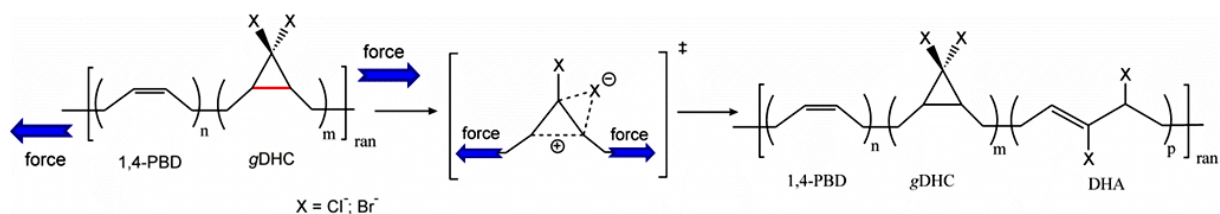


Figure 14. Force induced electrocyclic ring opening reaction of *gem*-dihalocyclopropane (gDHC) modified poly(1,4-butadiene) (PBD) generates 2,3-dihaloalkene (DHA) moieties.

The activation event itself was demonstrated in solution by ultrasound as well as in bulk either by compression, extrusion or tension, whereas strong differences in the activation efficiency were observed. Ultrasound induced activation in THF solutions yielded good activation rates up to 80% of gDHC²⁸, whereas a limiting molecular weights of at least 40 000 g/mol can be supposed as no cleavage can be determined below. In contrast, the activation via compression was applied in the pure mechanophore bulk state without additional matrix material and requires significant higher molecular

weights of 300 000 to 500 000 g/mol offering thereby much lower activation efficiencies of only 3% gDHC, while the activation by tension force was not possible at all, presumably due to the lower applicable maximal force^{29; 53}. Extrusion shows the most efficient activation of gDHC in bulk materials up to 30%, but is unsuitable for practical applications due to its destructive character²⁷.

However, in all cases the formation of 2,3-dihaloalkenes (DHA) can be observed, which were reactive to a subsequent nucleophilic substitution enabling thus *in situ* crosslinking reactions with dicarboxylates (Figure 15)²⁵. The random distribution of gDHC mechanophores along the complete polymer backbone offers the potential for a highly efficient crosslinking and increase the efficiency of activation as the chance for a central positioning of the mechanophore in focus of the applied force is more likely. Furthermore, the ring opening lead to an inherent change in material properties by self-strengthening²⁵ and elongates additionally the polymer scaffold releasing thereby partially stress and preventing thus damage which may lead otherwise to a catastrophic failure of the material. Thus, the gDHC mechanophores offers the potential for a well suitable mechanochemically induced self-healing behavior.

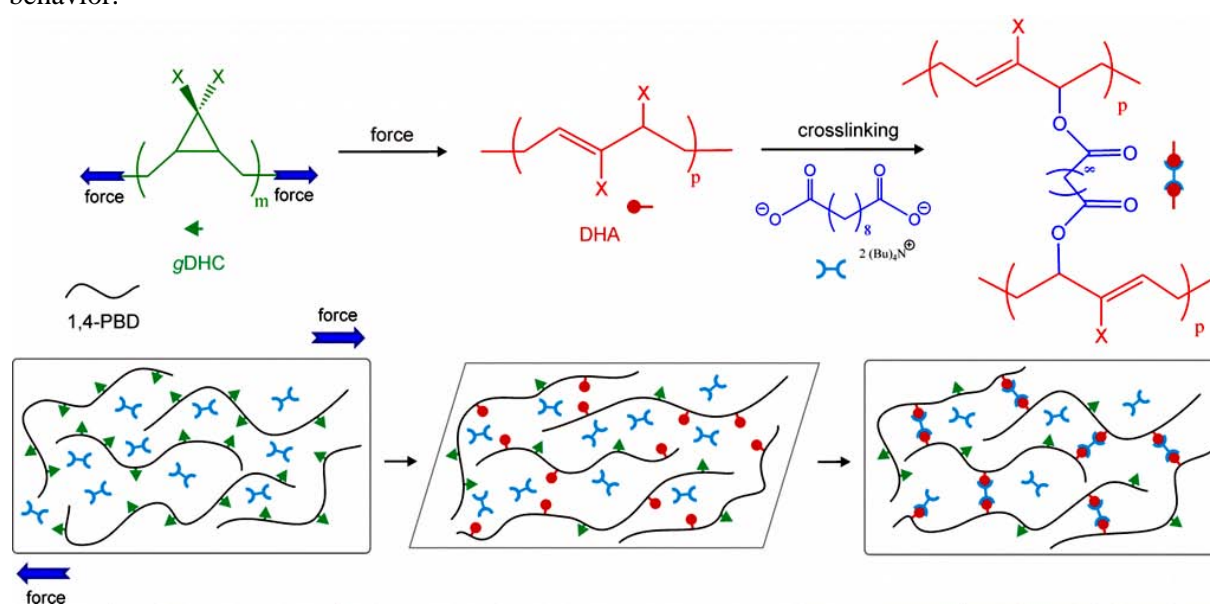


Figure 15. The mechanochemical activation of *gem*-dihalocyclopropane (gDHC) modified poly(1,4-butadiene) (PBD) generates 2,3-dihaloalkene (DHA) moieties within the polymer backbone enabling crosslinking reactions towards mild nucleophiles, like dicarboxylates and forms thus polymer networks leading in turns to self-healing.

Also the influence of the *cis/trans* isomerization of the gDHC mechanophores towards the electrocyclic ring opening was investigated^{24; 35; 52}. According to the orbital symmetry rules of Woodward-Hoffmann, the *cis-gem*-dihalocyclopropanes request the thermally allowed disrotatory pathway yielding the corresponding 2,3-dihaloalkene, while *trans-gem*-dihalocyclopropanes require the thermally forbidden conrotatory pathway. However, mechanochemical activation yielded in both cases the desired 2,3-dihaloalkene species as proven by practical investigations²⁸. Additional AFM measurements revealed, that significant higher forces of up to 1000 pN are required for the mechanochemical activation of the thermally forbidden reaction³⁵. Thus, the thermally allowed disrotatory ring opening of the *cis-gem*-dichlorocyclopropane (*cis*-gDCC) PBD based mechanophore required 1300 pN, while the conrotatory ring opening of the *trans-gem*-dichlorocyclopropane (*trans*-gDCC) requires 2290 pN. Additionally, the effect of the halogen atoms where investigated revealing lower forces required for the ring opening of the dibromo- (1210 pN for *cis*-gDBC PBD) than for the dichoro- (1300 pN for *cis*-gDCC PBD) or for the difluorocyclopropane (1290 pN for *cis*-gDFC PBD), which explains also the slightly higher reactivity of the dibromo compound.

Furthermore, the overall bond strength of the C-C bond within the gDHC ring was determined to ~170 kJ/mol and was thus significantly lowered by the highly strained cyclopropane ring compared to more than 300 kJ/mol for common C-C bonds^{33; 35}.

In order to investigate the effect of the stiffness and thus the force transmission efficiency of the polymer scaffold to the mechanolabile group, the 1,4-poly(butadiene) (PBD) backbone was replaced by *cis*-poly(norbornene) (PNB) and converted to a PNB based gDHC mechanophore using dihalocarbenes²⁴. AFM investigations revealed a drop-down of approximately one-third in the required ring opening force to 900 pN for PNB based *cis*-gDCC and 740 pN for PNB based *cis*-gDBC compared to their PBD based counterparts with 1300 pN for *cis*-gDCC PBD and 1210 pN for *cis*-gDBC PBD. As suitable explanation therefore was found in the intrinsic barriers of the cyclopentane rings within the PNB backbones, which limits chain internal conformational changes and leading to a lever-effect of the whole polymer scaffold and thus finally to a decrease in the scission barrier enabling in turns a bond cleavage at lower forces. These observations give a first hint for systematic screening of suitable polymer backbones to greater mechanical advantages and may prospectively enable to engineer mechanochemical reactivity.

1.3.2.2 *gem*-Dichlorocyclopropanated indenenes

Enhancing this concept led to the development of *gem*-dichlorocyclopropanated indene mechanophores which were incorporated into a crosslinked PMA-based matrix material³⁶. Subjecting this material to compression led - in comparison to the previously discussed gDHC mechanophores (see Chapter 1.3.2.1) - to a different ring-opening reaction via a pericyclic rearrangement under elimination of HCl and a re-aromatization of the bicyclic ring system to 2-chloronaphthalene (Figure 16). The force-dependent release of HCl featured the material for acid-catalyzed cross-linking reactions and thus finally for self-healing behavior albeit no final proof was accomplished. However, the bulk activation efficiency via compression was found to 20% and is thus significantly higher compared to the non-crosslinked gDHC (only 3%) presumably due to the incorporation of the mechanophore into the polymeric network as well as the enhanced driving force through the re-aromatization.

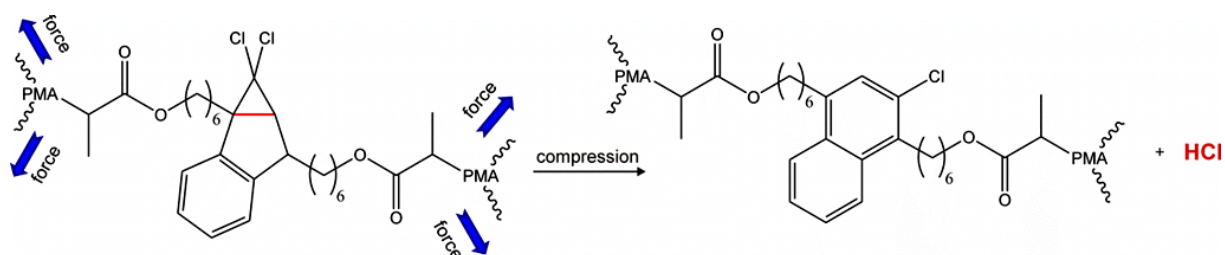


Figure 16. Bulk activation of *gem*-dichlorocyclopropanated indene incorporated into a crosslinked PMA matrix by compression generated via a pericyclic rearrangement 2-chloronaphthalene and eliminate HCl able to catalyze further crosslinking reactions.

1.3.2.3 Epoxides

Epoxidized polymers represent another group of high strained three-membered cyclic mechanophores which generate under applied mechanical force reactive compounds³⁷. For that purpose, PBD as well as PNB with a molecular weight ranging from 380 000 to 965 000 g/mol had been epoxidized by the means of *meta*-chloroperoxybenzoic acid (*m*CPBA) with 50 – 80% conversion in respect to its double bonds (Figure 17). Subjecting this mechanophores to ultrasonication led in case of the PNB to a formation of reactive ylides, while in case of PBD based mechanophores no activation could be

observed. The reason therefore is the higher force transmission efficiency due to the lever-effect of the PNB in comparison the PBD (see Chapter 1.3.2.1). Thus, the transmitted force is for PBD insufficient to open the more stable epoxides with bond dissociation energies of 272 kJ/mol in comparison to the easier cleavable gDHC (126 – 188 kJ/mol)³⁷. Nevertheless, the formed reactive ylides enabled in case of PNB an efficient crosslinking with primary alcohols as well as terminal alkenes (Figure 17) and reveals thus the potential for an efficient self-healing material.

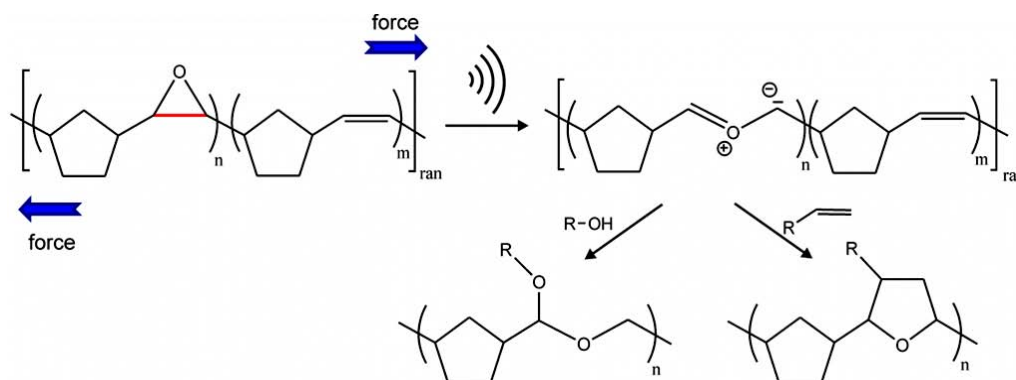


Figure 17. Ultrasound induced electrocyclic ring opening of epoxidized PNB under formation of reactive ylides and subsequent crosslinking reaction with primary alcohols or terminal alkenes.

1.3.2.4 Annulated cyclobutanes

Also a large diversity of four-membered cyclic mechanophores were developed, whereas these kind of mechanophores required additional functionalities close to the cyclobutene ring, like annulated strained ring systems³⁸⁻⁴¹, diesters or electron withdrawing groups⁴²⁻⁴³, in order to enable an efficient activation under external force.

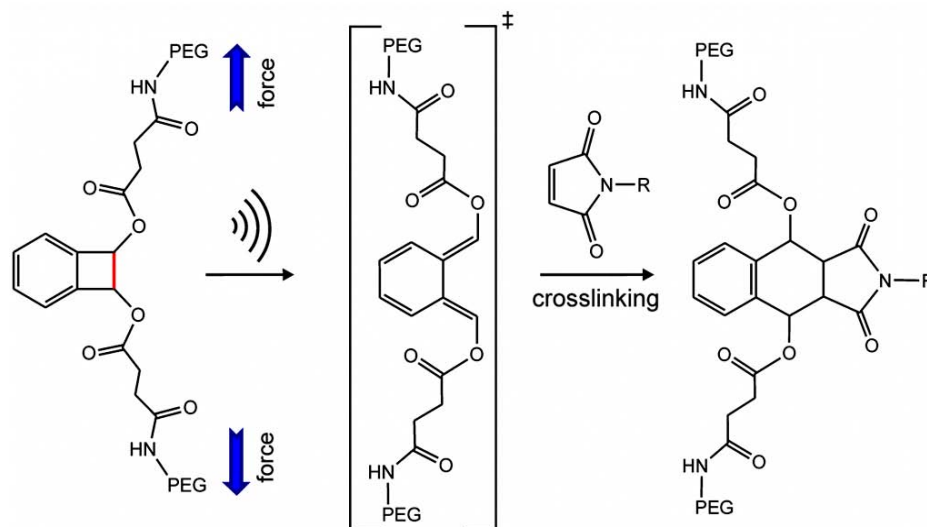


Figure 18. The mechanochemical activation of PEG-based benzocyclobutene (BCB) by ultrasound yields in the formation of *E,E*-*ortho*-quinodimethide dienes (*oQDM*) and a subsequent crosslinking reaction with substituted maleinimides.

One of the first examples was developed by Moore *et al.*, who used benzocyclobutene (BCB) mechanophores linked either to PEG³⁸ or PMA polymer chains³⁹. Subjecting them to ultrasound facilitated a pericyclic rearrangement including a 4π electrocyclic ring-opening reaction and resulted in an almost quantitative formation of an *ortho*-quinodimethide diene (*oQDM*), which was able to conduct a Diels-Alder (DA) crosslinking reaction in the presence of substituted maleimides (Figure 18) and opened thus the potential for self-healing applications.

Additionally, the salient different reaction pathways for the thermally, photo- and mechanochemically triggered electrocyclic ring opening reactions had been investigated for the single isomers of BCB demonstrating thus clearly the potential for predicting and directing reaction pathways by mechanical force^{35; 38}. The orbital symmetry rules of Woodward-Hoffman requires for the thermally triggered ring opening reaction a conrotatory movement generating for the *cis*-BCB mechanophore the E,Z-*o*QDM, while *trans*-BCB yielded the E,E-*o*QDM isomer (Figure 19). The light induced reaction showed the opposite behavior and requested a disrotatory ring-opening generating for *cis*-BCB the E,E-*o*QDM and for *trans*-BCB the E,Z-*o*QDM. Contrary to both, the mechanochemical reaction revealed for both BCB isomers the same E,E-*o*QDM isomer, which is essential as it is preferred in the subsequent DA crosslinking reaction, while the E,Z-*o*QDM is unsuited. AFM investigations showed surprisingly a slightly higher required force of 1500 pN for the symmetry allowed scission of the *trans*-BCB compared to symmetry forbidden 1370 pN for the *cis*-BCB isomer³⁵. Implementing additional double bonds next to the strained ring system acted in the same way as for the epoxide and gDHC mechanophores as a kind of lever, reducing the required force to 900 pN⁵².

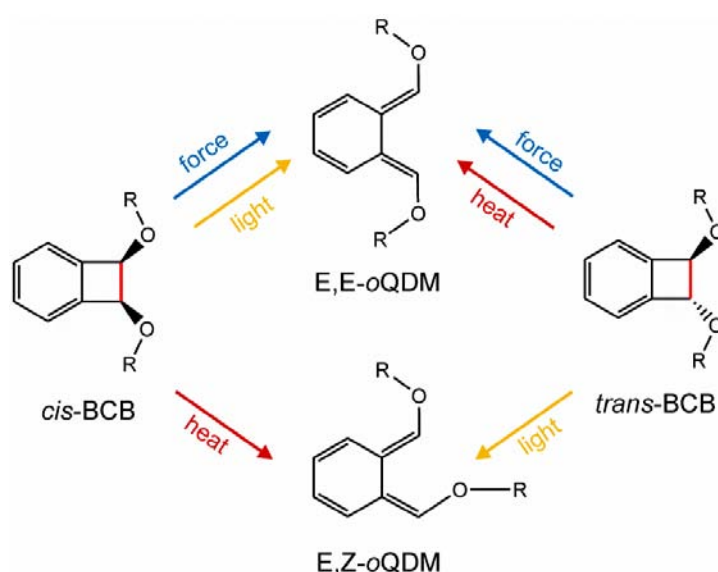


Figure 19. Different reaction pathways for *cis/trans*-BCB: Thermal (red arrows), photochemical (yellow) and mechanochemical (blue) and the corresponding E,E- or E,Z-*o*QDM isomers.

Similarly, other cyclobutene mechanophores with annulated strained rings had been developed leading in turns under ultrasonication to the formation of double bonds via [2+2] cyclo-reversions of cyclobutene (Figure 20)⁴⁰⁻⁴¹. In contrast to the aforementioned example, two σ -bonds were broken generating reactive α,β -unsaturated carbonyl groups up to 48% which are highly reactive for Michael additions of e.g. secondary amines (Figure 20A)⁴⁰ or thiol-ene reactions using bifunctional thiols forming sulfide functionalized crosslinked polymer networks within 1 min under ambient conditions (Figure 20B)⁴¹. Furthermore, a significant elongation of the polymer chain due to the mechanophore scission (up to 7Å compared to gDHC 1-2Å) allows a partial stress release preventing thus damage which may lead otherwise to a catastrophic failure of the material. The very fast and efficient crosslinking reactions especially under ambient conditions as well as their ability for chain elongation make these kinds of mechanophores to promising candidates for well suitable autonomous self-healing materials, albeit none of them were realized in the solid state.

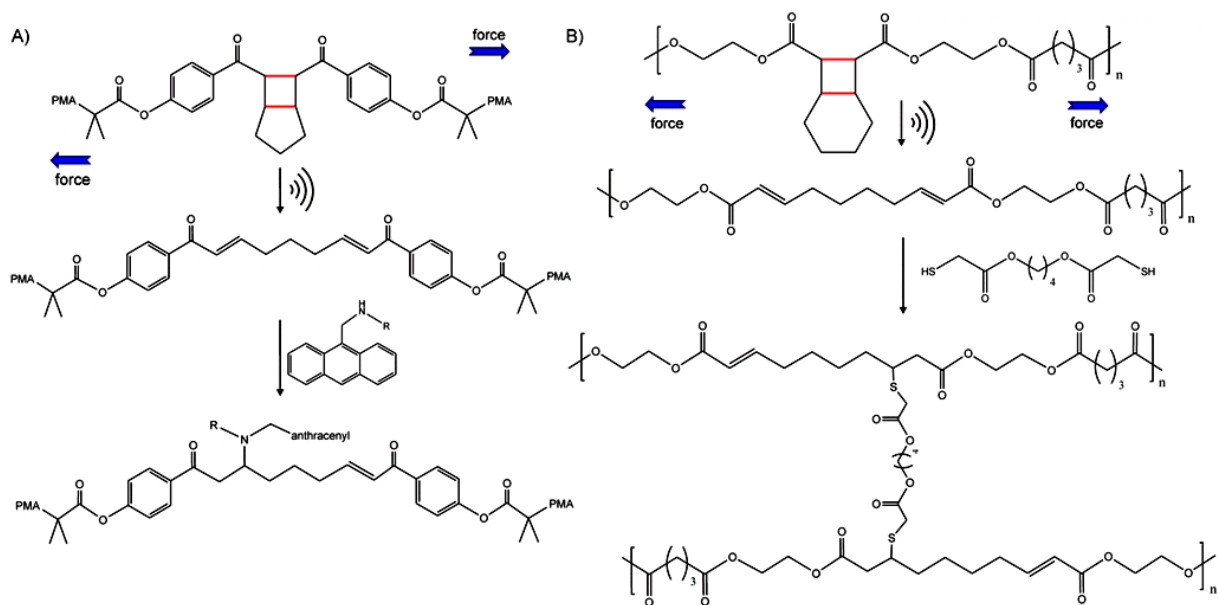


Figure 20. Ultrasound induced activation of annulated cyclobutane mechanophores: A) PMA-based bicyclo[3.2.0]-heptane mechanophores enabling a pericyclic rearrangement under applied force and subsequent Michael additions of secondary amines. B) Polyester-based bicyclo[4.2.0]octane mechanophore undergoes a [2+2] cycloreversion generating α,β -unsaturated carbonyl groups which are reactive in thiol-ene reactions to bifunctional thiols forming under mild conditions crosslinked networks.

1.3.2.5 Dicyano-substituted cyclobutane-di-esters

Dicyano-substituted cyclobutane-di-esters linked symmetrically to two PMA chains are another group of well suited four-membered ring mechanophores as they generate under applied ultrasound stable, but highly reactive cyanoacrylates which are able to conduct Michael additions e.g. with secondary amines to form crosslinked structures (Figure 21)⁴²⁻⁴³. Contrary to the previously discussed cyclic mechanophores, the sonification of substituted dicyanocyclobutanes led to a selective cleavage via a [2+2] cycloreversion into two molecules with the half of original molecular weight.

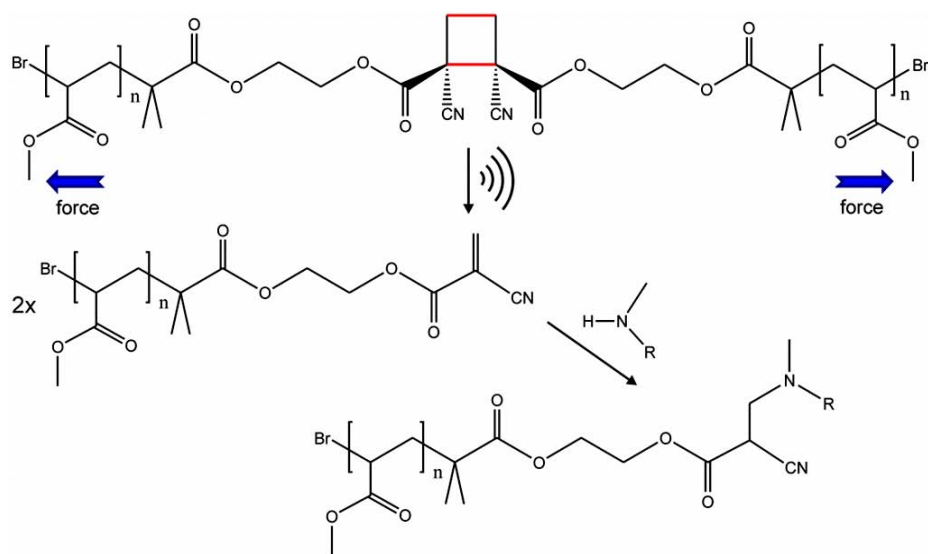


Figure 21. Ultrasound induced [2+2] cycloreversion of *cis*-dicyano-substituted cyclobutane-di-esters with attached PMA handles transmitting the applied force yielding cyanoacrylates reactive for Michael additions of secondary amines forming crosslinked structures.

Additionally, the influences of the substituents as well as its conformational arrangement on the activation behavior of the mechanophore had been investigated in detail considering di- and monocyano as well as unsubstituted cyclobutane-di-esters in their different conformations⁴². Subsequently performed CoGEF calculations revealed a decrease of the required scission force for higher substituted mechanophores stepwise decreasing from 4370 pN for the unsubstituted *cis*-cyclobutane-di-ester over 3670 pN for the *cis*-monocyano- and 3300 pN for the *cis*-dicyano-substituted cyclobutane-di-ester. Accordingly, the molecular weight threshold necessary for an efficient chain cleavage is also decreasing from around 24 000 g/mol for the un- and monocyano-substituted to 11 700 g/mol for the dicyano-substituted cyclobutan-di-ester. The corresponding *trans*-conformations always require forces of at least 1000 pN and molecular weight thresholds of around 10 000 g/mol over their corresponding *cis*-isomers and are thus significantly less reactive for mechanochemical reactions. The most reactive *cis*-dicyano-substituted cyclobutane-di-ester (100 000 g/mol) showed a significant mechanochemical reactivity of 24% towards the Michael addition of secondary amines and an almost quantitative chain scission according to GPC⁴³, which highlighted the potential for self-healing application.

1.3.2.6 Retro-Staudinger cycloaddition of β -lactams

Similarly, the mechanochemical activation of PMA-based β -lactams by ultrasound generated high reactive ketenes as well as imines with a cleavage efficiency of 65% via a [2+2]-cycloreversion (Figure 22)⁴⁴, which is in the present case a kind of the retro Staudinger cycloaddition. The bond dissociation force for a β -lactam was determined to 284 kJ/mol which require an applied force of 3470 pN for an efficient bond cleavage and is thus in the range of the previous discussed examples. The obtained ketenes and imines are high reactive compounds which extend the current repertoire of covalent mechanophores enabling fast and efficient crosslinking reactions for self-healing applications. Therefore, the highly efficient addition of alcohols to the ketene moiety was demonstrated as an example.

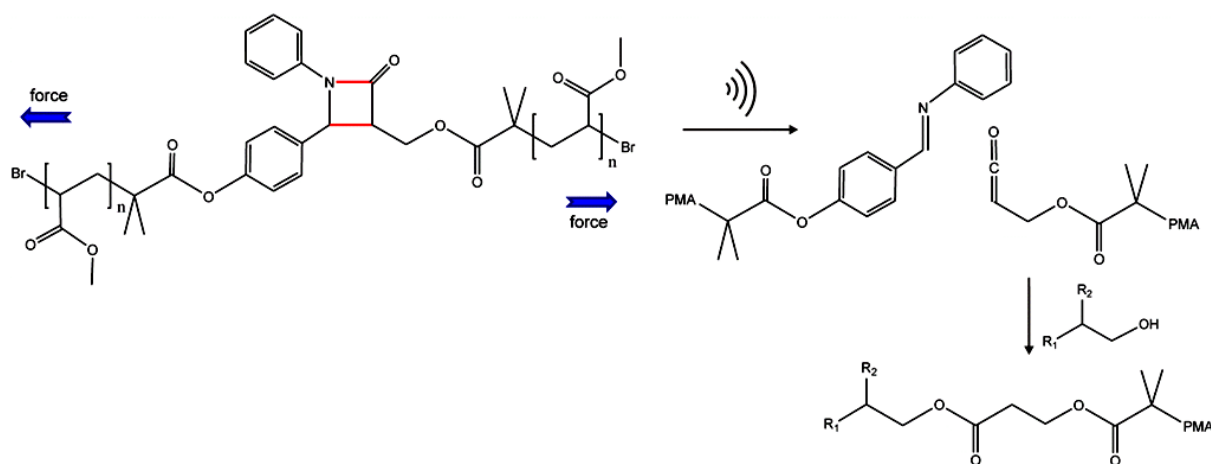


Figure 22. Retro-Staudinger cycloaddition of β -lactam mechanophores yielding under ultrasonication imines and highly reactive ketenes able to trigger further crosslinking reactions.

1.3.2.7 Bergmann cyclization of enediynes

Another type of cyclic mechanophores is based on larger ten-membered rings, which require especially strained or activated functionalities in order to enable an efficient activation via mechanical force⁴⁵⁻⁴⁷. For that purpose, enediyne rings were incorporated into crosslinked PMMA networks (Figure 23)⁴⁵ and subjected to mechanical force by swelling in MMA which induced a stretching of the labile bonds. The occurred Bergmann cyclization generated a biradical species which has shown to be

an efficient initiator for radical polymerizations of various acrylates in yield up to 93%⁴⁶. Performed CoGEF calculations had shown a theoretical force of ~5000 pN to induce the Bergmann cyclization which suggest that enediynes are potential useful mechanophores⁴⁵.

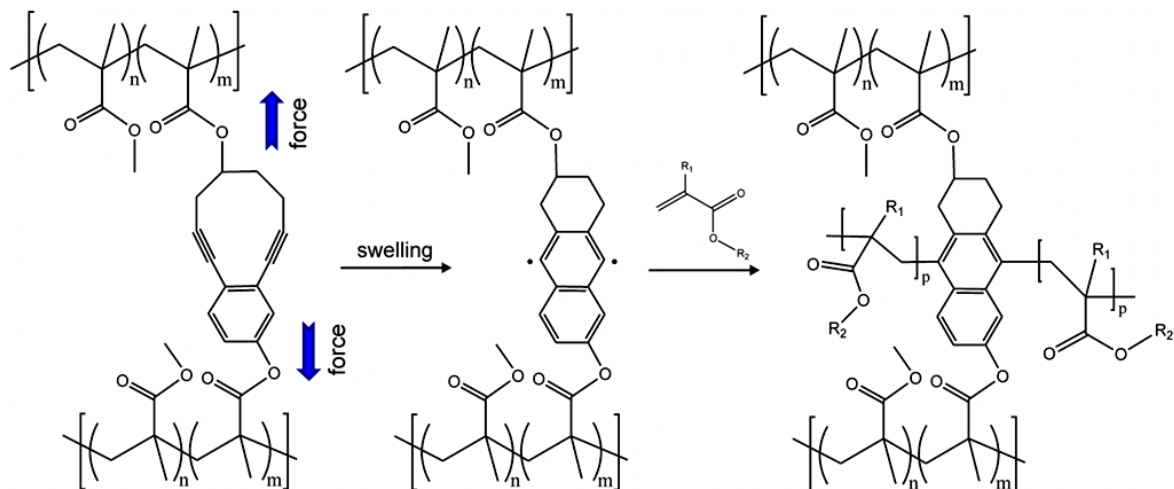


Figure 23. Force-driven Bergmann cyclization of enediyne mechanophores generating biradical moieties which are suitable as initiators for radical polymerizations of acrylates.

1.3.2.8 Cyclobutane-1,3-diones

A likewise unusual, but quite interesting example for mechanophores is the ring opening of cyclobutane-1,3-diones which is centered within two PTHF chains⁸⁵. Subjecting this -according to theoretical considerations weakest link in the molecule - to ultrasound should lead to a [2+2]-cycloreversion generating two reactive ketenes (Figure 24).

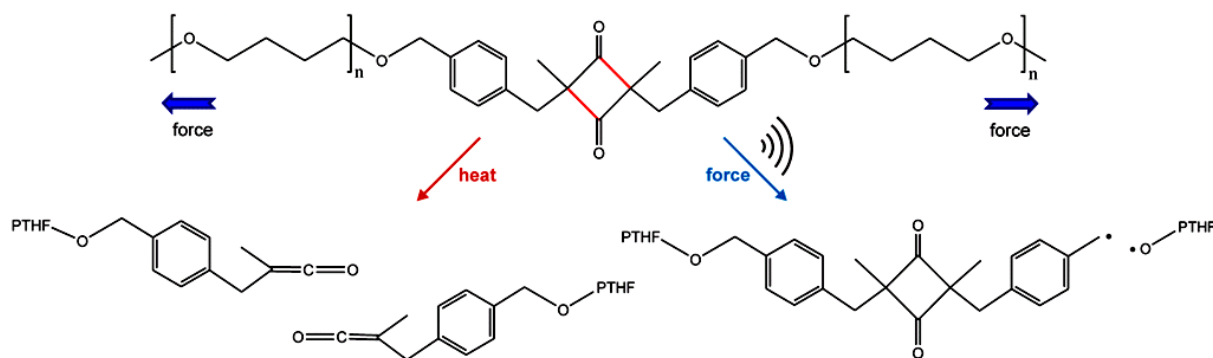


Figure 24. Mechanochemical versus thermal scission of cyclobutane-1,3-diones linked symmetrically to two PTHF chains.

However, theoretical investigations as well as ultrasound experiments revealed in contrast to other mechanophores a strengthening of the four-membered ring bonds in the presence of external force for the *cis*-isomer from 185 kJ/mol at zero force to ~220 kJ/mol at 2500 pN, while the bond strength of the C-O bond close to the cyclobutane-1,3-dione decreased simultaneously from 350 kJ/mol to ~50 kJ/mol. The strengthening of the cyclobutane-1,3-dione ring is a quite unusual behavior as normal chemical bonds are weakened due to their elongation under the influence of external force, but DFT calculations revealed that the energy barrier to acquire the adequate orthogonal transition state for the ring opening of the ketene dimer is increasing under applied force as the orbital symmetry does not allow the [2+2]-cycloreversion. Thus, the desired ring opening of the cyclobutane-1,3-dione ring does not take place by applying mechanical force; instead, a homolytic scission of the weakened C-O bond

appears and cleave the molecule elsewhere. The amazing and the up-to now unique observation of the bond strengthening of the cyclobutane-1,3-dione ring under applied external force indicates clearly that not all labile groups embedded centrally to two polymer chains are suitable for mechanochemical application.

1.3.3 Other mechanophores

Beside the already discussed mechanocatalysts and cyclic mechanophores, several other approaches like the acid generation by degradation of oxime sulfonates⁴⁸, the formation of cations by heterolysis of triarylsulfonium salts⁴⁹ as well as the liberation of small molecules by mechanical force^{50; 168} are known in the field of self-healing mechanochemistry (Figure 25). A totally different approach based on the stress release by deracemization respectively isomerization of 1,1'-bi-2-naphthol to prevent thus damage⁸⁸. Some characteristic benchmarks of those mechanophores are summed-up in Table 3.

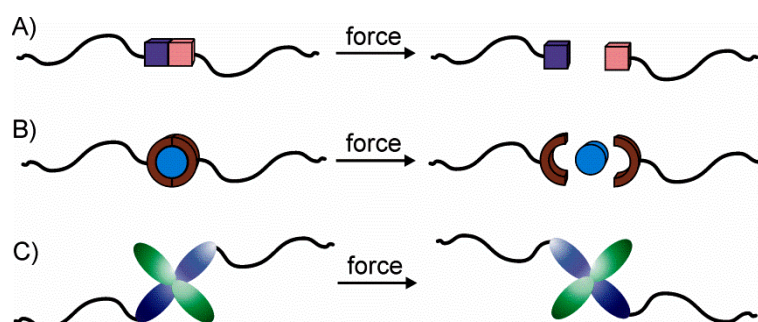


Figure 25. Generalized examples for polymer embedded mechanophores: A) Selective scission generates reactive compounds, B) exclusion of small molecules and C) isomerization.

Table 3. Benchmarks of mechanophores generating different kinds of reactive species (mechanolabile bonds are highlighted in red).

	Mechanophore	Polymer handle (T _g [K])	Activation	Limiting molecular weight [g/mol]	Cleavage efficiency [%]	Activation force/bond strength	Ref
1		PMA (282) ¹⁵²	<u>Solution:</u> Ultrasound	>38 000	-	264 kJ/mol	48
2		PMA (282) ¹⁵²	<u>Solution:</u> Ultrasound	-	-	-	49
3		poly(o-phthalaldehyde)	<u>Solution:</u> Ultrasound	>26 000	60%	-	50
4		PMA (282) ¹⁵²	<u>Solution:</u> Ultrasound	<52 000	-	126 kJ/mol	88

1.3.3.1 Oxime sulfonates

PMA-chain centered symmetrical oxime sulfonates degraded under applied ultrasound forming aryl sulfonic acid and oximes, which in turns are able to react in a Beckmann rearrangement under catalysis of the formed acid yielding carboxamides or in the presence of water ketones (Figure 26)⁴⁸. Both functionalities as well as the likewise formed acid can be used for developing autonomous self-healing materials by triggering different kinds of crosslinking reactions. The experimental observed mechanochemical scission above a molecular weight of 38 000 g/mol were supplemented by CoGEF calculations, which revealed a preferred cleavage of the relative strong S-O bond (264 kJ/mol) compared to the weaker N-O bond (201 kJ/mol) due to orbital symmetry reasons.

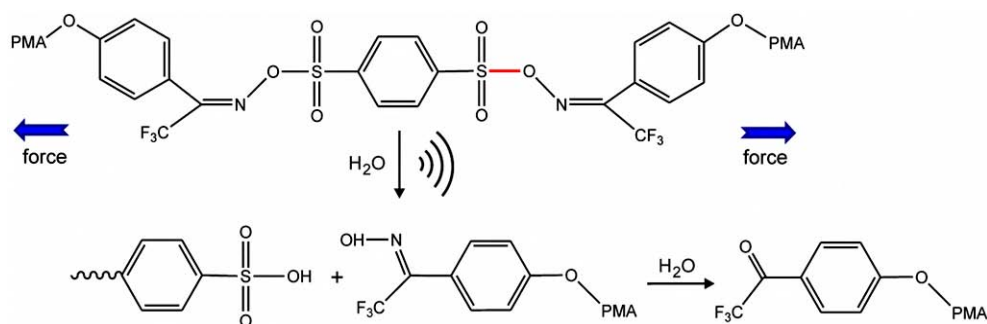


Figure 26. Mechanochemical activation of oxime sulfonates by ultrasound generates aryl sulfonic acid and oximes respectively ketones.

1.3.3.2 Triarylsulfonium salts

The mechanochemical activation of triarylsulfonium salts by ultrasound caused a heterolytic scission of the labile S-aryl-bond and generated thus a neutral thioether moiety as well as a reactive aryl cation (Figure 27)⁴⁹. This was subsequently able to crosslink e.g. with secondary amines under the formation of polymeric networks, which offers the potential to restore material properties and leading thus to a self-healing behavior of the material.

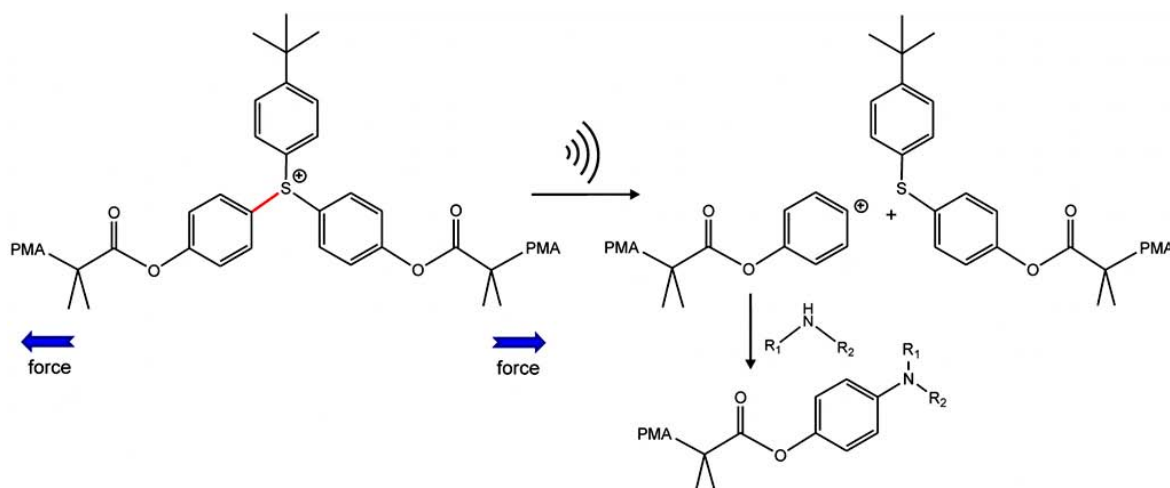


Figure 27. Ultrasound induced heterolytic scission of labile S-aryl- bond generating reactive aryl cation which enables e.g. a crosslinking reaction with secondary amines.

1.3.3.3 Poly(*o*-phthalaldehyde)s

Another approach for self-healing force-responding material was demonstrated by metastable end-capped poly(*o*-phthalaldehyde)s which are able to depolymerize under mechanical stress yielding back the initial *ortho*-phthalaldehyde monomers within a yield of 60% (Figure 28)⁵⁰. The obtained aldehyde offered the potential for further crosslinking reactions with amines as well as thiols¹⁶⁹ or can be re-initiate to restore the original polymer.

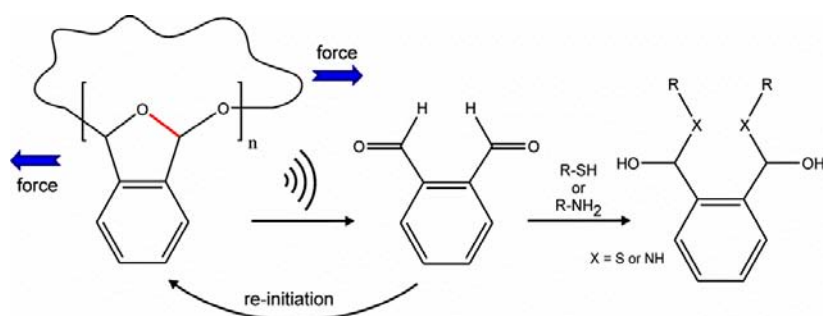


Figure 28. Ultrasound induced depolymerization of poly(*o*-phthalaldehyde) generating initial *ortho*-phthalaldehyde monomers which are able to react with primary amines or thiols.

1.3.3.4 1,1'-Bi-2-naphthol

A totally different approach based on the stress release by deracemization respectively isomerization of 1,1'-bi-2-naphthol (Binol) centered in a PMA chain⁸⁸. Applied force e.g. by ultrasound led to a deracemized intermediate state, which is only stable under sustained force and relax either to S- or R-Binol when the force was released (Figure 29). The intermediate state elongates the polymer scaffold and absorbs parts of the applied force due to its high isomerization barrier of 126 kJ/mol, which reduce the intensity of the acting force and prevents thus the appearing of damage.

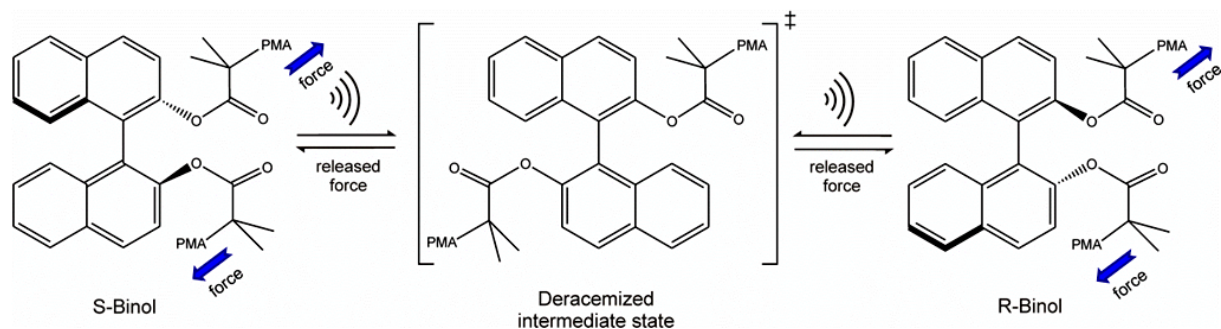


Figure 29. Force-driven isomerization of 1,1'-bi-2-naphthol (Binol) leading to a partial absorbents of the applied force which prevent damage events.

1.4 Mechanochemical damage-sensing approaches

Sensing stress or occurred, usually microscopic damage is one of the crucial points in the development of polymeric materials, especially as common detection methods are quite expensive or even fail for polymer composites. Hence, the development of weak covalent bonds able to translate applied macroscopic force to the molecular level, facilitates the development of self-sensing materials reporting stress or occurred damage autonomously. Various mechanolabile functionalities display at least two different stages, one “unstressed” inactive and one “stressed” activated and can therefore be used as mechanochromophores or for mechanoluminescence (Figure 30). Common examples like spiropyranes^{1, 39; 55-72}, spirothiopyranes⁷³, coumarines⁷⁴, anthracenes⁷⁵⁻⁸⁰ or 1,2-dioxetanes⁸¹⁻⁸⁷ had been investigated and systematically enhanced in order to enable an efficient detection and subsequent repair of microcracks during or directly after their formation. This prevents redundant preliminary replacement of polymeric materials and composites which helps to minimize waste and enhance simultaneously the capability and safety of items like airplane or automotive components.

Moreover, the direct visualization of the strict spatial and temporal restricted application of force facilitate a deeper understanding of the crack propagation during the damage event and enable a detailed insight into the activation process of the mechanophores itself, like the role of the mechanophore orientation or the strength as well as the direction of tensile or compression forces. Table 4 summed-up some of the most vivid examples for mechanochemical induced damage-sensing approaches by mechanochromism or mechanoluminescence, which are discussed in the following section.

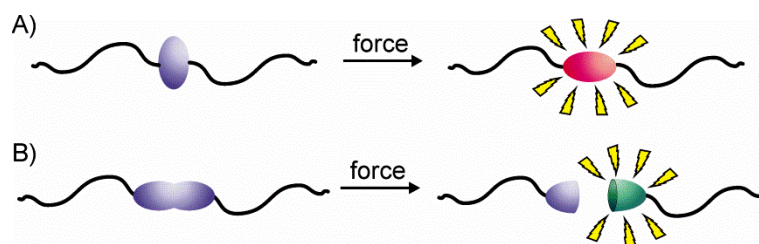


Figure 30. Generalized examples for polymer embedded mechanochromophores and mechanochemiluminescent functionalities.

Table 4. Benchmarks of the most vivid mechanochemical induced damage-sensing approaches (mechanolabile bonds are highlighted in red).

	Mechanophore	Polymer handle (T _g [K])	Activation	Limiting molecular weight [g/mol]	Cleavage efficiency [%]	Activation force/bond strength	Ref
1		PMA (282) PMMA (378) PU/PTHF PDMS	<u>Solution:</u> Ultrasound <u>Bulk:</u> Tension; Torsion; Compression; Swelling; Shock waves	linear < 75 000 network ^{a)}	-	CoGEF ⁵⁸ 2000 - 3000 pN AFM ⁶¹ 260 pN 100 kJ/mol	1; 39; 55- 72
2		PU (HDMI/BD) (213)	<u>Solution:</u> Ultrasound <u>Bulk:</u> Tension	> 14 000	-	400 pN	73
3		PMA (282) ¹⁵²	<u>Solution:</u> Ultrasound	> 28 000	71%	-	74
4		PVA (358) ¹⁵²	<u>Solution:</u> Ultrasound; <u>Bulk:</u> Grinding	network ^{b)}	-	-	75
5		PMA (282) ¹⁵²	<u>Solution:</u> Ultrasound; <u>Bulk:</u> Compression	-	-	-	76
6		PMA (282) ¹⁵² PU (HDMI/BD) PMMA (363) ⁸¹	<u>Solution:</u> Ultrasound; <u>Bulk:</u> Tension, Compression	> 18 000	54%	147 kJ/mol	81- 87

^{a)}prepared either by radical polymerization of the corresponding monomer using the mechanophore as crosslinking points or used as crosslinkers for PDMS within a Karstedt reaction or used as comonomer in polycondensations generating copolymers which were subsequently crosslinked e.g. by hydrogen bonding moieties; ^{b)}mechanophore used as crosslinking points for 31 000 – 50 000 g/mol PVA

1.4.1 Mechanochromophore

Mechanochromism is the property of a usually polymeric material to change its colour in the visible (vis) or ultraviolet (UV) range of the light spectra when external mechanical force is applied². The most vivid examples for mechanochromophore are spiropyranes^{1; 39; 55-72}, spirothiopyranes⁷³, coumarines⁷⁴ or anthracenes⁷⁵⁻⁸⁰ which are incorporated centrally into linear polymer chains or crosslinked polymeric networks and will be discussed in the following chapters.

1.4.1.1 Spiropyranes

Spiropyranes (SP) consist out of two orthogonal arranged heterocyclic rings connected via one C-atom and are able to generate upon thermal treatment, UV-light irradiation or mechanochemical activation the purple coloured merocyanine (MC) within a 6π electrocyclic ring-opening reaction (Figure 31A)^{1; 39; 55-72}. For that purpose, the SPs were incorporated either centrally into linear PMA chains or were crosslinked with MMA yielding glassy polymeric networks and subjected subsequently to tensile testing, torsional shear force or compression.

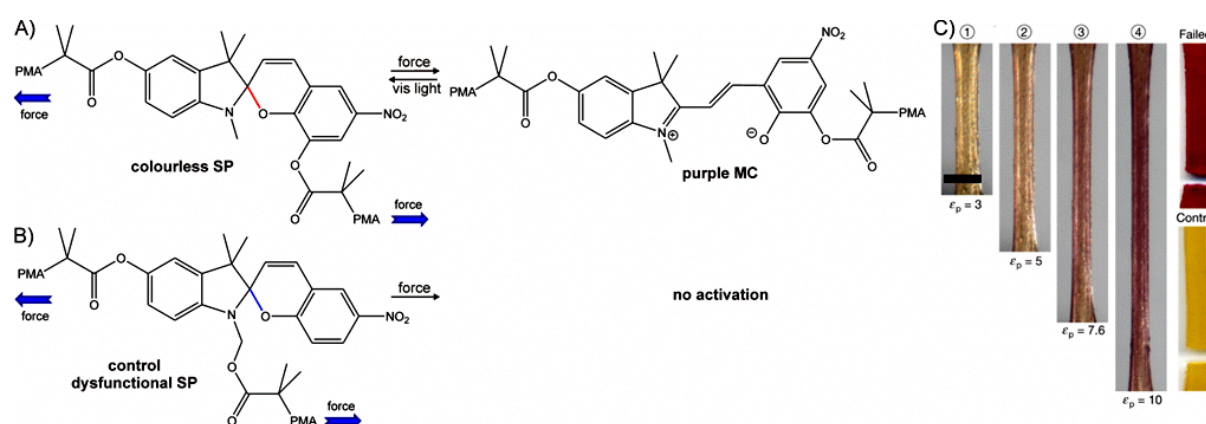


Figure 31. A) The mechanochemical activation of colourless spiropyranes (SP) by tensile force generates purple coloured merocyanine (MC) via a 6π electrocyclic ring-opening reaction. B) Control experiment with dysfunctional SP unable to transmit the applied force to the labile C-O bond (blue) showing no activation and thus no colour change (see C right bottom). C) Optical images of colour changing from linear PMA-based SP mechanochromophore ($M_n = 80\,000$ g/mol) after applied tension force in dependence of the plastic deformation strain (ϵ_p) as well as the failed specimen and control sample (Optical image reprinted by permission from Macmillan Publishers Ltd: Nature⁵⁸, copyright 2009).

Continuous stretching of SP linked flexible PMA ($T_g \sim 282$ K) by tensile testing led to an efficient mechanochemical activation of the colourless SP indicated by the gradually increase of the purple MC colour (Figure 31C)⁵⁸, whereas a parallel orientation of the mechanophores along the direction of the tensile force facilitated strongly their activation⁵⁶. However, a relative large plastic deformation strain (ϵ_p) of up to 500% was required in order to achieve a suitable activation of the mechanophores. In contrast, tensile testing as well as compression experiments of the glassy PMMA-SP samples generated only above or close to the T_g of ~ 378 K the activated MC. Otherwise a brittle failure of the material was observed preventing a mechanochemical activation at room temperature as the restricted chain mobility prohibits a chain rearrangement and inhibits thus the accommodation of the applied force (see Chapter 1.2.2)⁵⁵. Adding a plasticizer, like MeOH into the polymer matrix can skip this drawback and implement an enhanced chain mobility enabling thus a mechanochemical activation also below the T_g , albeit lower efficiencies compared to PMA were observed. In all cases, the obtained isomerization from SP to MC can be reversed multiple times upon irradiation of the open MC-form with visible (vis) light reforming the initial SP. Nevertheless, elongating the SP specimen beyond the reversible linear deformation range of Hooke's law led to a failure of the specimen and to a colour change to deep purple shortly before breaking into two pieces (Figure 31C right top).

However, a quantification of the absolute values of activated SP is hard to determine as two transition states for the isomerization from SP to MC were hypothesized (Figure 32)^{60; 62}. A first transition can be referred to the ring-opening of SP to MC and is represented by a shift from colourless to blue, while a second color transition from blue to purple is a result of an isomerization of the MC methane bridge. Thus, a defined quantification in RGB color analysis is difficult as both spectra are overlapped and behave partially opposing, why usually only a comparative quantification is used.

Control experiments were performed using beside the un-functionalized and end-capped spiropyran also a dysfunctional spiropyran, whereat the second polymeric handle was attached to the spiro-N instead of the spiro-O inhibiting the transmission of the applied force to the most labile C-O-bond across the spiro-junction (Figure 31B+C). Thus, no mechanochemical activation was observed for all kinds of control experiments. These observations were supported by theoretical CoGEF calculations which show a selective spiro C-O bond rupture at 2000 – 3000 pN⁵⁸, while the dysfunctional control sample (Figure 31B) revealed a bond scission at much higher forces at one of the side chains which led in turns to no colour change⁵⁸. However, subsequently performed AFM measurement revealed a force induced cleavage of the most labile C-O bond of the functional SP (100 kJ/mol) at 260 pN⁶¹, which is much lower compared to the previously conducted CoGEF calculations⁵⁸.

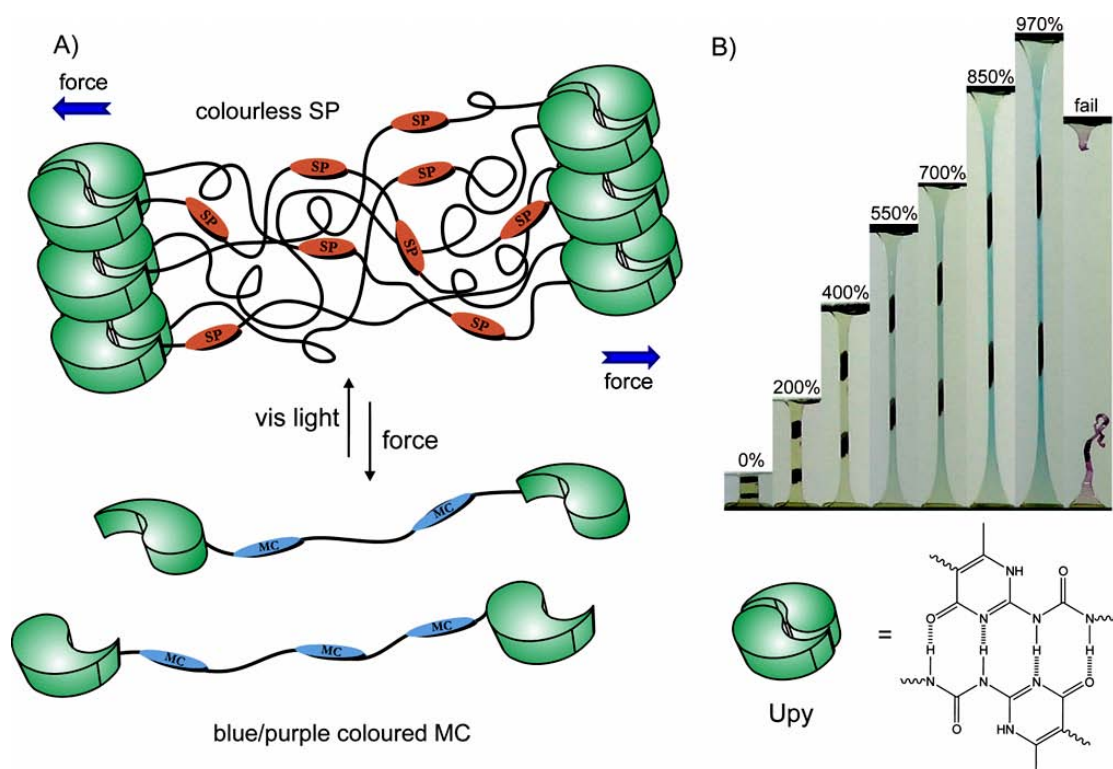


Figure 32. A) Mechanochemical activation of SP incorporated into hard segments of 2-ureido-4-pyrimidone (UPy) crosslinked PU/PTHF copolymer networks by tensile testing forming blue/purple coloured MC passing two transition states. B) Optical images during tensile testing showing gradually colour change from colourless SP over the blue to purple coloured MC shortly before respectively after occurred failure. (Adapted with permission from (A)¹⁷⁰ and (B)⁶⁴. Copyright (A) 2015 Wiley and Sons and (B) 2013 American Chemical Society.)

In order to increase the activation efficiency, the SP mechanochromophore were embedded into polymeric networks, crosslinked either via purely physical interaction, like hydrogenbonds^{59; 62-64} or metal-ligand interactions⁶⁵ or via covalent bonds^{60; 68-70}. The additional crosslinking points enables a more efficient transmission of the applied external force as also its perpendicular parts are transformed into a mechanochemical response (see Chapter 1.2.2). Furthermore, SP were incorporated into various

polymer matrices, like poly(urethane)/poly(tetrahydrofuran) (PU/PTHF) copolymers^{59; 62-65}, poly(dimethylsiloxane) (PDMS)⁶⁰, PMMA^{55-56; 58} and PMA^{39; 56; 72} in order to investigate stress-sensing behavior into such widely-used technical polymers. PU/PTHF has turned out to be the best matrix for the mechanochemical activation of SP as PMA as well as PDMS are too soft requiring thus quite high strains for an efficient activation, while PMMA is too brittle providing to low plastic deformation to yield suitable activation². Moreover, PU/PTHF copolymers enables the formation of hard(PU)/soft(PTHF) domains and ensure a crosslinked structure by hydrogen bonding of the PU moieties (often supported by additional 2-ureido-4-pyrimidone (UPy) units) as well as a strain induced crystallization of the PTHF enhancing both the efficiency of mechanochemical activation (Figure 32)^{59; 62-64}.

Additionally, some likewise unusual approaches for mechanochemical activation, like the solvent-swelling⁶⁶ or laser-generated shock waves⁷¹ had been investigated opening some new opportunities for mechanochromophore applications. Overall, SP has been established as an efficient and repeatable molecular force probe, permitting a (semi)quantification of mechanically-induced polymeric damage and facilitates a deeper insight into microcrack propagation process.

1.4.1.2 Spirothiopyranes

This concept was taken up very recently and extended to spirothiopyranes (STP) which enables beside the aforementioned mechanochromism additionally a mechanochemical induced crosslinking with bismaleimides (Figure 33)⁷³. Colourless STP incorporated randomly into a (PU-STP)-PU copolymer can be converted by ultrasonication into green thiomercyanine (TMC), while in the presence of a large excess of maleimide 60% of the initial STP can be trapped. Additionally the activation in solid state had been instigated by tensile testing revealing an activation of about 20% of the STP and crosslinking conversions up to 35% were achieved. These observations offer one of the rare combinations of autonomous damage-sensing with autonomous self-healing in solution as well as in bulk state.

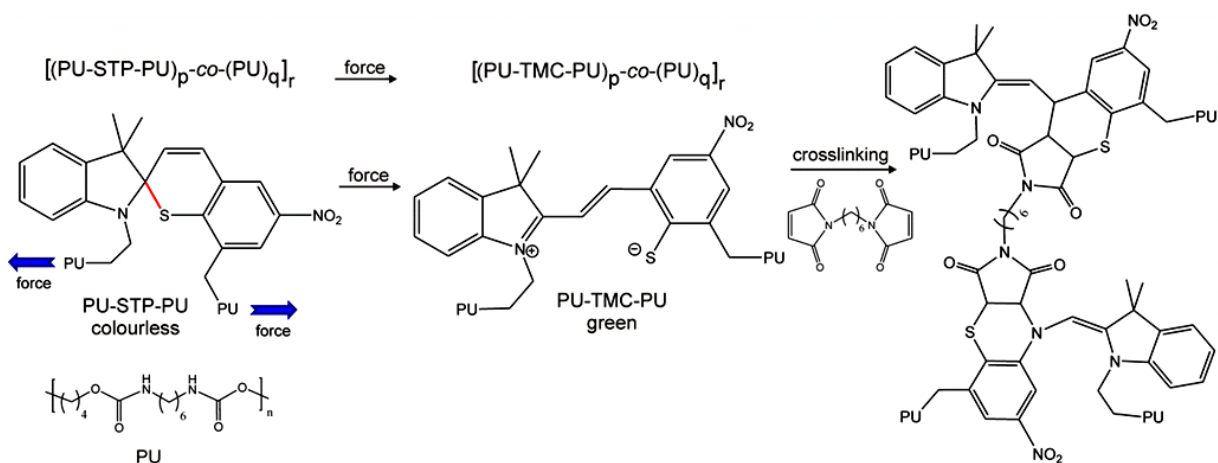


Figure 33. Mechanochemical activation of colourless spirothiopyranes (STP) embedded into poly(urethane)-STP-poly(urethane) (PU-STP-PU)-*co*-poly(urethane) (PU) polymers generating either in solution or bulk green thiomercyanine (TMC) which is able to form with bismaleimides crosslinked networks indicating thus autonomously damages and triggering self-healing at once.

1.4.1.3 Coumarins

Another smart concept for mechanochromophores based on coumarin-dimers which were embedded centrally close to the mid-point of a PMA chain (Figure 34)⁷⁴. Mechanochemical activation by ultrasound led to an efficient scission of the dimeric structure within a [2+2] cycloreversion yielding two highly fluorescent coumarin-telechelic PMAs, which are in contrast to the previously discussed SP and STP examples well suitable for quantitative analyses. Thus, cleavage efficiencies up to 71%

could be determined via highly sensitive fluorescence measurements. Moreover, the positioning of the coumarin-dimer within the polymer chain was quantitatively investigated revealing significant higher efficiencies of 71% when more than 74% of the mechanophore was located in 15% of the midst of the chain compared to 35% activation when only 47% were positioned centrally. Control experiment revealed no mechanochemical activity below a molecular weight of 28 000 g/mol and proving thus the chromophore activation solely due to mechanochemical activation.

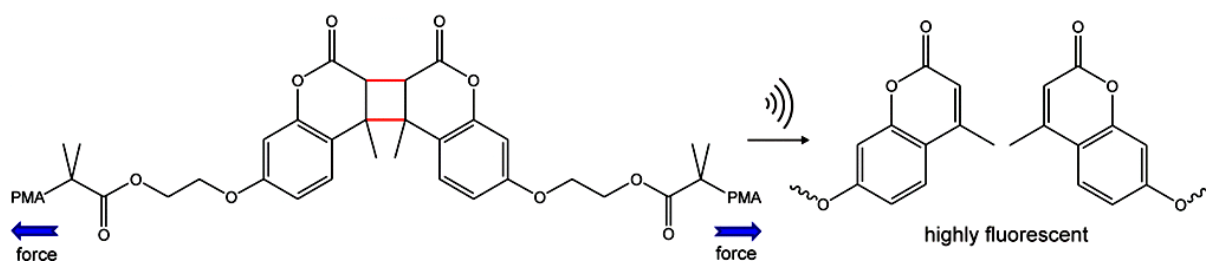


Figure 34. Ultrasound induced activation of dimeric coumarins yielding the highly fluorescent coumarin-telechelic PMA.

1.4.1.4 Anthracene

Dimerized non-fluorescent anthracene moieties linked between two poly(vinyl alcohol) (PVA) chains can be used as fluorescent crack sensors as applied mechanical force led to the formation of the highly fluorescent mono-anthracene derivatives within a [4+4] cycloreversion reaction (Figure 35A)⁷⁵. Spatially resolved fluorescence measurements enable a direct visualization of the crack plane and thus the investigation of the crack propagation behavior (Figure 35B). The opportunity for light induced re-dimerization of the anthracene moieties regenerating the crosslinking structure revealed the potential for healing properties.

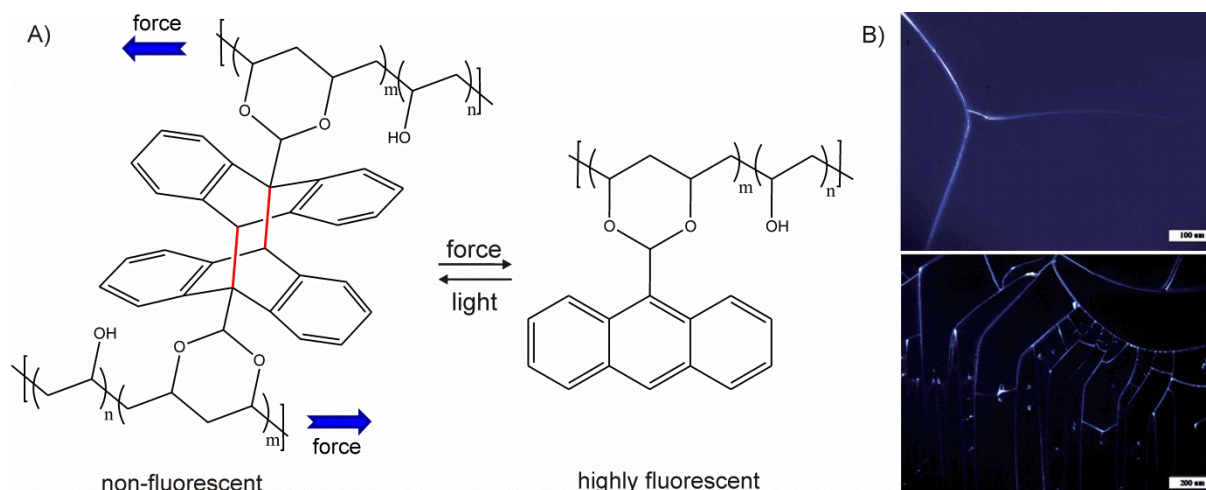


Figure 35. A) Force-depending [4+4] cycloreversion of dimerized non-fluorescent anthracene generates highly fluorescent anthracene by rearomatization of the planar system. B) Fluorescence microscopical images of the dimerized anthracene PVA under 330-385 nm UV light after mechanochemical activation detecting the crack planes by appearing fluorescence of mono-anthracene enabling a real-time monitoring of the propagating crack (Adapted from ref⁷⁵ with permission from The Royal Society of Chemistry.)

Similar mechanochromophores were developed based on substituted anthracene-maleimides⁷⁶⁻⁸⁰. Subjecting PMA centered non-fluorescent π -extended anthracene derivatives to ultrasound or compression triggers a retro-Diels-Alder (rDA) reaction releasing maleimides under the formation of high fluorescent anthracene (Figure 36)⁷⁶. Remarkable high quantum yields of up to 0.72 can be

determined for the anthracene-maleimide adducts which are thus two orders of magnitude higher compared to the previously discussed and widely used spiropyranes (SP) increasing the sensitivity of mechanochromophoric investigations significantly. Moreover, the implementation of well understood DA/rDA chemistry enables an exact fine-tuning of the light absorption and emission behavior establishing thus a versatile tool-box for modularly adjustment and designing of mechanochromophores.

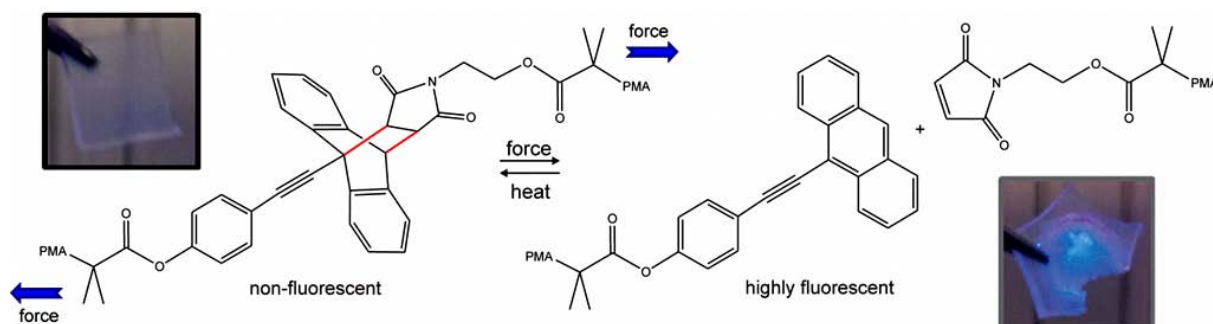


Figure 36. Mechanochemical activation of non-fluorescent π -extended PMA based anthracene-maleimides via retro-Diels-Alder (rDA) reaction generating highly fluorescent anthracene. Optical images under UV-light (365 nm) before and after compression. (Adapted from ref⁷⁶ - Published by The Royal Society of Chemistry.)

1.4.2 Mechanoluminescence of dioxetanes

Mechanochemiluminescence describes the ability of a functional group to emit light under applied external stress². In contrast to the previously described mechanochromophores no additional excitation by visible or UV-light is required increasing thus the sensitivity of the chemiluminescence measurements significantly. Additionally, the stress response is transient in time, rather than cumulative as the chemiluminescence is a short single time event, which enables a better time and spatial resolution facilitating *in situ* real-time observation of the propagating crack and represents thus a versatile tool for studying how damage occurs and propagate within polymeric materials.

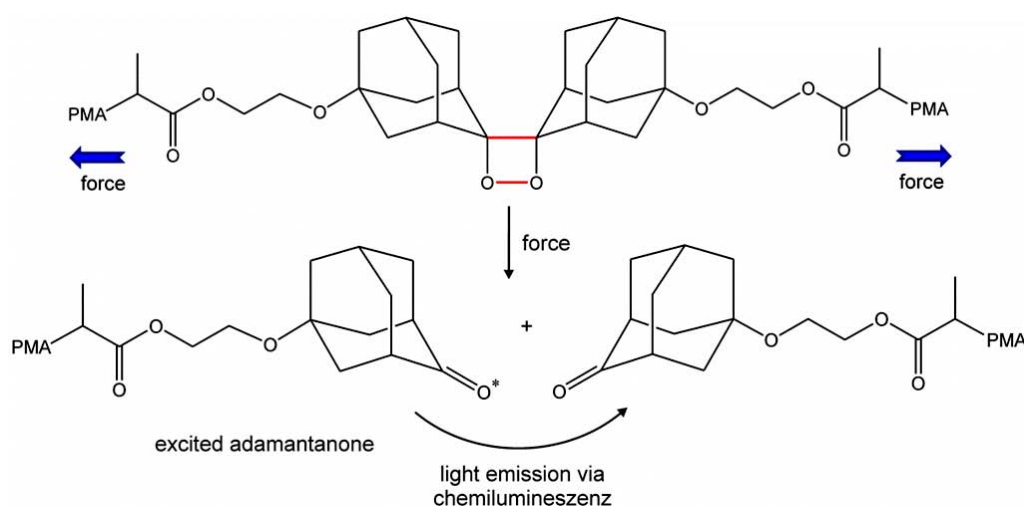


Figure 37. Force-induced chemiluminescence of bis(adamantyl)-1,2-dioxetane (BAD). Subjecting polymer bounded BAD to ultrasound, compression or tension generates under cleavage of the four-membered dioxetane ring one blue light emitting excited and one unexcited adamantanone moiety.

Bis(adamantyl)-1,2-dioxetanes (BAD) embedded either centrally into linear PMA⁸¹, randomly along the polymer backbone of PU (HDMI/BD)⁸² or as crosslinker into interwoven acrylic networks⁸⁴ were found as one of the most suitable mechanoluminescent compounds as BAD derivatives are known to

be highly stable with half-life times of ~ 40 years under ambient conditions and a dissociation energy barrier of ~ 147 kJ/mol^{2, 171}. Activating the mechanophore in solution via ultrasound or the bulk state by compression or tension force led to a cleavage of the four-membered dioxetan ring generating two adamantanone moieties: one in the excited singlet and the other in the non-excited triplet state (Figure 37)⁸¹⁻⁸⁷. The excited singlet adamantanone is able to emit blue light as chemiluminescence by direct relaxation to the triplet state (Figure 38A) or can transmit its energy to a suitable acceptor (i.e. diphenylanthracenes or perylenes) which allows a tuning of the emission wavelength and an energy harvesting contributing thus to a higher sensitivity⁸¹. Similarly to the observations of the previous discussed SP, no mechanochemical activation could be observed for glassy polymers. Neither cooling the PMA based BAD mechanophores below the T_g of 282 K nor its central implementation to PMMA ($T_g \sim 363$ K) revealed significant mechanoluminescence under fracturing the brittle films⁸¹.

Embedding the BAD mechanophore into single (SN), double (DN) or triple acrylic networks (TN) by swelling the previous network each time by monomer as well as initiator and subsequent polymerization obtaining thus multiple interwoven networks with defined pre-stretched BAD bonds enables a detailed investigation of the crack propagation behavior⁸⁴. Chemiluminescence measurements revealed under applied stress by single edge notch tests an enhanced scission of BAD for TN compared to DN or SN, which offers the lowest mechanophore activation efficiency (Figure 38B). In case of the not pre-stretched SN a highly localized mechanoluminescence at the propagating crack tip can be seen, while for pre-stretched DNs and especially for stronger pre-stretched TNs a more intense, broader activation zone of the BAD can be observed. These observations facilitate detailed information about the yielding zone of the applied stress in respect to its extend and shape and gives a first insight into the crack propagation behavior in polymeric materials by direct time- and spatially-resolved visualization and may thus help to develop more precise damage prediction models.

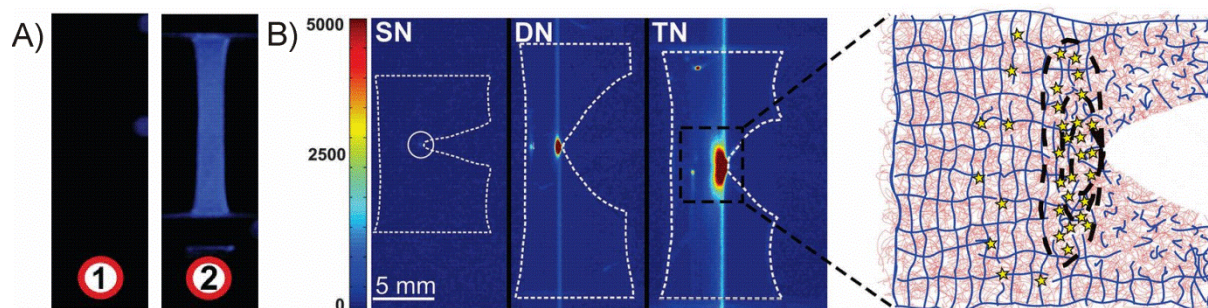


Figure 38. A) Optical image of obtained blue chemiluminescence ($\lambda_{\text{emission}} = 420$ nm) of bis(adamantyl)-1,2-dioxetane (BAD) (1) before applied stress and (2) during elongation by tensile testing. B) Intensity-colored mapping of BAD bond rupturing during the crack propagation into single (SN), double (DN) or triple interwoven acrylic networks (TN) by single edge notch tests. (Reproduced from ref⁸⁴. Reprinted with permission from AAAS.)

Moreover, networks with tunable toughening properties had been investigated combining supramolecular metal-ligand or hydrogen bonding moieties together with covalent BAD-based crosslinkers into various polymers, like poly(vinylpyridine), poly(ester)s, PTHF or PU^{82, 86}. It was found, that stronger hydrogen bonding interactions hamper the chain disentanglement and reduce the amount of slipping chains which prevents otherwise the accommodation of the external force and leading in turns to an increased chain scission. Adjusting the supramolecular interaction as well as the crosslinking density enabled a defined setting of the fracturing behavior of the BAD mechanophores and led in case of the incorporation into hard(PU)-soft(PTHF) phase-separated polymers to an activation with a total light intensity of about 56%.

1.5 Copper(I)-catalyzed alkyne-azide cycloaddition reaction

The copper(I)-catalyzed alkyne-azide cycloaddition (CuAAC) reaction¹⁷²⁻¹⁷⁶ is a special kind of the thermal Huisgen's 1,3-dipolar cycloaddition¹⁷⁷⁻¹⁷⁹ between terminal alkynes and alkyl or aryl azides yielding 1,4-disubstituted 1,2,3-triazole rings. The catalyzed CuAAC is according to the general definition of Sharpless *et al.* a so called "click" reaction¹⁸⁰, which is in turns characterized as a rapid, almost quantitative reaction which generate only one, usually stereospecific pure product with a thermodynamic driving force of at least 84 kJ/mol and proceed under ambient reaction conditions in benign solvents, like water. Ideally an insensitivity against water and oxygen is given and no or only simple purification procedures such as crystallization or distillation, but no chromatographic methods are required. Moreover, "click" reactions must be modular and should tolerate a wide range of functional groups enabling its application in a large scope^{149; 172; 181-189}.

The CuAAC fulfilled almost all criteria of Sharpless to be called "click" reaction; solely the insensitivity against oxygen and water is not given. Usually, Cu(I) is oxygenized by air to Cu(II) and disproportionate in water into Cu(0) and Cu(II) which requires a protection of the catalytic active Cu(I) species from these influences. This can be achieved in two different ways: The first is the *in situ* generation of the active Cu(I) species by reducing Cu(II) compounds, oxidizing elemental copper or the comproportionation of Cu(II) species with elemental Cu(0). Another method is the stabilization of the active Cu(I) moiety by protecting ligands, which shields the active centre from disturbing influences and enhance thus its tolerance towards oxygen and water. Furthermore, the additional ligand increase the solubility of the Cu(I) species and enhance the reaction rate significantly^{172-173; 184}. Table 5 provides an overview of the most common catalysts, ligands, reducing agents and solvents which are well suited for CuAAC reactions^{172-173; 176; 184; 190-194}.

Table 5. Overview of common catalytic systems¹⁹⁰⁻¹⁹¹, ligands^{190; 192} and solvents for the CuAAC^{172-173; 176; 184; 190-194}.

catalysts/reducing agent	ligands/bases	solvents
Cu(II)SO ₄ /sodium ascorbate	<i>N,N,N',N'',N'''</i> - pentamethyl-diethylenetriamine (PMDETA)	hexane
Cu(II)SO ₄ /elemental copper	<i>N,N</i> -diisopropylethylamine (DIPEA)	toluene
Cu(II)(OAc) ₂ /sodium ascorbate	tris[(1-benzyl-1 <i>H</i> -1,2,3-triazol-4-yl)methyl]amine (TBTA)	butanol
Cu(I)Br; Cu(I)I	2,2'-bipyridine (bpy)	CH ₂ Cl ₂
[Cu(I)(MeCN) ₄]PF ₆	hexamethyltriethylenetetramine (HMTETA)	CHCl ₃
[Cu(I)(PPh ₃) ₃]Br	tris[(2-pyridyl)-methyl]amine (TPMA)	DMF
Cu(I)OTf · C ₆ H ₆	tris[(2-dimethylamino)ethyl]amine (Me ₆ -TREN)	DMSO
Cu(I)I · P(OEt) ₃	2,2':6',2''-terpyridine (tpy)	THF
elemental copper/NEt ₃	1,8-diazabicyclo[5.4.0]undec-7-ene (DBU)	diethyl ether
copper cluster	triethylamine (NEt ₃)	dioxane
	<i>N</i> -heterocyclic carbenes (NHC)	water

Studying the CuAAC since 2001 has revealed multidental *N*-donor ligands, like TBTA, tpy or PMDETA as some of the best suited ligands preventing oxygenation or disproportion, which enhance at the same time the reactivity significantly¹⁹⁰⁻¹⁹². However, Nolan *et al.* developed a series of *N*-heterocyclic carbene (NHC) based ligands and coordinated two of them to one copper(I) centre obtaining a [Cu(NHC)₂]X catalyst which can even applied directly into water and catalyze a large variety of CuAAC reactions in quantitative yields^{158-161; 190; 195-200}. Thus a library of NHC-based copper catalysts were synthesized ranged from *N,N'*-disubstituted imidazol-2-ylidenes (A), imidazolin-2-ylidenes (B), over cyclic diamidocarbenes (C) and pyrimidine-2-ylidenes (D) to triazolylidenes (E)

(Figure 39) and were investigated systematically in respect to its reactivity and stability. It has turned out, that especially for the imidazol-2-ylidenes as well as for the imidazolin-2-ylidenes the attached substituents R' and R'' play a crucial role: Bulkier and electron-donating substituents, like 2,6-diisopropylphenyl (*iPr*), mesityl (*Mes*) or adamantly (*Ad*) revealed a higher stability but less reactivity compared to less bulkier or electron-withdrawing groups, like cyclohexyl (*Cy*), *tert*-butyl (*tBu*) or alkyl (Figure 40)^{157-161; 190; 195-205}. Moreover, the imidazol-2-ylidenes (Figure 39A) shows usually a higher reactivity but less stability compared to the corresponding imidazolin-2-ylidenes (Figure 39B), presumably due to its planar aromatic structure compared to the angled non-aromatic imidazoline based scaffold¹⁵⁸⁻¹⁶¹.

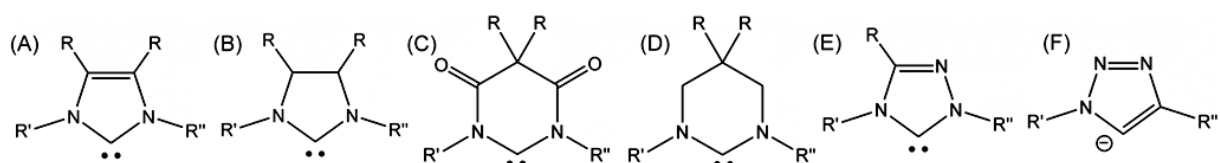


Figure 39. Some frequently used examples for *N*-heterocyclic carbene (NHC) ligands synthesizing copper(I) carbene catalysts for CuAAC. (A) *N,N'*-disubstituted imidazol-2-ylidenes, (B) imidazolin-2-ylidenes, (C) cyclic diamidocarbene, (D) pyrimidine-2-ylidenes, (E) triazolylidenes and (F) 1,2,3-triazoles.

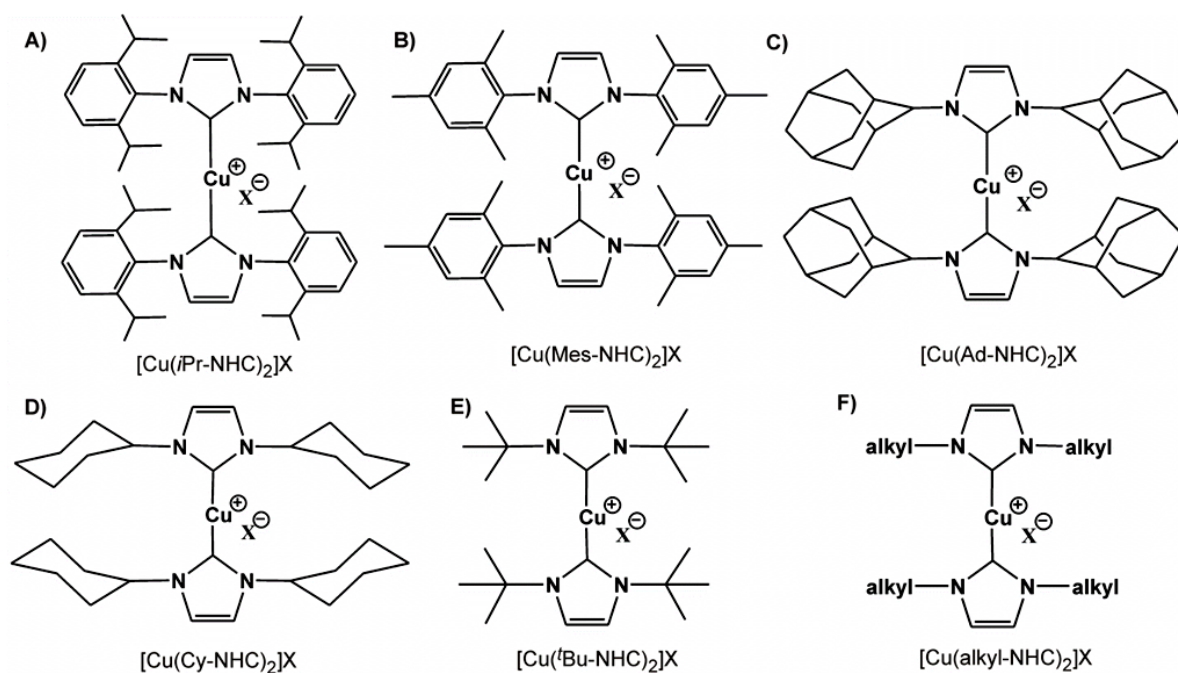


Figure 40. Tuning of catalytic reactivity and stability (from A stable to F unstable) of copper(I) *N*-heterocyclic carbene ($[\text{Cu}(\text{NHC})_2]\text{X}$) complexes by modification of the substituents R' and R'' in respect to bulkiness and electron-donating effects.

Mechanistic investigations show for the CuAAC of these highly efficient and stable $[\text{Cu}(\text{NHC})_2]\text{X}$ catalysts a slightly different activation step^{159; 161} compared to other copper(I) salts (Figure 41)^{173; 180; 184; 206-207}. In the first step (**I**), one of the NHC ligands has to be replaced and re-protonated by the alkyne compound activating thus the catalyst for the CuAAC under formation of a copper(I)-acetylide (**II**). Contrary to the simple Cu(I)-salts no additional base is required as the NHC-ligand itself is able to act as internal base. Kinetic studies as well as theoretical considerations revealed a multi-copper-center based mechanism for the azide addition step (**III**), where at least two copper centers are involved^{184; 206-207}. It was found, that the energy of the transition states for the subsequently formed copper including six-membered cyclic intermediate (**IV**) is significant lower in case of multiple involved copper centers as the formation of otherwise obtained allene structure is prevented. However,

the exact number of participating copper species is hard to predict as the large number of possible interactions (e.g. π -complexation or ligation to versatile nitrogen atoms) enables different pathways for steps **III** and **IV**. The subsequent exclusion of the copper from the ring generates a copper-bounded 1,2,3-triazole intermediate (**V**) which is afterwards protonated by the previously cleaved (protonated)NHC ligand regenerating the initial biscarbene-copper(I)-catalyst ($[\text{Cu}(\text{NHC})_2]\text{X}$) as well as the final 1,4-disubstituted-1,2,3-triazole and close thus the catalytic cycle.

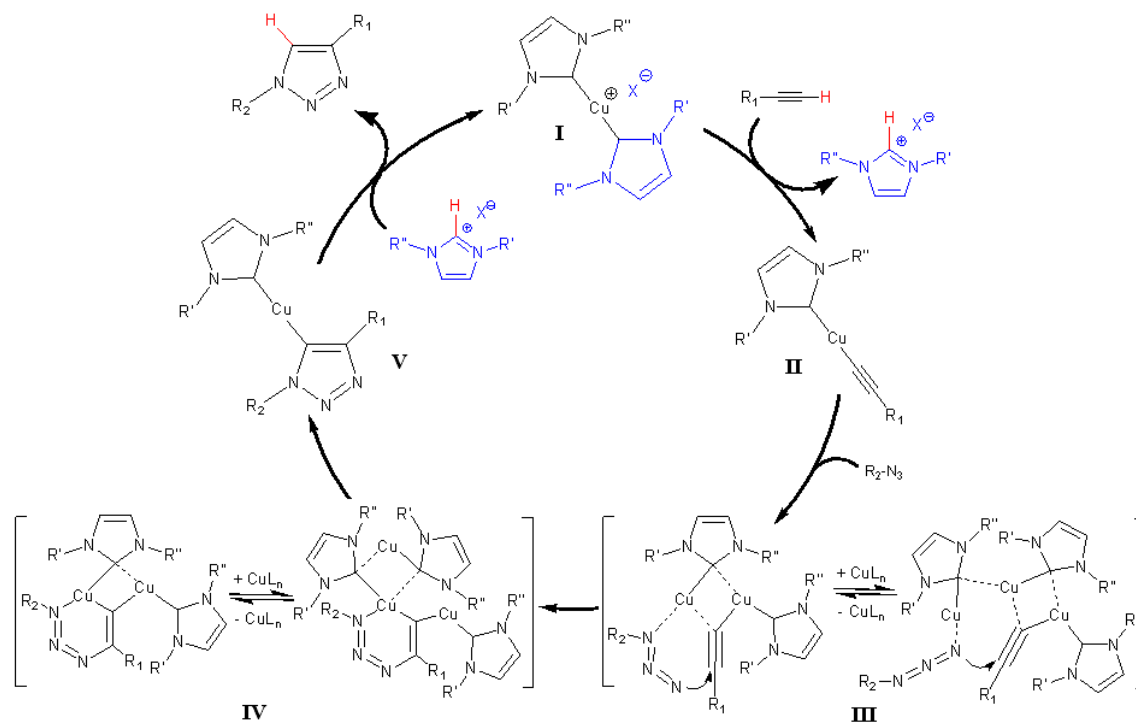


Figure 41. Mechanism of copper(I)-catalyzed alkyne-azide cycloaddition (CuAAC) reaction using biscarbene $[\text{Cu}(\text{NHC})_2]\text{X}$ catalysts. **I**) Activation of $[\text{Cu}(\text{NHC})_2]\text{X}$ by replacing one NHC ligand by the alkyne compound and protonation of the cleaved NHC yielding the copper(I)-acetylide (**II**). **III**) Coordination of the azide compound and subsequent ring closure (**IV**) involving multiple copper(I) centers. **V**) Exclusion of the copper moiety from the six-membered intermediate and regeneration of the initial catalyst via protonation of the formed triazole by the previously cleaved (protonated)NHC ligand.

The elucidation of the CuAAC mechanism for the $[\text{Cu}(\text{NHC})_2]\text{X}$ catalysts opens the opportunity for the development of a latent Cu(I)-based catalyst in form of a mechanocatalyst. For that purpose, it would be necessary to prevent the cleavage of one of the NHC-ligands within the first step (**I**) of the catalytic cycle (Figure 41) and inhibit thus the formation of the copper(I)-acetylide (**II**). This can be reached for instance by increasing the bulkiness of the attached substituents on both NHCs to shield the active center from the attacking alkyne and preventing thus the NHC-replacement. A suitable method would be the attachment of polymers which exerts a large bulkiness especially in its randomly coiled state. Another possibility to protect the copper center would be the change of the electronic properties of the NHC to accomplish a stabilization of the active center, e.g. by carbonyl or sulfonyl groups, as shown by Nolan *et al.* for copper-carbenes while using acetone or DMSO¹⁹⁸. In both cases, the applied mechanical force should be able to remove one of the shielding NHC ligands enabling thus the formation of the copper-acetylide which would start the catalytic cycle.

Thus, the CuAAC “click” reaction seem to be an ideal candidate for developing truly autonomous self-healing materials due to their previously discussed intrinsic beneficial properties, like high yields or substrate independency, together with their ability to introduce a mechanochemical behavior enabling a defined triggering of the self-healing or damage-sensing reaction solely when damage occurs.

2 Aim of the thesis

2.1 Objective and motivation

Aim of this thesis was the development of a latent copper(I) *N*-heterocyclic carbene (NHC) catalyst which can be activated by mechanical force via two attached polymer handles (Figure 42). The activation of the obtained Cu(I) mechanophore should be investigated into bulk as well as into solution proving its ability to trigger a copper(I) alkyne azide “click” reaction (CuAAC) of terminal alkynes and azides. Thus, an up to now unique combination of a mechanophoric approach with an autonomous self-healing and damage-sensing concept based on the network formation via CuAAC reactions of multivalent liquid alkynes and azides would be accomplished^{124; 208-210}.

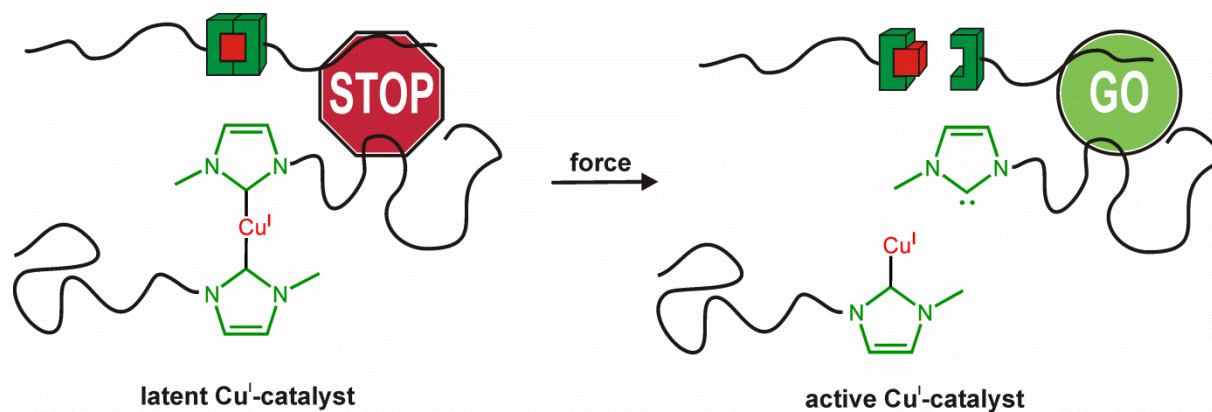


Figure 42. The activation of the latent copper(I) bis-*N*-heterocyclic carbene catalyst through cleaving of one shielding polymeric-NHC ligand via applied mechanical force generating the catalytic active monocarbene complex.

Up to now, the reactive alkyne and azide compounds were embedded into nano- or microcontainers, like microcapsules or microvascular networks, in order to prevent premature reactions without occurred damage which consume otherwise the reactants inhibiting a later healing or leading to false-positive indications of damage¹²⁴. The application of latent Cu(I) mechanophores as catalysts in the CuAAC would eliminate the need of such protecting nano- or microcontainers and avoid thus their often negative influences onto the material properties, like enhanced stiffness or delamination and allows a direct embedding of the healing agents together with the latent Cu(I)-catalyst into the matrix material (Figure 43). Thus, truly autonomous self-healing and damage-sensing materials activatable solely by applied external force during the damage event itself would be feasible, requiring no additional external stimulus, like heat or light.

For that purpose, especially the influence of the initial molecular weight as well as the glass transition temperature (T_g) and thus the rigidity of the attached polymer handles should be evaluated in respect to the efficiency of the Cu(I)-mechanophore activation as well as its effectivity within the CuAAC reaction in solution as well as in bulk state. Additionally, a first insight into the activation mechanism should be provided differing into thermal and mechanochemical scission of the attached shielding NHC-ligand. Furthermore, the ability for damage-sensing should be investigated via a so called fluorogenic “click” reaction within the solid state.

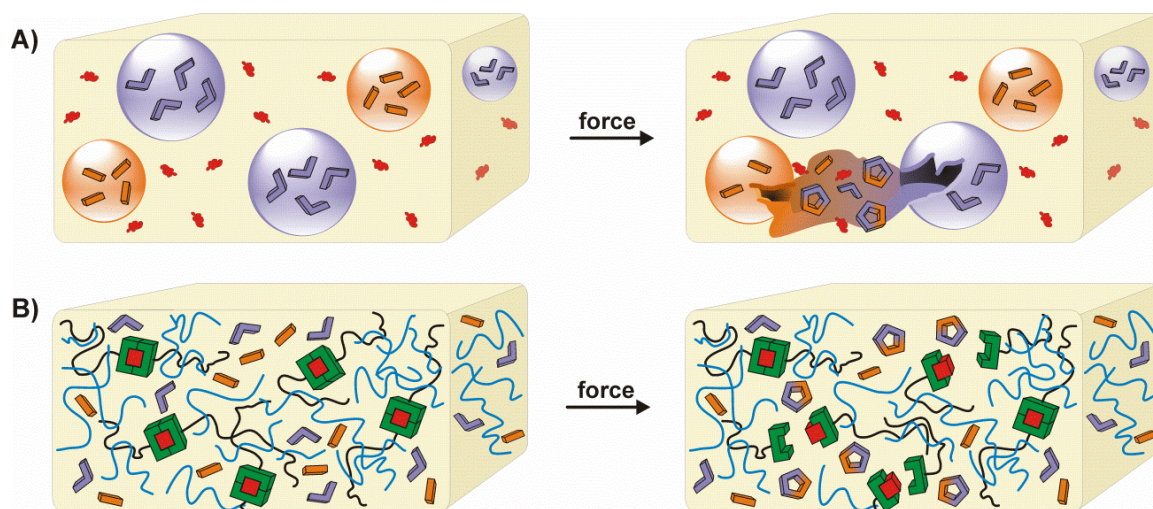


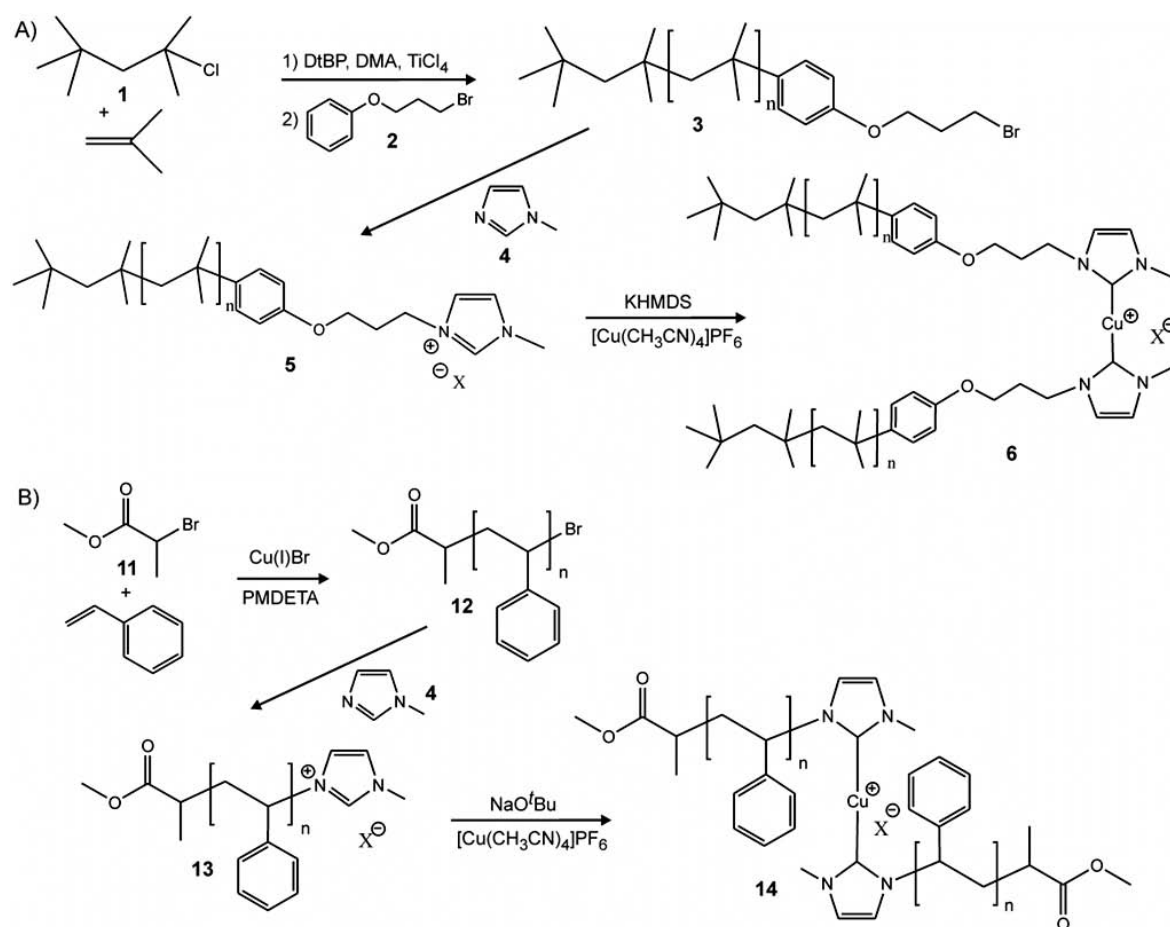
Figure 43. A) Former CuAAC based self-healing concept of multivalent liquid alkynes () and azides () encapsulated separately into microcapsules in order to protect them from the free copper(I)-catalyst () preventing thus premature reactions. After occurred damage the capsules were ruptured, their liquid content flue out, mix with each other and react under catalysis of the free Cu(I) under formation of triazole rings (). B) The latent Cu(I)-biscarbene-mechanocatalysts () allow a direct embedding of the catalyst together with the unprotected alkynes and azides into the polymer matrix as they are unable to catalyze the CuAAC in its initial form. Applied mechanical force led to a scission of one polymeric-NHC ligand () in order to generate the active monocarbene catalyst () triggering thus the CuAAC. In both cases the formed triazole rings are able to act as crosslinking points for self-healing applications or can trigger fluorescence via a fluorogenic “click” reaction by the elongation of the conjugated system ensuring thus autonomous damage detection.

2.2 Concept

In order to combine the CuAAC “click” reaction with mechanophoric behavior, a latent polymer based bis-*N*-heterocyclic carbene copper(I) complex ($[\text{Cu}(\text{polymer-NHC})_2]\text{X}$) had to be designed, which is able to cleave-off one NHC-ligand under mechanical force and generate thus an active catalyst (for theoretical considerations see Chapter 1.5) (Figure 42). For that purpose, NHC-telechelic polymers with homogeneous chain length had to be synthesized, as previous studies revealed the most efficient activation of mechanophores when positioned the mechanolabile group centrally in 15% of the midst of the polymer chain (see Chapter 1.2.1). Hence, living respectively controlled polymerization methods were chosen ensuring defined endgroups and narrow molecular weight distribution with polydispersity indices (PDI) close to 1. Moreover, different kinds of polymers were selected in order to investigate the influence of the T_g and the stiffness of the polymer backbone on the activation behavior. The therefore selected polymers were the highly flexible poly(isobutylene) (PIB) displaying a low T_g of around 193K and the rigid poly(styrene) (PS) with a T_g of above 373K.

For practical realization, bromo-telechelic poly(isobutylene)s (PIB-Br) (**3**) should be synthesized in a first step through living carbocationic polymerization (LCCP), while bromo-telechelic poly(styrene)s (PS-Br) (**12**) should be polymerized by atom transfer radical polymerization (ATRP). Both types of bromo-telechelic polymers enable a nucleophilic substitution by sodium iodide/15-crown-5-ether generating thereby *in situ* iodo-telechelic moieties which can be subsequently quaternized by *N*-methylimidazole (**4**) yielding *N*-methylimidazolium telechelic PIBs (**5**) respectively PSs (**13**) (Figure 44). The thus obtained macroligands can be deprotonated in a second step either by sodium *tert*-butoxide or potassium hexamethyldisilazide (KHDMS) to form the free carbene and transformed finally to the copper(I)-biscarbene complexes $[\text{Cu}(\text{NHC})_2]\text{X}$ (**6** and **14**). Three different chain lengths should be synthesized for each polymer to enable a systematic investigation of the initial molecular

weight dependency of the mechanochemical activation behavior. Moreover, low molecular weight model complexes (**10**) should be prepared without attached polymer handles to investigate the activation behavior of the copper(I)-biscarbene complex without attached polymer chains.



Furthermore, the catalytic activity of the obtained polymeric biscarbene copper(I) complexes (**6** and **14**) should be investigated in solution as well as in the solid state. Accordingly, a model CuAAC “click” reaction of phenylacetylene (**17**) and benzyl azide (**19**) was chosen to examine the mechanochemical activation in solution proving thus the initial latency of the origin [Cu(polymer-NHC)₂]X catalysts as well as its ability for mechanochemical activation.

Additionally, details of the activation mechanism during the decomposition of the latent biscarbene Cu(I)-mechanocatalyst by cleaving one of the shielding polymeric-NHC ligands to form the active monocarbene catalyst should be investigated by the means of ¹H-NMR spectroscopy as well as GPC investigations.

In order to prove the mechanochemical activation in the bulk state, a so called fluorogenic “click” reaction of non-fluorescent 3-azido-7-hydroxy-coumarin (**16**) with phenylacetylene (**17**) generating the highly fluorescent 7-hydroxy-3-(4-phenyl-*1H*-[1,2,3]triazole-1-yl)-coumarin dye (**18**) was chosen (Figure 45). Detailed investigations through fluorescence measurements should be performed proving the ability of the designed mechanocatalyst to act as a kind of indirect mechanosensors for damage detection.

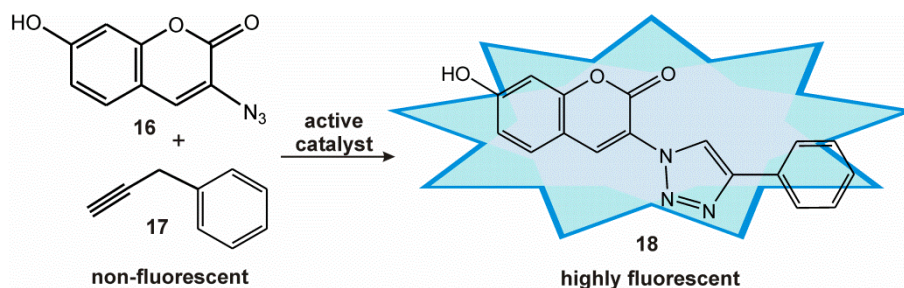


Figure 45. Fluorogenic “click” reaction of non-fluorescent 3-azido-7-hydroxy-coumarin (**16**) with phenylacetylene (**17**) generating highly fluorescent 7-hydroxy-3-(4-phenyl-*1H*-[1,2,3]triazole-1-yl)-coumarin (**18**).

3 Results and Discussion

Parts of the Results and Discussion as well as of the Experimental Part were already published in “A Mechanochemically Triggered “Click” Catalyst” (Michael, P.; Binder, W. H. *Angew. Chem. Int. Ed.* **2015**, *54*, 13918. <http://dx.doi.org/10.1002/anie.201505678>⁹⁷; Michael, P.; Binder, W. H. *Angew. Chem.* **2015**, *127*, 14124. <http://dx.doi.org/10.1002/ange.201505678>²¹¹) and were in parts adapted with permission from John Wiley and Sons (Copyright 2015).

3.1 Synthesis and characterization of PIB-based bis(*N*-methylimidazol-2-ylidene) copper(I)X mechanocatalysts (**6**)

The synthesis of the PIB-based bis-*N*-heterocyclic carbene copper(I) mechanocatalysts [Cu(PIB-NHC)₂]X (**6**) were accomplished within a three step synthesis starting with the polymerization of the linear bromo-telechelic PIB (**3**) via living carbocationic polymerization (LCCP) of isobutylene using 2,4,4-trimethyl-pentane (TMPCl) (**1**)/TiCl₄ as initiator and 3-(bromopropoxy)benzene (BPB) (**2**) as quenching agent (see Figure 46).

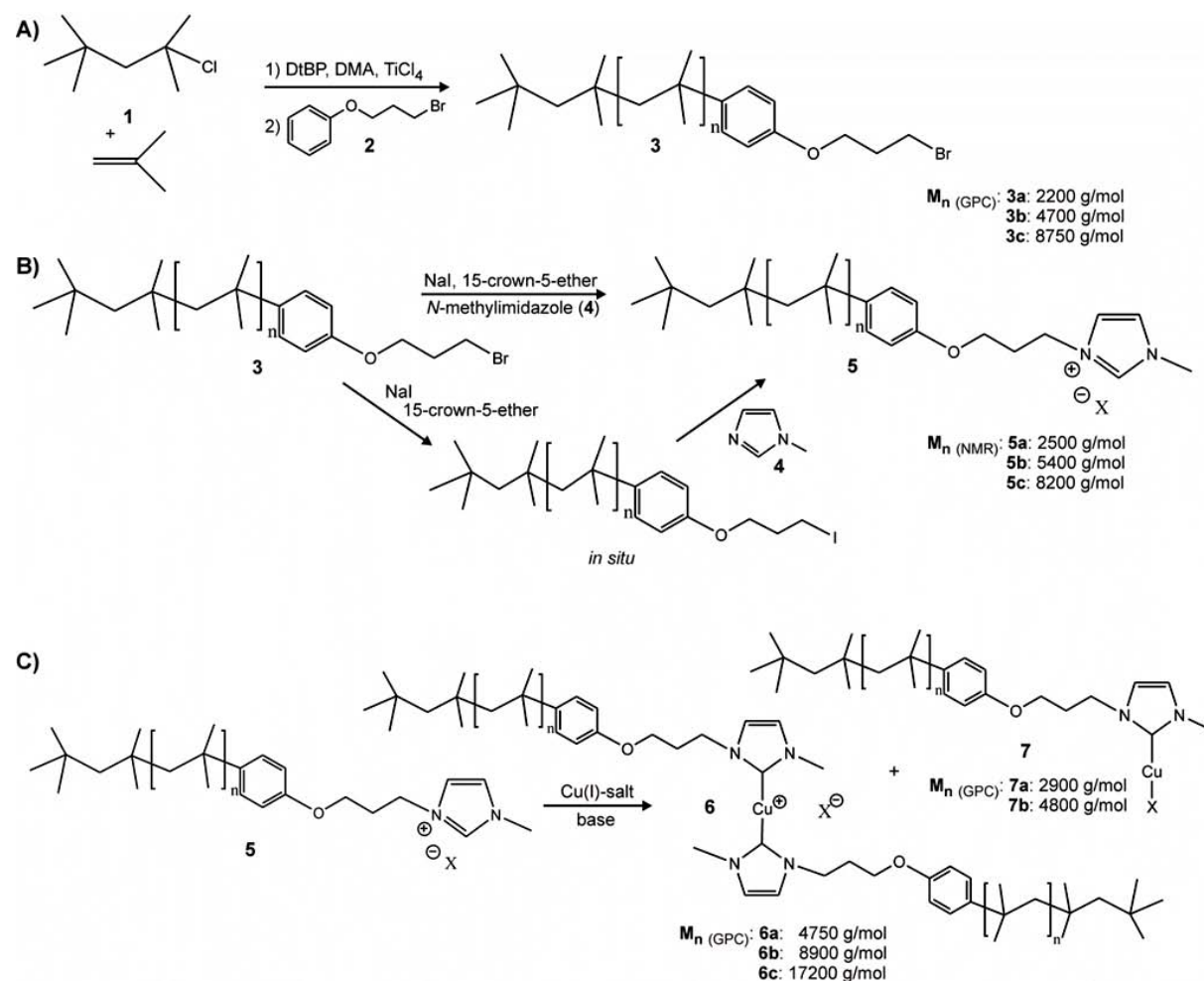


Figure 46. Three step synthetic route for the PIB-based bis(*N*-heterocyclic carbene) copper(I) mechanocatalysts [Cu(PIB-NHC)₂]X (**6**). A) In a first step, linear bromo-telechelic PIB (**3**) was synthesized using TMPCl (**1**)/TiCl₄ as initiator and BPB (**2**) as quenching agent. B) In a second step, *N*-methylimidazolium telechelic PIB (**5**) was prepared through nucleophilic substitution of **3** with sodium iodide in order to generate *in situ* the more reactive iodo-telechelic PIB, which was subsequently quaternized with *N*-methylimidazole (**4**). C) In a third step, the bis(*N*-methylimidazol-2-ylidene-telechelic PIB) copper(I)X complexes [Cu(PIB-NHC)₂]X (**6**) were obtained after deprotonating **5** with a strong base like KHMDS or KO^tBu followed by the coordination of the thus generated free NHC macroligand to a copper(I) salt.

3 was obtained in three different molecular weights ranging from 2200 to 8750 g/mol (Table 6) with PDI around 1.2. Thus, it was possible to synthesize the initial polymers in a well suited living way with small molecular weight distributions ensuring the later centrally embedding of the mechanolabile copper-carbene bond, which is crucial for an efficient activation of the mechanophore (according to theoretical discussions see chapter 1.2).

Table 6. Overview of synthesis PIB-based polymers: bromo-telechelic PIB (**3**) and *N*-methylimidazolium telechelic PIB (**5**).

	PIB-Br (3)		PIB-Imi (5)			
	M_n^a (GPC) [g/mol]	M_n^b (NMR) [g/mol]	M_n^c (GPC) [g/mol]	M_n^d (NMR) [g/mol]	M_n (MALDI) [g/mol]	
					measured	simulated
a	3a : 2200	2500	5a : -	2500	1675.751	1675.765
b	3b : 4700	5200	5b : -	5400	5604.165	5604.165
c	3c :8750	9000	5c : -	8200	9588.761	9588.627

^a)in THF using PIB standard; ^b)determined by the resonances at 6.81 ppm (2x CH eng group), 0.99 (15H head group) in respect to the resonance at 1.42 ppm (CH₂ group of repetitive unit); ^c)could not be determined in THF or toluene because of the low signal intensity due to the ionic nature of **5**; ^d) determined by the resonances at 6.77 ppm (2x CH eng group) and 1.41 ppm (CH₂ group of repetitive unit).

In a second step, the *N*-methylimidazolium telechelic PIB (**5**) was prepared via a quaternization of **3** with *N*-methylimidazole (**4**). However, a direct quaternization yielded only poor conversions of 8% (Table 7 ent. 6), which required an optimization of the applied reaction conditions. For that purpose, first sodium iodide and later also 15-crown-5-ether (increasing the solubility of sodium iodide) were added to generate *in situ* the more reactive iodo-telechelic PIB, which were afterwards quaternized by **4** (Figure 46, Table 7 ent. 1 – 5). Thus, the yield of **5** could be improved to 57% (ent. 5). Moreover, the reaction temperature was varied revealing the best results for 90°C (57%) as higher temperatures (120°C) led to an increased elimination of the phenoxy endgroup from the PIB (17% yield of **5**, ent. 3 – 5), while too low temperatures prevented the quaternization at all. Furthermore, the solvent was varied using different mixtures of *n*-heptane/DMF, toluene/DMF or pure toluene to increase the solubility of the sodium iodine further, while preventing the foiling precipitation of the PIB compound. Thus, the optimal conditions for the quaternization of **3** with **4** were found using 5 eq. sodium iodine, 5.5 eq. 15-crown-5-ether and 100 eq. *N*-methylimidazole (**4**) heating in pure toluene to 90°C for 120h offering yields up to 95% of **5** (Table 7 ent. 8 – 11).

Table 7. Experimental details for the synthesis of *N*-methylimidazolium telechelic PIB (**5**).

Ent.	PIB-Br (3)	NaI	15-crown-5- ether	<i>N</i> -methyl- imidazole (4)	solvent	T [°C]	time [h]	isolated yield [%]	
1	5T1	1 eq.	10 eq.	-	100 eq.	heptane/DMF 1:1	90	72	36
2	5T2	1 eq.	10 eq.	-	100 eq.	heptane/DMF 1:1	90	210	24
3	5T3	1 eq.	10 eq.	-	100 eq.	heptane/DMF 1:1	120	72	17
4	5T4	1 eq.	10 eq.	-	100 eq.	toluene/DMF 7:2	145	90	11
5	5T5	1 eq.	5 eq.	5.5 eq.	100 eq.	heptane/DMF 5:1	90	90	57
6	5T6	1 eq.	-	-	225 eq.	heptane/DMF 5:1	90	90	8
7	5T7	1 eq.	5 eq.	5.5 eq.	100 eq.	toluene	90	90	74
8	5T8	1 eq.	5 eq.	5.5 eq.	100 eq.	toluene	90	120	95
9	5a	1 eq.	5 eq.	5.5 eq.	100 eq.	toluene	90	120	83
10	5b	1 eq.	5 eq.	5.5 eq.	100 eq.	toluene	90	120	74
11	5c	1 eq.	5 eq.	5.5 eq.	100 eq.	toluene	90	120	66

The obtained polymers **5** were successfully characterized by ^1H - and ^{13}C -NMR spectroscopy as well as MALDI-TOF-mass spectrometry proving the true attachment of the *N*-methylimidazolium moiety to the polymer. Detailed information are given in Table 6 as well as in the Experimental Part 4.2.3, while selected spectra are shown in Appendix 7.2 and compared with its derivatives in Figure 48 (page 54). GPC measurements of **5** were not successful neither in THF nor in toluene because of the low intensity of RI- as well as light scattering detection signal due to the ionic nature of **5**²¹². For that reason discussed M_n were calculated directly from ^1H -NMR spectra. The thus observed molecular weights were in the range of 2500 to 8200 g/mol and stayed thus almost constant during the transformation from **3** to **5** (Table 6).

The synthesis of the PIB-based bis(*N*-methylimidazol-2-ylidene) copper(I)X complexes $[\text{Cu}(\text{PIB-NHC})_2]\text{X}$ (**6**) was accomplished in a third step according to three different reaction pathways which differ mainly in the applied bases and copper(I) sources. However, for all three approaches the *N*-methylimidazolium telechelic PIB (**5**) was deprotonated by a strong base yielding the free *N*-heterocyclic carbene which is able to coordinate as a kind of macroligand to the copper(I) center. In the first approach, potassium hexamethyldisilazide (KHMDS) was used to deprotonate **5** followed by the coordination to $[\text{Cu}(\text{CH}_3\text{CN})_4]\text{PF}_6$, which was selected as Cu(I) source because of its good solubility in common organic solvents. In a second approach potassium *tert*-butoxide (KO^tBu) was used as base and $[\text{Cu}(\text{CH}_3\text{CN})_4]\text{PF}_6$ as Cu(I) source, while Cu_2O was used in a third approach as Cu(I) source and base at once.

The choice of the base plays a crucial role within the synthesis of the copper(I) biscarbene complexes: On the one hand the base must be strong enough to enable a quantitative deprotonation of **5** ($\text{pK}_{\text{a}}(\text{water}) = 19 - 23$ ^{203; 213-214}), but on the other hand several side reactions involving such strong bases could be observed within the practical realization (Figure 47).

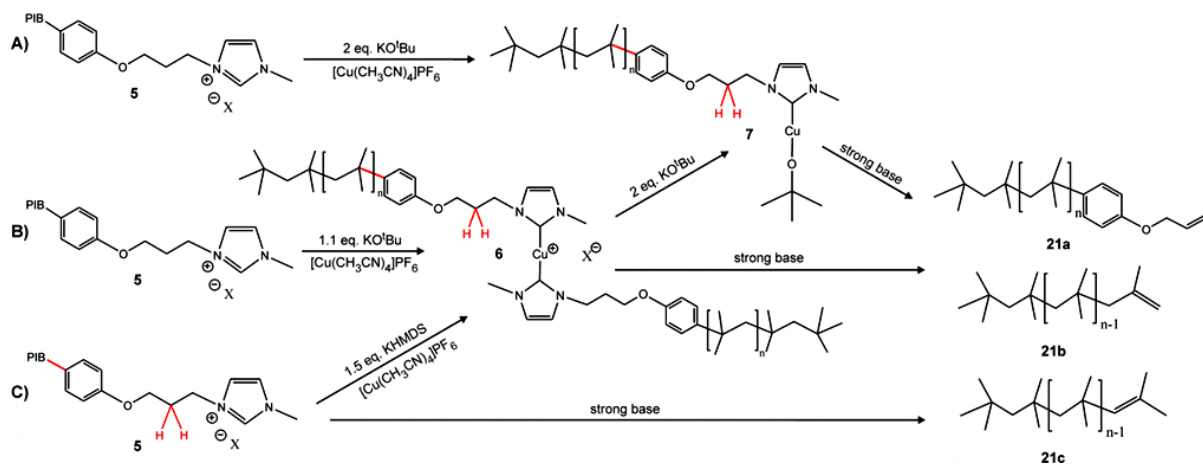


Figure 47. Side reactions during the formation of **6** by strong or coordinative bases. The excess of KO^tBu (2 eq.) favored the formation of the monocarbene complex **7** either by A) direct coordination to the free coordination site of the Cu(I) or B) by attacking the once formed biscarbene complex **6** generating thus also **7** with attached *tert*-butoxide. C) Using strong bases like KHMDS or KO^tBu led to the deprotonation of the over next CH_2 group of the *N*-heterocyclic carbene precursor (**5**) or the catalysts (**6**, **7**) enforcing thus the elimination of the *N*-methylimidazolium endgroup (**21a**) or led to the elimination of the whole phenoxy endgroup of the PIB generating PIB with terminal double bonds (**21b+c**) (^1H -NMR spectrum see Appendix 7.3).

Thus, applying 2 eq. potassium *tert*-butoxide (KO^tBu) ($\text{pK}_{\text{a}}(\text{water}) = 19$ ²¹⁵) to deprotonate **5** led solely to the formation of the monocarbene complex **7** in a yield of 25%, but no biscarbene catalyst **6** was formed (Table 8 ent. 4 and 5). Reasons therefore are the quite high nucleophilicity of KO^tBu and its too low steric hindrance to prevent a nucleophilic attack or a coordination to the copper(I) center respectively. Two possibilities are feasible: Either the *tert*-butoxide anion coordinates directly to the

Cu(I) center preventing thus the formation of **6** blocking the second free coordination site of the copper(I) (Figure 47A) or the used excess of KO^tBu attacked the once formed biscarbene complex and led to its decomposition (Figure 47B)¹⁶⁰. This hypothesis was supported as the reduction of the excess of KO^tBu from 2 to 1.1 eq. led to the formation of the desired PIB-based biscarbene complex **6** up to 45%, while in parallel only 11% of **7** was formed (Table 8 ent. 6). Another prominent side reaction observed during the synthesis of **6** was the elimination of the complete *N*-methylimidazolium endgroup from the polymer by trapping the proton of the over next CH₂-group to the imidazolium ring (see Figure 47C highlighted red) by the applied strong bases, which led in turn to the formation of PIBs with double bonds (**21**) up to 23% and prevented thus the formation of the desired biscarbene complex **6**.

Table 8. Experimental approaches for the synthesis of PIB-based bis(*N*-methylimidazol-2-ylidene) copper(I)X complexes [Cu(PIB-NHC)₂]X (**6**) using different bases and copper(I) sources.

Ent.	M _{n(NMR)} PIB-Imi (5) [g/mol]	Cu(I) source	base	T [°C]	t [h]	isolated yields ^{a)} [%]			
						decomp. PIB (21)	regained 5	monocarbene complex (7)	biscarbene complex (6)
A KHMDS + [Cu(CH ₃ CN) ₄]PF ₆									
1	5a :2500	[Cu(CH ₃ CN) ₄]PF ₆ 0.5 eq.	KHMDS 1.5 eq.	RT	24	15	25	7a : 7	6a : 52
2	5b :5400	[Cu(CH ₃ CN) ₄]PF ₆ 0.5 eq.	KHMDS 1.5 eq.	RT	24	10	35	7b : 5	6b : 49
3	5c :8200	[Cu(CH ₃ CN) ₄]PF ₆ 0.5 eq.	KHMDS 1.5 eq.	RT	24	7	40	7c : - ^{b)}	6c : 42
B KO ^t Bu + [Cu(CH ₃ CN) ₄]PF ₆									
4	5T :4400	[Cu(CH ₃ CN) ₄]PF ₆ 0.5 eq.	KO ^t Bu 2.0 eq.	RT	24	0	80	7d : 20	0
5	5T :4400	[Cu(CH ₃ CN) ₄]PF ₆ 0.5 eq.	KO ^t Bu 2.0 eq.	40	72	10	65	7e : 25	0
6	5T :4400	[Cu(CH ₃ CN) ₄]PF ₆ 0.5 eq.	KO ^t Bu 1.1 eq.	RT	24	23	9	7f : 11	6f : 45
C Cu ₂ O									
7	5T :4400	Cu ₂ O 5 eq.	without	RT	120	0	98	0	0
8	5T :4400	Cu ₂ O 5 eq.	without	80	72	3	60	7h : 2	6h : 35
9	5T :4400	Cu ₂ O 50 eq.	without	120	120	33	11	7i : 7	6i : 49

^{a)}isolated yields after column, missing percentages to 100% are either mixed fractions or lost during the purification; ^{b)}elimination of the *N*-methyl-imidazolium endgroup from PIB generates decomposed PIB with terminal double bonds

To minimize this disturbing side reactions, KO^tBu was replaced by KHMDS which is known as a strong (pK_a (water) = 26²¹⁶), non-nucleophilic, but highly sterically hindered base able to form free carbenes without coordinating to the central metal atoms^{157; 160; 217}. Similarly to the previous attempt [Cu(CH₃CN)₄]PF₆ was used as copper(I) source and the PIB-based biscarbene complex **6** was obtained in slightly higher yields up to 52% (Table 8 ent. 1-3), while the monocarbene complex **7** occurred solely as a side product in yields up to 7%. Simultaneously, the amount of decomposition products **21** could be minimized to ~10% and the major part of the not converted educt **5** (up to 40% see Table 8 ent. 1-3) could be regained allowing a subsequently reuse for further attempts.

In another approach Cu₂O was used as Cu(I) source and base at once. As no additional strong base was added, the minimization of the endgroup elimination was expected. However, Cu₂O itself is a kinetically hindered reactant²¹⁸⁻²¹⁹ and requires thus usually higher reaction temperatures compared to the previously described examples which were commonly performed at room temperature (see Table 8). Accordingly, no reaction of **5** with Cu₂O could be observed at room temperature (also no decomposition), while an increasing of the reaction temperature to 120°C triggered the formation of the desired Cu(I)-biscarbene complex **6** in yields of ~49% (Table 8 ent. 9). Unfortunately, the high reaction temperature caused again a decomposition of the PIB moieties and led to the formation of the elimination products **21** in yields of 33% and is thus higher compared to the approach which applies KHMDS as base.

Also other bases, like weaker, non-nucleophilic 1,8-diazabicyclo[5.4.0]undec-7-en (DBU) (pK_a(water) = 12) and stronger non-nucleophilic *tert*-butylimino-tri(pyrrolidino)phosphazene phosphazene base (pK_a = 28) were tested in a Master Thesis²²⁰ accomplished within the scope of this work. However, DBU led neither to the formation of the mono- nor to the formation of the biscarbene copper(I) complexes as it is either too weak to deprotonate the *N*-methylimidazolium macroligand (pK_a(water) = 19 – 23^{203; 213-214}) or form complexes with Cu(I) shielding thus the free coordination sites which prevented the attachment of the NHC-ligands, while the phosphazene base increased the amount of polymer which eliminates the imidazolium endgroup significantly. For that reason, the approach applying KHMDS as base was selected for the preparation of **6**.

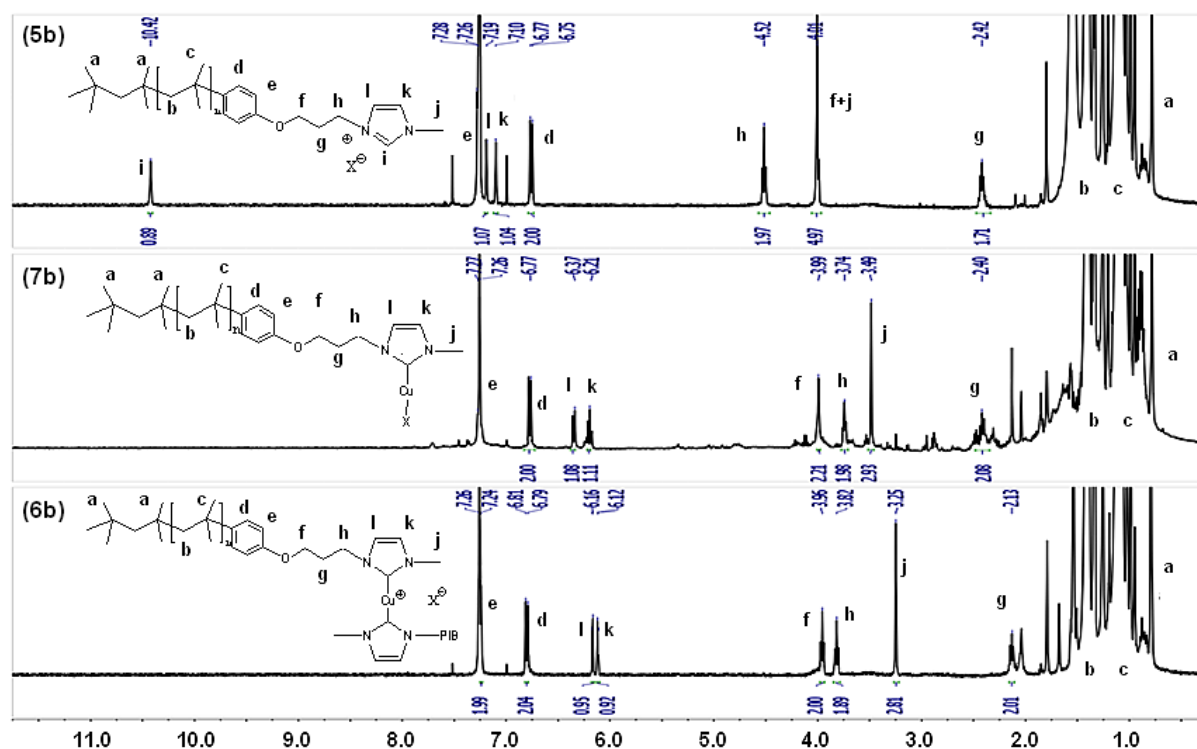


Figure 48. ¹H-NMR spectra of *N*-methylimidazolium-telechelic PIB (**5b**) and the corresponding mono- (**7b**) and biscarbene copper(I) complexes (**6b**) in CDCl₃.

The structural proof of the synthesized complexes **6** and **7** was accomplished by ¹H-NMR spectroscopy as well as MALDI-TOF-MS analysis. Comparing the ¹H-NMR-spectra from the PIB-based biscarbene [Cu(PIB-NHC)₂]X (**6**) as well as the monocarbene [Cu(PIB-NHC)]X complex (**7**) to the initial *N*-methylimidazolium-telechelic PIB (**5**) showed clearly the disappearance of the imidazolium proton (NCH₃N) at 10.42 ppm and the shift of the CH-groups (H_l and H_k) of the respective NHC-moieties from 7.10 and 7.19 ppm for **5** to 6.21 and 6.37 ppm for the monocarbene

complex **7** respectively 6.12 and 6.16 ppm for the biscarbene complex **6** (Figure 48). Also the resonances H_f, H_g, H_h and H_j of the neighboring CH₂ respectively CH₃ groups of the NHC-ring were shifted significantly as assigned in Figure 48. Further NMR spectra of the catalysts with different molecular weights are shown in Appendix 7.2 and 7.3.

During MALDI-TOF-MS analysis only spectra showing two series for different Cu(I)-moieties could be determined (Figure 49). The first series with its maximum at 1956.846 g/mol could be identified as the desired PIB-based bis(*N*-methylimidazol-2-ylidene) Cu(I)-complex (**6a**) detected without counterion or additional cation, which fits well with its simulation of 1956.829 g/mol (err. 9 ppm) ($[M]^+ C_{130}H_{242}Cu_1N_4O$) (Figure 49C) as well as with the isotope pattern. The second series could be assigned to a decomposition product of **6a** whereby one shielding polymeric NHC-ligands is cleaved-off. The residual $[Cu(PIB-NHC)]^+$ could be determined with a maxima at 2752.534 g/mol without counterion together with CF₃COOH (from salt). Also the simulation of this series (C₁₈₃H₃₅₆Cu₁F₃N₂O₃⁺; 2752.706 g/mol; err. 62 ppm) as well as the isotope pattern fits very well to the obtained peaks (Figure 49D).

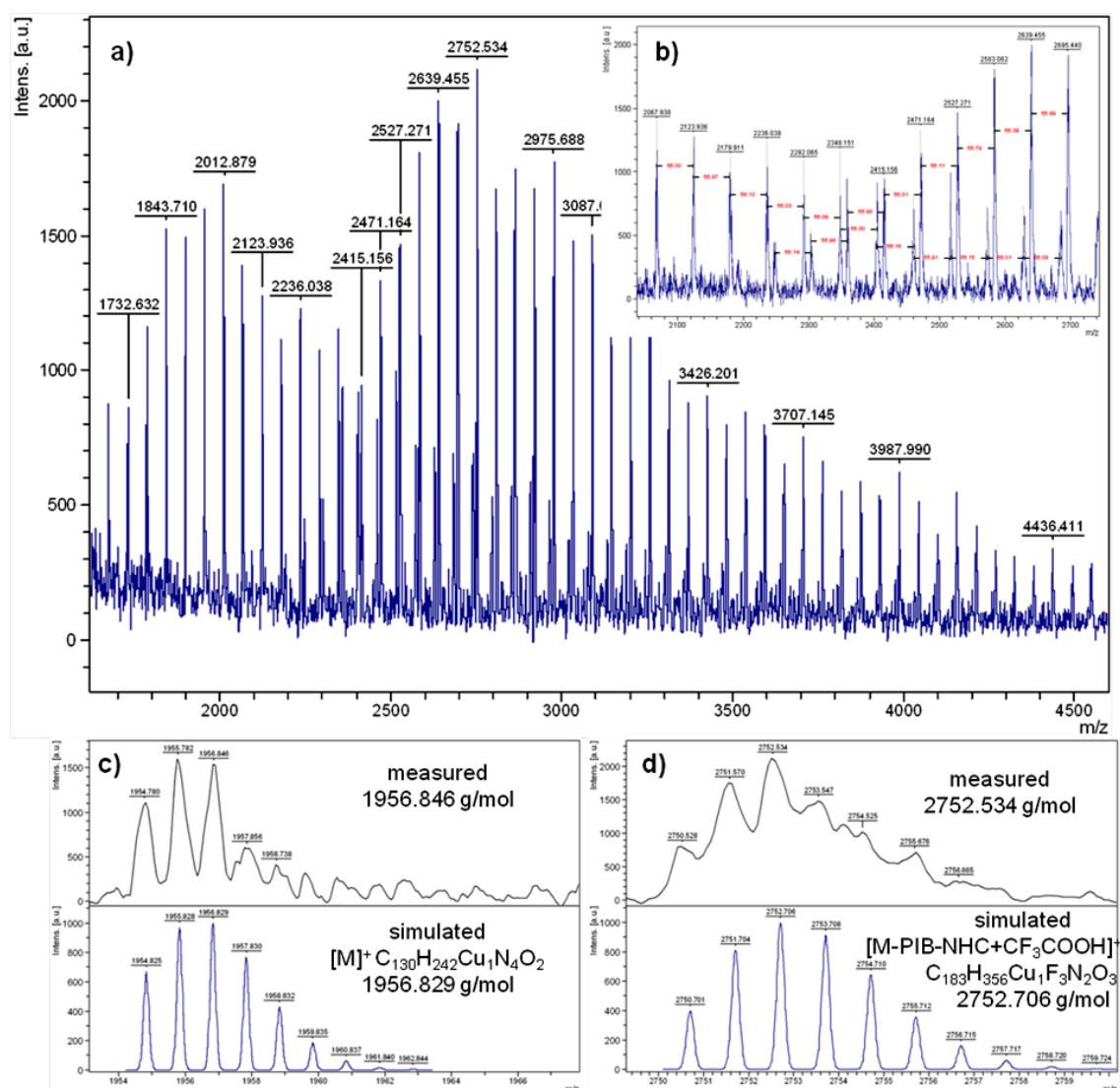


Figure 49. MALDI-TOF-mass spectrum of bis(*N*-methylimidazol-2-ylidene telechelic PIB copper(I)X $[Cu(PIB-NHC)_2]X$ (**6a**) using DCTB as matrix and LiTFA as salt. a) Full spectrum of **6a** showing two series, b) enlargement of overlay area of both series, c) isotopic pattern as well as simulation of 1st series assigned to the biscarbene complex **6a** without counterion and d) isotopic pattern as well as simulation of 2nd series assigned to decomposed **6a** (without counterion and one cleaved-off polymeric ligand detected together with CF₃COOH). (Reproduced from ref⁹⁷ with permission of Wiley and Sons)

The observed scission of one polymeric NHC-ligand during the MALDI-TOF-MS analysis was expectable so far as the mechanocatalysts were designed to be labile. Catalysts with longer polymer chains are more labile in comparison to catalysts with shorter chains which was also shown in literature for other mechanocatalysts^{15; 17}. Thus, the more labile, higher molecular weight fractions of **6a** were disrupted during the ionization process, while the more stabile, lower molecular weight fractions could be determined as unfractured catalyst. This is also the reason, while suitable mass-spectra could only be obtained for complex **6a** as the higher molecular weight catalysts decompose much rapidly during the ionization process. Nevertheless, the performed MALDI-TOF-mass spectroscopy of the mechanocatalyst **6** proved the prospected structure.

The final proof obtaining the desired biscarbene catalysts **6** was accomplished comparing the molecular weights from GPC and ¹H-NMR spectroscopy for the bromo-telechelic (**3**) and the *N*-methylimidazolium-telechelic PIB (**5**) with the corresponding mono- (**7**) respectively biscarbene mechanocatalysts (**6**) (Table 9). GPC investigations revealed a clear doubling of the molecular weight during the synthesis of PIB-based biscarbene mechanocatalysts e.g. **6a** (4750 g/mol) compared to the starting polymer **3a** (2200 g/mol), while in case of the monocarbene catalysts e.g. **7a** (2900 g/mol) the molecular weight stayed constant (Figure 50; Table 9). This indicates the true attachment of two polymeric-NHC ligands to one copper(I) center in case of **6** and solely one in case of **7**. The doubling of the molecular weights could be proven by GPC for all obtained biscarbene complexes **6** as can be seen in Table 9 as well as Appendix 7.3.

Table 9. Overview of synthesis PIB-based polymers and catalysts: bromo-telechelic PIBs (**3**); *N*-methylimidazolium telechelic PIBs (**5**), bis(*N*-methylimidazol-2-ylidene-telechelic PIB) copper(I)X complexes [Cu(PIB-NHC)₂]X (**6**) and mono(*N*-methylimidazol-2-ylidene-telechelic PIB) copper(I)X complexes [Cu(PIB-NHC)]X (**7**).

	PIB-Br (3)		PIB-Imi (5)			[Cu(PIB-NHC)]X - monocarbene catalyst (7)		[Cu(PIB-NHC) ₂]X - biscarbene catalyst (6)		
	M _n ^{a)} (GPC) [g/mol]	M _n ^{b)} (NMR) [g/mol]	M _n ^{c)} (GPC) [g/mol]	M _n ^{d)} (NMR) [g/mol]	M _n ^{e)} (MALDI) [g/mol]	M _n ^{a)} (GPC) [g/mol]	M _n ^{f)} (NMR) [g/mol]	M _n ^{a)} (GPC) [g/mol]	M _n ^{f)} (NMR) [g/mol]	M _n ^{e)} (MALDI) [g/mol]
a	3a : 2200	2500	5a : -	2500	1675.751	7a : 2900	2800	6a : 4750	2400	1956.846
b	3b : 4700	5200	5b : -	5400	5604.295	7b : 4800	5700	6b : 8900	5100	- ^{g)}
c	3c : 8750	9000	5c : -	8200	9588.761	7c : non-existent		6c : 17200	8900	- ^{g)}

^{a)}in THF using PIB standard; ^{b)}determined by the resonances at 6.81 ppm (2x CH eng group), 0.99 (15H head group) in respect to the resonance at 1.42 ppm (CH₂ group of repetitive unit); ^{c)}could not be determined in THF or toluene because of the low signal intensity due to the ionic nature of **5**; ^{d)}determined by the resonances at 6.77 ppm (2x CH eng group) and 1.41 ppm (CH₂ group of repetitive unit); ^{e)}simulated values are given in Experimental Part; ^{f)}determined according to the signals from phenylic end group (C₆H₄) around 6.80 ppm as well as from CH-groups from NHC ligand (6.17 ppm for **6**, 6.37 ppm for **5**) compared to the signals of the CH₂-group from the PIB backbone at 1.41 ppm; ^{g)}not determined due to the labile nature of the formed complexes.

Furthermore, the molecular weights obtained by ¹H-NMR spectroscopy revealed only the half of the real molecular weight which can be observed e.g. by GPC as the biscarbene catalysts **6** are symmetric molecules without a singular proton which could be used for the normalization. Thus, comparing the molecular weights obtained by GPC and ¹H-NMR spectroscopy proved the formation of the biscarbene complex **6** as the molecular weight of GPC (e.g. **6a**: 4750 g/mol) was double compared to the M_n from ¹H-NMR spectroscopy (**6a**: 2400 g/mol) (Table 9). In contrast, the molecular weights of the monocarbene catalysts (**7**) were the same in GPC (e.g. **7a**: 2900 g/mol) and ¹H-NMR spectroscopy (**7a**: 2800 g/mol). This behavior could be observed for all synthesized PIB-based catalyst (see Table 9).

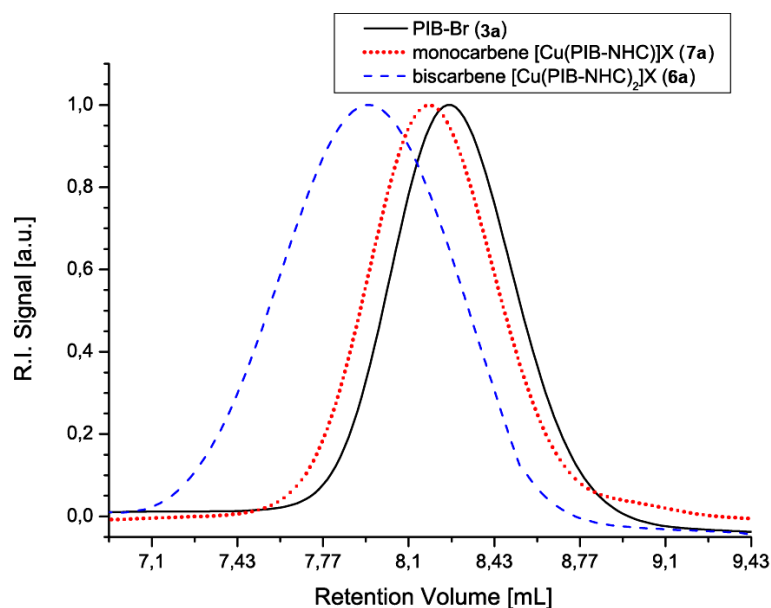


Figure 50. GPC traces of bromo-telechelic PIB (**3a**; PIB-Br; M_n (GPC) = 2200 g/mol) as well as corresponding mono- (**7a**; [Cu(PIB-NHC)]X; M_n (GPC) = 2900 g/mol) and biscarbene complexes (**6a**; [Cu(PIB-NHC)₂]X; M_n (GPC) = 4750 g/mol) indicating the doubling of molecular weight during the mechanocatalyst formation. (Reprinted from ref⁹⁷ with permission of Wiley and Sons)

Thus, GPC, ¹H-NMR spectroscopic as well as MALDI-TOF-MS analysis proved the successful synthesis of the desired PIB-based bis(*N*-methylimidazol-2-ylidene) copper(I)X complexes [Cu(PIB-NHC)₂]X (**6**) with three different molecular weight ranging from 4750, 8900 up to 17200 g/mol as well as of the corresponding mono(*N*-methylimidazol-2-ylidene-telechelic PIB) copper(I)X complex [Cu(PIB-NHC)]X (**7**). However, a slow decomposition of the biscarbene complexes (**6**) could be observed over a period of several months by cleaving/re-protonating one of the carbene ligands (proven by GPC and ¹H-NMR spectroscopy), while the monocarbene complexes (**7**) oxidized during the purification process as the second shielding carbene ligand is missing and can solely be activated for later CuAAC reactions by adding an additional reducing agent like sodium ascorbate.

3.2 Synthesis and characterization of PS-based bis(*N*-methylimidazol-2-ylidene) copper(I)X mechanocatalysts (**14**)

The poly(styrene)-based bis(*N*-methylimidazol-2-ylidene) copper(I)X mechanocatalysts [Cu(PS-NHC)₂]X (**14**) were synthesized and characterized in a similar way like their PIB-based counterparts (**6**) described above. The synthesis was accomplished in three steps starting with the atom transfer radical polymerization (ATRP) of styrene using methyl 2-bromopropionate (**11**) as initiator (Figure 51A). Linear bromo-telechelic PSs (**12**) were achieved in three different molecular weights ranging from 3100 to 7100 g/mol (determined by GPC; Table 10) with PDI of 1.1 to 1.3 (see Experimental Part). The narrow molecular weight distributions ensure a central embedding of the mechanolabile copper-carbene bond within the later formed mechanophore, which is a crucial requirement for an efficient activation by external force (see theoretical discussions chapter 1.2).

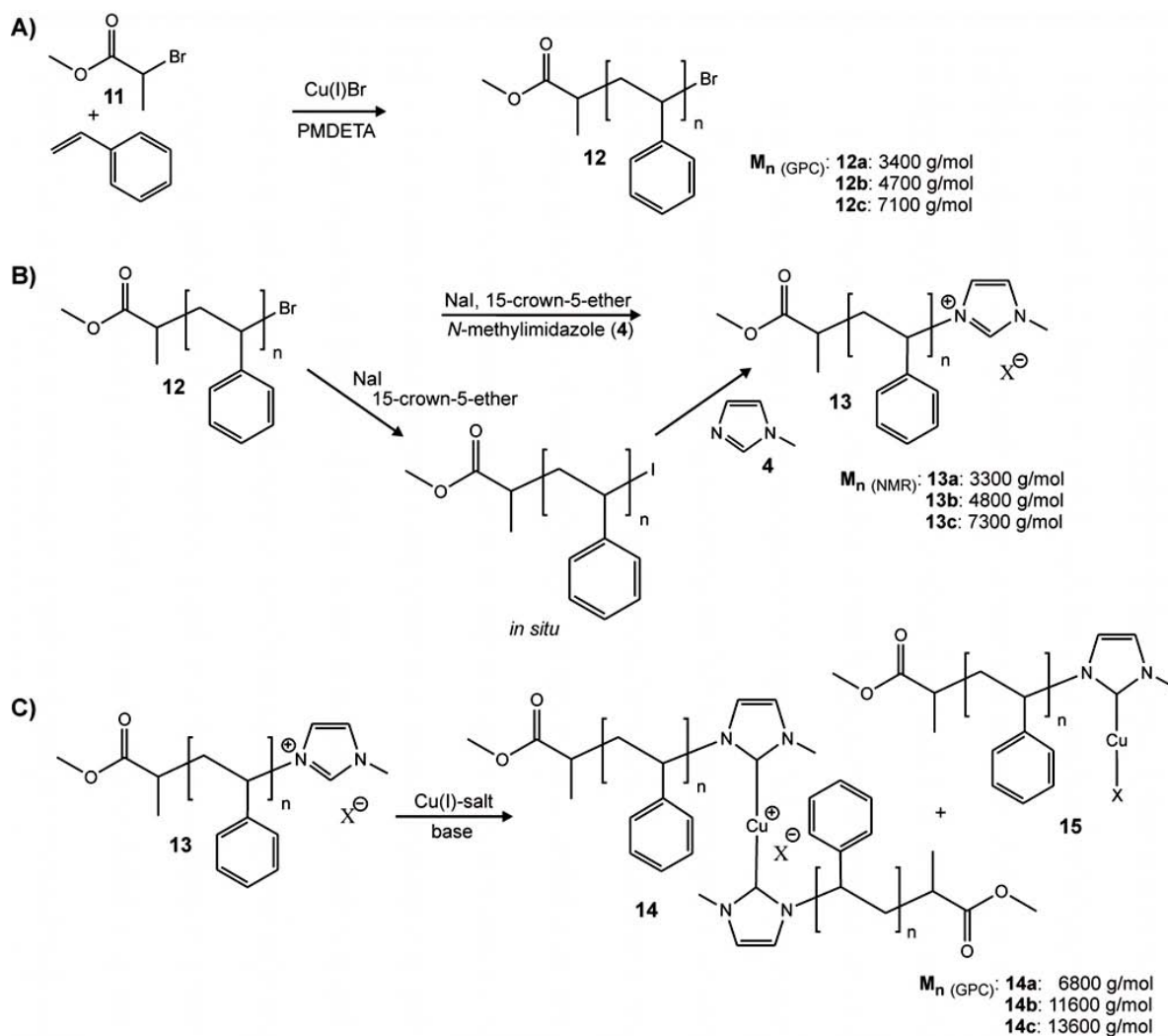


Figure 51. Three step synthetic route for the PS-based bis(*N*-heterocyclic carbene) copper(I) mechanocatalyst [Cu(PS-NHC)₂]*X* (**14**). A) In the first step, linear bromo-telechelic PS (**12**) was synthesized via ATRP using methyl 2-bromopropionate (**11**) as initiator. B) In a second step, *N*-methylimidazolium telechelic PS (**13**) was synthesized through nucleophilic substitution of **12** with sodium iodide in order to generate *in situ* the more reactive iodo-telechelic PS, which was subsequently quaternized with *N*-methylimidazole (**4**). C) In a third step, the bis(*N*-methylimidazol-2-ylidene)-telechelic PS copper(I)*X* complexes [Cu(PS-NHC)₂]*X* (**14**) were obtained after deprotonating **13** with NaO^tBu followed by the coordination of the thus generated free NHC macroligand to [Cu(CH₃CN)₄]*PF*₆.

Table 10. Overview of synthesized PS-based polymers: bromo-telechelic PS (**12**) and *N*-methylimidazolium telechelic PS (**13**).

Ent.	PS-Br (12)		PS-Imi (13)		M_n (MALDI)	
	$M_n^a)$ (GPC)	$M_n^b)$ (NMR)	$M_n^a)$ (GPC)	$M_n^b)$ (NMR)	M_n [g/mol]	
	[g/mol]	[g/mol]	[g/mol]	[g/mol]	measured	simulated
a	12a: 3100	2800	13a: - ^{c)}	3200	3605.512	3605.017
b	12b: 5000	4900	13b: - ^{c)}	4800	5999.157	5999.461
c	12c: 7100	7200	13c: - ^{c)}	7300	8499.507	8499.973

^{a)}PS standards were used for GPC; ^{b)} M_n of ¹H-NMR spectroscopy were calculated out of the ratio of signals from the CH₃ of the initiator head group at 0.88 ppm and the superimposed signals of the CH and CH₂-groups of the polymer chain at 1.87 - 1.45 ppm as well as the CH₂-group of the last repetitive unite close to the NHC (CH₂CHBr) at 3.17 ppm. ^{c)}GPC analysis not possible due to the low detection intensity of ionic polymer.

Subsequently, the bromo-telechelic PS (**12**) was quaternized by *N*-methylimidazole (**4**) (Figure 51B) applying the optimized conditions found for the previously described preparation of the PIB-based imidazolium (**5**). Thus, *N*-methylimidazolium-telechelic PS (**13**) was obtained in yields up to 49% treating 1 eq. **12** with 5 eq. sodium iodine, 5.5 eq. 15-crown-5-ether and 100 eq. *N*-methylimidazole (**4**) for 120h at 90°C in toluene (for details see Table 26 Experimental Part 4.4.2). ¹H-NMR spectroscopy as well as MALDI-TOF-mass spectrometry proved the successful attachment of the *N*-methylimidazolium moiety to the polymer. Detailed information are given in the Experimental Part 4.4.2 and selected spectra are shown in Appendix 7.7. Similarly to **5**, GPC measurements of **13** were not possible neither in THF nor in toluene because of the low intensity of RI- as well as light scattering detection signal due to the ionic nature of the *N*-methylimidazolium-telechelic polymers²¹². Therefore, the discussed M_n s were calculated directly from ¹H-NMR spectra revealing molecular weights in the range of 3200 to 7300 g/mol and stayed thus almost constant during the transformation from **12** to **13** (Table 10).

The synthesis of the PS-based bis(*N*-methylimidazol-2-ylidene) copper(I)X complexes [Cu(PS-NHC)₂]X (**14**) was accomplished applying in principle the same three methods as described for the PIB-based copper(I) complexes **6** using either KHMDS or NaO^tBu as base with [Cu(CH₃CN)₄]PF₆ as copper(I) source or Cu₂O as base and copper source at once. However, the most suitable method for **6** utilizing KHMDS caused in case of the PS-based copper(I) complexes **14** solely the decomposition of **13** by elimination of the *N*-methylimidazolium endgroup from the PS chain forming terminal double bonds (**23**) (Figure 52). Contrary to the complex formation of **6**, no formation of PS-based mono- or biscarbene complex (**14**, **15**) could be observed (Table 11 ent. 1), which founded on the higher acidity of the protons of the CH₂ group next to the *N*-methylimidazolium endgroup for **13** compared to **5** (red highlighted in Figure 52 respectively Figure 47 for **5**). Also the application of Cu₂O at elevated temperatures of 120°C caused solely the decomposition of **13**, but led not to the formation of **14** or **15** (Table 11 ent. 5).

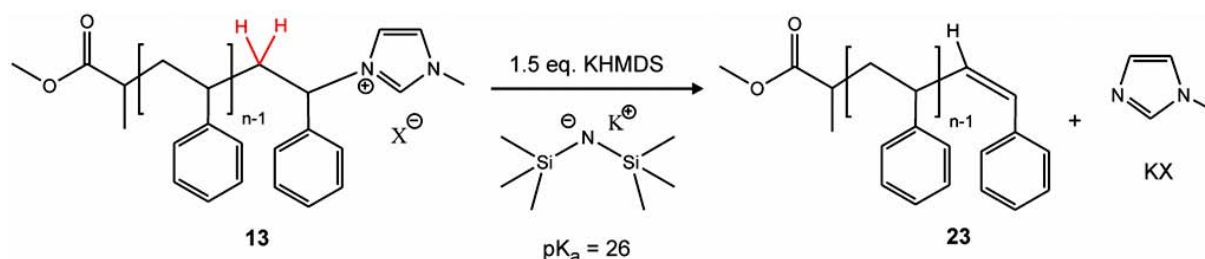


Figure 52. Most prominent side reaction during the synthesis of PS-based bis(*N*-methylimidazol-2-ylidene) copper(I)X mechanocatalysts (**14**). The application of strong bases led to the elimination of the *N*-methylimidazolium endgroup and the formation of terminal double bonds.

The application of 1.3 eq. NaO^tBu ($pK_{a(\text{water})} = 19$ ²¹⁵) for the deprotonation of **13** ($pK_{a(\text{water})} = 19 - 23$ ^{203; 213-214}) as a weaker base compared to KHMDS ($pK_{a(\text{water})} = 26$ ²¹⁶) led under mild conditions to the formation the desired PS-based biscarbene complexes **14** in yields up to 39% (Table 11 ent. 2 - 4; Figure 51C). However, the formation of the corresponding PS-based monocarbene complex **15** could not be observed due to its lower stability compared to the biscarbene Cu(I) complex **14** which led thus to a faster decomposition during the purification by column chromatography.

Table 11. Experimental approaches for the synthesis of PS-based bis(*N*-methylimidazol-2-ylidene) copper(I)X complexes [Cu(PS-NHC)₂]X (**14**) using different bases and copper(I) sources.

Ent.	M _n (NMR) PS-Imi (13): [g/mol]	Cu(I) source	base	T [°C]	t [h]	isolated yields ^{a)} [%]		
						decomp. PS ^{b)} (23)	regained 13	biscarbene complex (14)
A KHMDS + [Cu(CH ₃ CN) ₄]PF ₆								
1	13a: 3200	[Cu(CH ₃ CN) ₄]PF ₆ 0.5 eq.	KHMDS 1.5 eq.	RT	24	34	23	0
B NaO ^t Bu + [Cu(CH ₃ CN) ₄]PF ₆								
2	13a: 3200	[Cu(CH ₃ CN) ₄]PF ₆ 0.5 eq.	NaO ^t Bu 1.3 eq.	40	48	16	0	32
3	13b: 4800	[Cu(CH ₃ CN) ₄]PF ₆ 0.5 eq.	NaO ^t Bu 1.3 eq.	40	48	11	23	39
4	13c: 7300	[Cu(CH ₃ CN) ₄]PF ₆ 0.5 eq.	NaO ^t Bu 1.3 eq.	40	48	4	32	35
C Cu ₂ O								
5	13a: 3200	Cu ₂ O 5 eq.	without	RT	120	43	12	0

^{a)}isolated yields after column, missing percentages to 100% are either mixed fractions or lost during the purification; ^{b)}elimination of the *N*-methylimidazolium endgroup from PS

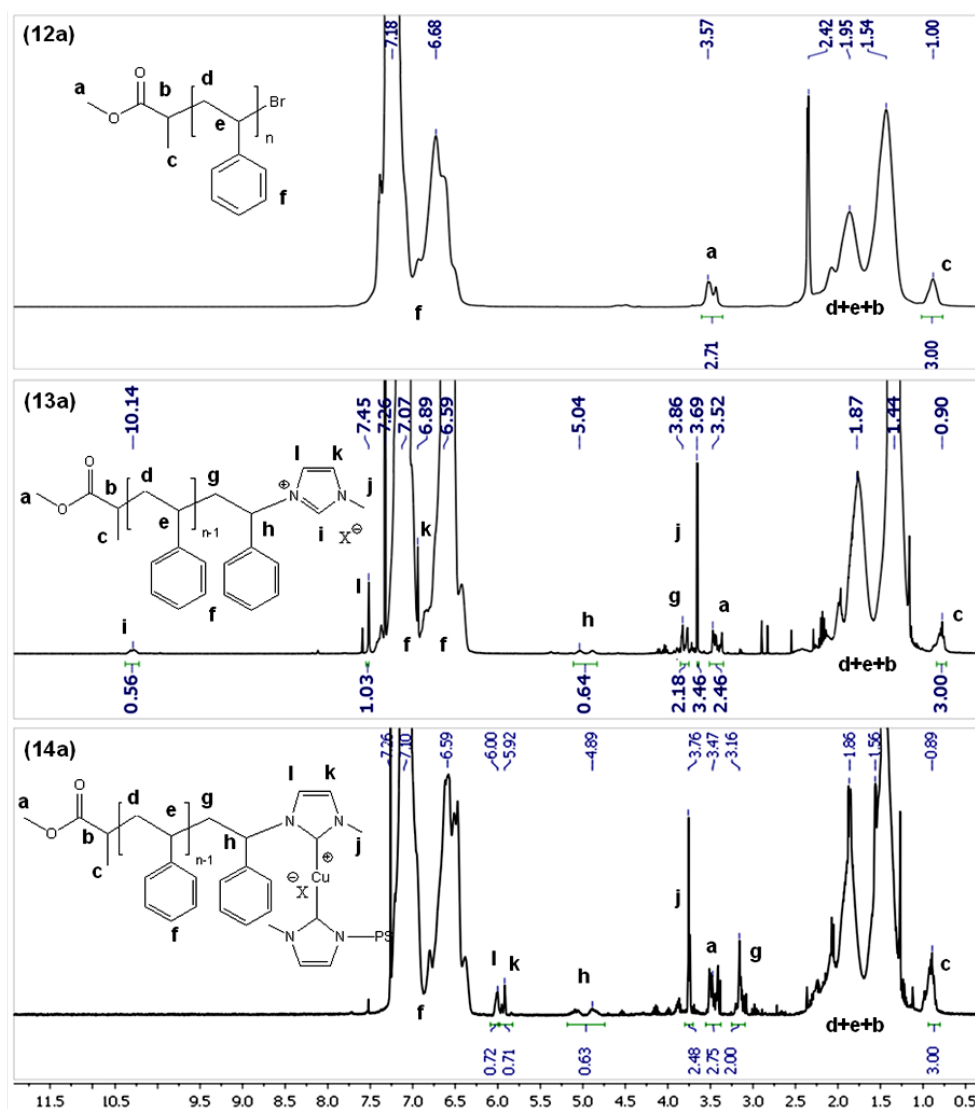


Figure 53. ¹H-NMR spectra of bromo-telechelic PS (**12a**), *N*-methylimidazolium-telechelic PS (**13a**) and the corresponding PS-based biscarbene copper(I) complex (**14a**) in CDCl₃.

The structural proof of the obtained polymers was done by $^1\text{H-NMR}$ spectroscopy as well as GPC. Comparing the $^1\text{H-NMR}$ -spectra from the PS-based biscarbene $[\text{Cu}(\text{PS-NHC})_2]\text{X}$ (**14**) with its direct precursor the *N*-methylimidazolium-telechelic PS (**13**) revealed the disappearance of the imidazolium proton (NCH_3N) at 10.14 ppm and the shift of the CH -groups (H_i and H_k) of the corresponding NHC-moieties from 7.45 and 6.89 ppm for **13** to 6.00 and 5.92 ppm for the biscarbene complex **14** (Figure 53). Further NMR spectra are presented in Appendix 7.7 and 7.8.

Furthermore, GPC measurements were performed in order to prove finally the desired PS-based biscarbene structure **14**. For that purpose, the molecular weights of **14** obtained by GPC were compared to the molecular weights of the bromo-telechelic PS (**12**) revealing a doubling of the molecular weight during the synthesis of PS-based biscarbene mechanocatalysts; e.g. **14a** (6800 g/mol) compared to the starting polymer **12a** (3100 g/mol) (Figure 54; Table 12) which proved thus the real attachment of two polymeric NHCs to one copper(I) center. A comparison with the molecular weight of direct *N*-methylimidazolium-telechelic PS precursor (**13**) was not possible due to the low signal intensity in GPC of such ionic species²¹². Nevertheless, the doubling of the molecular weights could be proven by GPC for all obtained biscarbene complexes **14** as can be seen in Table 12 as well as Appendix 7.8.

Table 12. Overview of synthesis PS-based polymers and catalysts: bromo-telechelic PS (**12**); *N*-methylimidazolium telechelic PS (**13**) and bis(*N*-methylimidazol-2-ylidene-telechelic PS) copper(I)X complex $[\text{Cu}(\text{PS-NHC})_2]\text{X}$ (**14**).

Ent.	PS-Br (12)		PS-Imi (13)			biscarbene complex $[\text{Cu}(\text{PS-NHC})_2]\text{X}$ (14)	
	$M_n^{\text{a)}$ (GPC) [g/mol]	$M_n^{\text{b)}$ (NMR) [g/mol]	$M_n^{\text{a)}$ (GPC) [g/mol]	$M_n^{\text{b)}$ (NMR) [g/mol]	$M_n^{\text{c)}$ (MALDI) [g/mol]	$M_n^{\text{a)}$ (GPC) [g/mol]	$M_n^{\text{b)}$ (NMR) [g/mol]
a	12a: 3100	2800	13a: - ^{d)}	3200	3605.512	14a: 6800	3100
b	12b: 5000	4900	13b: - ^{d)}	4800	5999.157	14b: 11600	4800
c	12c: 7100	7200	13c: - ^{d)}	7300	8499.507	14c: 13600	9300

^{a)}PS standards were used for GPC; ^{b)} M_n of $^1\text{H-NMR}$ spectroscopy were calculated out of the ratio of signals from the CH_3 of the initiator head group at 0.88 ppm and the superimposed signals of the CH and CH_2 -groups of the polymer chain at 1.87 - 1.45 ppm as well as the CH_2 -group of the last repetitive unite close to the NHC (CH_2CHBr) at 3.17 ppm. ^{c)}simulated values are given in Experimental Part; ^{d)}GPC analysis not possible due to the low detection intensity of ionic polymer.

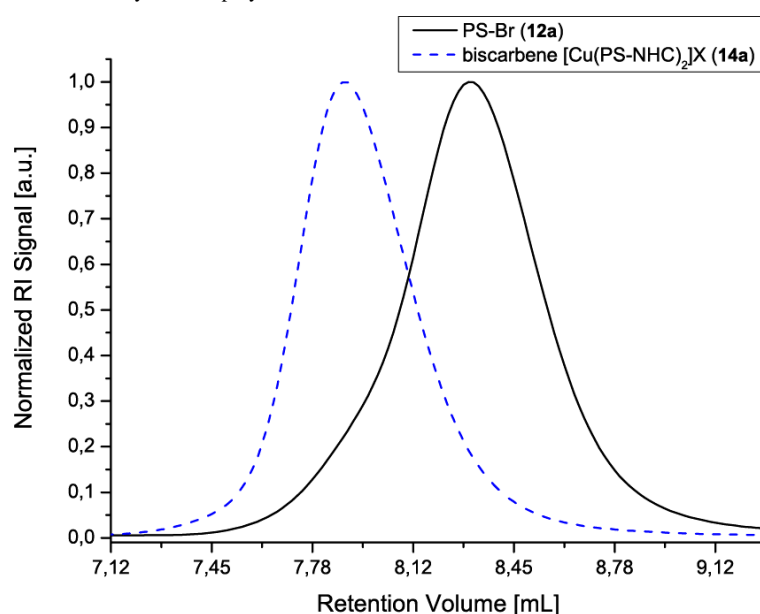


Figure 54. GPC traces of bromo-telechelic PS (**12a**; PS-Br; M_n (GPC) = 3400 g/mol) as well as corresponding biscarbene complexes (**14a**; $[\text{Cu}(\text{PS-NHC})_2]\text{Br}$; M_n (GPC) = 6800 g/mol) indicating the doubling of molecular weight during the mechanocatalyst formation. (Reprinted from ref⁹⁷ with permission of Wiley and Sons)

Moreover, the comparison of the molecular weights obtained through GPC and $^1\text{H-NMR}$ spectroscopy proved the attachment of two polymeric NHC-ligands as the observed M_n from $^1\text{H-NMR}$ spectroscopy (e.g. **14a**: 3100 g/mol) offers only the half M_n of the GPC measurements (**14a**: 6800 g/mol) (see Table 12). This conclusion can be drawn as the synthesized PS-based biscarbene catalyst **14** is - likewise the PIB-based complexes **6** - a symmetric molecule without a singular proton which could be used for the normalization. Thus, GPC and $^1\text{H-NMR}$ spectroscopic analysis proved the successful synthesis of the desired PS-based bis(*N*-methylimidazol-2-ylidene) copper(I)X complexes $[\text{Cu}(\text{PS-NHC})_2]\text{X}$ (**14**) in three different molecular weight ranging from 6800, 11600 up to 13600 g/mol. Albeit, a slow decomposition of the biscarbene complexes **14** could be observed over a period of several months by cleaving/re-protonating one of the carbene ligands (proven by GPC and $^1\text{H-NMR}$ spectroscopy).

3.3 Mechanochemical activation of polymeric bis(*N*-methylimidazol-2-ylidene) copper(I)X complexes **6** and **14** by external force

After the successful synthesis of the PIB- (**6**) and PS-based (**14**) bis(*N*-methylimidazol-2-ylidene) copper(I)X complexes in three different molecular weights, the catalytic properties of these complexes should be tested - especially in respect to the desired latency in the initial state and the subsequent activation by external mechanical force. This should enable the cleavage of one shielding NHC-ligand by transmitting the applied force through the attached polymeric handles to the labile copper-NHC bond generating thus a free coordination site on the copper which introduce a catalytic activity (Figure 55). In the scope of this thesis, ultrasound respectively compression are used for the mechano-chemical activation as they are generally accepted methodologies to simulate stress onto mechano-phores in solution^{4; 6; 98-102} respectively in the solid state^{19; 28-29; 36; 58; 97; 112-113} (see Chapter 1.2).

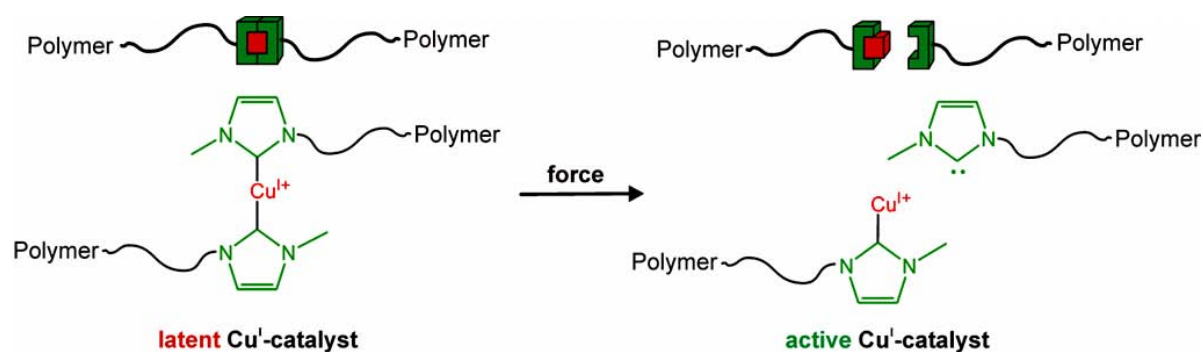


Figure 55. Proposed mechanochemical activation of the designed polymeric bis(*N*-methylimidazol-2-ylidene) copper(I)X complexes **6** and **14** triggered through applied external force (e.g. by ultrasound in solution or compression in solid state) leading thus to the scission of the labile Cu(I)-NHC bond and the cleavage of one shielding NHC-ligand generating thus a catalytic active site.

3.3.1 Ultrasound-induced scission of mechanocatalysts **6** and **14**

3.3.1.1 GPC investigations of ultrasound-induced scission of mechanocatalysts **6** and **14**

In order to prove the proposed cleavage of one shielding NHC-ligand, ultrasound experiments were performed subjecting solutions of the corresponding polymeric biscarbene catalysts **6** and **14** to sonication while monitoring the molecular weight during the course of the sonication process by GPC. However, to enable a quantification of the ultrasound induced scission, the linearity of the RI-response of the mechanocatalysts **6** and **14** and their corresponding monovalent scission products must be proven at the same concentrations, ensuring that one molecule of **6** respectively **14** have the same RI-response as one molecule of their scission products. For that purpose, a calibration of the RI-signal intensity in respect to the concentration of the polymeric bi- and monovalent species had to be

performed resulting in equations **eq1** for **6** and **eq2** for **14** (for details see Experimental Part 4.9.1 as well as for derivation Appendix 7.11).

$$X = \frac{M_n(\text{determined}) - M_n(\mathbf{6})}{M_n(\mathbf{7}) - M_n(\mathbf{6})} \cdot 100 \quad (\text{eq1})$$

$$X = \frac{M_n(\text{determined}) - M_n(\mathbf{14})}{M_n(\text{determined})} \cdot 100 \quad (\text{eq2})$$

Subsequently, a series of GPC experiments were conducted to investigate the influence of the initial chain length of the mechanocatalysts, the time of applied ultrasound as well as the kind of attached polymer to the scission process of the polymeric biscarbene complexes **6** and **14**. Therefore, mechanophore solutions were prepared in a concentration of 0.75 mM in 30:1 THF/MeOH mixtures and subjected to several ultrasonication cycles applying pulsed ultrasound for 90 min under intensive external cooling with a pulse sequence of 5s pulse-on and 10s pulse-off followed by 60 min without sonication ensuring temperatures below 25°C to avoid undesired thermal effect. Monitoring the molecular weight by GPC revealed a significant decrease during the sonication process (Figure 56): A clear shift to higher retention times and thus lower molecular weights could be observed with increasing sonication time (represented by different numbers of sonication cycles). The dashed lines in Figures 56 show the limit values of the initial, high molecular weight biscarbene complex and the corresponding half-molecular weight scission product, whereat the GPC traces of the proceeding scission are located in between. The shift from the double molecular weight biscarbene complexes **6c** (17200 g/mol; Figure 56A) and **14c** (13600 g/mol; Figure 56B) to the half molecular weight monocarbene moieties (8600 g/mol for **6c** and 6800 g/mol for **14c**) indicates clearly a progressing, symmetric chain scission by cleaving one of the two NHC-ligands during the course of the sonication. A likewise behavior could be observed for the lower molecular weight mechanocatalysts (see Appendix 7.11). The decreasing RI-signal intensity during the cleavage process in case of PIB-based mechanocatalysts **6** and its increase in case of PS-based mechanocatalysts **14** is an effect of the different RI-response for the individual compounds (see Experimental Part 4.9.1 and Appendix 7.11).

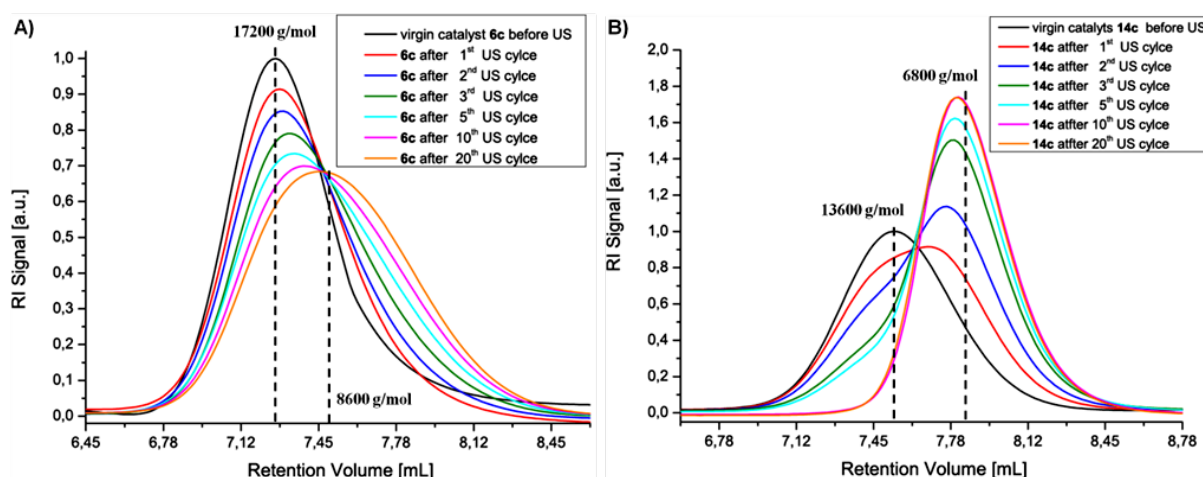


Figure 56. GPC traces of ultrasound induced scission experiments for the polymeric bis-*N*-heterocyclic carbene complexes: A) PIB-based biscarbene catalyst **6c** (17200 g/mol) (virgin - black line) and decreasing molecular weight indicated by increased retention volume after multiple sonication cycles (colored lines). B) PS-based biscarbene catalyst **14c** (13600 g/mol) (virgin - black line) and decreasing molecular weight indicated by increased retention volume after multiple sonication cycles (colored lines). The dashed lines represents the limiting values of the initial, high molecular weight biscarbene complexes and the corresponding half-molecular weight monocarbene moieties.

The quantification of the cleavage efficiencies via **eq1** for **6** and **eq2** for **14** revealed an increased cleavage efficiency with increased initial molecular weight (Table 13, Figure 57 and 58). The highest molecular weight PIB-based catalyst **6c** (17200 g/mol, Table 13 ent. 4) showed after 20 sonication cycles (corresponding to 50 h) a cleavage efficiency of 84%, while in case of the lower molecular weight mechanocatalysts **6b** (8900 g/mol, ent. 3) 55% and for **6a** (4750 g/mol, ent. 2) only 45% of the chains were cleaved after the same sonication time proving thus the more efficient force transmission by longer polymer chains to the labile Cu-NHC bond. Similar observations were made for the PS-based mechanocatalysts: 80% of the higher molecular weight complexes **14c** (13600 g/mol, ent. 10) were cleaved after 20 sonication cycles, while a cleavage efficiency of only 69% respectively 46% could be observed for the corresponding lower molecular weight complex **14b** (11600 g/mol) and **14a** (6800 g/mol) (Table 13). Thus, almost the same cleavage efficiencies could be determined for the PIB- (**6**) and PS-based (**14**) mechanocatalysts using ultrasound for activation. However, the employed PIB-based mechanophores were longer (**6c**: 17200 g/mol) compared to their PS-based counterparts (**14c**: 13600 g/mol), which allow to conclude a more efficient scission for **14** as the obtained cleavage efficiencies were in both cases around 80%. A reasonable explanation for that is the better solvent-polymer interactions of PS (**14**) with THF due to its higher polarity compared to PIB (**6**) which enables a faster coil-to-stretch transformation of the attendant polymer chains and thus a more efficient force transmission (theoretical background see Chapter 1.2.1).

Table 13. Cleavage of PIB-based mechanocatalysts **6a-c** as well as PS-based mechanocatalysts **14a-c** with different initial molecular weights applying either ultrasound or thermal energy to activate the labile Cu-NHC bond of the biscarbene catalysts (for time dependent investigations see Experimental Part 4.9.2).

Ent.	mechano- phore	US cycles ^{a)}	t [h]	T [°C]	solvent	M _n (GPC) ^{b)}		PDI ^{b)}		cleaved mechanophores ^{c)} [%]
						initial	end	initial	end	
PIB-based mechanocatalysts 6										
1	6c	-	168	20	THF/MeOH	17500	17500	1.30	1.31	0
2	6a	20	50	20	THF/MeOH	4750	3600	1.60	1.76	45
3	6b	20	50	20	THF/MeOH	8900	6600	1.25	1.52	55
4	6c	20	50	20	THF/MeOH	17200	10000	1.23	1.47	84
5	6c	20	50	20	THF	17450	16450	1.23	1.24	11
6	6c	-	72	65	THF/MeOH	17500	8950	1.29	1.49	97
PS-based mechanocatalysts 14										
7	14c	-	168	20	THF/MeOH	13600	11360	1.18	1.19	0
8	14a	20	50	20	THF/MeOH	6800	4450	1.20	1.42	46
9	14b	20	50	20	THF/MeOH	11600	5950	1.32	1.42	69
10	14c	20	50	20	THF/MeOH	13600	7900	1.19	1.26	80
11	14c	-	72	65	THF/MeOH	13600	7600	1.18	1.28	88

^{a)}Ultrasonication cycle: 90 min sonication with 30% of max. amplitude of 125 μm with pulse sequence 5s on, 10s off and 60 min without sonication and a sonication power intensity of 8.75 W cm^{-2} corresponding to an energy input of 21 kJ per US cycle..

^{b)}Determined by GPC in HPLC-grade THF using PIB standards for **6** and PS standards for **14**. ^{c)}Determined after 20 sonication cycles (50h) for entries 1-4 and after 72h for entries 5-6 from GPC values according to equation eq1 and after 20 sonication cycles (50h) for entries 7-9 and after 72h for entries 10-11 from GPC values according to equation eq2.

Moreover, mechanocatalysts with longer polymer chains (e.g. **6c** or **14c**) showed a significant faster molecular weight degradation compared to those with shorter appended polymer chains (**6a** respectively **14a**; see Figure 57 as well as Figure 58), proving thus that increased chain length favor

the transmittance of force, culminating finally in bond-cleavage of the most labile bond close to the midst point of the polymer chain^{4; 6; 13; 34; 96; 103}. Additionally, a broadening of the molecular weight distribution (PDI) e.g. from 1.2 to 1.5 for **6c** could be observed (Table 13).

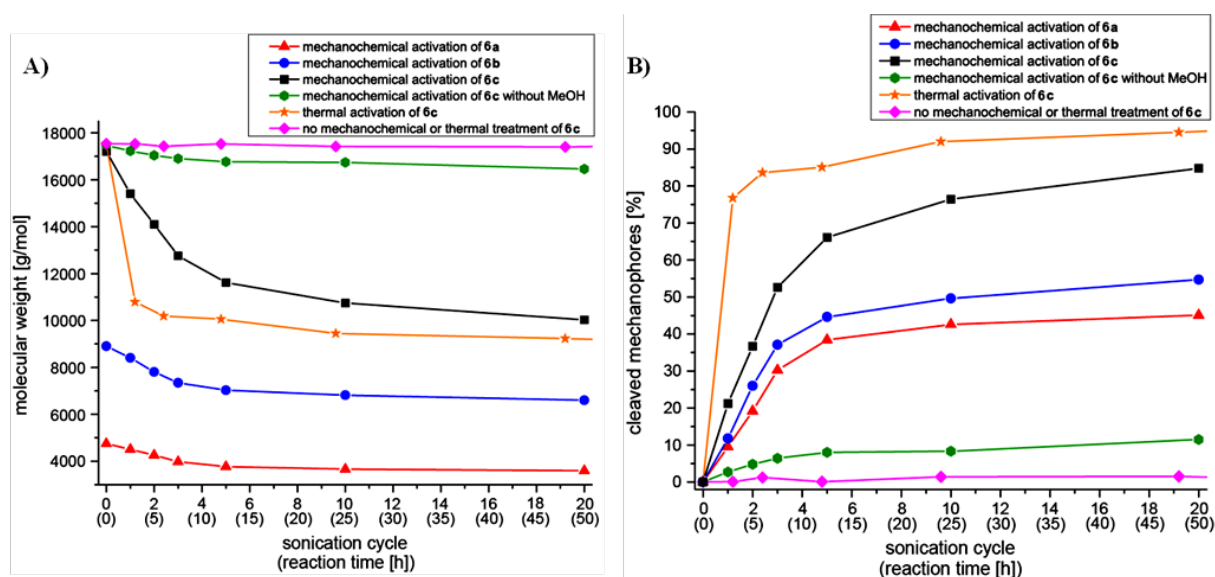


Figure 57. Quantification of the cleavage efficiencies for the PIB-based bis-*N*-methylimidazol-2-ylidene complexes **6**: A) GPC-determined molecular weight in dependency of the performed sonication cycles for the individual mechanocatalysts **6** performed under different conditions; B) cleavage efficiencies of **6** determined by **eq1** in dependence of the applied ultrasonication cycles under different conditions.

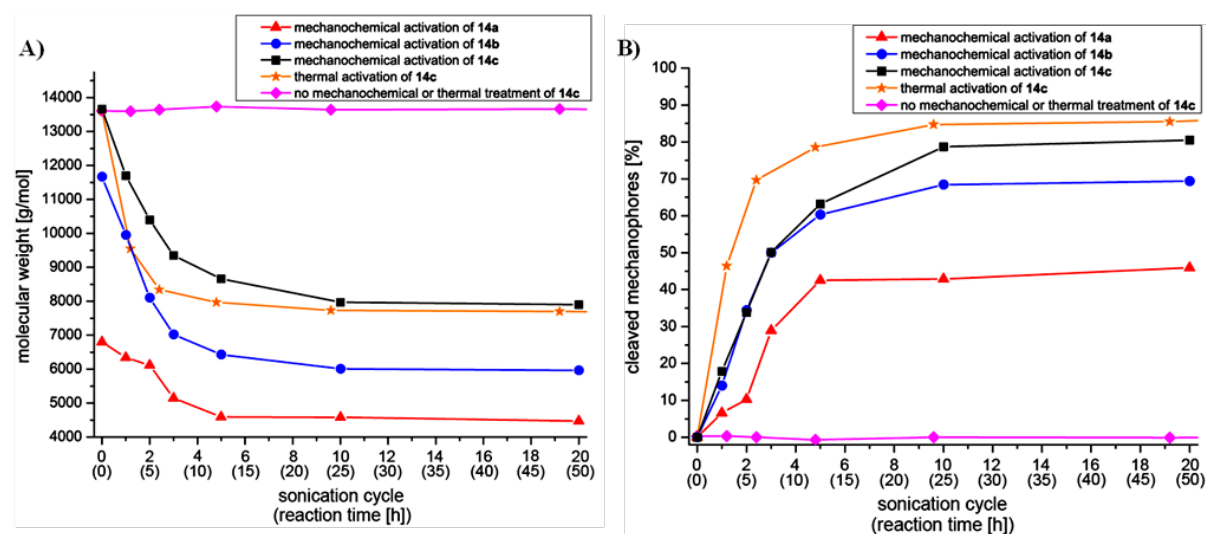


Figure 58. Quantification of the cleavage efficiencies for the PS-based bis-*N*-methylimidazol-2-ylidene complexes **14**: A) GPC-determined molecular weight in dependency of the performed sonication cycles for the individual mechanocatalysts **14** performed under different conditions; B) cleavage efficiencies of **14** determined by **eq2** in dependence of the applied ultrasonication cycles under different conditions.

Control experiments were performed stirring the mechanophore solution for 7 days at room temperature without ultrasound application while monitoring the molecular weights by GPC. However, in all cases no significant chain scission could be observed (Table 13 ent. 1 and 7) proving thus the stability of the mechanocatalysts and give a first hint for its latency.

The mechanocatalysts **6** were subjected to ultrasound applying several sonication cycles performed likewise to the GPC experiments described above. The concentration of **6** was adjusted to 0.75 mM in THF-d8/MeOH 30:1 solution and the $^1\text{H-NMR}$ spectra were determined before ultrasonication (US) and after the 1st, 2nd, 3rd, 5th 10th and 20th US cycle (each cycle correlates to 150 min) and are shown in Figure 61, while Figure 60 depicts the discussed structures and the appropriate assignments. The shown spectra are excerpts of the full spectra pointing out the most decisive signal shifts for the investigated scission of the mechanocatalysts. The assignments and labeling (d, l, k and i) were made according to the individual $^1\text{H-NMR}$ spectra obtained during the synthesis of **5**, **6** and **7** which were discussed in Chapter 3.1 Figure 48.

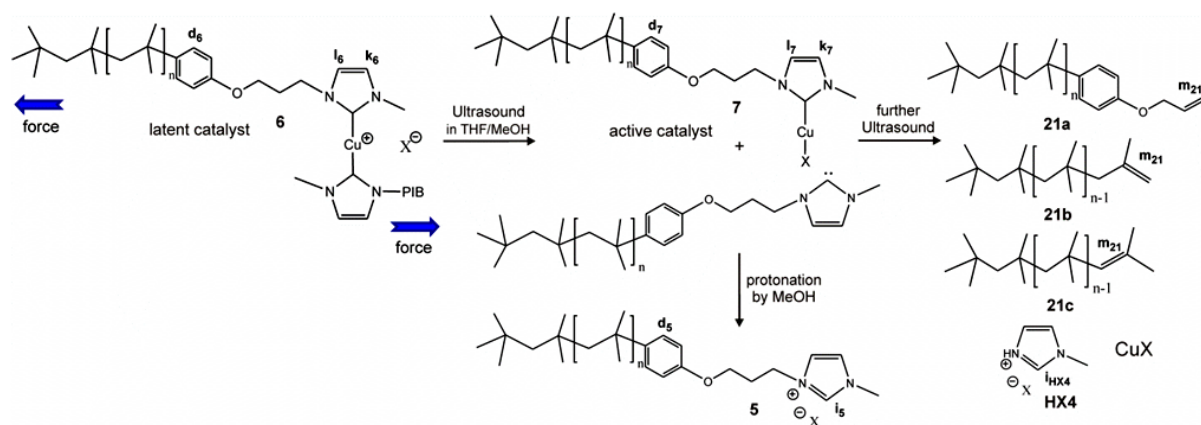


Figure 60. Obtained products during the ultrasound-induced scission of the latent PIB-based mechanophores **6** generating the desired active monocarbene catalyst **7** and the free polymeric carbene which is immediately protonated by MeOH leading to the formation of the *N*-methylimidazolium telechelic PIB **5**. Further application of ultrasound led to the elimination of the propoxyphenyl respectively the *N*-methylimidazolium endgroup generating thus PIB with terminal double bonds (**21**).

The $^1\text{H-NMR}$ spectrum of the virgin bis-*N*-methylimidazolium-2-ylidene copper(I)X mechanocatalyst **6c** (Figure 61) displayed before sonication in the selected range solely the two signals of the *NCH-CHN* groups of the imidazol-2-ylidene scaffold at 6.20 (k_6) and 6.25 ppm (l_6) as well as the resonance at 6.81 ppm corresponding to the both CH-groups of the phenoxy group (d_6). Ultrasonication up-to the 2nd sonication cycle led to an increasing amount of the cleaved monocarbene species **7** (Figure 62), indicated through the appearing resonances at 6.40 (k_7) and 6.63 ppm (l_7) as well as of the phenoxy group at 6.75 ppm (d_7). The simultaneously formed and through MeOH protonated NHC-macro ligand **5** was obtained displayed, by the proton of the *NCHN*-group (i_5) at 9.98 ppm as well as of the phenoxy group (d_5) at 6.85 ppm), which prove the specific cleavage of the Cu-carbene-bond in the mechanophore **6** (Figure 60). After the 3rd sonication cycle the intensity of the monocarbene species **7** decreased until its complete disappearance after the 10th cycle (Figure 61 and Figure 62) revealing a further decomposition of the Cu(I)-monocarbene complex **7** as a kind of background reaction with continuing ultrasonication. The additional and during the cures of the sonication continuously increasing resonances at 8.98 ppm (i_{HX4}) and around 5.75 ppm (m_{21}) can be assigned to the decomposition products **HX4** and **21a-c** (Figure 62), which were formed either through the elimination of the methylimidazol-2-ylidene end group (**HX4** and **21a**) or the complete elimination of the methylimidazol-2-ylidene bearing phenoxy end group from the PIB chain generating internal and terminal double bonds (**21b** and **21c**) (see Figure 60). These observations proved a change in the decomposition pathway of the latent mechanocatalysts **6** after the third sonication cycle from the desired ultrasound induced cleavage into **5** and **7** to a destructive mechanism leading to a breakdown of the polymer-carbene scaffold and is thus in compliance with the obtained results of the previously discussed GPC investigations.

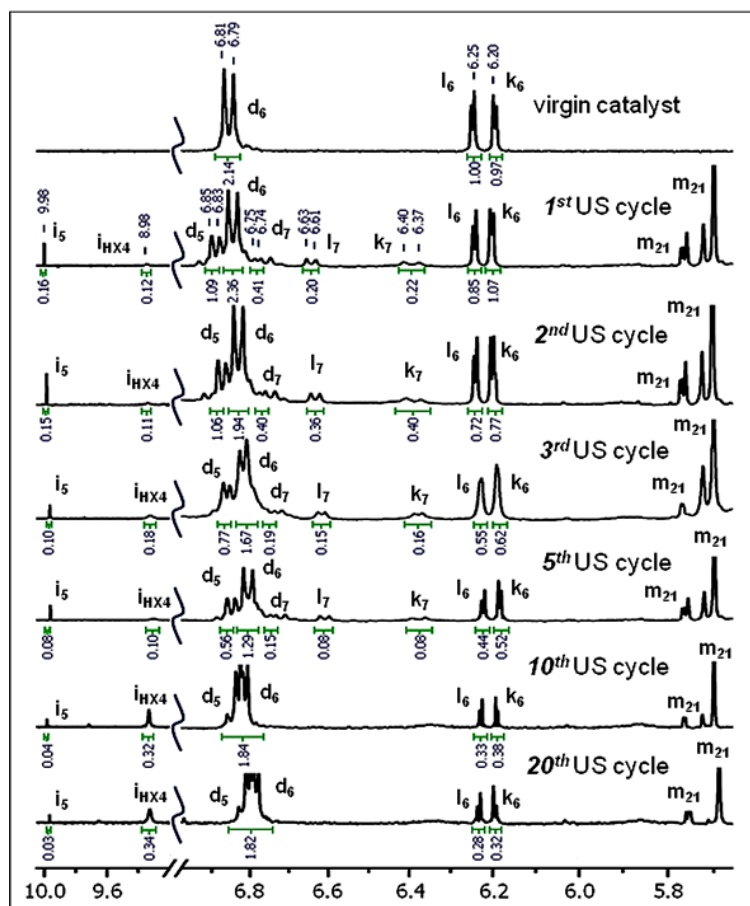


Figure 61. $^1\text{H-NMR}$ spectroscopic investigations of mechanochemical activation from the PIB-based bis-*N*-methylimidazol-2-ylidene copper(I)*X* complex $[\text{Cu}(\text{PIB-NHC})_2]\text{X}$ (**6c**) in dependence of the applied ultrasound (US) cycles. The formation of the desired monocarbene complex **7** as well as the cleaved and through MeOH protonated polymeric NHC-ligand **5** could be observed within the first three US cycles, while after the fifth cycle the decomposition products **21** were formed predominantly by elimination of the phenoxypropyl or *N*-methylimidazolium endgroup (**4**). The shown spectra are excerpts of the full spectra pointing out the most decisive signal shifts for the investigated scission of the mechanocatalysts and were recorded in THF- d_8 /MeOH 30:1.

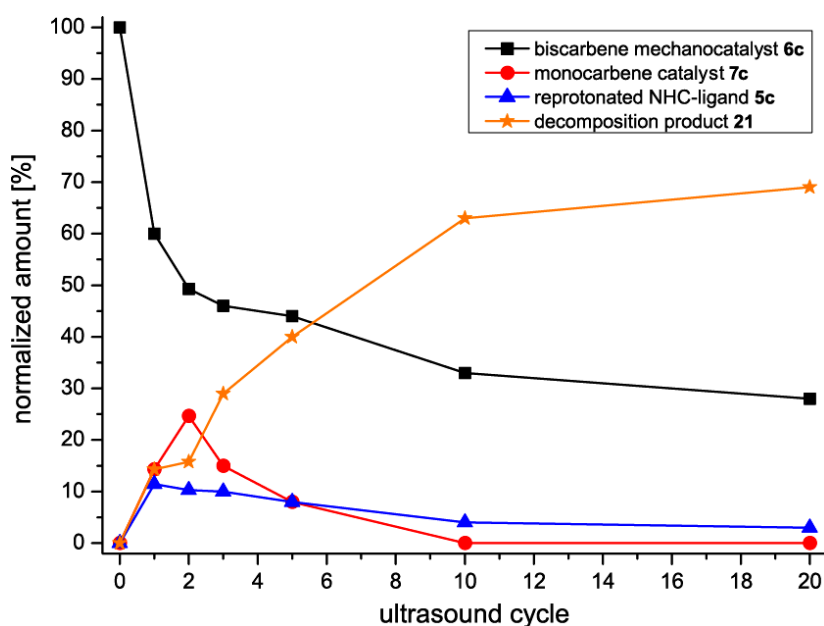


Figure 62. Quantification of the normalized amount of the obtained species (**5**, **6**, **7** and **21**) during the ultrasonication of the PIB-based biscarbene Cu(I)*X* complexes **6** according to the $^1\text{H-NMR}$ spectroscopic investigations.

Similarly, the thermally induced scission of the mechanocatalysts **6** observed during the previously discussed GPC investigations were studied by $^1\text{H-NMR}$ spectroscopy. For that purpose, a 0.75 mM solution of **6** in THF-d₈/MeOH was heated to 65°C and the NMR samples were taken after 3, 6, 12, 24, 48 and 72h. The thus obtained $^1\text{H-NMR}$ spectra (Figure 63) revealed strong changes after three hours heating at 65°C in compliance to the observed chain scission determined by the GPC investigations. Instead of the formation of the Cu(I)-monocarbene species **7**, the formation of the re-protonated *N*-methylimidazol-2-ylidene telechelic PIB macroligand **5** at 9.98 ppm (i_5) as well as the elimination products **HX4** at 8.85 ppm (i_{HX4}) and **21a-c** around 5.75 ppm (m_{21}) were observed. These results imply a decomposition of the initial biscarbene copper(I) complexes **6** without the intermediate activation of the catalyst under formation of the catalytic active Cu(I)-monocarbene species **7**.

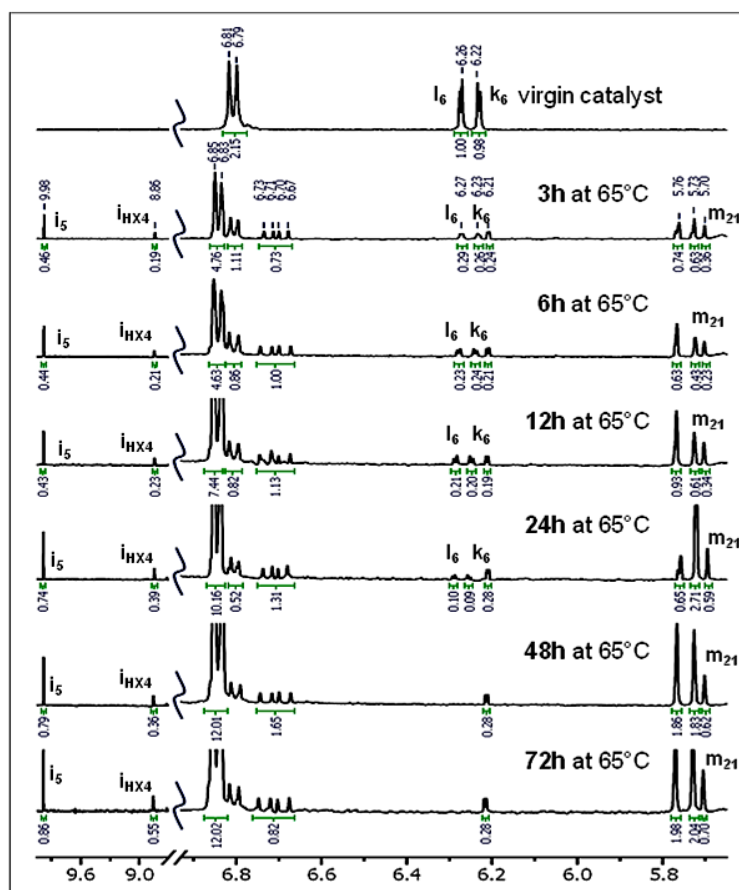


Figure 63. $^1\text{H-NMR}$ spectroscopic investigations of thermal control experiments treating the PIB-based bis-*N*-methylimidazol-2-ylidene copper(I)X complex $[\text{Cu}(\text{PIB-NHC})_2]\text{X}$ (**6c**) at 65°C in THF-d₈/MeOH 30:1 revealed a decomposition of the mechanocatalyst **6** without intermediate formation of the desired active monocarbene complex **7**. The shown spectra are excerpts of the full spectra pointing out the most decisive signal shifts for the investigated decomposition of the mechanocatalysts **6**.

Furthermore, the formation of solid particles could be observed during the sonication as well as the thermal decomposition process and flame atomic absorption spectroscopy (FAAS) proved the presence of copper in significant amounts within the particles. Probing the exact nature of the copper species via STEM-EDXS measurements revealed the presence of Cu and O in a ratio of 63.4 : 36.6 ($\approx 2 : 1$), indicating the formation of copper(I)-oxide (Cu_2O) (Figure 64). The small, brighter region on the left side of the particle consist predominantly out of Cu_2O but contains also Cu(II) halides (Br, I). The formation of these copper nanoparticles supports the decomposition of the Cu(I)-monocarbene complex **7** by ultrasound in the presence of oxygen traces. Blind experiments in the absence of ultrasonication or thermal treatment were performed without significant changes in $^1\text{H-NMR}$ spectra or the formation of particles even after one week.

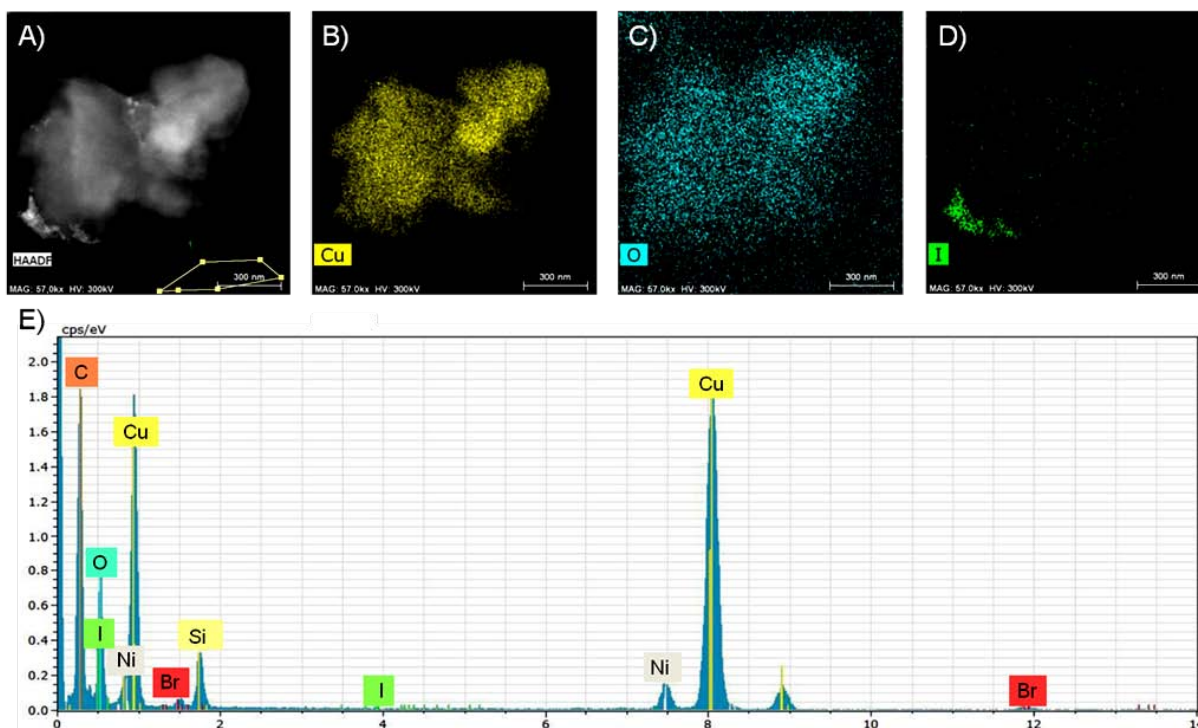
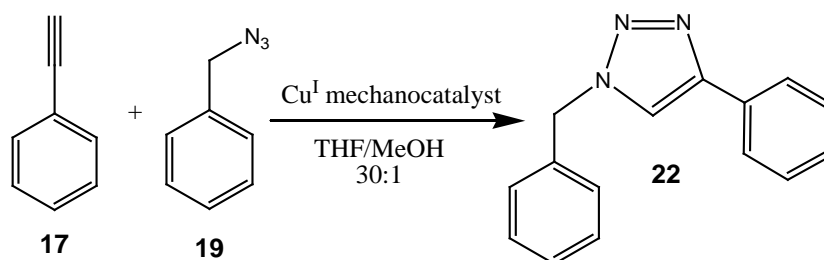


Figure 64. STEM-EDX measurements of Cu-precipitates obtained during cleavage of mechanophores **6** indicating the formation of copper(I)-oxide (Cu_2O) as well as Cu(II) halides (Br, I). A - D) STEM-EDXS measurements of different elements; E) STEM-EDXS spectra of the central region of the particle.

3.3.2 Mechanochemical triggered CuAAC “click” reaction of benzyl azide (**19**) and phenylacetylene (**17**) using latent mechanocatalysts

In order to investigate the catalytic activity of the initial as well as the activated mechanocatalysts **6** and **14** in solution, a model copper(I)-catalyzed alkyne/azide “click” reaction (CuAAC) of phenylacetylene (**17**) with benzyl azide (**19**) was performed (Figure 65) and monitored through *in situ* ^1H -NMR-spectroscopy. Additionally the activation behavior of the monocarbene catalyst **7** was investigated figuring out the catalytic activity even without attached second shielding NHC-ligand.



Scheme 65. Model “click” reaction of phenylacetylene (**17**) with benzyl azide (**19**) in order to determine the activation of latent mechanocatalysts **6** and **14** by *in situ* ^1H -NMR spectroscopic investigations.

For that purpose, the biscarbene mechanophores **6** and **14** as well as the monocarbene complexes **7** were dissolved either in pure THF- d_8 or THF- d_8 /MeOH (30:1) mixtures and subjected in concentrations of 0.75 mM in presence of 100 eq. **17** and **19** to several ultrasonication cycles and the conversion of the “click” reaction was determined by *in-situ* ^1H NMR spectroscopy after the 1st, 2nd, 3rd, 5th and 10th cycle monitoring the increasing triazole resonance at 8.12 ppm as well as the shift of the CH_2 resonance from 4.34 to 5.58 ppm (time-dependent ^1H -NMR spectra are presented in

Appendix 7.13). The obtained results are summed-up in Table 14 and are depicted in Figures 67 - 69. Blind experiments proved no “click” reaction of **17** and **19** without Cu(I) catalyst treating them with or without ultrasound excluding thus any influence of the ultrasound to the alkyne-azide cycloaddition reaction (Table 14 ent. 1 and 2).

Table 14. Time and sonication cycle dependent investigation of click reaction from phenylacetylene (**17**) and benzyl azide (**19**) using either PIB-based biscarbene [Cu(PIB-NHC)₂]X catalysts (**6**) or monocarbene [Cu(PIB-NHC)]X catalysts (**7**), PS-based biscarbene [Cu(PS-NHC)₂]X catalysts (**14**) as well as model complex **10**^{a)} (sonication cycle dependent values are given in the Experimental Part).

Ent	type of catalyst	type of activation	Cu(I) catalyst	M _n (GPC) [g/mol]	solvent	T [°C]	t _{End} [h]	US cycles ^{b)}	final conversion [%] ^{c)}	
1	no catalyst	A	Blind experiments	without	-	THF/MeOH	20	168	off	0
2				without	-	THF/MeOH	20	168	10	0
3				without	-	THF/MeOH	65	72	off	2
4	PIB-based catalysts	B	Control experiments without US	6a	4750	THF/MeOH	20	168	off	0
5				6c	17200	THF/MeOH	20	168	off	0
6				7a+Asc^{d)}	2900	THF/MeOH	20	7.5	off	11
7				7b	4800	THF/MeOH	20	25	off	0
8	PIB-based catalysts	C	Mechanochemical activation	6a	4750	THF	20	7.5	3	2
9				6a	4750	THF/MeOH	20	25	10	11
10				6b	8900	THF/MeOH	20	25	10	19
11				6c	17200	THF/MeOH	20	25	10	28
12				D	Thermal activation	6a	4750	THF/MeOH	65	72
13	6c	17200	THF/MeOH			65	72	off	3	
14	B	Control experiments without US	14c	13600	THF/MeOH	20	144	off	0	
15	PS-based catalysts	C	Mechanochemical activation	14a	6800	THF/MeOH	20	25	10	23
16				14b	11600	THF/MeOH	20	25	10	34
17				14c	13600	THF/MeOH	20	25	10	52
18				D	Thermal activation	14c	13600	THF/MeOH	65	72
19	Model catalyst	B+D	Control experiments and thermal activation	10	-	THF/MeOH	20	24	off	2
20				10	-	THF/MeOH	65	24	off	39
21	Model catalyst	C	Mechanochemical activation	10	-	THF/MeOH	20	25	10	49
22				10+Asc^{d)}	-	THF/MeOH	20	25	10	40
23				10	-	THF	20	25	10	17
24				10+Asc^{d)}	-	THF	20	25	10	8

^{a)}For all reaction an equimolar mixture of **17** and **19** in either pure THF-d₈ or THF-d₈/MeOH 30:1 where used together with 0.01 equiv. of mechanocatalyst **6**, **7**, **10** or **14** (c = 0.75 mM). ^{b)}Each ultrasonication cycle consists of 90 min sonication with 30% of max. amplitude of 125 μm with pulse sequence of 5 s on, 10 s off and 60 min without sonication corresponding to a sonication power intensity of 8.75 W/cm² and an energy input of 21 kJ per US cycle. ^{c)}Determined by ¹H-NMR spectroscopy in THF-d₈/MeOH 30:1 monitoring the increasing triazole resonance at δ=8.12 ppm as well as the shift of the CH₂ resonance from δ=4.34 to 5.58 ppm. ^{d)}1.1 eq. Na/ascorbate were additionally used for “click” reaction of **7a** and **10**.

First of all, the true latent nature of the PIB- (**6**) and PS-based (**14**) mechanocatalysts was proven as no catalytic activity towards the CuAAC of **17** with **19** could be determined without applied ultrasound or thermal treatment even after one week (Table 14 ent. 4, 5 and 14). Thus, it is in good compliance with the previously performed GPC and ¹H-NMR spectroscopic investigations, which also revealed no cleavage of the mechanophores **6** and **14** under silent conditions at ambient temperatures.

Even heating the catalysts **6** or **14** to a temperature of 65°C induced only an extremely poor activity of 3% conversion in the “click” reaction for **6** (Table 14 ent. 13 and 14) and 4% in case of **14** (ent. 18) and is thus in the range of the thermal 1,3-dipolar Huisgen cycloaddition which showed 2% “click” conversion (ent. 3). Hence, the reduction of the molecular weight observed in GPC experiments during the thermal scission of the mechanocatalysts **6** and **14** does not lead to no significant formation of the catalytic active Cu(I) monocarbene species, as also discussed via ¹H-NMR spectroscopic investigations above.

However, subjecting the biscarbene catalysts **6** and **14** to ultrasonication introduced the desired catalytic activity (Table 14 ent. 9 – 11 and 15 – 17) as the applied force led according to the previously discussed GPC and ¹H-NMR spectroscopic investigations to a cleavage and protonation of one of the shielding polymeric-NHC ligands (**5**, **13**), activating in turns the initially latent catalysts under formation of an active Cu(I)-monocarbene moiety (**7**, **15**) (Figure 66).

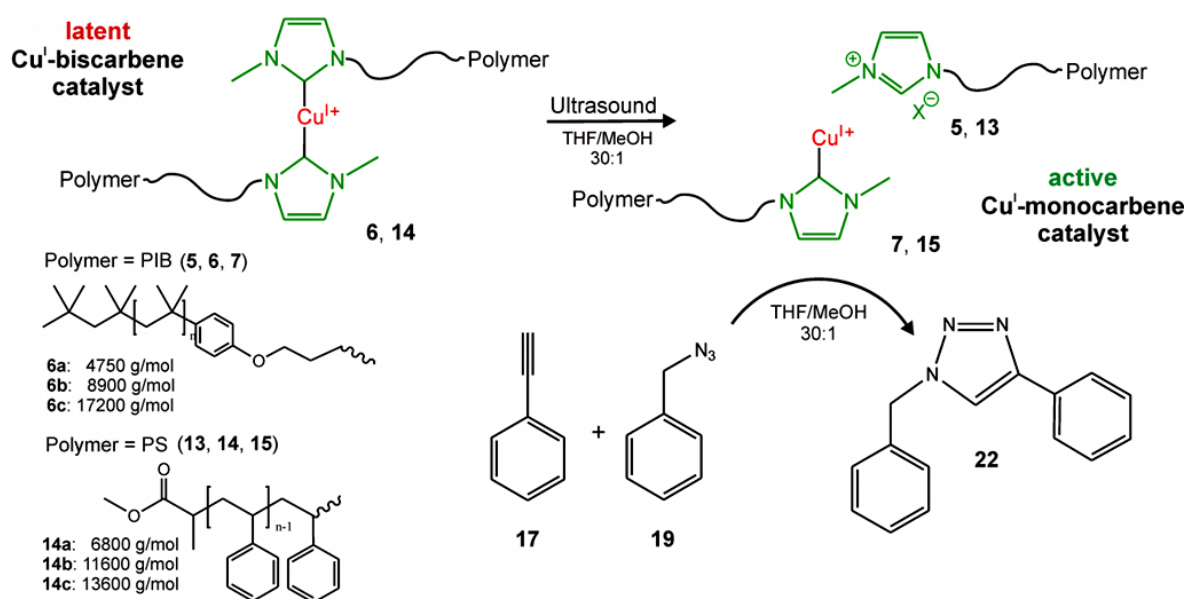


Figure 66. Mechanochemical activation of the polymeric bis(*N*-methylimidazol-2-ylidene) copper(I)X complexes **6** and **14** by ultrasound in solution leading to the scission of the labile Cu(I)-NHC bond and the cleavage of one shielding NHC-ligand generating thus a catalytic active site which is able to trigger the CuAAC of phenylacetylene (**17**) and benzyl azide (**19**).

The observed catalytic activity scaled directly with the initial chain-length of the attached polymer chains: An increasing molecular weight from 4750 g/mol (**6a**) to 17200 g/mol (**6c**) led in case of the PIB-based biscarbene catalyst **6** to an increased “click” conversion from 11 to 28% after 10 sonication cycles (Table 14 ent. 9 – 11; Figure 67), while in case of the PS-based mechanophores **14** an enhanced “click” conversion from 23 to 52% could be observed increasing the molecular weight from 6800 g/mol (**14a**) to 13600 g/mol (**14c**) (Table 14 ent. 15 – 17; Figure 68). PS-based mechanocatalysts **14** revealed thus a higher reactivity compared to their PIB-based counterparts **6** even at lower molecular weight, due to their higher rigidity and better solvent-polymer interactions (for theoretical considerations see Chapter 1.2.1).

Moreover, analyzing the time dependent ¹H-NMR measurements revealed a flattened, non-linear increasing of the “click” conversion after the third sonication cycle converging to a plateau value, irrespective of the initial molecular weight of the mechanophore (Figure 67 and 68). Thus, it is in compliance with the observations of GPC as well as the ¹H-NMR investigations described before, where the amount of the monocarbene-species decreased after the third cycle significantly and disappear finally after the fifth sonication cycle.

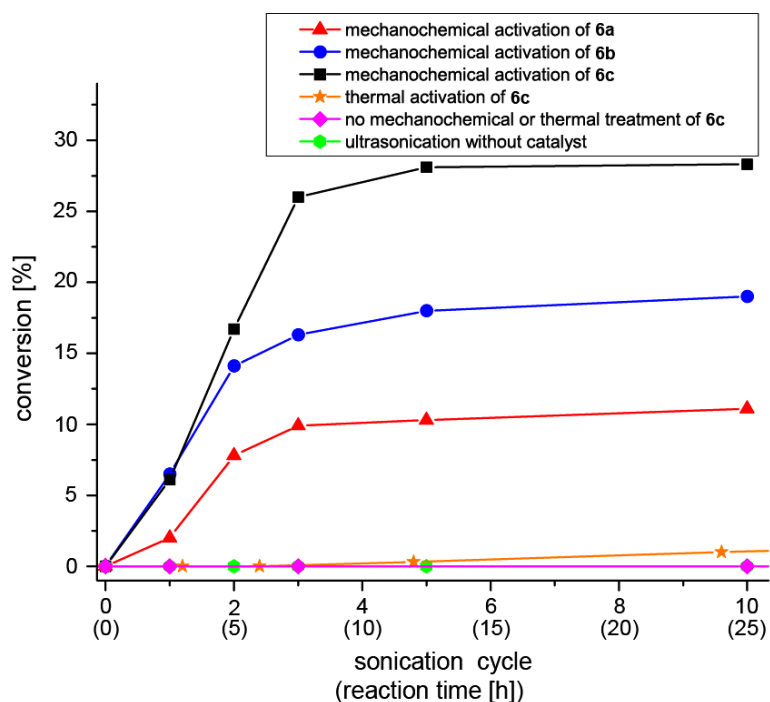


Figure 67. Time and sonication cycle dependent investigation of click reaction from an equimolar mixture of phenylacetylene (**17**) and benzyl azide (**19**) in THF/MeOH 30:1 (75 mM) using the PIB-based biscarbene catalysts $[\text{Cu}(\text{PIB-NHC})_2]\text{X}$ (**6**) (0.75 mM) under sonication or pure thermal activation (for more detailed information see Experimental Part 4.9.4 as well as Appendix 7.13).

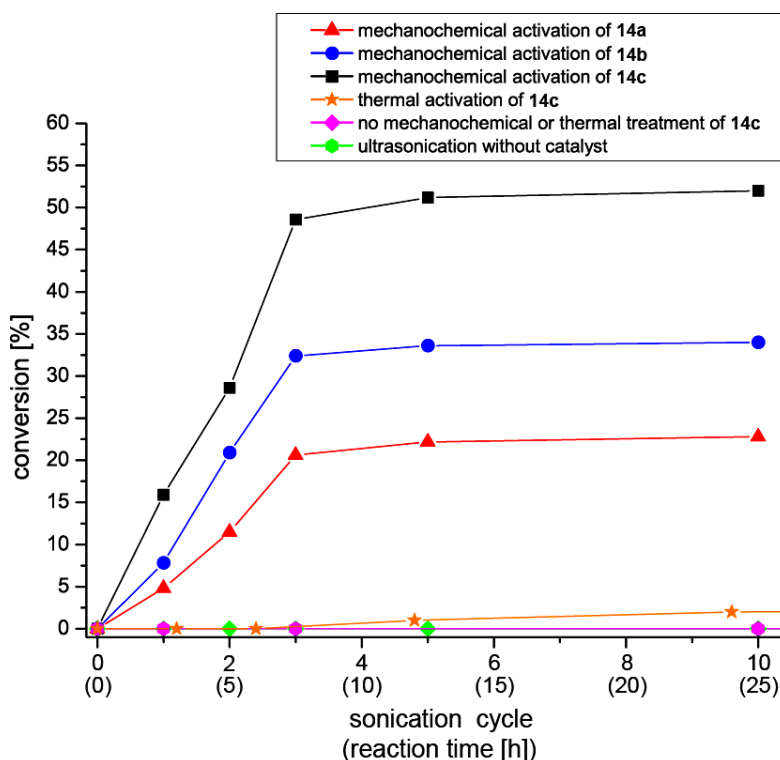


Figure 68. Time and sonication cycle dependent investigation of click reaction from an equimolar mixture of phenylacetylene (**17**) and benzyl azide (**19**) in THF/MeOH 30:1 (75 mM) using the PS-based biscarbene catalysts $[\text{Cu}(\text{PS-NHC})_2]\text{X}$ (**14**) (0.75 mM) under sonication or pure thermal activation (for more detailed information see Experimental Part 4.9.4 as well as Appendix 7.13).

Furthermore, the effect of methanol addition was investigated as it was already been proven by conducted GPC experiments (see Chapter 3.3.1.1), that MeOH is able to protonate the cleaved free polymeric *N*-heterocyclic carbenes and prevents thus the otherwise possible back reaction with the Cu(I)-monocarbene complexes **7** and **15** re-forming the latent biscarbene mechanocatalysts. Accordingly, the addition of MeOH increased the amount of cleaved mechanophores significantly (e.g. for **6c** 84% in THF/MeOH compared to 11% in pure THF; Table 13 ent. 4+5). Using pure THF-d8 as solvent for the ultrasound triggered CuAAC “click” reaction of **17** with **19** showed a significant lower conversion of only 2% compared to 11% when THF-d8/MeOH 30:1 mixtures were used (Table 14 ent. 8 and 9).

Moreover, the PIB-based monocarbene complexes **7** were tested within the CuAAC of **17** and **19** revealing a catalytic activity even without applied ultrasound, as no shielding second ligand blocks the catalytic active site of the copper. For instance, the monocarbene catalyst **7a** (2900 g/mol) showed without applied ultrasound a “click” conversion of 11% (Table 14 ent. 6), which is exactly the same as obtained subjecting the corresponding biscarbene mechanophore **6a** (4750 g/mol) to 10 ultrasonication cycles (11%; ent. 9).

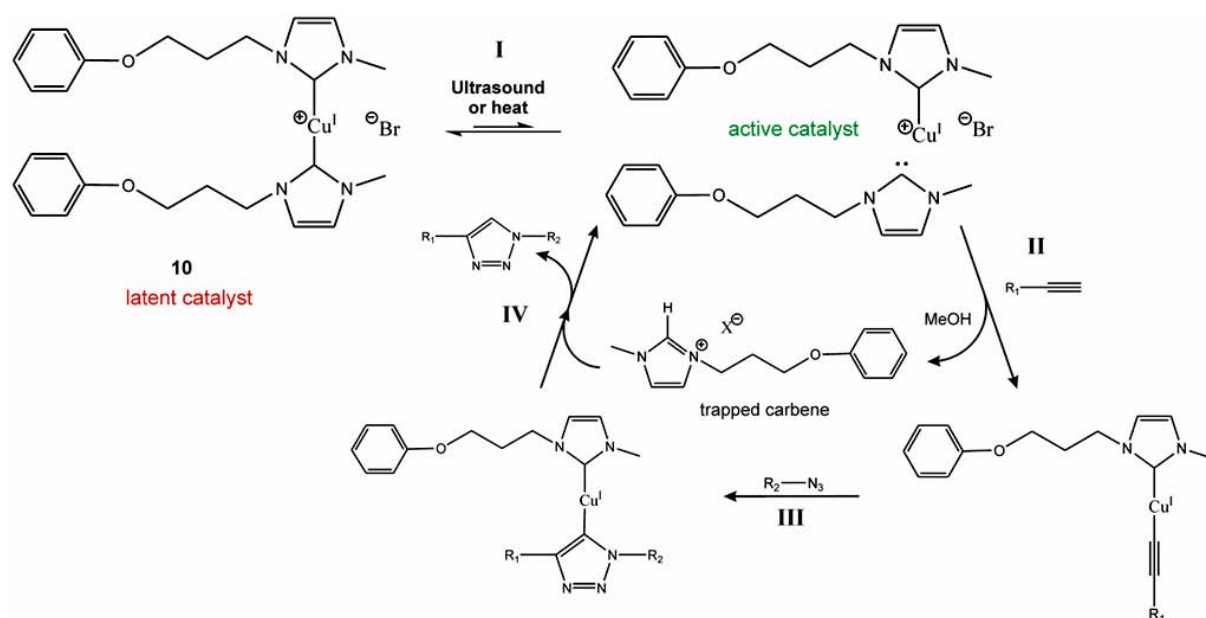


Figure 69. During the mechanochemical and thermal activation of the latent model complex **10** one shielding NHC-ligand is cleaved (I) and re-protonated forming the a monocarbene copper(I) acetylene structure as well as the trapped carbene (II). The subsequent cycloaddition with the azide compound (III) yielded after the protonation with by means of the trapped carbene the final triazole product (IV).

Additionally, the reactivity of a model biscarbene Cu(I) complex (**10**) without attendant polymer chains (Figure 69) was investigated towards the CuAAC of **17** with **19** (Figure 70). Expectedly, **10** showed at room temperature only a low catalytic activity of 2% when no ultrasound was applied (Table 14 ent. 19). As **10** has no polymer chains attached which would enable the transmission of the applied force to the most labile bond, a lower activation efficiency and thus in turns a lower catalytic activity could be expected triggering the catalyst by ultrasound or thermal treatment. However, subjecting **10** in the presence of **17** and **19** to ultrasonication revealed a strongly increased reactivity yielding “click” conversions of 49% in THF:MeOH mixtures (Table 14 ent. 21; Figure 70). The reason for that is the missing bulkiness of the attached polymer chains which prevent the replacement of the second NHC-ligand on the copper(I) center by the alkyne moiety enabling thus the initiation of the catalytic cycle (Figure 69; for more detailed information see Chapter 1.5). Accordingly, thermal

treatment introduced also a catalytic activity which triggered the “click” reaction with 39% conversion (Table 14 ent. 20).

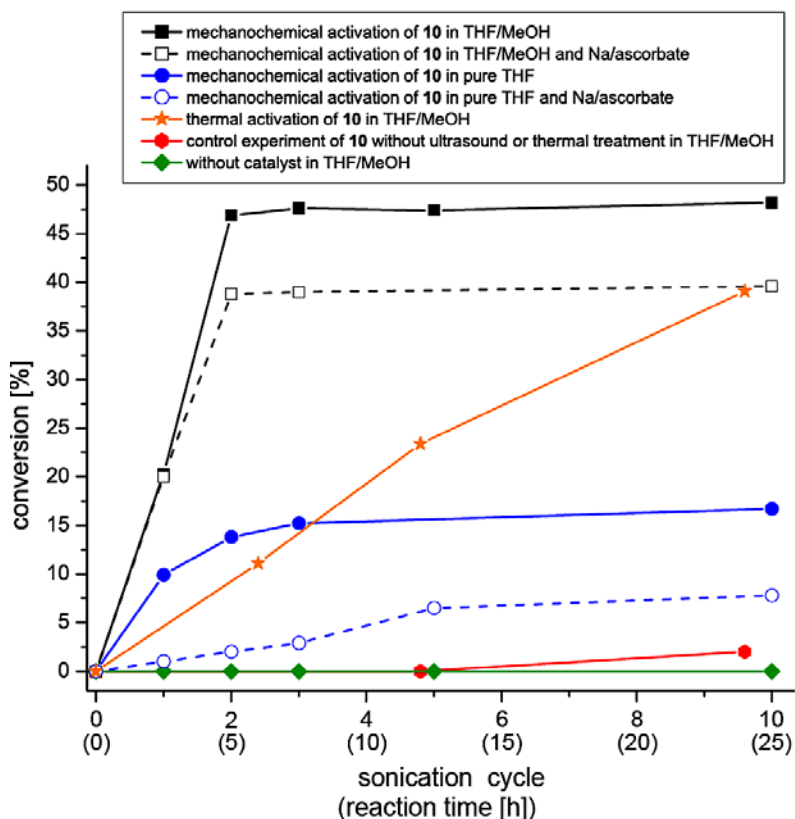


Figure 70. Time and sonication cycle dependent investigation of click reaction from an equimolar mixture of phenylacetylene (**17**) and benzyl azide (**19**) in THF/MeOH 30:1 (75 mM) using the model biscarbene catalysts $[\text{Cu}(\text{BPB-NHC})_2\text{X}]$ (**10**) (0.75 mM) under sonication or pure thermal activation (for more detailed information see Experimental Part 4.9.4).

These results were supported comparing the energy minimized 3D-structures of the model catalyst **10** (Figure 71A) (without polymer chains; $n = 0$) with the corresponding PIB-based catalysts **6** (B: $n = 10$; C: $n = 20$). Increasing the chain length of the attached polymers increased in turns their bulkiness which enabled a much better shielding of the active copper(I) center as illustrated in Figure 71. The red labeled copper(I) center is almost perfect covered increasing the chain length about 20 monomer units. Thus, the complete latency of polymeric catalysts **6** compared to the low molecular weight model complex **10** could be explained as the degree of polymerization for all synthesized mechanophores is higher (**6a**: $n = 40$; **6b**: $n = 77$; **6c**: $n = 151$).

Also the potential thermal activation of the low molecular weight model complex **10** compared to the polymeric mechanophores **6** and **14** could be explained as the elongated polymer chains strongly restrict the thermal movement of the copper covering propoxyphenyl respectively phenyl groups preventing thus its thermal activation, albeit the complete absence of the thermal activation is in case of **6** and **14** more likely due to its previous decomposition.

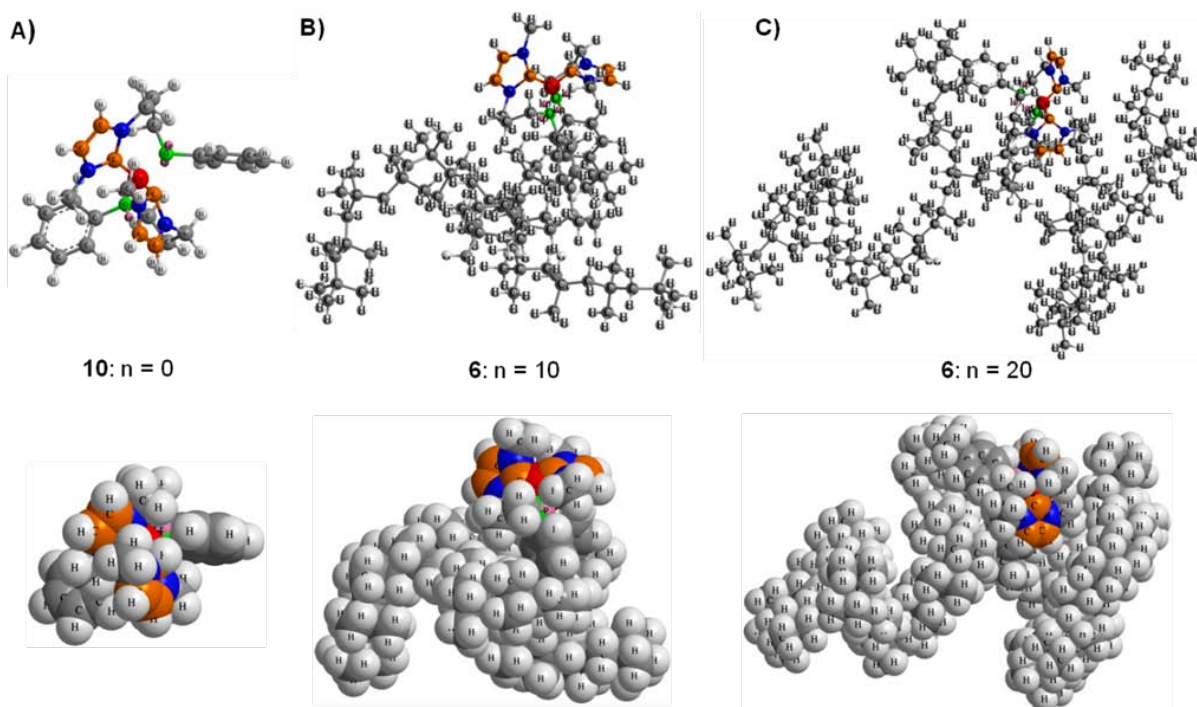


Figure 71. Energy minimized 3D-structures of (A) the model catalyst **10** (without polymer chains; $n = 0$) as well as of mechanocatalysts **6** with increased attached PIB chains (B) $n = 10$ and (C) $n = 20$ assuming an attractive propoxy-copper interaction. The upper row shows the modeled structures in the clear stick-ball view, while the bottom row shows the space filling view. The copper atoms are highlighted in red, the nitrogen atoms in blue, the oxygen atoms in green and the carbon atoms of the imidazol-2-ylidene scaffold orange other carbon atoms are marked dark gray, while hydrogen atoms are shown in bright gray.

Moreover, the effect of the MeOH addition was investigated for the model complex **10**: Likewise to the polymer based mechanophores **6** and **14**, the catalytic activity of **10** increased significantly from 17% to 49% when MeOH was added (Table 14 ent. 21 and 23; Figure 70). To exclude the literature known reduction effect of MeOH from Cu(II) to Cu(I)²²¹⁻²²³, sodium ascorbate (Asc.) were added as a well known alternative reducing agent for Cu(II)^{172-173; 184}. The determined “click” conversion of **17** and **19** using **10** in prescience of sodium ascorbate within pure THF-d8 was with only 8% (Table 14 ent. 24) even lower than without sodium ascorbate (17%; ent. 23) proving thus that the acceleration by the MeOH addition did not based on the reduction of partially oxidized Cu(II) to Cu(I). Instead, the aforementioned re-protonation of the cleaved free carbene ligand is the reason for an accelerated “click” reaction applying THF/MeOH solvent mixtures as it prevents the back reaction of the monocarbene complexes with the NHC to the corresponding biscarbene complexes and shifts thus the equilibrium to the side of the catalytic active monocarbene complexes. This observation was further supported as the additional use of sodium ascorbate (Asc.) within the THF/MeOH mixtures revealed no acceleration of the “click” reaction (49% without Asc., 40% with Asc.; Table 14 ent. 21 and 22).

3.3.3 Mechanochemical activation of latent catalysts in solid state by compression

Finally and most importantly, the mechanochemical activation was probed within a real solid polymer matrix, devoid of any solvent. As it is known that an optimal transmittance of mechanochemical force is achieved when the structural polymer contains crystalline regions. Thus, high molecular weight poly(tetrahydrofuran) (PTHF)¹⁹ ($M_{n,(GPC)} = 112\ 000\ \text{g/mol}$; crystallinity 68%) was chosen as the structural polymer, into which the mechanocatalysts **6** and **14** were embedded to check the pressure induced activation (for theoretical considerations see Chapter 1.2.2). Critical for the detection of the so generated, mechanically induced catalytic activity is a reliable detection system able to monitor the progress of the “click” reaction directly within a solid polymer matrix. Based on previous knowledge of the fluorogenic “click”-reaction²²⁴⁻²²⁶, the highly fluorescent 7-hydroxy-3-(4-phenyl-*1H*-[1,2,3]triazole-1-yl)-coumarin dye (**18**) ($\lambda_{em} = 427\ \text{nm}$, $\lambda_{ex} = 260\ \text{nm}$ as well as $360\ \text{nm}$) was chosen to probe and quantify the catalyst-activity in the solid state developing thus a stress- and damage-sensing material.

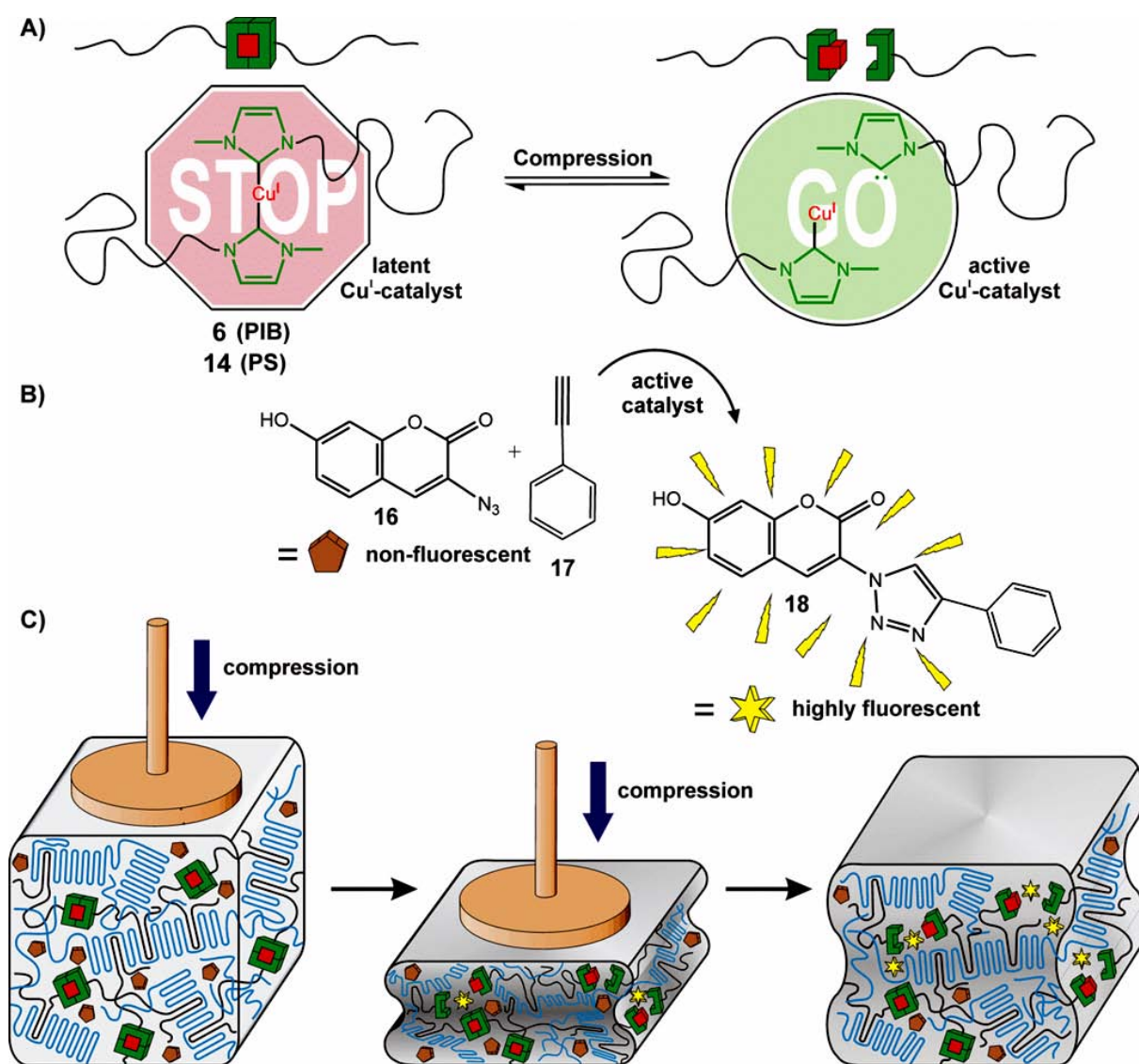


Figure 72. A) Mechanochemical activation of latent copper(I) *N*-heterocyclic carbene (NHC) catalysts (**6**, **14**) through compression. B) Fluorogenic “click” reaction of non-fluorescent 3-azido-7-hydroxy-coumarin dye (**16**) with phenylacetylene (**17**) catalyzed by the activated mechanocatalysts **6** or **14** resulting in the formation of highly fluorescent 7-hydroxy-3-(4-phenyl-*1H*-[1,2,3]triazole-1-yl)-coumarin dye (**18**). C) Mechanochemical activation of the latent polymeric NHC-copper(I)-catalysts (**6**, **14**) within the crystalline poly(tetrahydrofuran) (PTHF) matrix (**20**) by compression. (Reprinted from ref⁹⁷ with permission of Wiley and Sons)

For that purpose, the initial non-fluorescent compounds 3-azido-7-hydroxy-coumarin (**16**) and phenylacetylene (**17**) were embedded in a concentration of $1.56 \cdot 10^{-4}$ mmol_{dye}/mg_{sample} together with the mechanocatalysts **6** and **14** (concentration $5.17 \cdot 10^{-6}$ mmol_{Cu}/mg_{sample}) within the high molecular weight PTHF-matrix (**20**) and subjected after crystallization for one week into dark (65% crystallinity after embedding; determined through DSC) to several compression cycles via an automatic hydraulic press, applying 10 tons pressure (corresponding to 0.74 GPa) for 30 min followed by 30 min without pressure (Figure 72). The thus triggered CuAAC “click” reaction yielded the highly fluorescent 7-hydroxy-3-(4-phenyl-1*H*-[1,2,3]triazole-1-yl)-coumarin dye (**18**) which was subsequently used for quantifying the obtained fluorescence in dependency of the compression cycles via fluorescence spectroscopy according to **eq3** and **eq4**.

The calibration equations **eq3** (for $\lambda_{\text{ex}} = 360$ nm) and **eq4** (for $\lambda_{\text{ex}} = 260$ nm) were recorded within separate experiments to determine the fluorescence intensity at 427 nm of fluorescence dye **18** as well as the non-fluorescent dyes **16** and **17** in dependency of their corresponding concentrations into the high molecular weight PTHF matrix (for details see Experimental Part 4.10.1 as well as Appendix 7.14).

$$\text{for excitation at 360 nm: } y = 1.330 \cdot 10^{13} (\pm 4.325 \cdot 10^{12}) x + 5.359 \cdot 10^6 (\pm 9.094 \cdot 10^7) \quad (\text{eq3})$$

$$\text{for excitation at 260 nm: } y = 1.118 \cdot 10^{13} (\pm 3.392 \cdot 10^{12}) x - 6.479 \cdot 10^7 (\pm 7.132 \cdot 10^7) \quad (\text{eq4})$$

The calculated conversions of mechanochemically triggered “click” reaction of **16** and **17** within PTHF matrix using the mechanocatalyst **6** and **14** (Figure 72) are sum-up in Table 15 and shown graphically in Figure 73.

Table 15. Calculated conversions for the “click” reaction of the non-fluorescent 3-azido-7-hydroxy-coumarin (**16**) with phenylacetylene (**17**) yielding highly fluorescent 7-hydroxy-3-(4-phenyl-1*H*-[1,2,3]triazole-1-yl)-coumarin (**18**) after activating the latent mechanophores **6** and **14** in bulk PTHF matrix by multiple compression cycles via a hydraulic press (time and compression cycle dependent values are given in the Experimental Part).

Ent.	mechanocatalyst		compression cycle	fluorescence intensity [a.u.] ^{a)}	“click” conversion [%] ^{b)}		
	Nr.	M _n (GPC) [g/mol]					
1	A	Control experiment	without catalyst	20	$1.29 \cdot 10^7$	0.3 ± 0.2	
2	B	Thermal activation	6c	17200	no compression:	$2.52 \cdot 10^7$	0.9 ± 0.2
3			14c	13600	heating to 60°C for 72h	$2.21 \cdot 10^7$	0.8 ± 0.3
4	C	Mechanochemical activation of PIB-based mechanophores 6 by compression	6a	4750	20	$1.53 \cdot 10^7$	0.5 ± 0.2
5			6b	8900	20	$1.39 \cdot 10^7$	0.4 ± 0.2
6			6c	17200	20	$1.55 \cdot 10^8$	7.2 ± 0.3
7	D	Mechanochemical activation of PS-based mechanophores 14 by compression	14a	6800	20	$1.51 \cdot 10^7$	0.5 ± 0.2
8			14b	11600	20	$4.75 \cdot 10^7$	2.0 ± 0.3
9			14c	13600	20	$1.69 \cdot 10^8$	7.9 ± 0.5

^{a)}average value of multiple determined fluorescence spectra at different positions of the sample after excitation at 360 nm and fluorescence emission at 427 nm; ^{b)}calculated according to eq.3 assuming a maximum concentration of **18** of $1.56 \cdot 10^{-4}$ mmol_{dye}/mg_{sample}.

The applied compression force activated the catalyst as described above by cleaving one shielding NHC-ligand generating thus the catalytic active monocarbene copper(I) catalysts. This led to a stepwise increase of the fluorescence at 427 nm in dependence of the number of compression cycles proving thus the mechanochemical activation of the latent copper catalyst (Figure 73). Increasing the chain length of the attached polymer handles increased the activation efficiency due to the better entanglement with the polymer matrix preventing thus the drag-out of the anchoring polymers. Accordingly, an increased fluorescence intensity from $1.24 \cdot 10^7$ to $1.55 \cdot 10^8$ could be determined for the PIB-based mechanocatalyst **6c** (17200 g/mol) after 20 compression cycles which corresponds to a “click” conversion of 7.2% (Table 15 ent. 6). However, shorter PIB-based mechanophores (**6a**: 4750 g/mol and **6b**: 8900 g/mol) revealed no significant increase of fluorescence indicating thus an insufficient entanglement with the matrix material to activate the catalyst (Table 15 ent. 4 and 5). Similarly, for the longest PS-based biscarbene mechanocatalysts **14c** (13600 g/mol) an increased fluorescence of $1.45 \cdot 10^7$ to $1.69 \cdot 10^8$ corresponding to a “click” conversion of 7.9% could be determined (Table 15 ent. 9), while **14b** (11600 g/mol) showed only an increased fluorescence from $1.34 \cdot 10^7$ to $4.75 \cdot 10^7$ after 20 compression cycles which corresponds to 2.0% conversion (Table 15 ent. 8). In parallel to the PIB-based mechanophores revealed the shortest PS-mechanophore **14a** an insignificant increase of the fluorescence intensity (Table 15 ent. 7). However, no significant differences in the conversion of the catalyzed “click” reaction could be observed, even when the PS-based mechanocatalysts showed the same reactivity at lower molar masses (7.9% for PS **14c**: 13600 g/mol vs. 7.2% for PIB **6c**: 17200 g/mol) indicating a more efficient scission for **14**.

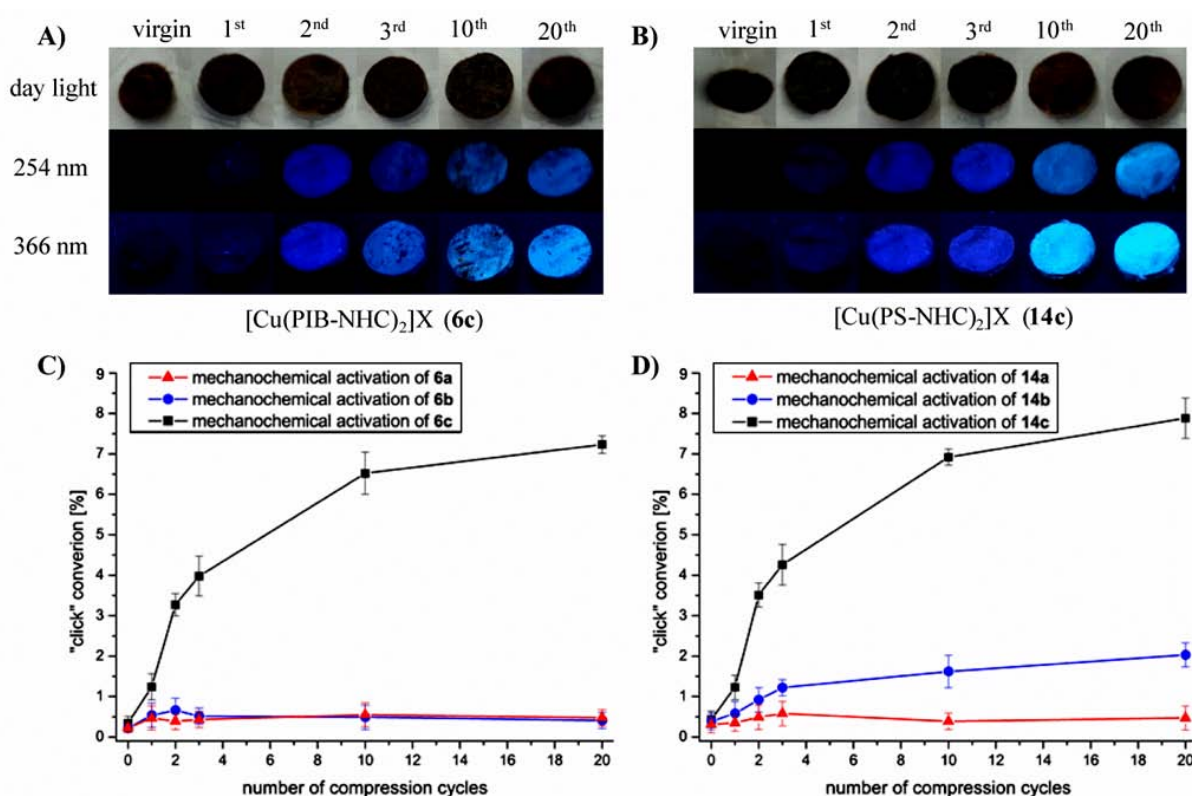


Figure 73. Mechanochemical activation of the latent copper(I) mechanocatalysts **6** (A, C: PIB) and **14** (B, D: PS) through compression led to an increased fluorescence with increased number of compression cycles consisting out of 30 min pressing and 30 min without compression. A, B) Optical images of the prepared PTHF samples with embedded dyes **16** and **17** as well as mechanocatalysts **6c** (17200 g/mol) respectively **14c** (13600 g/mol) under day light or UV-vis light with a wavelength of 254 nm respectively 366 nm. Subjecting these samples to multiple compression cycles led in case of sufficient long polymer chains to a significant increase of fluorescence.

A possible explanation was the potential depleting of the educts **16** and **17** due to the propagating “click” reaction, especially as both types of mechanophore showed a flattening of the “click” conversion after the third compression cycle (Figure 73 C and D). However, a re-dissolving and subsequent re-crystallization of the investigated sample revealing no further increase of fluorescence after 10 additional compression cycles excluding thus the depleting theory. More likely is a slow decomposition of the catalytic active species similar to the solution experiments described before (Chapter 3.3.1 and 3.3.2).

Moreover, the absence of fluorescence within the control experiments without compression of the embedded mechanocatalysts (**6** and **14**) with **16** and **17** into the PTHF matrix proved the latency of the mechanocatalysts also within the bulk state (Figure 74B). Also thermal treatment of **6c** or **14c** within the PTHF matrix at 60°C without compression induced no fluorescence and thus in turns no activation of the catalyst triggering the “click” reaction of **16** with **17** (Figure 74C, Table 15 ent. 2 and 3). Likewise, no fluorescence increase could be detected in the blind experiments without mechanocatalyst excluding thus any influence of the compression event itself to the CuAAC “click” (Figure 74D, Table 15 ent. 1).

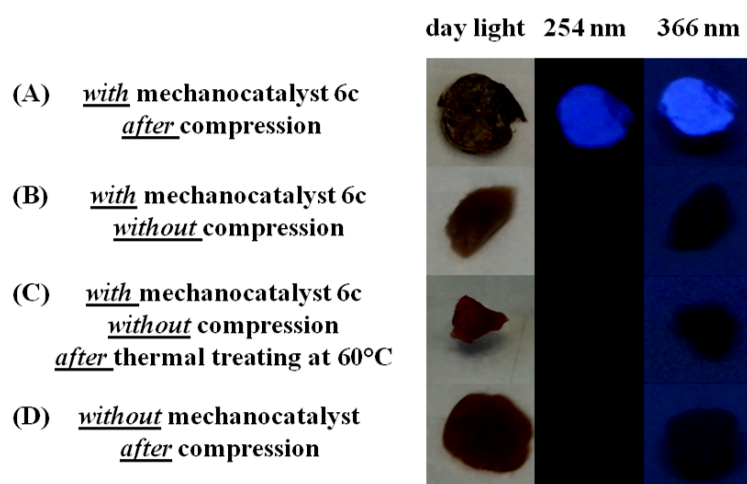


Figure 74. A) Optical images of embedded non-fluorescent coumarin dye **16** and **17** within a high molecular PTHF matrix (**20**) together with latent mechanocatalyst **6c** (17200 g/mol) after mechanochemical activation through 3 compression cycles. B) The absence of fluorescence within the control experiment without compression proved the latency of the mechanocatalyst **6c**, while thermal treatment at 60°C for 72h without compression C) also revealed no fluorescence. D) The blind experiment without mechanocatalyst excluded any influence of the compression event to the “click” reaction. (Reprinted from ref⁹⁷ with permission of Wiley and Sons)

Summed up, the synthesized and investigated mechanocatalytical system of PIB- (**6**) and PS-based (**14**) mechanocatalysts showed its potential within the CuAAC “click” reaction of the non-fluorescent 3-azido-7-hydroxy-coumarin dye (**16**) with phenylacetylene (**17**) generating the highly fluorescent 7-hydroxy-3-(4-phenyl-*1H*-[1,2,3]triazole-1-yl)-coumarin dye (**18**). Moreover, it could be verified that the fluorogenic “click” reaction using **6** and **14** as catalyst is truly latent and could solely be triggered by mechanical compression force, but not due to thermal treatment at 60°C even for several days. A well suitable quantifiability has been demonstrated enabling thus the potential application of the designed mechanocatalytical system within autonomous stress- reporting or damage-sensing materials.

4 Experimental Part

4.1 Materials and methods

The following reactions were carried out under dry, inert argon atmosphere using common Schlenk techniques unless noted. All solvents were purchased in technical grade and were distilled before further use. THF was predried over potassium hydroxide, while toluene was predried over calcium chloride. Final drying was done by heating under reflux conditions over sodium/benzophenone for several hours until the blue colour persists. Dichloromethane and acetonitrile were predried over calcium chloride and dried finally by refluxing over calcium hydride for several hours. *n*-Hexane was refluxed over oleum and concentrated sulphuric acid in order to remove olefins. Afterwards the organic layer was washed with a NaHCO₃ solution and distilled water, dried over Na₂SO₄ and stored over KOH. Finally it was freshly distilled under argon atmosphere over sodium and KOH before used. 1,4-Dioxane and methanol (MeOH) were dried with small portions of metallic sodium under intense cooling. Dimethyl sulfoxide (DMSO) was dried over a molecular sieve 4Å, stored over calcium hydride and distilled freshly before use.

Potassium hexamethyldisilazide (KHMDs, 95%), sodium *tert*-butoxide (NaO^tBu, 97%), tetrakis(acetonitrile)copper(I) hexafluorophosphate ([Cu(MeCN)₄]PF₆, 97%), *N*-methylimidazole (97%), sodium iodide (99.9%), 1,4,7,10,13-pentaoxacyclopentadecane (15-crown-5-ether, 98%), phenylacetylene (98%), copper(II) sulfate pentahydrate, sodium ascorbate, anhydrous sodium acetate (99%), sodium nitrite (99%), sodium azide (99.5%), methyl trifluoromethanesulfonate (98%), 2,6-di-*tert*-butylpyridine (97%), copper(I) bromide, *N,N,N',N'',N'''* - pentamethyldiethylenetriamine (PMDETA) (99%) and acetic acid (99.8%) were purchased from Sigma-Aldrich. *N*-acetyl glycine as well as acetic anhydride (99%) were purchased from VWR, 2,4-dihydroxy benzaldehyde (98%) was purchased from Alfa-Aesar and hydrochloric acid (37%) was purchased from Grüssing, while styrene and magnesium sulfate (97%) were ordered from Acros Organics. Benzyl bromide (98%) and ammonia hydroxide solution (25%) were received from Fluka. All chemicals were used without further purification unless *N*-methylimidazole, DIPEA and PMDETA, which were dried over molecular sieve and were distilled one time after purchasing from Sigma-Aldrich. Styrene was destabilized by extracting with 10wt% sodium hydroxide solution, distillation from calcium hydride and stored in a freezer at -16°C. Before using, the styrene was distilled freshly under dry inert gas atmosphere. Cu(I)Br was washed three times with acetic anhydride, dry ethanol and finally with dry diethylether and was stored in a Schlenk tube within the glove box.

Column chromatography was performed using Merck silica gel 60 (230 – 400 mesh). Thin-layer chromatography (TLC) was carried out on Merck TLC aluminium sheets (silica gel 60 F₂₅₄). Spots on TLC plates were visualized either by UV light with a wavelength of 254 or 366 nm or by oxidizing agents like cerium or “blue” stain. The cerium stain was prepared by dissolving Ce(SO₄)₂·4H₂O (1 g) in a mixture of distilled water (47 mL) and subsequent addition of concentrated sulphuric acid (2.75 mL). The “blue” stain consists of Ce(SO₄)₂·4H₂O (1 g) and (NH₄)₆Mo₇O₂₄·4H₂O (1 g) dissolved in a mixture of distilled water (90 mL) and concentrated sulphuric acid (6 mL).

All NMR-spectra were recorded on a Varian Gemini 400 (¹H-NMR 400 MHz; ¹³C-NMR 100 MHz) or 500 (¹H-NMR 500 MHz; ¹³C-NMR 125 MHz) spectrometer at 27°C in CDCl₃ (Chemotrade, 99.8 Atom%D), THF-d₈ (Chemotrade, 99.5 Atom%D) or DMSO-d₆ (Chemotrade, 99.8 Atom%D). Chemical shifts (δ) are reported in ppm and referred to the solvent residual signal (CDCl₃ 7.26 ppm for ¹H and 77.0 ppm for ¹³C; THF-d₈ 3.58 and 1.72 ppm for ¹H as well as 67.2 and 25.3 ppm for ¹³C; DMSO-d₆ 2.50 ppm for ¹H and 39.5 ppm for ¹³C²²⁷⁻²²⁸. MestReNova v. 6.0.2-5475 was used for interpretations of NMR-data.

Gel permeation chromatography (GPC) was performed on a Viscotek GPCmax VE 2002 using a columns set of a H_{HR}H Guard-CLM3008 and a GMH_{HR}-N-18055 main column in THF (exclusion limit of 400 000 g/mol) with a column temperature of 22°C. The injection volume was 100 µL with a standard sample concentration of 5 mg/ml in THF unless noted and the flow rate was adjusted to 1 mL/min. Detection was accomplished by refractive index with a VE 3580 RI detector of Viscotek at 35°C. External calibration was done using poly(isobutylene) (PIB) standards (purchased from PSS) in a molecular weight range from 340 to 87 600 g/mol for PIB-based samples, while poly(styrene) (PS) standards (also purchased from PSS) with a molecular weight range from 1050 to 115 000 g/mol were used for all other polymers. GPC data of *N*-methylimidazolium-telechelic polymers could not be obtained due to the low detection intensity of ionic polymer species.

MALDI-TOF-MS experiments were conducted on a Bruker Autoflex III system equipped with a smart beam laser (355 nm, 532 nm, 808 nm and 1064 nm ± 5 nm; 3 ns pulse width; up to 2500 Hz repetition rate) accelerated by a voltage of 20 kV and detected as positive ions operating either in reflectron or linear mode. Baseline subtraction and smoothing of the recorded spectra were performed using a three point Savitzky–Golay algorithm. The data evaluation was carried out on flexAnalysis software (version 3.0). Samples preparation was done by dissolving the polymer in THF at a concentration of 10 mg/mL. 1,8-Dihydroxy-9,10-dihydroanthracen-9-one (dithranol) or *trans*-2-[3-(4-*tert*-butylphenyl)-2-methyl-2-propenylidene] malononitrile (DCTB) were used as matrix and dissolved in THF at a concentration of 20 mg/mL. LiTFA or NaTFA were used as salts dissolved in THF at a concentration of 10 mg/mL. The ratio of matrix:analyte:salt was 100:10:1 and 1 µL of the solution was spotted on the MALDI-target plate.

ESI-TOF-MS measurements were performed on a Bruker Daltonics microTOF via direct injection with a flow rate of 180 µL/h using the negative mode with an acceleration voltage of 4.5 kV. The spectra were processed on Bruker Daltonics ESI compass 1.3 for microTOF (Data Analysis 4.0). Samples were prepared by dissolving sample in HPLC grade solvent at a concentration of 1 mg/mL without additional salt.

ATR-IR measurements were done on a Bruker Tensor VERTEX 70 spectrometer equipped with a Golden Gate Heated Diamond ATR Top-plate. Opus 6.5 was used for data analyzing. IR spectra of KBr pellets were recorded on a 205 FT-IR spectrometer from Nicolet.

DSC thermograms were measured on a Netzsch Phoenix® DSC 204 F1 after crystallization for one week under inert conditions into dark. Typically 2 – 5 mg sample were weight into standard alumina pans. Measurements were performed with a heating rate of 5 K/min in a temperature range from -40 to 80°C.

The UV-vis spectra were recorded on a Perkin-Elmer Lambda 18 UV-vis spectrometer in HPLC grade THF or methanol in a wavelength range from 700 nm to 200 nm with a data interval of 1 nm, a scan speed of 240 nm/min and a slit size of 2 nm.

Fluorescence measurements were carried in the bulk state out on a FlouoroMax-2 instrument, whereat the samples were fixed with a special solid sample holder between two object slides out of quartz glass. Emission spectra were recorded in a range from 380 to 700 nm observing the maximum emission at a wavelength of 427 nm, when excited at 260 respectively 360 nm, while excitation spectra were recorded in wavelength range from 220 to 500 nm revealing a maximum in emission at 427 nm when samples were excited at 260 respectively 360 nm. All fluorescence experiments were repeated at least three times at three different positions of the investigated pellet.

Ultrasonication experiments were performed with a Sonics VCX 500 ultrasonic processor at a frequency of 20 kHz with 30% of the maximal amplitude of 125 µm. A 254 mm long full wave solid probe out of titanium alloy (Ti-Al-4V) with a diameter of 13 mm was used together with an internally

threaded stainless steel adapter (fitting to probe at nodal point). All sonication experiments were conducted under inert and dry conditions in a 10 mL reaction vessel with two additional 14/20 side necks which was temperate at 20°C by an external cooling bath. The sonication intensity in THF/MeOH 30:1 mixtures was determined to 8.75 W/cm², while the energy input was obtained as 21 kJ per applied ultrasonication cycle consisting out of 90 min sonication with a pulse sequence of 5s on and 10s off.

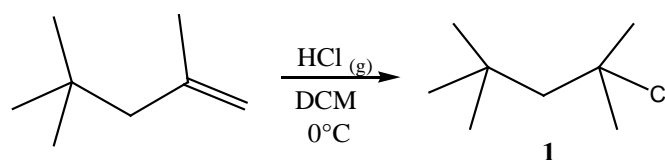
The compression experiments were conducted on the automatic hydraulic Atlas Power Presses T15 from Specac together with an Atlas 13 mm evacuable pellet die applying 10 tons pressure.

STEM-EDXS analyses (Scanning Transmission Electron Microscopy - Energy Dispersive X-ray Spectroscopy) were performed on FEI TITAN³ G2 80-300 using carbon-coated Ni TEM grids. The sample preparation was done by ultrasonic dispersion of the powder in isopropyl alcohol, followed by putting one droplet of the dispersion onto the TEM grid and drying on a hot plate.

Microwave irradiation experiments were performed in a Discover SP Microwave Synthesizer of CEM applying the SPS method.

4.2 Synthesis of PIB-based bis(*N*-methylimidazol-2-ylidene) copper(I) mechanocatalysts (6)

4.2.1 Synthesis of TMPCl (1)

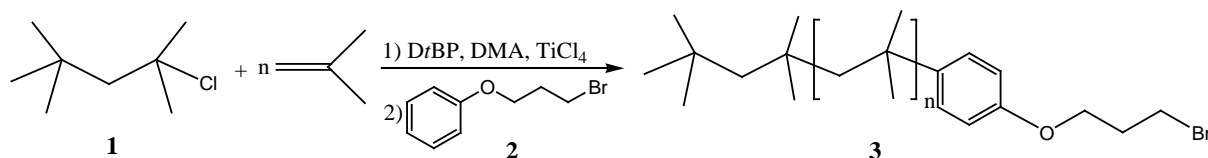


Scheme 1. Synthesis of 2-chloro-2,4,4-trimethyl-pentane (TMPCl) (1).

The synthesis of 2-chloro-2,4,4-trimethyl-pentane (TMPCl) (1) was done according to literature procedure²²⁹ as shown in Scheme 1. 2,4,4-Trimethylpent-1-ene (3.0 mL; 18.9 mmol) diluted in dry dichloromethane (5 mL) was cooled to 0°C by the means of an ice bath and kept at these temperature during the whole reaction time. A slow steam of gaseous HCl produced *in situ* out of NaCl and H₂SO₄ was dried by passing through a column of CaH₂ and bubbled 5 hours through the solution. Removing the solvent at 0°C under reduced pressure yielded TMPCl as colourless liquid in quantitative yield. The obtained product was stored under argon atmosphere at 0°C until use.

¹H-NMR (400 MHz, CDCl₃): δ [ppm] 1.85 (s, 2H, CH₂); 1.65 (s, 6H, C(CH₃)₂Cl); 1.03 (s, 9H, C(CH₃)₃)

4.2.2 Synthesis of bromo-telechelic PIB (3)



Scheme 2. Synthesis of linear bromo-telechelic PIB (3) via LCCP.

The synthesis of linear bromo-telechelic poly(isobutylene) (3) was done via living carbocationic polymerization (LCCP) with slide changes according to common literature procedure of Binder *et al.*²⁰⁹ as well as Morgan and Storey²³⁰⁻²³¹ using TMPCl(1)/TiCl₄ as initiating system and 3-

(bromopropoxy)benzene (**2**) for termination as shown in Scheme 2. For that purpose, a 250 mL three-neck round bottom flask equipped with mechanical stirrer, gas tap and rubber septum was attached to a Schlenk line and heated several times under vacuum, flushed with argon and filled with a mixture of dry and degassed dichloromethane/*n*-hexane (2:3 v/v). *N,N*-dimethylacetamide (DMA; adjusting a concentration of 5 mM), 2,6-di-*tert*-butylpyridin (*DtBP*; 5 mM) and **1** were added while cooling to -80°C by methanol/liquid nitrogen followed by the addition of TiCl₄ (7.5 eq. per **1**) when reaching the desired temperature. The stirring speed was adjusted to 300 rpm and condensed, dry and oxygen-free isobutylene (*IB*; 1 M) was added rapidly via syringe. The thus started polymerization was stirred vigorously for 15 minutes at -80°C. Subsequently, 3-(bromopropoxy)benzene (**2**) (2.5 eq. per **1**) was added and the reaction mixture was stirred for 180 min at -60°C, followed by decomposing the residual TiCl₄ by an excess of MeOH, while warming up to room temperature. The solvent was evaporated and the crude product was precipitated three times out of *n*-hexane in a large excess of MeOH. The pure product was obtained as a colourless, highly viscous polymer after drying in high vacuum. For experimental details and for characterization data see Table 16 and Table 17. Selected spectra are shown in Appendix 7.1.

¹H-NMR (500 MHz, CDCl₃): δ [ppm] 7.28 (d, 2H, C₆H₄, ³J_{H,H} = 8.8 Hz), 6.81 (d, 2H, C₆H₄, ³J_{H,H} = 8.8 Hz), 4.08 (t, 2H, CH₂Br, ³J_{H,H} = 5.8 Hz), 3.60 (t, 2H, OCH₂, ³J_{H,H} = 6.6 Hz), 2.31 (quint, 2H, CH₂CH₂Br, ³J_{H,H} = 6.1 Hz), 1.42 (bs, CH₂ polymer), 1.11 (bs, 2x CH₃ polymer), 0.99 (s, 15H, C(CH₃)₂CH₂C(CH₃)₃).

¹³C-NMR (125 MHz, CDCl₃): δ [ppm] 156.2 (C_{Ar}-O), 142.8 (C_{Ar}-C(CH₃)₂), 127.1 (CH_{Ar}C_{Ar}-C(CH₃)₂), 113.7 (CH_{Ar}C_{Ar}-O), 65.3 (O-CH₂), 59.5 (CH₂ polymer backbone), 58.8 (CH₂ last repetitive unit), 58.2 (CH₂ polymer head group), 38.1 (C(CH₃)₂ polymer backbone), 37.9 (C(CH₃)₂ last repetitive unit), 37.8 (C(CH₃)₂ polymer head group), 32.4 (C(CH₃)₃ polymer head group), 31.2 (C(CH₃)₂ polymer backbone), 30.8 (CH₂CH₂Br), 30.1 (CH₂Br).

Table 16. Experimental details for the synthesis of bromo-telechelic poly(isobutylene)s (**3**).

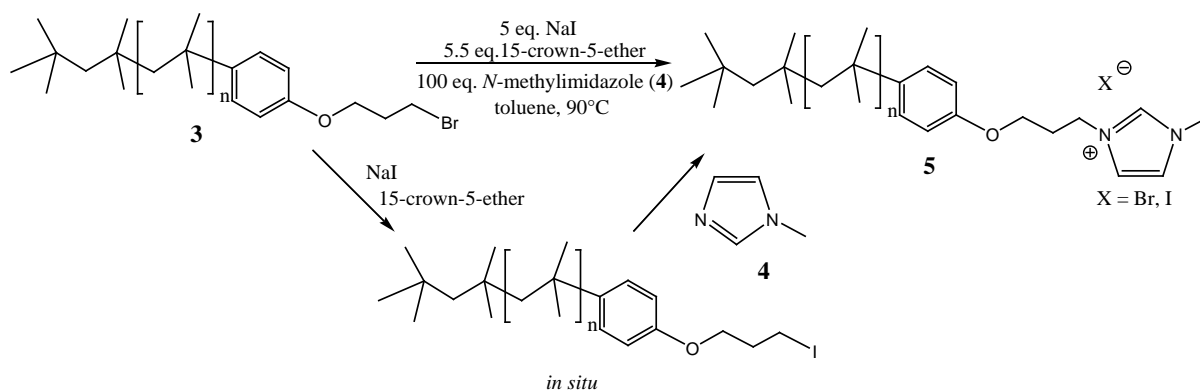
	Ini 1	Qu 2	DMA	<i>DtBP</i>	<i>IB</i>	TiCl ₄	DCM	<i>n</i> -hexane	isolated yield
3a	513 μL 3.0 mmol	1182 μL 7.5 mmol	62 μL 0.67 mmol	150 μL 0.67 mmol	11.0 mL 133.7 mmol	2.5 mL 22.5 mmol	53 mL	80 mL	87%
3b	171 μL 1.0 mmol	394 μL 2.5 mmol	42 μL 0.45 mmol	100 μL 0.45 mmol	7.3 mL 89.1 mmol	0.8 mL 7.5 mmol	36 mL	54 mL	92%
3c	103 μL 0.6 mmol	237 μL 1.5 mmol	50 μL 0.5 mmol	120 μL 0.5 mmol	8.8 mL 107 mmol	0.5 mL 4.5 mmol	43 mL	64 mL	97%

Table 17. Characterization data of bromo-telechelic poly(isobutylene)s (**3**).

Ent.	M _n (theo) [g/mol]	M _n (GPC) ^{a)} [g/mol]	M _n (NMR) ^{b)} [g/mol]	PDI
3a	2500	2200	2500	1.2
3b	5000	4700	5200	1.4
3c	10000	8750	9000	1.2

^{a)}using PIB standards in THF with a flow rate of 1 mL/min; ^{b)}For calculation, the resonances of the end group at 6.81 ppm were set to 2H and brought into ratio to the resonance of the CH₂-groups of the polymer chain at 1.42 ppm. The obtained degree of polymerization (DP) was multiplied with 56.11 g/mol yielding the molecular mass of the synthesized polymer. In order to prove a quantitative quench process the resonances of the end group at 6.81 ppm was set to 2H and the resonance of the initiating group at 0.99 ppm had to result in 15H.

4.2.3 Synthesis of *N*-methylimidazolium telechelic PIB (**5**)



Scheme 3. Synthesis of *N*-methylimidazolium telechelic PIB (**5**) from bromo-telechelic PIB (**3**) via nucleophilic substitution with sodium iodide generating *in situ* the iodo-telechelic PIB-moiety and subsequent quaternization reaction with *N*-methylimidazole (**4**).

The subsequently described reaction conditions were figured out as the best according to several optimization attempts summed-up in Table 18 (Ent. 5TX), whereat different solvent (mixtures), reaction temperatures as well as the effect of adding NaI/15-crown-5-ether (to increase the nucleophilicity) were tested. The following reactions were carried out under a dry argon atmosphere and under exclusion of light. Bromo-telechelic poly(isobutylene) (**3**) was placed in a two-neck round bottom flask equipped with rubber septum, gas tap and reflux condenser and subjected to several vacuum-argon cycled. Subsequently dry, degassed toluene was added adjusting a concentration of ~15 mM, followed by the addition of sodium iodide (5 eq.) in the countercurrent of Argon. 15-crown-5-ether (5.5 eq.) as well as freshly distilled *N*-methylimidazole (**4**; 100 eq.) were added by means of an Eppendorf pipette. The reaction mixture was stirred in the dark at 90°C for 5 days. Subsequently, the cold reaction mixture was precipitated two times into -18°C cold MeOH and dried into vacuum. The crude polymer mixture was purified by column chromatography on silica gel using first pure CHCl₃ and changing afterwards slowly the polarity to CHCl₃/MeOH 25:1 (TLC: CHCl₃/MeOH 15:1; R_f(**5**) = 0.1; blue stain; for details see below). The pure *N*-methylimidazolium telechelic PIB (**5**) was obtained as a slightly yellow, viscose polymer and was stored under argon atmosphere into dark until further use. The experimental details as well as the characterization data shown in Table 18 and Table 19 resulted on the combined fractions F3-F5 (see TLC information). Selected spectra are shown in Appendix 7.2.

TLC information for column chromatography:

During the column chromatography typically 5 fractions could be isolated and identified through ¹H-NMR spectroscopy: The 1st fraction (R_{f1} = 0.95 - 1.00) belongs to unreacted PIB bromide (**3**), while the 2nd fraction (R_{f2} = 0.43) represent an elimination product, whereby the *N*-methylimidazolium end group is cleaved showing characteristic terminal double bond on PIB. The fractions 3 - 5 were combined for further reactions. Moreover, higher molecular weight polymers **5b** and **5c** reveal higher R_f-values compared to the lower molecular weight polymer **5a**.

- | | |
|--|---|
| 1 st Fraction: R _{f1} = 0.95 - 1.00 | → unreacted PIB bromide 3 |
| 2 nd Fraction: R _{f2} = R _{f2} = 0.43 | → PIB-elimination product with terminal double bonds |
| 3 rd Fraction: R _{f3} = 0.2 | → high M _n fraction of <i>N</i> -methylimidazolium telechelic PIB 5 |
| 4 th Fraction: R _{f4} = 0.05 - 0.15 | → medium M _n fraction of 5 |
| 5 th Fraction: R _{f5} = 0 | → low M _n fraction of 5 |

¹H-NMR (400 MHz, CDCl₃): δ [ppm] 10.30 (s, 1H, NCHN), 7.28 (d, 2H, C₆H₄, ³J_{H,H} = 8.8 Hz), 7.21 (d, 2H, NCHCHN), 6.77 (d, 2H, C₆H₄, ³J_{H,H} = 8.8 Hz), 4.54 (t, 2H, CH₂N, ³J_{H,H} = 6.9 Hz), 4.03 (m, 5H, overlay of OCH₂ and NCH₃), 2.44 (quint, 2H, OCH₂CH₂, ³J_{H,H} = 6.1 Hz), 1.41 (bs, CH₂ polymer backbone), 1.10 (bs, 2x CH₃ polymer backbone), 0.99 (s, 15H, C(CH₃)₂CH₂C(CH₃)₃).

¹³C-NMR (100 MHz, CDCl₃): δ [ppm] 155.7 (C_{Ar}-O), 143.3 (C_{Ar}-C(CH₃)₂), 138.2 (NCHN), 127.2 (CH_{Ar}C_{Ar}-C(CH₃)₂), 122.9 (NCHCHN), 122.3 (NCHCHN), 113.6 (CH_{Ar}C_{Ar}-O), 63.4 (O-CH₂), 59.5 (CH₂ polymer backbone), 58.8 (CH₂ last repetitive unit) 58.2 (CH₂ polymer head group), 47.3 (NCH₂CH₂), 38.1 (C(CH₃)₂ polymer backbone), 38.0 (C(CH₃)₂ last repetitive unit), 37.8 (C(CH₃)₂ polymer head group), 36.4 (NCH₃), 32.4 (C(CH₃)₃ polymer head group), 31.2 (C(CH₃)₂ polymer backbone), 29.8 (NCH₂CH₂).

GPC measurements of **5** were not possible due to the low intensity of RI- respectively light scattering detection signal. Thus, no signal was detected neither in THF not in toluene.

MALDI-TOF-MS (Dithranol, NaTFA) [m/z]: *N*-methylimidazolium-telechelic PIB species found without counterion or additional cation [M-X]⁺. (**5a**) C₁₁₇H₂₂₅N₂O₁⁺ simulated 1675.765 g/mol, found 1675.751 g/mol (err. 8 ppm); (**5b**) C₃₉₇H₇₈₅N₂O₁⁺ simulated 5604.165 g/mol, found 5604.295 g/mol (err. 23 ppm); (**5c**) C₆₈₁H₁₃₅₅N₂O₁⁺ simulated 9588.627 g/mol, found 9588.761 g/mol (err. 14 ppm).

Table 18. Experimental details for the synthesis of *N*-methylimidazolium telechelic PIB (**5a-c**). The attempts **5TX** were accomplished as pre-experiments in order to optimize the reaction conditions. The here presented examples are a selection of a wide series of attempts.

Ent.	PIB-Br (3)		NaI	15-crown-5-ether	<i>N</i> -methylimidazole (4)	solvent	T [°C]	time [h]	isolated yield [%]
	M _n (GPC) [g/mol]	m; n							
5T1	3	3900 1 eq. 102 mg 26.2 μmol	10 eq. 40 mg 267 μmol	-	100 eq. 210 μL 2.6 mmol	heptane/DMF 1:1	90	72	36
5T2	3	3900 1 eq. 102 mg 26.2 μmol	10 eq. 40 mg 267 μmol	-	100 eq. 210 μL 2.6 mmol	heptane/DMF 1:1	90	210	24
5T3	3	3900 1 eq. 101 mg 25.9 μmol	10 eq. 38 mg 254 μmol	-	100 eq. 205 μL 2.5 mmol	heptane/DMF 1:1	120	72	17
5T4	3	3900 1 eq. 105 mg 26.9 μmol	10 eq. 41 mg 274 μmol	-	100 eq. 220 μL 2.8 mmol	toluene/DMF 7:2	145	90	11
5T5	3	3900 1 eq. 100 mg 25.6 μmol	5 eq. 19 mg 128 μmol	5.5 eq. 28 μL 142 μmol	100 eq. 204 μL 2.5 mmol	heptane/DMF 5:1	90	90	57
5T6	3	3900 1 eq. 110 mg 28.2 μmol	-	-	225 eq. 509 μL 6.4 mmol	heptane/DMF 5:1	90	90	8
5T7	3	3900 1 eq. 116 mg 29.7 μmol	5 eq. 23 mg 153 μmol	5.5 eq. 32 μL 162 μmol	100 eq. 237 μL 3.0 mmol	toluene	90	90	74
5T8	3	3900 1 eq. 250 mg 64.0 μmol	5 eq. 48 mg 320 μmol	5.5 eq. 70 μL 354 μmol	100 eq. 510 μL 6.4 mmol	toluene	90	120	95

Ent.	PIB-Br (3)		NaI	15-crown-5-ether	N-methylimidazole (4)	solvent	T [°C]	time [h]	isolated yield [%]	
	M _n (GPC) [g/mol]	m; n								
5a	3a	2200	1 eq. 500 mg 227 μmol	5 eq. 170 mg 1140 μmol	5.5 eq. 247 μL 1250 μmol	100 eq. 1810 μL 22.7 mmol	toluene	90	120	83
5b	3b	4700	1 eq. 750 mg 158 μmol	5 eq. 118 mg 790 μmol	5.5 eq. 172 μL 868 μmol	100 eq. 1260 μL 15.8 mmol	toluene	90	120	74
5c	3c	8750	1 eq. 760 mg 87 μmol	5 eq. 66 mg 440 μmol	5.5 eq. 96 μL 485 μmol	100 eq. 684 μL 8.68 mmol	toluene	90	120	66

Table 19. Characterization data of *N*-methylimidazolium telechelic PIB (5a-c).

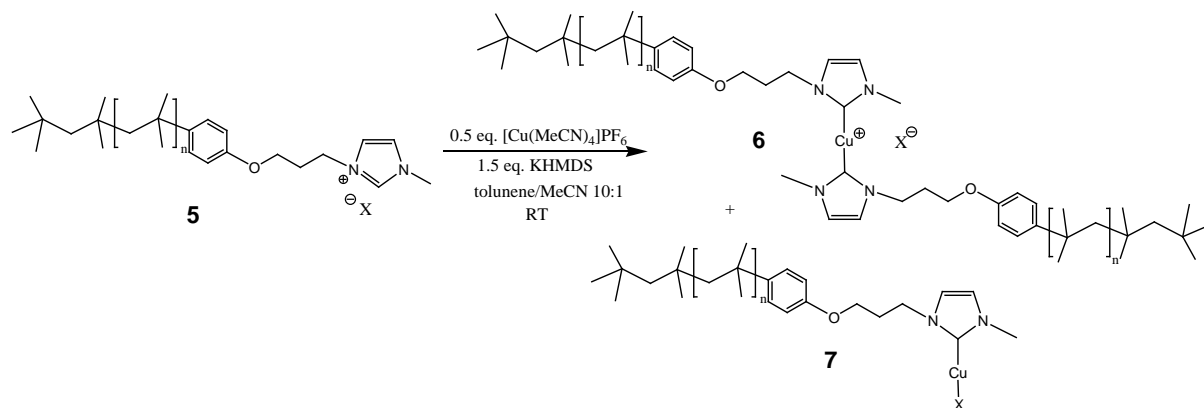
Ent.	used PIB-Br: M _n (NMR) [g/mol]	M _n (NMR) ^{a)} [g/mol]	M _n (MALDI) [g/mol]	
			simulated	measured
5a	3a: 2500	2500	1675.765	1675.751
5b	3b: 5200	5400	5604.165	5604.295
5c	3c: 9000	8200	9588.627	9588.761

^{a)} Calculated according to the resonances at 6.77 ppm (2H of phenylic endgroup) and at 1.41 ppm (CH₂-group of the repetitive unit) in order to determine the molecular weight as well as the 1:1 ratio of the CH₂-group close to the imidazolium (at 4.54 ppm) in respect to the aforementioned CH₂-group of the phenylic endgroup proofing a complete functionalization with *N*-methylimidazolium.

4.2.4 Synthesis of bis(*N*-methylimidazol-2-ylidene-telechelic PIB) copper(I)X complex [Cu(PIB-NHC)₂]X (6) and PIB-monocarbene complex [Cu(PIB-NHC)]X (7)

The preparation of mono- (7) and biscarbene copper complexes (6/10/14) was done with several modifications according to adopted literature procedures for the preparation of symmetric low molecular weight copper(I) biscarbene complexes^{160; 217-219}. In case of the PIB-based mechanocatalyst, the monocarbene catalysts (7) were obtained as a side product during the synthesis of 6. Moreover, a slow decomposition of the biscarbene complexes (6 and 14) could be observed over a period of several months by cleaving/re-protonating one of the carbene ligands (proven by GPC and ¹H-NMR spectroscopy), while the monocarbene complexes (7) oxidized during the purification process as the second shielding carbene ligand is missing and can solely be activated for CuAAC reactions by adding an additional reducing agent like sodium ascorbate.

4.2.4.1 Synthesis of 6 and 7 by KHMDS and [Cu(CH₃CN)₄]PF₆



Scheme 4. Synthesis of bis(*N*-methylimidazol-2-ylidene-telechelic poly(isobutylene) copper(I)X complex [Cu(PIB-NHC)₂]X (6) as well as corresponding monocarbene complex [Cu(PIB-NHC)]X (7).

N-methylimidazolium telechelic PIB (**5**) was placed in a two-necked round-bottom flask, subjected to several vacuum-argon cycles and was dissolved in dry, degassed toluene adjusting a concentration of ~20 mM. Potassium hexamethyldisilazide (KHMDS) (1.5 eq.) was dissolved in dry toluene inside the glove box (concentration ~30 mM), added to **5** and the reaction mixture was stirred for 15 min at room temperature. Subsequently, tetrakis(acetonitrile)copper(I) hexafluorophosphate [Cu(CH₃CN)₄]PF₆ (0.5 eq.) was dissolved inside the glove box into dry acetonitrile (concentration ~50 mM), added to the reaction mixture and stirred overnight at room temperature into dark. Removing of the solvent yields the crude product **6** which was finally purified by column chromatography on silica (solvent mixture CHCl₃/*n*-hexane 5:1 changing gradually to pure CHCl₃; TLC: pure CHCl₃, R_f = 0.1 (**6a**), R_f = 0.4 (**7a**), blue stain, for details see below). The pure products were obtained as brownish, viscose polymers and were stored under argon atmosphere into dark until use. Experimental details and characterization data are shown in Table 20 and Table 21, while selected spectra are presented in Appendix 7.3.

TLC information for column chromatography:

During the column chromatography typically 5 fractions could be isolated and identified partially through ¹H-NMR spectroscopy: The 1st fraction (R_{f1} = 0.95 - 1.00) belongs to an elimination product, whereat the *N*-methylimidazolium end group is cleaved showing characteristic terminal double bond on PIB, while the 2nd fraction (R_{f2} = 0.35-0.45) could be identified as monocarbene complexes **7**. The 3rd fraction (R_{f3} = 0.2) could not be identified, whereas the 4th fraction (R_{f4} = 0.05-0.15) can be assigned to the biscarbene complexes **6**. The 5th isolated fraction (R_{f5} = 0) was the unreacted educt **5**. Moreover, higher molecular weight complexes **6b** and **6c** revealed higher R_f-values compared to the lower molecular weight complex **6a**, while the R_f-values of complexes **7** stayed almost constant. Hence, in case of the highest M_n complexes the R_f-values of **6** and **7** are coincident which prevent an isolation of **7c** as solely mixed fractions of **6c** and **7c** can be obtained. After elution of **7c**, a pure fraction of **6c** could be isolated. Changing the polarity of the eluent could not solve this problem as the retention time and the stationary/mobile-phase interaction for **6c** and **7c** are obviously too similar.

- 1st Fraction: R_{f1} = 0.95 - 1.00 → elimination product; PIB without *N*-methyl-imidazolium end group bearing terminal double bonds **21**
 2nd Fraction: R_{f2} = 0.35 - 0.45 → monocarbene complex **7**
 3rd Fraction: R_{f3} = 0.2 → unidentified side product
 4th Fraction: R_{f4} = 0.05 - 0.15 → biscarbene complexes **6**
 5th Fraction: R_{f5} = 0 → unreacted educt **5**

¹H-NMR of **6** (400 MHz, CDCl₃): δ [ppm] 7.24 (d, 2H, C₆H₄), 6.81 (d, 2H, C₆H₄, ³J_{H,H} = 8.8 Hz), 6.17 (d, 2H, NCHCHN), 3.96 (t, 2H, OCH₂, ³J_{H,H} = 5.7 Hz), 3.82 (t, 2H, NCH₂, ³J_{H,H} = 7.2 Hz), 3.25 (s, 3H, NCH₃), 2.13 (quint., 2H, OCH₂CH₂), 1.41 (s, CH₂ polymer backbone), 1.11 (s, 2x CH₃ polymer backbone), 0.99 (s, 15H, C(CH₃)₂CH₂C(CH₃)₃).

¹H-NMR of **7** (400 MHz, CDCl₃): δ [ppm] 7.26 (d, 2H, C₆H₄), 6.77 (d, 2H, C₆H₄, ³J_{H,H} = 8.8 Hz), 6.37 (d, 2H, NCHCHN), 3.99 (t, 2H, OCH₂, ³J_{H,H} = 5.7 Hz), 3.74 (t, 2H, NCH₂, ³J_{H,H} = 7.2 Hz), 3.49 (s, 3H, NCH₃), 2.40 (quint., 2H, OCH₂CH₂), 1.41 (s, CH₂ polymer backbone), 1.11 (s, 2x CH₃ polymer backbone), 0.99 (s, 15H, C(CH₃)₂CH₂C(CH₃)₃).

¹³C-NMR spectroscopy shows only the signals of the polymer backbone as the quadruple moment of the attached Cu(I) suppress the intensity of the relevant signals of the *N*-methylimidazol-2-ylidene end group.

MALDI-TOF-MS (DCTB, LiTFA, Laser intensity 20%) [m/z]: A suitable spectrum could only be obtained for complex **6a** as the higher molecular weight catalysts decompose much rapidly during the ionization process. For **6a** two series could be identified, 1st series belongs to bis-carbene complex **6a** without counterion $[M]^+ C_{130}H_{242}Cu_1N_4O_2^+$: simulated 1956.829 g/mol, found 1956.846 g/mol (err. 9 ppm), while the 2nd series belongs to decomposed **6a** whereat one shielding polymeric ligand is cleaved-off. Hence, the residual $[Cu(PIB-NHC)]^+$ flies without counterion together with CF_3COOH (from salt) yielding $C_{183}H_{356}Cu_1F_3N_2O_3^+$ simulated 2752.706 g/mol, found 2752.534 g/mol (err. 62 ppm).

Table 20. Experimental details for the synthesis of PIB-based copper(I)-biscarbene complex $[Cu(PIB-NHC)_2]X$ (**6**) and monocarbene complex $[Cu(PIB-NHC)]X$ (**7**) by 1.5 eq. KHMDS and 0.5 eq. $[Cu(CH_3CN)_4]PF_6$. For all reactions toluene/acetonitrile 10:1 were used as solvent adjusting according to the previously described protocol the overall polymer concentration to ~10 mM and stirred overnight at room temperature.

Ent.	PIB-Imi (5)		$[Cu(CH_3CN)_4]PF_6$	KHMDS	isolated yields ^{b)} [%]			
	M_n (NMR) [g/mol]	m; n			decomp. PIB (21) ^{a)}	regained 5	monocarbene complex (7)	biscarbene complex (6)
6a/7a	5a: 2500	680 mg 272 μ mol	51 mg 136 μ mol	81 mg 408 μ mol	15	25	7a: 7	6a: 52
6b/7b	5b: 5400	551 mg 102 μ mol	19 mg 51 μ mol	31 mg 154 μ mol	10	35	7b: 5	6b: 49
6c/7c	5c: 8200	601 mg 73 μ mol	14 mg 37 μ mol	22 mg 110 μ mol	7	40	7c: - ^{c)}	6c: 42

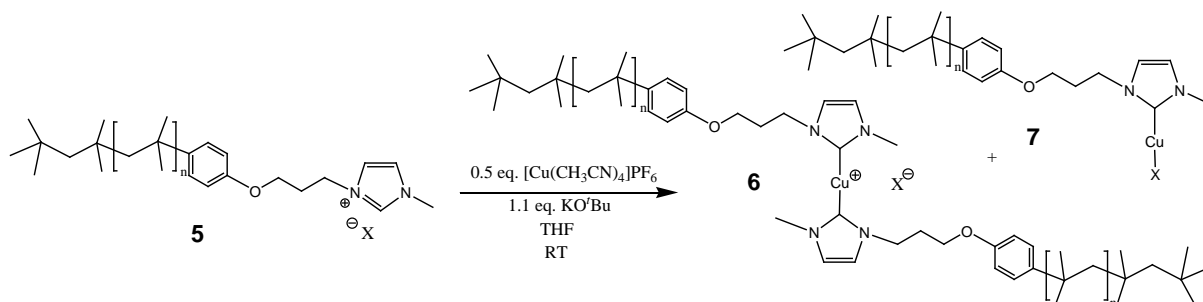
^{a)}¹H-NMR spectroscopy revealed decomposed PIB with terminal double bonds (4.50 – 5.50 ppm) caused by the elimination of the *N*-methylimidazolium endgroup from PIB; ^{b)}isolated yields after column, missing percentages to 100% are either mixed fractions or lost during the purification; ^{c)}solely mixed fractions of **6c** and **7c** could be isolated

Table 21. Characterization data of $[Cu(PIB-NHC)_2]X$ (**6**) and $[Cu(PIB-NHC)]X$ (**7**) synthesized by KHMDS and $[Cu(CH_3CN)_4]PF_6$.

Ent	PIB-Imi (5)		monocarbene complex $[Cu(PIB-NHC)]X$ (7)		biscarbene complex $[Cu(PIB-NHC)_2]X$ (6)			
	M_n ^{a)} (GPC) [g/mol]	M_n ^{b)} (NMR) [g/mol]	M_n ^{a)} (GPC) [g/mol]	M_n ^{b)} (NMR) [g/mol]	M_n ^{a)} (GPC) [g/mol]	M_n ^{b)} (NMR) [g/mol]	M_n (MALDI)	
							simulated [g/mol]	measured [g/mol]
6a/7a	- ^{c)}	2500	2900	2800	4750	2400	1956.829	1956.846
6b/7b	- ^{c)}	5400	4800	5700	8900	5100	-	-
6c/7c	- ^{c)}	8200	non-existent		17200	8900	-	-

^{a)}PIB standards were used for GPC; ^{b)} M_n of ¹H-NMR spectroscopy were calculated out of the ratio of signals from phenylic endgroup (C_6H_4) around 6.80 ppm as well as from *CH*-groups from NHC ligand (6.17 ppm for **6**, 6.37 ppm for **5**) compared to the signals of the CH_2 -group as well as CH_3 -groups of PIB backbone. ^{c)}GPC analysis not possible due to the low detection intensity of ionic polymer

4.2.4.2 Synthesis of **6** and **7** by KO^tBu and [Cu(CH₃CN)₄]PF₆



Scheme 5. Synthesis of bis(*N*-methylimidazol-2-ylidene-telechelic poly(isobutylene) copper(I)X complex [Cu(PIB-NHC)₂]X (**6**) as well as corresponding monocarbene complex [Cu(PIB-NHC)]X (**7**).

5 was placed in a two-necked round-bottom flask equipped with rubber septum and gas tap and subjected to several vacuum-argon cycles. Dry and degassed THF was added adjusting a concentration of ~10 mM and the flask was transferred into a glove box. Potassium *tert*-butoxide (NaO^tBu) (1.1 eq.) was added and the resultant mixture was stirred for 15 min inside the glove box. Subsequently, [Cu(CH₃CN)₄]PF₆ (0.5 eq.) was added and the sealed flask was transferred out of the glove box. The rubber septum was replaced by a reflux condenser and the reaction mixture was heated for several hours into dark. Removing of the solvent yields the crude products **6/7** which were finally purified by column chromatography on silica (solvent mixture CHCl₃/*n*-hexane 5:1 changing gradually to pure CHCl₃; for details see above). The pure products were obtained as brownish, viscose polymers and were stored under argon atmosphere into dark until use. Experimental details are shown in Table 22. For characterization see Chapter 4.2.4.1.

Table 22. Experimental details for the synthesis of PIB-based copper(I)-biscarbene complex [Cu(PIB-NHC)₂]X (**6**) and monocarbene complex [Cu(PIB-NHC)]X (**7**) using KO^tBu and [Cu(CH₃CN)₄]PF₆. For all reactions THF was used as solvent adjusting the polymer concentration to ~10 mM.

Ent.	PIB-Imi (5)		[Cu(CH ₃ CN) ₄]PF ₆	KO ^t Bu	T [°C]	t [h]	isolated yields ^b [%]			
	M _n (NMR) [g/mol]	m; n					decomp. PIB (21) ^a	regained 5	mono-carbene complex (7)	bis-carbene complex (6)
6d/7d	5T : 4400	1 eq. 105 mg 24 μmol	0.5 eq. 5 mg 12 μmol	2 eq. 6 mg 48 μmol	RT	24	0	80	7d : 20	0
6e/7e	5T : 4400	1 eq. 93 mg 21 μmol	0.5 eq. 4 mg 11 μmol	2 eq. 5 mg 42 μmol	40	72	10	65	7e : 25	0
6f/7f	5T : 4400	1 eq. 102 mg 23 μmol	0.5 eq. 5 mg 12 μmol	1.1 eq. 5 mg 46 μmol	RT	24	23	9	7f : 11	6f : 45

^a) ¹H-NMR spectroscopy revealed decomposed PIB with terminal double bonds (4.50 – 5.50 ppm) caused by the elimination of the *N*-methylimidazolium endgroup from PIB; ^b) isolated yields after column, missing percentages to 100% are either mixed fractions or lost during the purification

4.2.4.3 Synthesis of **6** by Cu₂O

5 was placed in a two-necked round-bottom flask equipped with reflux condenser, rubber septum and gas tap and subjected to several vacuum-argon cycles. Cu₂O (5 eq.) was added in the counter current of Argon and the flask was evacuated and flushed with Argon one more time. Dry and degassed

toluene was added adjusting a polymer concentration of 2 mM and heated to reflux at 120°C. The solution was vigorously stirred for 120 h, cooled to room temperature and filtered in order to remove the excess Cu₂O. The crude products **6/7** were obtained after removing the solvent and were finally purified by column chromatography on silica (solvent mixture CHCl₃/*n*-hexane 5:1 changing gradually to pure CHCl₃; for details see above). The pure products were obtained as brownish, viscose polymers and were stored under argon atmosphere into dark until use. Experimental details are shown in Table 23. For characterization see Chapter 4.2.4.1.

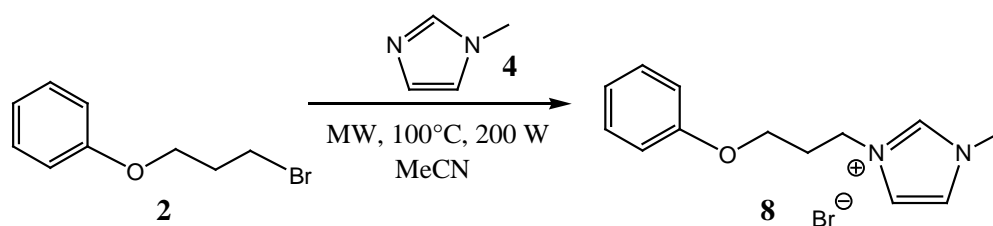
Table 23. Experimental details for the synthesis of **6** and **7** using Cu₂O as copper(I) source and base at once. For all reactions toluene was used as solvent adjusting a polymer concentration to ~2 mM.

Ent.	PIB-Imi (5)		Cu ₂ O	T [°C]	t [h]	isolated yields ^{b)} [%]			
	M _n (NMR) [g/mol]	m; n				decomp. PIB (21) ^{a)}	regained 5	monocarbene complex (7)	biscarbene complex (6)
6g/7g	5T : 4400	1 eq. 83 mg 19 μmol	5 eq. 14 mg 95 μmol	RT	120	0	98	0	0
6h/7h	5T : 4400	1 eq. 156 mg 35 μmol	5 eq. 25 mg 175 μmol	80	72	3	60	7h : 2	6h : 35
6i/7i	5T : 4400	1 eq. 75 mg 17 μmol	50 eq. 122 mg 850 μmol	120	120	33	11	7i : 7	6i : 49

^{a)}¹H-NMR spectroscopy revealed decomposed PIB with terminal double bonds (4.50 – 5.50 ppm) caused by the elimination of the *N*-methylimidazolium endgroup from PIB; ^{b)}isolated yields after column, missing percentages to 100% are either mixed fractions or lost during the purification

4.3 Synthesis of [Cu(BPB-NHC)₂]X model complex (**10**)

4.3.1 Synthesis of 1-(3-phenoxypropyl)-3-methylimidazolium bromide (**8**)



Scheme 6. Synthesis of 1-(3-phenoxypropyl)-3-methylimidazolium bromide (**8**).

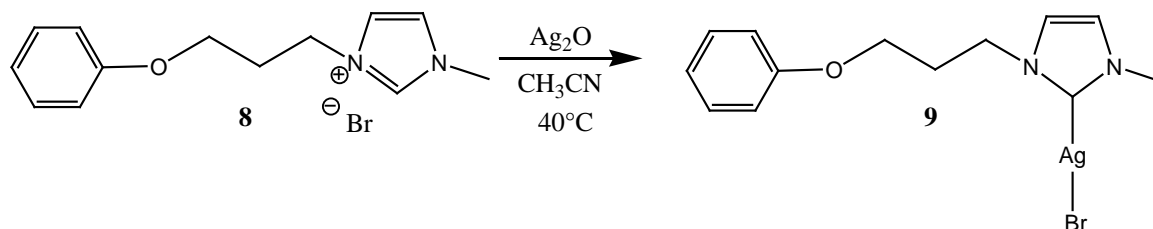
3-Phenoxypropyl bromide (BPB; **2**) (2364 μL, 15 mmol), *N*-methylimidazole (**4**) (396 μL, 5 mmol) and acetonitrile (3 mL) were added to a 10 mL microwave vial and stirred vigorously for 10 min at room temperature. Subsequently, the reaction mixture was placed in a microwave and heated for 4 h to 100°C with a power of 200W. The solution was concentrated in vacuum until an oily consistence was obtained, diluted with CHCl₃ (50 mL) and transferred into a separation funnel, followed by the addition of water (50 mL). The aqueous phase was extracted with CHCl₃ (3 x 50 mL) and the combined organic phases were washed twice with water (2 x 30 mL) until no product can be observed in the organic phase by TLC (ethyl acetate/MeOH 9:1; R_f (**8**) = 0.1; R_f (**2**) = 0.85; R_f (**4**) = 0.4). The combined aqueous phases were concentrated and finally dried for several days in high vacuum. The pure product was obtained as highly viscose oil in a yield of 94%. Selected spectra are presented in Appendix 7.4.

$^1\text{H-NMR}$ (400 MHz, CDCl_3): δ [ppm] 10.39 (s, 1H, NCHN), 7.45 (d, 2H, $m\text{C}_6\text{H}_5$, $^3J_{\text{H,H}} = 10.7$ Hz), 7.24-7.22 (m, 3H, overlay of 2H of $p\text{C}_6\text{H}_5$ and 1H of NCHCHNCH₃), 6.93 (t, 1H, NCHCHNCH₃, $J_{\text{H,H}} = 7.4$ Hz), 6.83 (d, 2H, $o\text{C}_6\text{H}_5$, $^3J_{\text{H,H}} = 7.8$ Hz), 4.58 (t, 2H, NCH₂, $^3J_{\text{H,H}} = 7.0$ Hz), 3.95 (m, 5H, OCH₂ and NCH₃), 2.44 (quint., 2H, OCH₂CH₂, $^3J_{\text{H,H}} = 5.9$ Hz).

$^{13}\text{C-NMR}$ (100 MHz, CDCl_3): δ [ppm] 158.0 ($i\text{C}_6\text{H}_5$), 137.8 (NCHN), 129.6 ($m\text{C}_6\text{H}_5$), 123.2 (NCHCHN), 122.5 (NCHCHN), 121.3 ($p\text{C}_6\text{H}_5$), 114.3 ($o\text{C}_6\text{H}_5$), 63.8 (OCH₂), 47.4 (NCH₂), 36.7 (NCH₃), 29.9 (OCH₂CH₂).

ESI-TOF-MS (direct injection, without salt or tune mix, 2.2 mg/mL in MeOH) [m/z]: two species were found $[\text{M}]^+$ without counterion or additional cation $\text{C}_{13}\text{H}_{17}\text{N}_2\text{O}^+$ simulated: 217.1335 g/mol, measured: 217.1898 g/mol and $[\text{2M}+\text{Br}]^+$ bromo-bridged dimer of **8** $\text{C}_{26}\text{H}_{34}\text{BrN}_2\text{O}^+$ simulated: 513.1860 g/mol, measured: 513.2109 g/mol.

4.3.2 Synthesis of 1-(3-phenoxypropyl)-3-methylimidazol-2-ylidene silver (I) bromide (**9**)

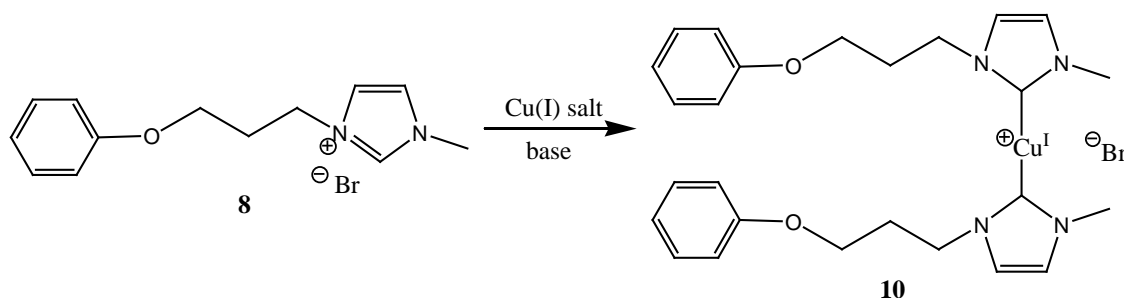


Scheme 7. Synthesis of 1-(3-phenoxypropyl)-3-methylimidazol-2-ylidene silver (I) bromide (**9**).

1-(3-phenoxypropyl)-3-methylimidazolium bromide (**8**) (102 mg, 343 μmol) was weighed into a previously under vacuum dried two-necked round bottom flask and silver(I) oxide (80 mg, 345 μmol) was added. The flask was sealed and subjected to several vacuum-argon cycles. Dry, degassed acetonitrile (10 mL) was added and the reaction mixture heated to 40°C for 48h in the dark until TLC shows no remaining educt (ethyl acetate/MeOH 9:1, R_f (**8**) = 0.1, R_f (**9**) = 0.95). Subsequently the solvent was removed and the crude product was flushed over a short frit of silica in order to remove residual particles. Pure **9** was obtained as highly viscose, slightly brownish product in a yield of 98% and was stored in the dark.

$^1\text{H-NMR}$ (400 MHz, CDCl_3): δ [ppm] 7.30 (d, 2H, $m\text{C}_6\text{H}_5$), 6.98-6.87 (m, 6H, superimposition of $p\text{C}_6\text{H}_5$, $o\text{C}_6\text{H}_5$, NCHCHNCH₃), 4.34 (t, 2H, NCH₂, $^3J_{\text{H,H}} = 6.9$ Hz), 3.94 (t, 2H, OCH₂, $^3J_{\text{H,H}} = 5.71$ Hz), 3.82 (s, 3H, NCH₃), 2.30 (quint., 2H, OCH₂CH₂, $^3J_{\text{H,H}} = 6.3$ Hz).

4.3.3 Synthesis of bis(1-(3-phenoxypropyl)-3-methylimidazol-2-ylidene) copper (I) bromide (**10**)



Scheme 8. Synthesis of bis(1-(3-phenoxypropyl)-3-methylimidazol-2-ylidene) copper (I) bromide (**10**).

4.3.3.1 Synthesis of **10** from **8** by NaO^tBu and CuBr

1-(3-phenoxypropyl)-3-methylimidazolium bromide (**8**) (118 mg, 397 μmol) was weighed in a previously under vacuum dried two-neck round-bottom flask and subjected to several vacuum-argon cycles. Sodium *tert*-butoxide (NaO^tBu) (42 mg, 437 μmol) and dry, degassed acetonitrile (10 mL) were added inside the glove box to **8** and the reaction mixture was allowed to stir at room temperature for 15 min. Subsequently, CuBr (28 mg, 195 μmol) was added and the sealed flask was heated outside the glove box in the dark to 40°C for 48h. Removing the solvent in vacuum yielded the crude product **10**, which was isolated via column chromatography on silica changing the eluent polarity gradually from ethyl acetate/MeOH 50:1 to 10:1 (TLC ethyl acetate/MeOH 9:1 R_f (**8**) = 0.1, R_f (**10**) = 0.25). The pure product **10** was obtained as slightly brownish crystals in a yield of 54%. Selected spectra are presented in Appendix 7.5.

¹H-NMR (400 MHz, CDCl₃): δ [ppm] 7.25 (m, 2H, *mC*₆H₅), 6.88 (m, 3H, superimposition of *pC*₆H₅ and *oC*₆H₅), 6.16 (d, 2H, NCHCHN, $J_{\text{H,H}} = 15.3$ Hz), 3.95 (t, 2H, OCH₂, $^3J_{\text{H,H}} = 5.7$ Hz), 3.84 (t, 2H, NCH₂, $^3J_{\text{H,H}} = 6.1$ Hz), 3.27 (s, 3H, NCH₃), 2.13 (quint., 2H, OCH₂CH₂, $^3J_{\text{H,H}} = 6.0$ Hz).

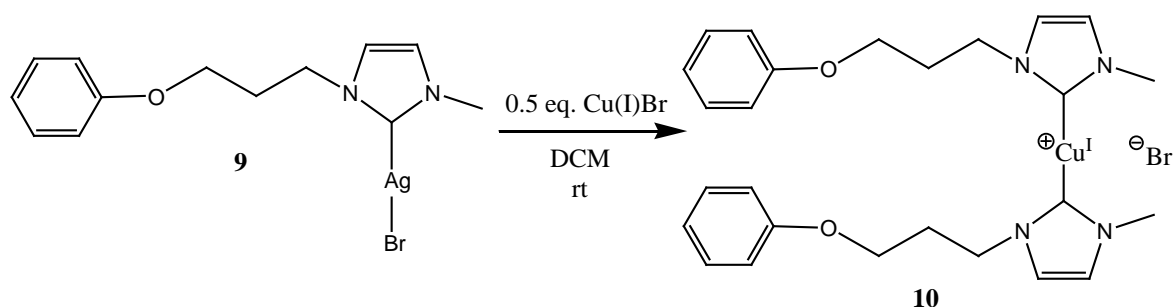
¹³C-NMR (100 MHz, CDCl₃): δ [ppm] 158.6 (*iC*₆H₅), 152.9 (NCCuN), 129.5 (*mC*₆H₅), 120.8 (*pC*₆H₅), 114.4 (*oC*₆H₅), 111.4 (NCHCHN), 110.8 (NCHCHN), 64.4 (OCH₂), 40.7 (NCH₂), 30.3 (NCH₃), 29.0 (OCH₂CH₂).

ESI-TOF-MS: was not possible as solely fractured products could be obtained

4.3.3.2 Synthesis of **10** from **8** by Cu₂O

8 (110 mg, 370 μmol) and Cu₂O (260 mg, 1817 μmol) were added to a previously under vacuum dried two-neck round-bottom flask, which was equipped with rubber septum, gas tap and reflux condenser and subjected to several vacuum-argon cycles. Dry and degassed acetonitrile (10 mL) was added and the reaction mixture was heated to 110°C for 48h. Removing the solvent in vacuum yielded the crude product **10**, which was isolated via column chromatography on silica changing the eluent polarity gradually from ethyl acetate/MeOH 50:1 to 10:1 (TLC ethyl acetate/MeOH 9:1: R_f (**8**) = 0.1, R_f (**10**) = 0.25). The pure product **10** was obtained as slightly brownish crystals in a yield of 68%. For characterization see Chapter 4.3.3.2.

4.3.3.3 Synthesis of **10** from **9** by CuBr



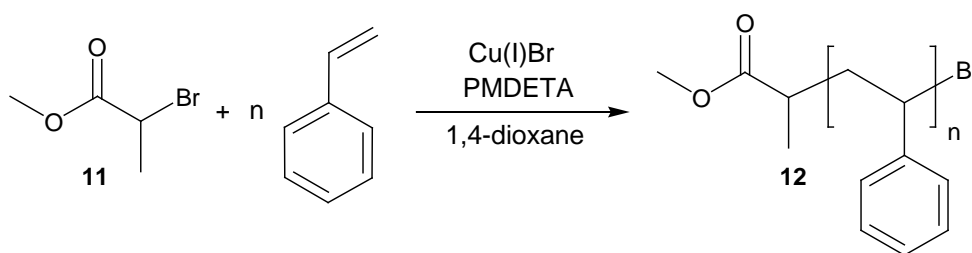
Scheme 9. Synthesis of bis(1-(3-phenoxypropyl)-3-methylimidazol-2-ylidene) copper (I) bromide (**10**) starting from 1-(3-phenoxypropyl)-3-methylimidazol-2-ylidene silver (I) bromide (**9**).

1-(3-phenoxypropyl)-3-methylimidazol-2-ylidene silver (I) bromide (**9**) (159 mg, 393 μmol) was added into a Schlenk tube and transferred into a glove box. Cu(I)Br (28 mg, 196 μmol) as well as dry, degassed dichloromethane (DCM) (15 mL) were added and the reaction mixture was stirred at room temperature in the dark for 24h. Removing the solvent in vacuum yielded the crude product **10**, which

was isolated via column chromatography on silica changing the eluent polarity gradually from ethyl acetate/MeOH 50:1 to 10:1 (TLC ethyl acetate/MeOH 9:1: R_f (**8**) = 0.1, R_f (**9**) = 0.95, R_f (**10**) = 0.25). The pure product **10** was obtained as slightly brownish crystals in a yield of 44%. For characterization see Chapter 4.3.3.2.

4.4 Synthesis PS-based bis(*N*-methylimidazol-2-ylidene) copper(I)X mechanocatalysts (**14**)

4.4.1 Synthesis of bromo-telechelic poly(styrene) (**12**)



Scheme 10. Synthesis of bromo-telechelic poly(styrene) (**12**) via ATRP.

The synthesis of **12** was done according to a general ATRP (atom transfer radical polymerization) literature procedure²³². A two-necked round bottom flask equipped with rubber septum, stirrer and three-way gas tap was attached to a Schlenk line and heated under vacuum and flushed with argon for several times. An appropriate amount freshly distilled, destabilized styrene (see Table 24) was degassed separately and added to the flask by the means of a syringe. Methyl 2-bromopropionate (MBPP) (**11**) (1 eq.) as well as *N,N,N',N',N''*-pentamethyldiethylenetriamine (PMDETA) (2 eq.) were added in the countercurrent of argon via Eppendorf pipette and the solution was diluted with degassed 1,4-dioxane. The sealed flask was transferred into the glove box, where Cu(I)Br (1 eq.) was added. Subsequently, the reaction mixture was stirred for 15 min at room temperature until a homogenous mixture was obtained and placed afterwards into a preheated oil bath at 80°C outside the glove box until the desired molecular weight was achieved (GPC control). Cooling the flask in an ice bath terminated the ATRP reaction and the crude product was precipitated into a large excess of methanol, re-dissolved in THF and flushed over column packed with neutral alumina using THF as eluent and precipitated again in large excess of methanol. The final product was obtained as a fine whiter powder in a yield of 60% after drying in high vacuum. Experimental details and characterization data are given in Table 24 and Table 25, while selected spectra are shown in Appendix 7.6.

$^1\text{H-NMR}$ (400 MHz, CDCl_3): δ [ppm] 7.18-6.68 (broad m, C_6H_5 of repetitive unit), 3.57 (s, 3H, OCH_3), 1.95-1.54 (broad m, CH as well as CH_2 of repetitive unit), 0.92 (s, 3H, $\text{CH}_3\text{OC(O)CH(CH}_3\text{)}$).

$^{13}\text{C-NMR}$ (100 MHz, CDCl_3): δ [ppm] 177.1 ($\text{CH}_3\text{OC(O)}$), 145.4 ($i\text{C}_6\text{H}_5$ of repetitive unit), 129.1-125.7 ($o\text{C}_6\text{H}_5$, $m\text{C}_6\text{H}_5$, $p\text{C}_6\text{H}_5$ of repetitive unit), 51.3 (CHBr), 46.5 (CH_3O), 44.3-40.5 (CH and CH_2 of repetitive unit as well as superposition of $\text{CH}_3\text{OC(O)CH(CH}_3\text{)-PS}$), 21.5 ($\text{CH}_3\text{OC(O)CH(CH}_3\text{)-PS}$).

MALDI-TOF-MS analyses were conducted with different matrices, salts and ionization methods, but no suitable spectrum could be obtained.

Table 24. Experimental details for the synthesis of bromo-telechelic poly(styrene)s (**12**).

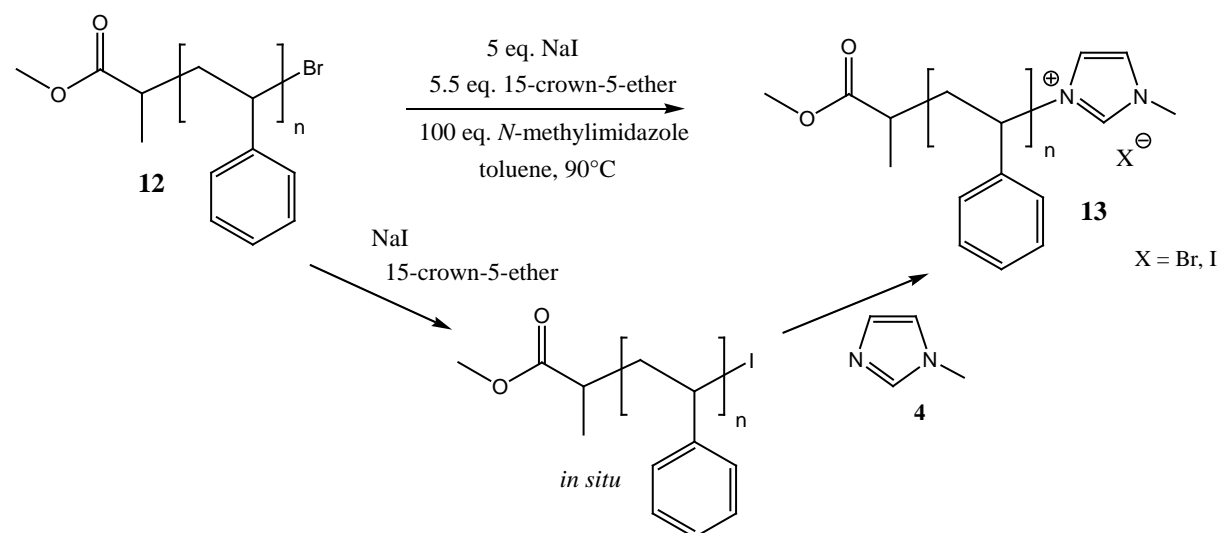
Ent.	styrene	MBPP (11)	Cu(I)Br	PMDETA	1,4-dioxane	time	isolated yield
12a	10 mL 87.4 mmol	340 μ L 3.0 mmol	436 mg 3.0 mmol	1270 μ L 6.0 mmol	3.3 mL	20h	98%
12b	10 mL 87.4 mmol	170 μ L 1.5 mmol	218 mg 1.5 mmol	635 μ L 3.0 mmol	3.3 mL	17h	76%
12c	23 mL 201 mmol	80 μ L 0.7 mmol	104 mg 0.7 mmol	300 μ L 1.4 mmol	bulk	20h	60%

Table 25. Characterization data of bromo-telechelic bromo-telechelic poly(styrene)s (**12**).

Ent.	$M_{n(\text{theo})}$ [g/mol]	$M_{n(\text{GPC})}^{\text{a)}$ [g/mol]	$M_{n(\text{NMR})}^{\text{b)}$ [g/mol]	PDI
12a	3100	3100	2800	1.3
12b	6000	5000	4900	1.1
12c	29000	7100	7200	1.1

^{a)}using PS standards in THF with a flow rate of 1 mL/min; ^{b)}For calculation, the resonances of the CH₃-group of the initiator at 0.92 ppm were normalized to 3H and brought into ratio to the resonance of the superpositioned signals of the CH and CH₂-groups of the polymer chain at 1.95-1.54 ppm. The obtained degree of polymerization (DP) was multiplied with 104.15 g/mol yielding the molecular mass of the synthesized polymer. The quantity of the quench process cannot be determined via ¹H-NMR spectroscopy due to the overlay of the CHBr resonance with the resonances of the CH/CH₂ groups of the polymer backbone (1.95-1.54 ppm).

4.4.2 Synthesis of *N*-methylimidazolium-telechelic PS (**13**)

**Scheme 11.** Synthesis of *N*-methylimidazolium-telechelic PS (**13**).

The subsequently described reaction conditions were figured out as the best according to several optimization attempts summed-up in Table 26. The following reactions were carried under a dry argon atmosphere as well as under exclusion of light. Bromo-telechelic poly(styrene) (**12**) was placed in a two-necked flask, subjected to several vacuum-argon cycled and was dissolved in dry, degassed

toluene adjusting a polymer concentration of 15 mM. Sodium iodide (5 eq.) was added in the countercurrent of argon. 15-crown-5-ether (5.5 eq.) as well as freshly distilled *N*-methylimidazole (100 eq.) were added by means of an Eppendorf pipette. The reaction mixture was stirred in the dark at 90°C for 5 days. Subsequently, the cold reaction mixture was precipitated two times into -18°C cold MeOH and dried into vacuum. The crude polymer mixture was purified by column chromatography on silica gel using first pure CHCl₃ and changing afterwards slowly the polarity to CHCl₃/MeOH 25:1 (TLC: CHCl₃/MeOH 25:1 R_f (**13**) = 0.15, blue stain). The pure *N*-methylimidazolium telechelic PS (**13**) was obtained as a slightly yellow, rigid polymer and stored under argon atmosphere into dark until further use. The experimental details as well as the characterization data are shown in Table 26 and Table 27, while selected spectra are shown in Appendix 7.7.

¹H-NMR (400 MHz, CDCl₃): δ [ppm] 10.14 (s, 1H, NCHN), 7.10-6.59 (broad m, C₆H₅ of repetitive unit), 6.89 (d, 2H, NCHCHN), 5.04 (m, 1H, CH₂CH(C₆H₅)N), 3.86 (m, 2H, CH₂CH(C₆H₅)N), 3.69 (s, 3H, NCH₃), 3.52 (s, 3H, OCH₃), 1.87-1.44 (broad m, CH as well as CH₂ of repetitive unit), 0.90 (s, 3H, CH₃OC(O)CHCH₃).

MALDI-TOF-MS [Dithranol, NaTFA] [m/z]: *N*-methylimidazolium-telechelic PS species found with additional sodium cation as [M+Na]⁺ for **13a** C₂₆₄H₂₆₉Br₁N₂Na₁O₂ simulated 3605.017 g/mol, found 3605.512 g/mol; for **13b** C₄₄₈H₄₅₃Br₁N₂Na₁O₂ simulated 5999.461 g/mol, found 5999.157 g/mol; for **13c** C₆₄₀H₆₄₅Br₁N₂Na₁O₂ simulated 8499.973 g/mol, found 8499.507 g/mol.

GPC analyses were not possible due to the low detection intensity of ionic polymer species even at concentrations of 5 mg/mL. Thus, no reliable signals of RI- respectively light scattering detection were observed, neither in THF not in toluene.

Table 26. Experimental details for the synthesis of *N*-methylimidazolium-telechelic PS (**13**).

Ent.	PS-Br (12)		NaI	15-crown-5-ether	<i>N</i> -methylimidazole (4)	solvent	T [°C]	time [h]	isolated yield [%]	
	M _n (GPC) [g/mol]	m; n								
13a	12a	3100	1 eq. 1043 mg 340 μmol	5 eq. 255 mg 1700 μmol	5.5 eq. 370 μL 1870 μmol	100 eq. 2710 μL 34.0 mmol	toluene	90	120	40
13b	12b	5000	1 eq. 1025 mg 203 μmol	5 eq. 152 mg 1015 μmol	5.5 eq. 221 μL 1117 μmol	100 eq. 1667 μL 20.3 mmol	toluene	90	120	49
13c	12c	7100	1 eq. 817 mg 115 μmol	5 eq. 86 mg 574 μmol	5.5 eq. 125 μL 632 μmol	100 eq. 936 μL 11.5 mmol	toluene	90	120	45

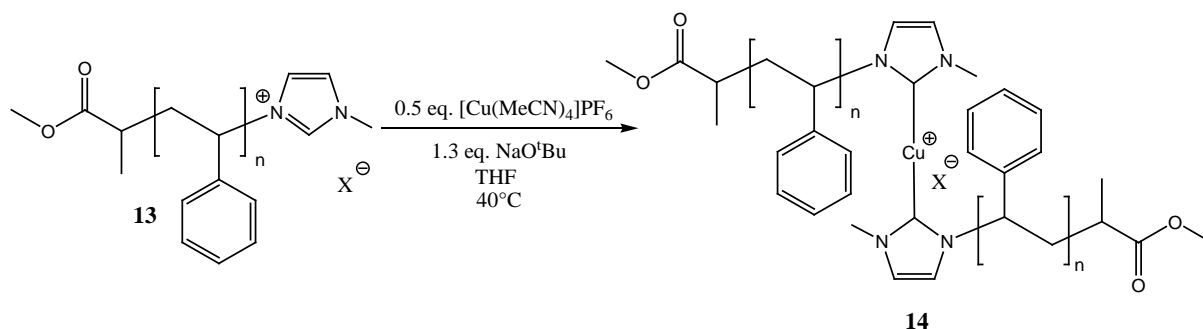
Table 27. Characterization data of *N*-methylimidazolium-telechelic PS (**13**).

Ent.	used PIB-Br: M _n (NMR) [g/mol]	M _n (NMR) ^{a)} [g/mol]	M _n (MALDI) [g/mol]	
			simulated	measured
13a	12a: 2800	3200	3605.017	3605.512
13b	12b: 4900	4800	5999.461	5999.157
13c	12c: 7200	7300	8499.973	8499.507

^{a)} Calculated according to the resonances of the CH₃-group of the initiator head group at 0.90 ppm and the superimposed signals of the CH and CH₂-groups of the polymer chain at 1.95-1.54 ppm.

4.4.3 Synthesis of bis(*N*-methylimidazol-2-ylidene-telechelic poly(styrene)copper(I)X complex [Cu(PS-NHC)₂]X (14)

4.4.3.1 Synthesis of 14 by NaO^tBu and [Cu(CH₃CN)₄]PF₆



Scheme 12. Synthesis of bis(*N*-methylimidazol-2-ylidene-telechelic poly(styrene)copper(I)X complex [Cu(PS-NHC)₂]X (14).

N-methylimidazolium telechelic PS (**7**) was placed in a two-necked flask, subjected to several vacuum-argon cycles and was dissolved in dry THF adjusting a concentration of 10 mM. Sodium *tert*-butoxide (1.3 eq.) was added by means of a stock solution in THF (20 mM) and the reaction mixture was stirred for 15 min at room temperature. Subsequently, tetrakis(acetonitrile)copper(I) hexafluorophosphate ([Cu(CH₃CN)₄]PF₆) (0.5 eq.) was added by means of stock solution in THF (10 mM). The reaction mixture was stirred at 40°C into dark for 48 h. Removing of the solvent yields the crude product **14** which was finally purified by column chromatography on silica (solvent mixture CHCl₃/*n*-hexane 2:1 changing gradually to pure CHCl₃; TLC: CHCl₃/*n*-hexane 10:1, R_f (**14**) = 0.1, for TLC details see below, blue stain). The pure products were obtained as yellowish, rigid polymers and were stored under argon atmosphere into dark until use. Experimental details and characterization data are shown in Table 28 and Table 29, while selected spectra are presented in Appendix 7.8.

TLC information for column chromatography:

During the column chromatography typically 3 fractions could be isolated and identified through ¹H-NMR spectroscopy. Moreover, higher molecular weight complexes **14b** and **14c** revealed higher R_f values compared to the lower molecular weight complex **14a**.

1st Fraction: R_{f1} = 0.35 - 0.5 → *N*-methylimidazolium eliminated PS

2nd Fraction: R_{f2} = 0.05 - 0.15 → desired PS complex **14**

3rd Fraction: R_{f3} = 0 → unreacted educt **13**

¹H-NMR (400 MHz, CDCl₃): δ [ppm] 7.06-6.59 (broad m, C₆H₅ of repetitive unit), 5.93 (d, 2H, NCHCHN), 4.90 (m, 1H, CH₂CH(C₆H₅)N), 3.77 (s, 3H, NCH₃), 3.49 (s, 3H, OCH₃), 3.17 (m, 2H, CH₂CH(C₆H₅)N), 1.87-1.45 (broad m, CH as well as CH₂ of repetitive unit), 0.88 (s, 3H, CH₃OC(O)CHCH₃).

¹³C-NMR spectroscopy shows only the signals of the polymer backbone as the quadruple moment of the attached Cu(I) suppress the intensity of the relevant signals of the *N*-methylimidazol-2-ylidene end group.

MALDI-TOF-MS analyses were conducted with different matrices, salts and ionization methods, but no suitable spectrum could be obtained.

Table 28. Experimental details for the synthesis of PS-based copper(I)-biscarbene complex $[\text{Cu}(\text{PS-NHC})_2]\text{X}$ (**14**) by 1.3 eq. NaO^tBu and 0.5 eq. $[\text{Cu}(\text{CH}_3\text{CN})_4]\text{PF}_6$. For all reactions THF was used as solvent adjusting according to the previously described protocol the overall polymer concentration to ~ 10 mM and stirred for 48h at 40°C .

Ent.	PS-Imi (13)		$[\text{Cu}(\text{CH}_3\text{CN})_4]\text{PF}_6$	NaO^tBu	isolated yields ^{b)} [%]		
	$M_n(\text{NMR})$ [g/mol]	m; n			decomp. PS ^{a)}	regained 13	biscarbene complex 14
14a	13a: 3200	258 mg 81 μmol	15.1 mg 40.5 μmol	10.1 mg 105 μmol	16	-	32
14b	13b: 4800	334 mg 70 μmol	13.0 mg 35 μmol	8.7 mg 91 μmol	11	23	39
14c	13c: 7300	408 mg 56 μmol	10.4 mg 28 μmol	7.0 mg 73 μmol	4	32	35

^{a)}elimination of the *N*-methylimidazolium endgroup from PS; ^{b)}isolated yields after column, missing percentages to 100% are either mixed fractions or lost during the purification

Table 29. Characterization data of PS-based copper(I)-biscarbene complexes $[\text{Cu}(\text{PS-NHC})_2]\text{X}$ (**14**) synthesized by NaO^tBu and $[\text{Cu}(\text{CH}_3\text{CN})_4]\text{PF}_6$.

Ent	PS-Br (12)		PS-Imi (13)				biscarbene complex $[\text{Cu}(\text{PS-NHC})_2]\text{X}$ (14)	
	$M_n^{\text{a)}$ (GPC)	$M_n^{\text{b)}$ (NMR)	$M_n^{\text{a)}$ (GPC)	$M_n^{\text{b)}$ (NMR)	M_n (MALDI) [g/mol]		$M_n^{\text{a)}$ (GPC)	$M_n^{\text{b)}$ (NMR)
	[g/mol]	[g/mol]	[g/mol]	[g/mol]	simulated	measured	[g/mol]	[g/mol]
a	3100	2800	- ^{c)}	3200	3605.017	3605.512	6800	3100
b	5000	4900	- ^{c)}	4800	5999.461	5999.157	11600	4800
c	7100	7200	- ^{c)}	7300	8499.973	8499.507	13600	9300

^{a)}PS standards were used for GPC; ^{b)} M_n of $^1\text{H-NMR}$ spectroscopy were calculated out of the ratio of signals from the CH_3 of the initiator head group at 0.88 ppm and the superimposed signals of the CH and CH_2 -groups of the polymer chain at 1.87-1.45 ppm as well as the CH_2 -group of the last repetitive unite close to the NHC (CH_2CHBr) at 3.17 ppm. ^{c)} GPC analysis not possible due to the low detection intensity of ionic polymer

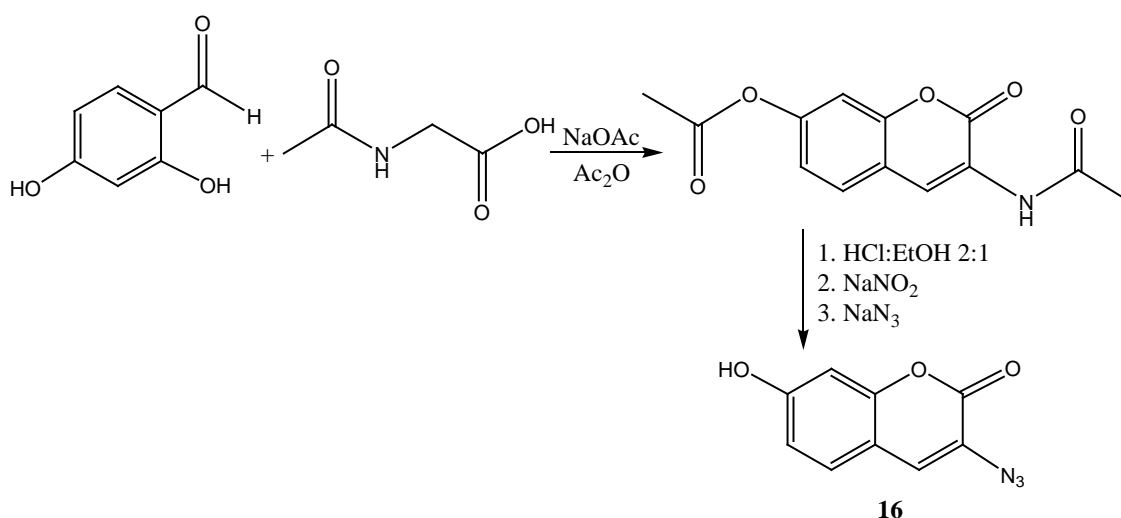
4.4.3.2 Synthesis of **14** by *KHMDS* and $[\text{Cu}(\text{CH}_3\text{CN})_4]\text{PF}_6$

N-methylimidazolium telechelic PS (**13a**) (262 mg, 82 μmol) was placed in a two-necked round-bottom flask, subjected to several vacuum-argon cycles and was dissolved in dry, degassed toluene (5 mL). Potassium hexamethyldisilazide (*KHMDS*) (1.5 eq., 25 mg, 123 μmol) was dissolved in dry toluene inside the glove box (concentration ~ 30 mM), added to **13** and the reaction mixture was stirred for 15 min at room temperature. Subsequently, tetrakis(acetonitrile)copper(I) hexafluorophosphate $[\text{Cu}(\text{CH}_3\text{CN})_4]\text{PF}_6$ (0.5 eq., 15 mg, 41 μmol) was dissolved inside the glove box into dry acetonitrile (concentration ~ 50 mM), added to the reaction mixture and stirred overnight at room temperature into dark. Removing of the solvent and conducted $^1\text{H-NMR}$ spectroscopic measurements revealed no detectable amount of desired biscarbene complex **14** as solely decomposition product (see above) could be observed.

4.4.3.3 Synthesis of 14 by Cu₂O

13a (203 mg, 63 μ mol) was placed in a two-necked round-bottom flask equipped with reflux condenser, rubber septum and gas tap and subjected to several vacuum-argon cycles. Cu₂O (5 eq., 45 mg, 315 μ mol) was added in the counter current of argon and the flask was evacuated and flushed with argon one more time. Dry and degassed toluene (5 mL) was added and the reaction mixture was heated to reflux at 120°C. The solution was vigorously stirred for 120 h and samples for ¹H-NMR spectroscopy were taken after each 24 h. However, also after 120 h only the decomposition of **13**, but no formation of product **14** could be observed.

4.5 Synthesis of 3-azido-7-hydroxy-coumarin (**16**)



Scheme 13. Synthesis of 3-azido-7-hydroxycoumarin (**16**).

The synthesis of 3-azido-7-hydroxycoumarin (**16**) was accomplished with several modifications according to an adopted literature procedure²²⁵. 2,4-dihydroxy benzaldehyde (2.77 g, 20 mmol), *N*-acetylglycine (2.35 g, 20 mmol) and anhydrous sodium acetate (6.00 g, 73 mmol) were placed in a two-necked round bottom flask equipped with rubber septum, gas tap and reflux condenser and dissolved in acetic anhydride (100 mL) and heated for 4 h to 160°C. Subsequently the hot solution was poured onto 1L ice leading to the formation of a yellow precipitate, which was filtered and washed with ice water (300 mL). The obtained double acetyl protected intermediate was placed into a two-necked round bottom flask equipped with a reflux condenser, rubber septum and gas tap and dissolved in a 2:1 mixture of concentrated hydrochloric acid and ethanol (30 mL). Refluxing this solution for 1 h was followed by dilution with ice water (40 mL). The mixture was cooled in an ice bath, treated with sodium nitrite (2.77 g, 40 mmol) and stirred for 15 min. Subsequently, sodium azide (3.90 g, 60 mmol) was added in small portions, while temperature of this strongly exothermic reaction was kept continuously below 5°C during the whole time of addition. After stirring for 15 min, the formed dark brown precipitate was filtered, washed with water (300 mL) and dried in high vacuum. The pure product was obtained as a dark brown solid with a yield of 30% and was stored under exclusion of light, oxygen and water in a desiccator. Selected spectra are presented in Appendix 7.9.

¹H-NMR (400 MHz, DMSO-d₆): δ [ppm] 10.50 (s, 1H, OH), 7.58 (s, 1H, CHC-N₃), 7.47 (d, 1, CHCHC(OH), ³J_{H,H} = 8.5 Hz), 6.80 (dd, 1H, CHCHC(OH), ³J_{H,H} = 8.5 Hz, ⁴J_{H,H} = 2.5 Hz), 6.75 (d, 1H, CCHC(OH), ⁴J_{H,H} = 2.5 Hz).

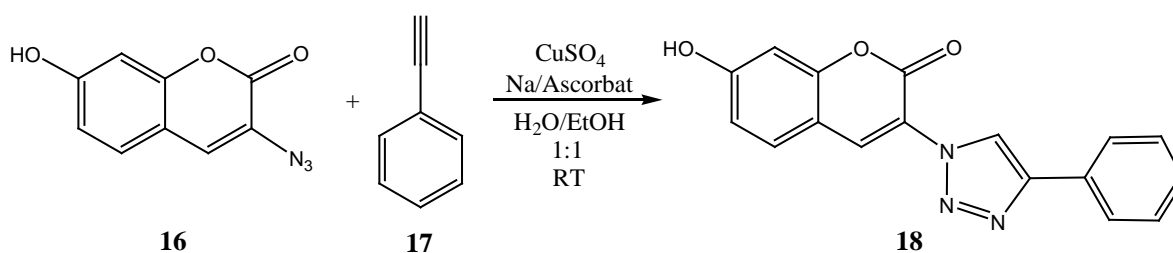
$^{13}\text{C-NMR}$ (100 MHz, DMSO- d_6): δ [ppm] 160.3 (C(OH)), 157.3 (C=O), 152.7 (C-O-C=O), 129.1 (CHCHC(OH)), 127.8 (CCHC(OH)), 121.1 (C-N₃), 113.8 (CHCHC(OH)), 111.3 (CCHC-N₃), 102.0 (CHC-N₃)

IR (bulk) [cm^{-1}]: 3284 (s), 3052 (m), 2106 (s) (azide), 1677 (s), 1620 (s), 1451 (w), 1342 (m), 1318 (m), 1220 (m), 1120 (w), 926 (w), 836 (w).

ESI-TOF-MS (direct injection, without salt or tune mix, THF/MeOH 20:1, 1.0 mg/mL) [m/z]: [M-H]⁻ C₉H₄N₃O₃: simulated 202.0247 g/mol, found 202.0322 g/mol; [M+Cl]⁻ C₉H₅ClN₃O₃: simulated 238.0014 g/mol, found 238.0053 g/mol; [2M-H]⁻ C₁₈H₉N₆O₆: simulated 405.0578 g/mol, found 405.0500 g/mol.

UV-vis : absorption maximum in THF 340 nm with relative intensity of 1.25.

4.6 Synthesis of 7-hydroxy-3-(4-phenyl-1*H*-[1,2,3]triazole-1-yl)-coumarin (**18**)



Scheme 14. Synthesis of 7-hydroxy-3-(4-phenyl-1*H*-[1,2,3]triazole-1-yl)-coumarin (**18**).

The synthesis of 7-hydroxy-3-(4-phenyl-1*H*-[1,2,3]triazole-1-yl)-coumarin (**18**) was accomplished according to an adopted literature procedure²²⁵. 3-azido-7-hydroxycoumarin (**16**) (100 mg, 492 μmol) was added to Schlenk tube, subjected to several vacuum-argon cycles to remove the oxygen and dissolved in an ethanol/water mixture (v:v = 1:1, 6 mL). Phenylacetylene (**17**) (54 μL , 492 μmol), sodium ascorbate (39 mg, 197 μmol) and Cu(II)SO₄ · 5H₂O (12 mg, 49 μmol) were added in the countercurrent of argon and the reaction mixture was stirred for 24 h at room temperature in the dark. Subsequently the ethanol was removed in vacuum and the residual aqueous solution was placed in the fridge overnight. The formed precipitate was filtered, washed with ice water (10 mL) and dried in high vacuum for several days. The final product was obtained as a dark brown solid in a yield of 46% and was stored under exclusion of light, oxygen and water in a desiccator. Selected spectra are presented in Appendix 7.10.

$^1\text{H-NMR}$ (400 MHz, DMSO- d_6): δ [ppm] 10.92 (s, 1H, OH), 8.99 (s, 1H, triazole), 8.65 (s, 1H, CHCN), 7.96 (d, 2H, *o*C₆H₅, ³J_{H,H} = 7.2 Hz), 7.78 (d, 1H, CHCHC(OH), ³J_{H,H} = 8.5 Hz), 7.49 (t, 2H, *m*C₆H₅, ³J_{H,H} = 7.6 Hz), 7.38 (t, 1H, *p*C₆H₅, ³J_{H,H} = 7.4 Hz), 6.92 (d, 1H, CHCHC(OH), ³J_{H,H} = 8.6 Hz), 6.87 (s, 1H, CCHC(OH)).

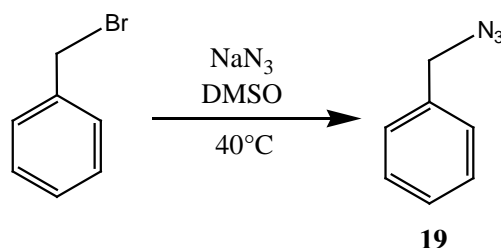
$^{13}\text{C-NMR}$ (100 MHz, DMSO- d_6): δ [ppm] 156.3 (C(OH)), 146.4 (C-O-C=O), 143.5 (C=O), 136.8 (N=N-NCHC), 131.0 (*i*C₆H₅), 130.1 (N=N-NCHC), 129.0 (*o*C₆H₅), 128.2 (CCHC-N), 125.4 (*m*C₆H₅), 122.1 (CHCHC(OH)), 120.8 (*p*C₆H₅), 119.2 (CCHC-N₃), 110.3 (CCHC-N), 107.5 (CHCHC(OH)), 102.2 (CCHC(OH)).

IR (bulk) [cm^{-1}]: 3379 (s), 3171 (m), 3083 (m), 1736 (s), 1713 (s), 1606 (s), 1413 (m), 1242 (s), 1178 (w), 1132 (w), 1051 (w), 767 (w).

UV-vis : absorption maxima in THF 250 nm (relative intensity 9.20) and 350 nm (relative intensity 9.80).

ESI-TOF-MS (direct injection, without salt or tune mix, THF/MeOH 20:1, 1.0 mg/mL) [m/z]: [M-H]⁻ C₁₇H₁₀N₃O₃: simulated 304.0717 g/mol, found 304.0673 g/mol, [2M-H]⁻ C₃₄H₂₁N₆O₆: simulated 609.1517 g/mol, found 609.1271 g/mol.

4.7 Synthesis of benzyl azide (**19**)



Scheme 15. Synthesis of benzyl azide (**19**).

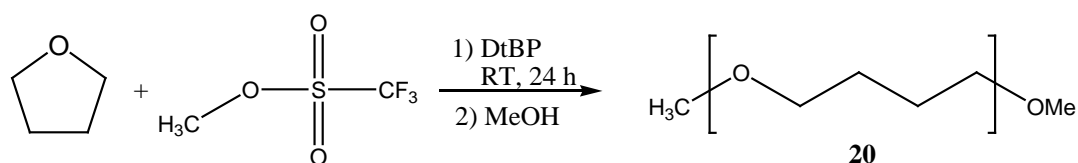
The synthesis of **19** was done according to literature procedure²³³. Sodium azide (15.0 g, 231 mmol) was dissolved in 300 mL dry DMSO into a two-necked round bottom flask equipped with magnetic stirrer, gas tap and rubber septum. Benzyl bromide (16.7 mL, 140 mmol) was added and the reaction mixture was heated to 40°C until a complete conversion was achieved after four days (TLC control in CHCl₃/*n*-hexane 4:1; R_f (benzyl bromide) = 0.37 and 0.73; R_f (**19**) = 0.50 and 0.68; blue stain). Subsequently, water (150 mL) was added and the solution was transferred into a separation funnel and extracted with diethyl ether (4x 150 mL). The combined organic layers were washed with water (2x 100 mL) and brine (100 mL) and dried over MgSO₄. After removing the solvent in vacuum, the pure product **19** was obtained with a yield of 96%.

¹H-NMR (400 MHz, CDCl₃): δ [ppm] 7.40-7.29 (m, 5H, C₆H₅), 4.33 (s, 2H, CH₂N₃).

¹³C-NMR (100 MHz, CDCl₃): δ [ppm] 135.4 (*i*C₆H₅), 128.8 (*m*C₆H₅), 128.3 (*p*C₆H₅), 128.2 (*o*C₆H₅), 54.9 (CH₂N₃).

IR data (bulk) [cm⁻¹]: 3032 (w), 2933 (w), 2090 (s) (azide), 1496 (w), 1455 (w), 1253 (m), 846 (w), 735 (w), 695 (m).

4.8 Synthesis of high molecular weight PTHF (**20**)



Scheme 16. Synthesis of high molecular weight poly(tetrahydrofuran) (PTHF) (**20**).

The synthesis of high molecular weight high molecular weight PTHF matrix was done according to general literature procedure^[1] via cationic ring opening polymerization. Methyl trifluoromethanesulfonate (60 μL, 547 μmol), DtBP (3 μL, 139 μmol) and freshly distilled, dry and degassed THF (600 mL, 7.4 mol) were placed in a previously under vacuum heated and with argon flushed 1L two-neck flask. The reaction mixture was stirred vigorously at room temperature until the desired high molecular weight was achieved (controlled by GPC). After 24 h, MeOH (50 mL) was added to the viscose solution and stirred overnight to quench the polymerization. Afterwards, the solution was diluted with THF and precipitated two times into a large excess of MeOH. The high

molecular weight PTHF was obtained after drying in vacuum until constant weight in a yield 10%. The final molecular weight of the isolated PTHF was determined to 112 000 g/mol by GPC. The melting point was determined by DSC to 46.3°C and a melting enthalpy of 117.8 J/g were obtained which corresponds to a crystallinity of 68% (according to literature $\Delta H_{m(100\%)} = 172 \text{ J/g}^{234}$).

4.9 Mechanochemical activation of latent catalysts in solution by ultrasonication

4.9.1 Concentration-RI-intensity calibration of GPC

In order to enable a quantification of ultrasound induced scission of the synthesized mechanocatalysts by GPC, a calibration of the RI-signal intensity in respect to the concentration of the polymeric bis- (**I**) and monovalent (**II**) species has to be performed. For that purpose, various samples of the corresponding PS- and PIB-based mechanocatalysts with concentration ranging from 0 mM to at least 1.5 mM, which correlates to the theoretical concentration of quantitative cleavage of the mechanocatalysts (as the cleavage of one biscarbene mechanophore yields two polymer chains of the half molecular weight) were prepared. Therefore, a stock solution of the appropriate polymer was prepared dissolving 35 mg in 3.5 mL HPLC-grade THF. Subsequently the required amounts were transferred via an Eppendorf pipette in the GPC vial and fill-up to a total amount of 1 mL (see Appendix 7.11 Table A1) and the GPC measurements were performed. The obtained calibration curves plotting the RI-response in dependency of the concentration are given in Appendix 7.11 Figures A38-A42 and the results are summed-up in Table 30. The slopes were obtained by linear regression over the whole concentration range.

Table 30. Results of RI-signal intensity calibration in respect to the concentration of the PIB-based as well as the PS-based bi- and monovalent moieties.

Ent.	Cu(I) mechanocatalyst initial M_n (GPC) ^{a)} [g/mol]	Slope [$\text{mV} \cdot \text{mL}^2 \cdot \text{mmol}^{-1}$]		Ratio of slopes bis(I)/mono(II)
		Bivalent species (I)	Monovalent species (II)	
PIB-based mechanocatalyst (6)				
6a	4750	20800	10900	1.91
6b	8900	40400	18700	2.16
6c	17200	68500	34800	1.97
PS-based mechanocatalyst (14)				
14a	6800	51000	50500	1.01
14b	11600	49000	43000	1.14
14c	13600	46200	42400	1.09

^{a)}determined by GPC in THF using PIB-standards for **6** and PS-standards for **14**,

The results summed-up in Table 30 show, that in case of the PIB-based mechanocatalyst (**6**) the ratio of slopes (which represents how fast the signal intensity of RI-detector changes with concentration) from bi- and corresponding monovalent (**I/II**) species is 2 independently of the initial molecular weight. That means one biscarbene mechanocatalyst **6** produces two polymeric species with the half molecular weight which should lead in turn to a doubling of RI-signal intensity. But as the calibration curves revealed that the cleaved, lower molecular weight polymers showed at the same concentration just the half RI-signal response, the RI-signal intensity during mechanocatalyst cleavage stays the same level. Thus, the equation **eq1** can be used for quantification of mechanocatalyst cleavage (with X - cleaved mechanophores in %; M_n (**I**) - number average molecular weight determined by GPC of bivalent species **6**; M_n (**II**) - number average molecular weight determined by GPC of monovalent species; M_n (determined) - number average molecular weight determined by GPC after z sonication cycles) (for derivation see Appendix 7.11).

$$X = \frac{M_n(\text{determined}) - M_n(\mathbf{6})}{M_n(\mathbf{7}) - M_n(\mathbf{6})} \cdot 100 \quad (\text{eq1})$$

In case of the PS-based mechanocatalysts (**14**), the ratio of the slopes from the bi- and corresponding monovalent species is around 1 and again independently of the initial molecular weight. This indicates that a doubling of the polymeric moieties due to the scission of one mechanocatalyst into two species with the half molecular weight led to a doubling in the RI-response. Thus, the equation **eq2** can be used for quantification of PS-based mechanocatalyst cleavage (for derivation see Appendix 7.11).

$$X = \frac{M_n(\text{determined}) - M_n(\mathbf{14})}{M_n(\text{determined})} \cdot 100 \quad (\text{eq2})$$

4.9.2 Ultrasound-induced cleavage of mechanocatalyst in solution

Ultrasonication experiments were performed with a Sonics VCX 500 ultrasonic processor at a frequency of 20 kHz. A 254 mm long full wave solid probe out of titanium alloy (Ti-Al-4V) with a diameter of 13 mm was used together with an internally threaded stainless steel adapter (fitting to probe at nodal point). All sonication experiments were conducted under inert and dry conditions in a 10 mL reaction vessel with two additional 14/20 side necks which was temperate at 20°C by an external cooling bath. The sonication intensity was 8.75 W/cm². The mixtures of mechanocatalysts **6** respectively **14** were prepared either in pure THF or in 30:1 THF/MeOH mixtures according to common Schlenk techniques. In case of ¹H-NMR spectroscopic investigations of **6** deuterated THF as well as non deuterated MeOH were used as solvents, while HPLC grade solvents were used for GPC experiments of **6** and **14**. The mechanophore concentration was adjusted in compliance to literature¹²⁻¹⁵ to 0.75 mM. Subsequently, ultrasound was applied with 30% of the maximal amplitude of 125 μm in several sonication cycles implementing thus energy of 21 kJ per sonication cycle. One cycle consists of 90 min sonication (with a pulse sequence of 5s on and 10s off) followed by 60 min without sonication. ¹H-NMR spectroscopy as well as GPC samples were directly taken out of the mixture at the end of the 1st cycle after 150 min, 2nd cycle after 300 min, 3rd cycle after 450 min, 5th cycle after 750 min, 10th cycle after 1500 min and 20th cycle after 3000 min. The results of the GPC monitored scission experiments are presented in Table 31 and 32, whereat the cleavage efficiencies were calculated for **6** according to equation **eq1** and for **14** according to equation **eq2**. Selected chromatograms and ¹H-NMR spectra are presented in Appendix 7.12.

Table 31. Results of GPC investigations from mechanochemical cleavage of PIB-based mechanocatalysts **6** by ultrasound (US).

Ent	US cycle ^{c)}	t [h]	6a ^{a)}			6b ^{a)}			6c ^{a)}			6c without MeOH ^{b)}		
			M _n ^{(GPC)^{d)}} [g/mol]	PDI	cleaved 6a [%] ^{e)}	M _n ^{(GPC)^{d)}} [g/mol]	PDI	cleaved 6b [%] ^{e)}	M _n ^{(GPC)^{d)}} [g/mol]	PDI	cleaved 6c [%] ^{e)}	M _n ^{(GPC)^{d)}} [g/mol]	PDI	cleaved 6c [%] ^{e)}
1	0	0	4750	1.60	0	8900	1.25	0	17200	1.23	0	17450	1.23	0
2	1	2.5	4500	1.68	9	8400	1.31	12	15400	1.30	21	17200	1.22	3
3	2	5	4250	1.69	19	7800	1.37	26	14100	1.33	37	17050	1.24	4
4	3	7.5	4000	1.77	30	7350	1.42	37	12750	1.40	53	16900	1.23	6
5	5	12.5	3750	1.77	38	7050	1.49	44	11600	1.45	66	16800	1.23	8
6	10	25	3650	1.76	42	6800	1.48	50	10700	1.46	76	16750	1.23	8
7	20	50	3600	1.76	45	6600	1.52	55	10000	1.47	84	16450	1.24	11

^{a)}Mechanocatalysts **6** in THF/MeOH 30:1 solvent mixtures in a concentration of 0.75 mM; ^{b)}Mechanocatalysts **6** in pure THF as solvent in a concentration of 0.75 mM; ^{c)}US cycle: consisting of 90 min sonication with a sonication intensity of 8.5 W/cm² applying a pulse sequence of 5s on, 10s off and 60 min without sonication corresponding to an energy input of 21 kJ per US cycle; ^{d)}Determined by GPC in HPLC-grade THF using PIB standard; ^{e)}Quantified by GPC using equation **eq1**.

Table 32. Results of GPC investigations from mechanochemical cleavage of PS-based mechanocatalysts catalysts **14** by ultrasound (US).

Ent	US cycle ^{e)}	t [h]	14a ^{a)}			14b ^{a)}			14c ^{a)}		
			M _n ^(GPC) ^{d)} [g/mol]	PDI	cleaved 14a [%] ^{e)}	M _n ^(GPC) ^{d)} [g/mol]	PDI	cleaved 14b [%] ^{e)}	M _n ^(GPC) ^{d)} [g/mol]	PDI	cleaved 14c [%] ^{e)}
1	0	0	6800	1.20	0	11650	1.32	0	13650	1.19	0
2	1	2.5	6350	1.23	6	9950	1.43	14	11700	1.25	17
3	2	5	6100	1.27	10	8100	1.51	34	10400	1.26	33
4	3	7.5	5150	1.33	28	7000	1.52	50	9350	1.23	50
5	5	12.5	4600	1.39	42	6400	1.49	60	8650	1.23	63
6	10	25	4550	1.39	42	6000	1.46	68	7950	1.16	78
7	20	50	4450	1.42	46	5950	1.42	69	7900	1.17	80

^{a)}Mechanocatalysts **14** in THF/MeOH 30:1 solvent mixtures in a concentration of 0.75 mM; ^{e)}Ultrasonication cycle: consisting of 90 min sonication at 20 kHz with 30% of max. amplitude of 125 μm with a sonication intensity of 8.5 W/cm² applying a pulse sequence of 5s on, 10s off and 60 min without sonication corresponding to an energy input of 21 kJ per US cycle; ^{d)}Determined by GPC in HPLC-grade THF using PS standard; ^{e)}Quantified by GPC using equation **eq2**.

4.9.3 Control and thermal scission experiments

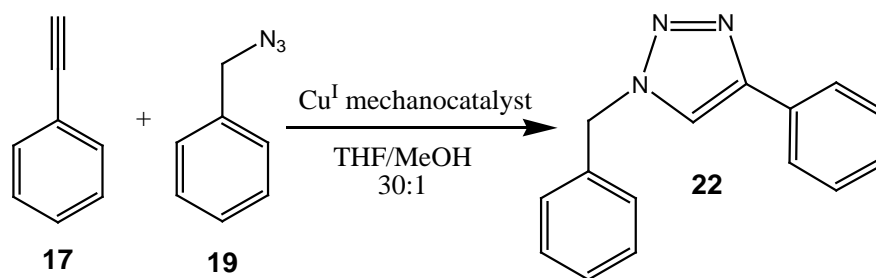
Control and thermal decomposition experiments were conducted under dry and inert conditions in normal two-necked flasks without ultrasonication. The concentration of the mechanophores **6c** and **14c** was kept constant at 0.75 mM in THF/MeOH 30:1 mixtures. The temperature was adjusted to 65°C under reflux conditions for the thermal experiments, while keeping at room temperature for the blind and control experiments. ¹H-NMR spectroscopy or GPC samples were directly taken out of the mixture after appropriate time. The results of the GPC monitored experiments are presented in Table 33 and selected chromatograms and ¹H-NMR spectra are presented in Appendix 7.12.

Table 33. Results of GPC investigations from thermal cleavage of PIB-based mechanocatalysts **6** as well as PS-based mechanocatalyst **14** at 65°C without ultrasound as well as control experiment without ultrasonication at 20°C.

Ent	t [h]	Thermal treatment of 6c without US at 65°C ^{a)}			Control experiment of 6c without US at 20°C ^{a)}			Thermal treatment of 14c without US at 65°C ^{a)}			Control experiment of 14c without US at 20°C ^{a)}		
		M _n ^(GPC) ^{b)} [g/mol]	PDI	cleaved 6c [%] ^{c)}	M _n ^(GPC) ^{b)} [g/mol]	PDI	cleaved 6c [%] ^{c)}	M _n ^(GPC) ^{d)} [g/mol]	PDI	cleaved 14c [%] ^{e)}	M _n ^(GPC) ^{d)} [g/mol]	PDI	cleaved 14c [%] ^{e)}
1	0	17500	1.29	0	17500	1.30	0	13600	1.18	0	13600	1.18	0
2	3	10750	1.49	77	17500	1.29	0	9550	1.25	46	13600	1.18	0
3	6	10200	1.48	84	17450	1.30	1	8350	1.27	70	13650	1.19	0
4	12	10050	1.49	85	17500	1.31	0	7950	1.26	79	13750	1.18	0
5	24	9450	1.49	92	17400	1.29	1	7750	1.28	85	13650	1.18	0
6	48	9250	1.49	95	17400	1.31	1	7700	1.28	86	13650	1.19	0
7	72	8950	1.45	97	17500	1.31	0	7600	1.26	88	13600	1.19	0

^{a)}Mechanocatalysts **6/14** in THF/MeOH 30:1 solvent mixtures in a concentration of 0.75 mM; ^{b)}Determined by GPC in HPLC-grade THF using PIB standard; ^{c)}Quantified by GPC using equation **eq1**. ^{d)}Determined by GPC in HPLC-grade THF using PS standard; ^{e)}Quantified by GPC using equation **eq2**.

4.9.4 Ultrasound triggered CuAAC “click” reaction of benzyl azide (19) and phenylacetylene (17) using latent mechanocatalysts



Scheme 17. Model “click” reaction of phenylacetylene (17) with benzyl azide (19) in order to determine the activation of latent mechanocatalysts **6** and **14** by *in situ* ¹H-NMR spectroscopic investigations.

The catalytic activity of the catalysts **6**, **7**, **10** and **14** was investigated by means of a model “click” reaction from phenylacetylene (**17**) and benzyl azide (**19**). For that purpose, an appropriate amount of **6**, **7**, **10** or **14** was weight directly into a 10 mL reaction vessel for ultrasound application with two additional side necks and was attached to a Sonics VCX 500 ultrasonic processor equipped with a long full wave solid probe (diameter 13 mm) and an internally threaded stainless steel adapter. The reaction vessel was subjected to several vacuum-argon cycles followed by the addition of **17** and **19** in an equimolar ratio (100 eq. per catalyst each) in the countercurrent of argon by means of an Eppendorf pipette. Afterwards either pure dry and degassed THF-d₈ or a mixture of THF-d₈ and MeOH (30:1) was added adjusting the mechanophore concentration to 0.75 mM (in compliance to literature^{12; 15}). Subsequently, ultrasound was applied at a frequency of 20 kHz with 30% of the maximal amplitude of 125 μm in several sonication cycles with a sonication intensity of 8.75 W/cm² implementing thus energy of 21 kJ per sonication cycle. One cycle consists of 90 min sonication (with a pulse sequence of 5s on and 10s off) followed by 60 min without sonication. The reaction vessel was cooled by external cooling system in order to avoid temperature increase during the sonication process. Temperature control was done by means of an inlet thermometer ensuring a temperature below 25°C. The conversion of the reaction was determined by ¹H-NMR spectroscopy at the end of the 1st cycle after 150 min, 2nd cycle after 300 min, 3rd cycle after 450 min, 5th cycle after 750 min and 10th cycle after 1500 min taking the NMR samples directly out of the mixture without further purification. Control and thermally triggered experiments were conducted under dry and inert conditions in normal two-necked flasks without ultrasonication. The concentration of the mechanophores **6**, **7**, **10** and **14** was kept constant at 0.75 mM either in pure THF-d₈ or in THF-d₈/MeOH 30:1 mixtures. The temperature was adjusted to 65°C under reflux conditions for the thermal experiments, while keeping at room temperature for the blind and control experiments. The samples for ¹H-NMR spectroscopy were directly taken out of the mixture after appropriate times without further purification. Experimental results are presented in Table 34 - Table 36 and selected ¹H-NMR spectra of the “click” kinetic are shown in Appendix 7.13.

Table 34. Blind experiments for time and sonication cycle dependent investigation of click reaction from phenylacetylene (**17**) and benzyl azide (**19**)^a.

Ent	Cu(I) catalyst	M _n (GPC) [g/mol]	solvent	T [°C]	US ^b	Conversion after US cycle ^c [%]						
						cycle	0	1	2	3	5	10
A	Blind experiments				cycle	0	1	2	3	5	10	t _{End}
					t [h]	0	2.5	5	7.5	12.5	25	168
1	without	-	THF/MeOH	20	off	0	0	0	0	0	0	0
2	without	-	THF/MeOH	20	on	0	0	0	0	0	0	0
					t [h]	0	3	6	12	24	72	
3	without	-	THF/MeOH	65	off	0	0	0	1	1	2	
B	Control experiments without US				cycle	0	1	2	3	5	10	t _{End}
					t [h]	0	2.5	5	7.5	12.5	25	168
4	6a	4750	THF/MeOH	20	off	0	0	-	0	-	0	0
5	6c	17200	THF/MeOH	20	off	0	0	-	0	-	0	0
6	7a ^d	2900	THF/MeOH	20	off	0	-	-	11	-	-	
7	7b	4800	THF/MeOH	20	off	0	-	-	0	-	0	
C	Mechanochemical activation											
8	6a	4750	THF	20	on	0	1	1	2	-	-	
9	6a	4750	THF/MeOH	20	on	0	2	8	10	10	11	
10	6b	8900	THF/MeOH	20	on	0	6	14	16	18	19	
11	6c	17200	THF/MeOH	20	on	0	6	17	26	28	28	
D	Thermal activation					t [h]	0	3	6	12	24	72
12	6a	4750	THF/MeOH	65	off	0	0	1	2	2	3	
13	6c	17200	THF/MeOH	65	off	0	0	0	0	1	3	

^aFor all reaction an equimolar mixture of **17** and **19** in either pure THF-d₈ or THF-d₈/MeOH 30:1 where used together with 0.01 equiv. of mechanocatalyst **6** or **7** (c = 0.75 mM). ^bEach ultrasonication cycle consists of 90 min sonication with 30% of max. amplitude of 125 μm with pulse sequence of 5 s on, 10 s off and 60 min without sonication corresponding to a sonication power intensity of 8.75 W/cm² and an energy input of 21 kJ per US cycle. ^cDetermined by ¹H-NMR spectroscopy in THF-d₈/MeOH 30:1 monitoring the increasing triazole resonance at δ=8.12 ppm as well as the shift of the CH₂ resonance from δ=4.34 to 5.58 ppm. ^d1.1 eq. Na/ascorbate were additionally used for reaction of **7a**.

Table 35. Time and sonication cycle dependent investigation of click reaction from phenylacetylene (**17**) and benzyl azide (**19**) using PS-based biscarbene [Cu(PS-NHC)₂]X catalysts (**14**)^a.

Ent	Cu(I) catalyst	M _n (GPC) [g/mol]	solvent	T [°C]	US ^b	Conversion after US cycle ^c [%]						
						cycle	0	1	2	3	5	10
B	Control experiments without US				cycle	0	1	2	3	5	10	t _{End}
					t [h]	0	2.5	5	7.5	12.5	25	144
14	14c	13600	THF/MeOH	20	off	0	-	-	-	0	0	0
C	Mechanochemical activation											
15	14a	6800	THF/MeOH	20	on	0	5	12	21	22	23	
16	14b	11600	THF/MeOH	20	on	0	0	8	32	34	34	
17	14c	13600	THF/MeOH	20	on	0	16	28	49	51	52	
D	Thermal activation					t [h]	0	3	6	12	24	72
18	14c	13600	THF/MeOH	65	off	0	0	1	2	3	4	

^aFor all reaction an equimolar mixture of **17** and **19** in either pure THF-d₈ or THF-d₈/MeOH 30:1 where used together with 0.01 equiv. of mechanocatalyst **14** (c = 0.75 mM). ^bEach ultrasonication cycle consists of 90 min sonication with 30% of max. amplitude of 125 μm with pulse sequence of 5 s on, 10 s off and 60 min without sonication corresponding to a sonication power intensity of 8.75 W/cm² and an energy input of 21 kJ per US cycle. ^cDetermined by ¹H-NMR spectroscopy in THF-d₈/MeOH 30:1 monitoring the increasing triazole resonance at δ=8.12 ppm as well as the shift of the CH₂ resonance from δ=4.34 to 5.58 ppm.

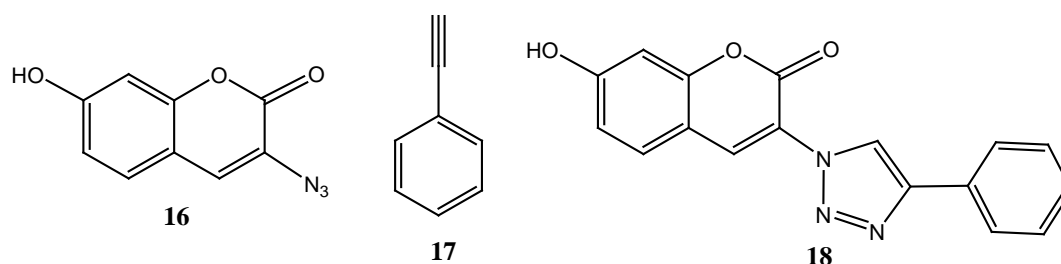
Table 36. Time and sonication cycle dependent investigation of click reaction from phenylacetylene (**17**) and benzyl azide (**19**) using model complex **10**^{a)}.

Ent	Cu(I) catalyst	M _n (GPC) [g/mol]	solvent	T [°C]	US ^{b)}	Conversion after US cycle ^{c)} [%]						
						t [h]	0	3	6	12	24	72
B+D	Control experiments and thermal activation					t [h]	0	3	6	12	24	72
19	10	-	THF/MeOH	20	off	0	-	-	0	2	-	
20	10	-	THF/MeOH	65	off	0	-	11	23	39	-	
C	Mechanochemical activation					cycle	0	1	2	3	5	10
						t [h]	0	2.5	5	7.5	12.5	25
21	10	-	THF/MeOH	20	on	0	20	47	48	47	49	
22	10	-	THF/MeOH ^{d)}	20	on	0	20	39	39	-	40	
23	10	-	THF	20	on	0	10	14	15	-	17	
24	10	-	THF ^{d)}	20	on	0	1	2	3	6	8	

^{a)}For all reaction an equimolar mixture of **17** and **19** in either pure THF-d₈ or THF-d₈/MeOH 30:1 where used together with 0.01 equiv. of mechanocatalyst **10** (c = 0.75 mM). ^{b)}Each ultrasonication cycle consists of 90 min sonication with 30% of max. amplitude of 125 μm with pulse sequence of 5 s on, 10 s off and 60 min without sonication corresponding to a sonication power intensity of 8.75 W/cm² and an energy input of 21 kJ per US cycle. ^{c)}Determined by ¹H-NMR spectroscopy in THF-d₈/MeOH 30:1 monitoring the increasing triazole resonance at δ=8.12 ppm as well as the shift of the CH₂ resonance from δ=4.34 to 5.58 ppm. ^{d)}1.1 eq. Na/ascorbate were additionally used for reaction of **10**.

4.10 Mechanochemical activation of latent catalysts in solid state by compression

4.10.1 Fluorescence calibration for fluorogenic “click” reaction



Scheme 22. Structures of embedded compounds, 3-azido-7-hydroxy-coumarin (**16**), phenylacetylene (**17**) and 7-hydroxy-3-(4-phenyl-1H-[1,2,3]triazole-1-yl)-coumarin (**18**).

200 mg of the high molecular weight PTHF (**20**, M_n = 112 000 g/mol, PDI = 1.4) and the corresponding amounts of **18** respectively the equimolare mixture of (**16** + **17**) were dissolved in dry THF in order to reach bulk concentrations in final material of 0, 1.63 · 10⁻⁵, 3.24 · 10⁻⁵, 6.42 · 10⁻⁵ as well as 1.56 · 10⁻⁴ mmol_{dye}/mg_{sample}. When everything was dissolved, the solvent was removed and the sample was brought roughly into a cylindrical form (diameter ~ 13 mm) using spatula and tweezer. Subsequently, the samples were allowed to crystallize for one week into dark and were subjected afterwards to compressing experiments under inert atmosphere using an automatic hydraulic press together with a 13 mm pellet die. 10 tons pressure (corresponding to 0.74 GPa) were applied for 3 compression cycles consisting out of 30 min compression interrupted each time by 30 minutes break and folded before the next compression cycle were started. The fluorescence measurements in bulk were carried out on FlouroMax-2 instrument fixing the PTHF tablets with dyes in a quartz glass holder (consisting out of two parallel quartz glass plates fixable into the fluorescence spectrometer). All measurements were repeated at least three times on three different positions. The sample was excited at two different wavelength namely 260 and 360 nm in accordance to their excitation maxima (see Figure 75a) excluding influences of wavelength, like quenching or absorption effects. Experimental results are presented in Table 37, Figure 76 as well as calibration curves in Figure 77. Images of prepared tablets are shown in Figure 76. Self-quenching effects of high concentrated coumarin dyes as

well as the increasing chromaticity of the investigated samples (see Figure 77) led to a non-linear increase of the fluorescence intensity for higher concentrations. Nevertheless, the calibration is applicable as the expected (and later on obtained) conversions are in the linear range of the calibration curve. Moreover, the fluorescence measurements of (**16** + **17**) in PTHF (Figure 75b) revealed a weak fluorescence even without “click” reaction of around 10% of fluorescence dye **3** (at equal concentrations) and is thus significantly lower (see Table 37).

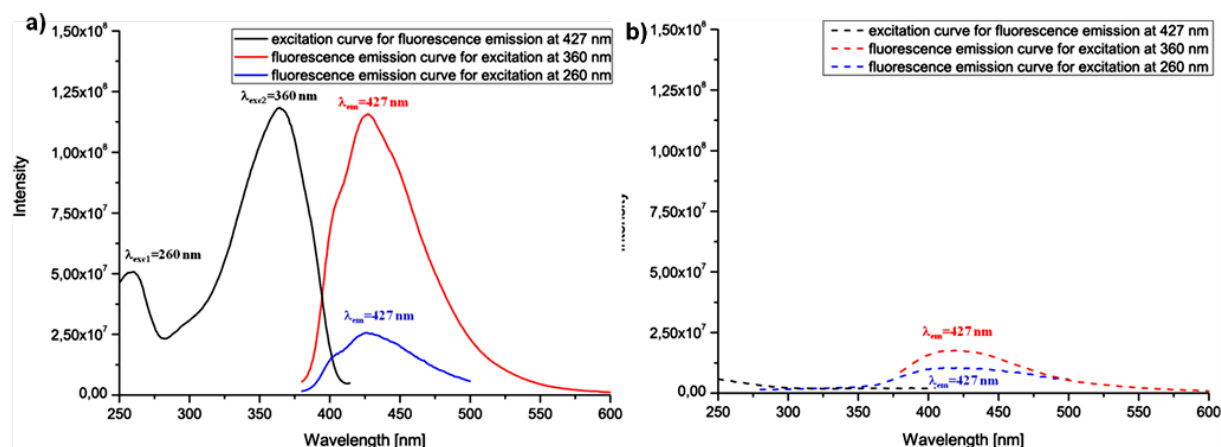


Figure 75. Representative fluorescence measurements of **a)** 7-hydroxy-3-(4-phenyl-*1H*-[1,2,3]triazole-1-yl)-coumarin (**18**) and **b)** 3-azido-7-hydroxy-coumarin (**16**) together with phenylacetylene (**17**) both within high molecular weight PTHF matrix (**20**). The red as well as the blue curves (solid line for **18**, dashed for **16+17**) show the measured fluorescence emissions at 427 nm after excitation with 360 nm (red) respectively 260 nm (blue). The black curves show the measured fluorescence at 427 nm when sample was excited with light of plotted wavelength. (Reprinted from ref⁹⁷ with permission of Wiley and Sons)

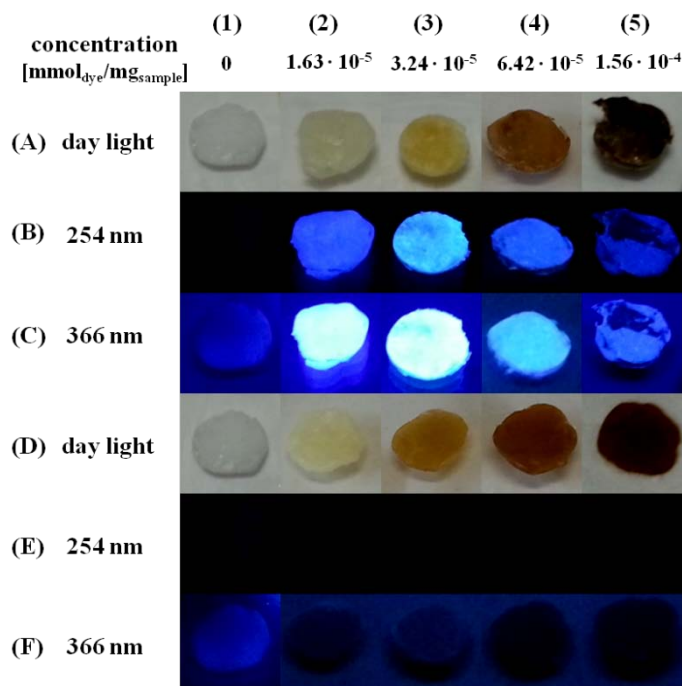


Figure 76. Optical images of reference samples for calibration for the fluorogenic “click” reaction: **(A)** - **(C)** optical images of fluorescence dye 7-hydroxy-3-(4-phenyl-*1H*-[1,2,3]triazole-1-yl)-coumarin (**18**) within the high molecular weight PTHF (**20**) and **(D)** - **(E)** of non-fluorescent dye 3-azido-7-hydroxy-coumarin (**16**) with phenylacetylene (**17**) within the PTHF matrix with different concentrations ranging from 0 mmol_{dye}/mg_{sample} (pure PTHF) (1) to $1.56 \cdot 10^{-4}$ mmol_{dye}/mg_{sample} (5) under normal daylight (**A**, **D**), UV light of 254 nm (**B**, **E**) and UV light of 366 nm wavelength (**C**, **F**). (Reprinted from ref⁹⁷ with permission of Wiley and Sons)

Table 37. Average fluorescence intensity of dyes (**16+17**; **18**) within high molecular weight PTHF matrix (**20**).

Ent.	Concentration [mmol _{dye} / mg _{sample}]	Fluorescence intensity for 18 within PTHF at 427 nm excitation at		Fluorescence intensity for 16+17 within PTHF at 427 nm excitation at	
		360 nm	260 nm	360 nm	260 nm
1	0	$1.36 \cdot 10^5$	$3.37 \cdot 10^5$	$1.36 \cdot 10^5$	$3.37 \cdot 10^5$
2	$1.63 \cdot 10^{-5}$	$2.91 \cdot 10^8$	$5.97 \cdot 10^7$	$1.75 \cdot 10^7$	$1.01 \cdot 10^7$
3	$3.24 \cdot 10^{-5}$	$3.99 \cdot 10^8$	$3.24 \cdot 10^8$	$3.60 \cdot 10^7$	$1.64 \cdot 10^7$
4	$6.42 \cdot 10^{-5}$	$1.46 \cdot 10^8$	$6.13 \cdot 10^7$	$1.42 \cdot 10^7$	$9.27 \cdot 10^6$
5	$1.56 \cdot 10^{-4}$	$1.16 \cdot 10^8$	$5.10 \cdot 10^7$	$4.29 \cdot 10^6$	$9.62 \cdot 10^5$

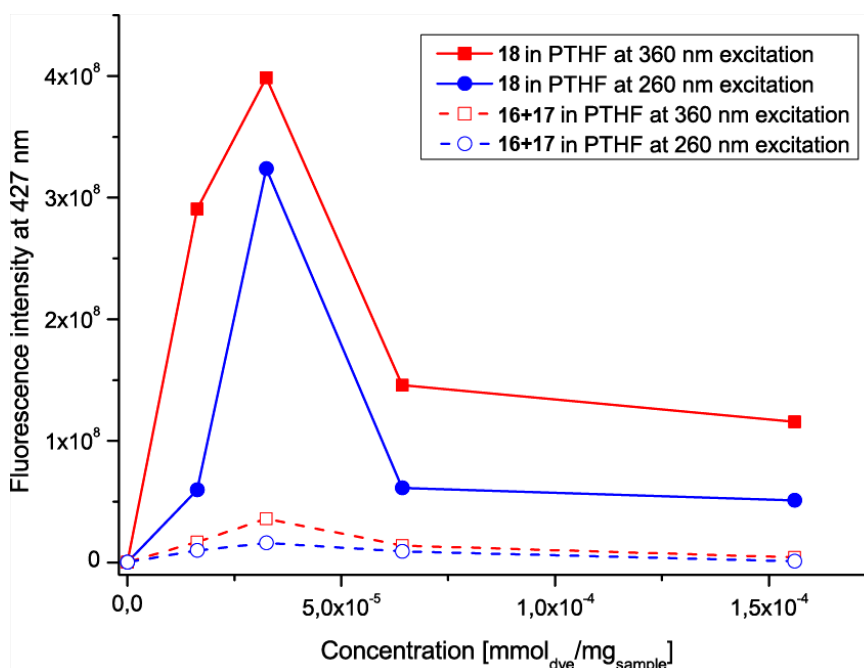


Figure 77. Calibration curve for fluorescence measurements of 7-hydroxy-3-(4-phenyl-*1H*-[1,2,3]triazole-1-yl)-coumarin (**18**) as well as of mixture of 3-azido-7-hydroxy-coumarin (**16**) together with phenylacetylene (**17**) in PTHF matrix (**20**) without catalyst. Red curves show fluorescence intensity after excitation at 360 nm, while blue show the fluorescence after excitation at 260 nm. Solid lines stand for **18** and dashed lines are for the mixture of (**16 + 17**). (Reprinted from ref⁹⁷ with permission of Wiley and Sons)

The fitting of calibration curves for 7-hydroxy-3-(4-phenyl-*1H*-[1,2,3]triazole-1-yl)-coumarin (**18**) in high molecular weight PTHF matrix yields in the concentration range of 0 to $3.24 \cdot 10^{-5}$ mmol_{dye}/mg_{sample} equations **eq3** and **eq4**:

for excitation at 360 nm

$$y = 1.330 \cdot 10^{13} (\pm 4.325 \cdot 10^{12}) x + 5.359 \cdot 10^6 (\pm 9.094 \cdot 10^7) \quad (\text{eq3})$$

and for excitation at 260 nm

$$y = 1.118 \cdot 10^{13} (\pm 3.392 \cdot 10^{12}) x - 6.479 \cdot 10^7 (\pm 7.132 \cdot 10^7). \quad (\text{eq4})$$

These equations were used afterwards for calculating conversions of mechanochemically triggered “click” reaction of **16** and **17** within PTHF matrix using the mechanocatalyst **6** and **14**.

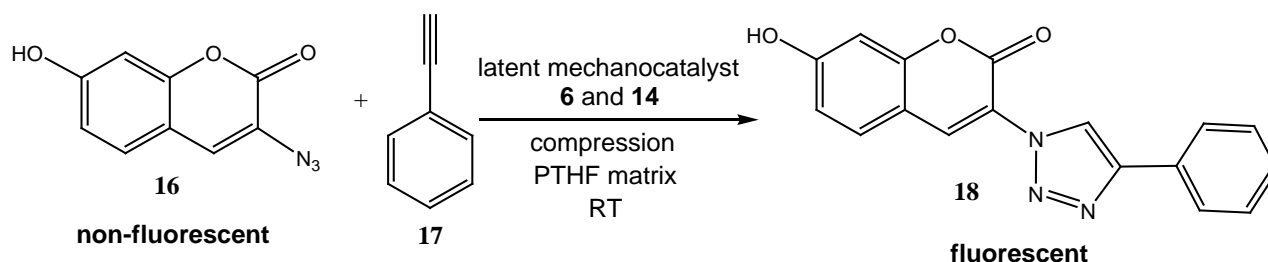
Moreover, the crystallinity of the PTHF samples with embedded fluorescence dye 7-hydroxy-3-(4-phenyl-*IH*-[1,2,3]triazole-1-yl)-coumarin (**18**) were determined and summarized in Table 38. No significant influence of embedding fluorescence dye **18** into PTHF matrix on crystallinity could be observed.

Table 38. DSC results of high molecular weight PTHF matrix with embedded **18**.

Ent.	Concentration [mmol _{dye} / mg _{sample}]	Melting point T _m [°C]	ΔH _m [J/g]	Degree of crystallinity [%] ^{a)}
1	0	46.3	117.8	68
2	1.63 · 10 ⁻⁵	43.1	103.4	60
3	3.24 · 10 ⁻⁵	42.3	100.9	59
4	6.42 · 10 ⁻⁵	45.3	112.6	65
5	1.56 · 10 ⁻⁴	48.8	110.9	65

^{a)}for determination 172 J/g was used as ΔH_m for 100% crystalline PTHF²³⁴

4.10.2 Fluorogenic “click” reaction of 3-azido-7-hydroxy-coumarin (**16**) and phenylacetylene (**17**) in solid state



Scheme 23. Fluorogenic “click” reaction of non-fluorescent 3-azido-7-hydroxy-coumarin (**16**) with phenylacetylene (**17**) yielding highly fluorescent 7-hydroxy-3-(4-phenyl-*IH*-[1,2,3]triazole-1-yl)-coumarin (**18**) triggered by mechanochemical activation of the latent PIB- (**6**) and PS-based mechanocatalysts (**14**) within the high molecular weight PTHF matrix (**20**) through compression.

The latent mechanocatalysts **6** respectively **14** (1.2 μmol, 6 μmol/mg_(PTHF)), the high molecular weight PTHF (**20**; 200 mg, M_n = 112 000 g/mol), 3-azido-7-hydroxy-coumarin (**16**; 7.3 mg, 0.036 mmol) and phenylacetylene (**17**; 4.0 μL, 0.036 mol) were dissolved in dry THF (5 mL). When everything was homogeneously dissolved, the solvent was removed and the sample was brought roughly into a cylindrical form (diameter ~ 13 mm) using spatula and tweezers. The sample was allowed to crystallize for one week into darkness. Afterward fluorescence was measured fixing the sample in a special quartz glass holder (λ_{ex} = 360 nm, λ_{em} = 427 nm). Subsequently, the sample was subjected to compressing experiments under inert atmosphere using an automatic hydraulic press together with a 13 mm pellet die. 10 tons pressure (corresponding to 0.74 GPa) were applied in several compression cycles consisting out of 30 min compression interrupted each time by 30 min without compression and folded before the next compression cycle were started. The fluorescence was measured at two different wavelengths after the 1st, 2nd, 3rd, 10th and 20th compression cycle, whereat all measurements were repeated at least three times on three different positions. The significantly increased fluorescence during the compression experiment proved the mechanochemical activation of the latent copper catalyst. The obtained results are summed-up in Table 39. Selected fluorescence spectra are shown in Appendix 7.14.

Control experiments were conducted in order to exclude the influence of the compression event itself (control experiment A) as well as the thermal influence (B) to the fluorogenic “click” reaction. Control experiments were performed following the same route for preparation of dye/polymer mixtures like described above. For control experiment A, no mechanocatalyst was added and the sample was subjected to compression experiment, followed by fluorescence measurements described above. Control experiment B should exclude a possible thermal acceleration of the “click” reaction of **16** with **17** due to the compression. Therefore, a mixture of **6c**, **16** and **17** with high molecular weight PTHF (**20**) was heated into dark to 60°C for 72 hours. Subsequently fluorescence measurements were performed. In both control experiments no significant fluorescence could be observed proving the mechanochemical activation of latent copper(I) catalyst by compression into a solid polymer matrix. The used amounts and obtained results are shown in Table 39. Selected fluorescence spectra are shown in Appendix 7.14.

Table 39. Fluorescence intensity and according to eq. 3 calculated conversions for the “click” reaction of **16** and **17** (30 eq. each) activating the latent mechanophores **6** and **14** (1.2 μmol) in bulk PTHF matrix (200 mg) by multiple compression cycles via a hydraulic press.

Ent.	mechanocatalyst			compression cycle	fluorescence intensity [a.u.] ^{a)}	“click” conversion [%] ^{b)}
	Nr.	M _n (GPC) [g/mol]	m [mg]			
A	Control experiment					
1				0	1.46 · 10 ⁷	0.4 ± 0.2
2				1	1.40 · 10 ⁷	0.4 ± 0.2
3				2	1.34 · 10 ⁷	0.4 ± 0.2
4				3	1.71 · 10 ⁷	0.6 ± 0.3
5				10	1.64 · 10 ⁷	0.5 ± 0.3
6				20	1.29 · 10 ⁷	0.3 ± 0.2
B	Thermal activation					
7	6c	17200	21	no compression: heating to 60°C for 72h	2.52 · 10 ⁷	0.9 ± 0.2
8	14c	13600	17		2.21 · 10 ⁷	0.8 ± 0.3
C	Mechanochemical activation of PIB-based mechanophores 6 by compression					
9	6a	4750	6	0	1.01 · 10 ⁷	0.2 ± 0.1
10				1	1.51 · 10 ⁷	0.5 ± 0.3
11				2	1.35 · 10 ⁷	0.4 ± 0.2
12				3	1.43 · 10 ⁷	0.4 ± 0.2
13				10	1.68 · 10 ⁷	0.6 ± 0.3
14				20	1.53 · 10 ⁷	0.5 ± 0.2
15	6b	8900	11	0	9.92 · 10 ⁶	0.2 ± 0.1
16				1	1.66 · 10 ⁷	0.5 ± 0.3
17				2	1.90 · 10 ⁷	0.7 ± 0.3
18				3	1.61 · 10 ⁷	0.5 ± 0.2
19				10	1.55 · 10 ⁷	0.5 ± 0.3
20				20	1.39 · 10 ⁷	0.4 ± 0.2
21	6c	17200	21	0	1.24 · 10 ⁷	0.3 ± 0.2
22				1	3.11 · 10 ⁷	1.2 ± 0.3
23				2	7.32 · 10 ⁷	3.3 ± 0.3
24				3	8.79 · 10 ⁷	4.0 ± 0.5
25				10	1.41 · 10 ⁸	6.5 ± 0.5
26				20	1.55 · 10 ⁸	7.2 ± 0.3

Ent.	mechanocatalyst			compression cycle	fluorescence intensity [a.u.] ^{a)}	“click” conversion [%] ^{b)}
	Nr.	M _n (GPC) [g/mol]	m [mg]			
D	Mechanochemical activation of PS-based mechanophores 14 by compression					
27	14a	6800	8	0	$1.18 \cdot 10^7$	0.3 ± 0.2
28				1	$1.26 \cdot 10^7$	0.4 ± 0.2
29				2	$1.55 \cdot 10^7$	0.5 ± 0.3
30				3	$1.74 \cdot 10^7$	0.6 ± 0.3
31				10	$1.35 \cdot 10^7$	0.4 ± 0.2
32				20	$1.51 \cdot 10^7$	0.5 ± 0.2
33	14b	11600	14	0	$1.34 \cdot 10^7$	0.4 ± 0.2
34				1	$1.73 \cdot 10^7$	0.6 ± 0.3
35				2	$2.44 \cdot 10^7$	0.9 ± 0.3
36				3	$3.07 \cdot 10^7$	1.2 ± 0.2
37				10	$3.89 \cdot 10^7$	1.6 ± 0.4
38				20	$4.75 \cdot 10^7$	2.0 ± 0.3
39	14c	13600	17	0	$1.45 \cdot 10^7$	0.4 ± 0.2
40				1	$3.09 \cdot 10^7$	1.2 ± 0.3
41				2	$7.82 \cdot 10^7$	3.5 ± 0.3
42				3	$9.37 \cdot 10^7$	4.3 ± 0.5
43				10	$1.49 \cdot 10^8$	6.9 ± 0.2
44				20	$1.69 \cdot 10^8$	7.9 ± 0.5

^{a)}average value of multiple determined fluorescence spectra at different positions of the sample after excitation at 360 nm and fluorescence emission at 427 nm; ^{b)}calculated according to eq.3 assuming a maximum concentration of **18** of $1.56 \cdot 10^{-4}$ mmol_{dye}/mg_{sample}.

5 Summary

The aim of this thesis was the development and characterization of latent mechanocatalysts for the copper(I) alkyne/azide catalyst cycloaddition (CuAAC) which can be activated under mechanical force, like ultrasound or compression. For that purpose, poly(isobutylene) (PIB) (**6**) as well as poly(styrene) (PS) based (**14**) bis(*N*-heterocyclic carbene) (NHC) copper(I)X complexes were synthesized carrying two bulky polymer chains onto the NHC-ligand (Figure 78) shielding thus the catalytic active Cu(I) center due to their steric hindrance. The synthesis for both mechanophores started with the preparation of bromo-telechelic polymers (**3** and **12**) once via living carbocationic polymerization (LCCP) in case of PIB (**3**) and through atom transfer radical polymerization (ATRP) for PS (**12**). Both types of polymers could be synthesized in three different molecular weights ranging from 2200 g/mol to 8750 g/mol in case of **3** and from 3400 g/mol to 7100 g/mol in case of **12**. The synthesis of **3** and **12** were accomplished in a well suited living way offering small molecular weight distributions with PDIs around 1.2 ensuring the later centrally embedding of the mechanolabile copper-carbene bond, which is crucial for an efficient activation of the mechanophore.

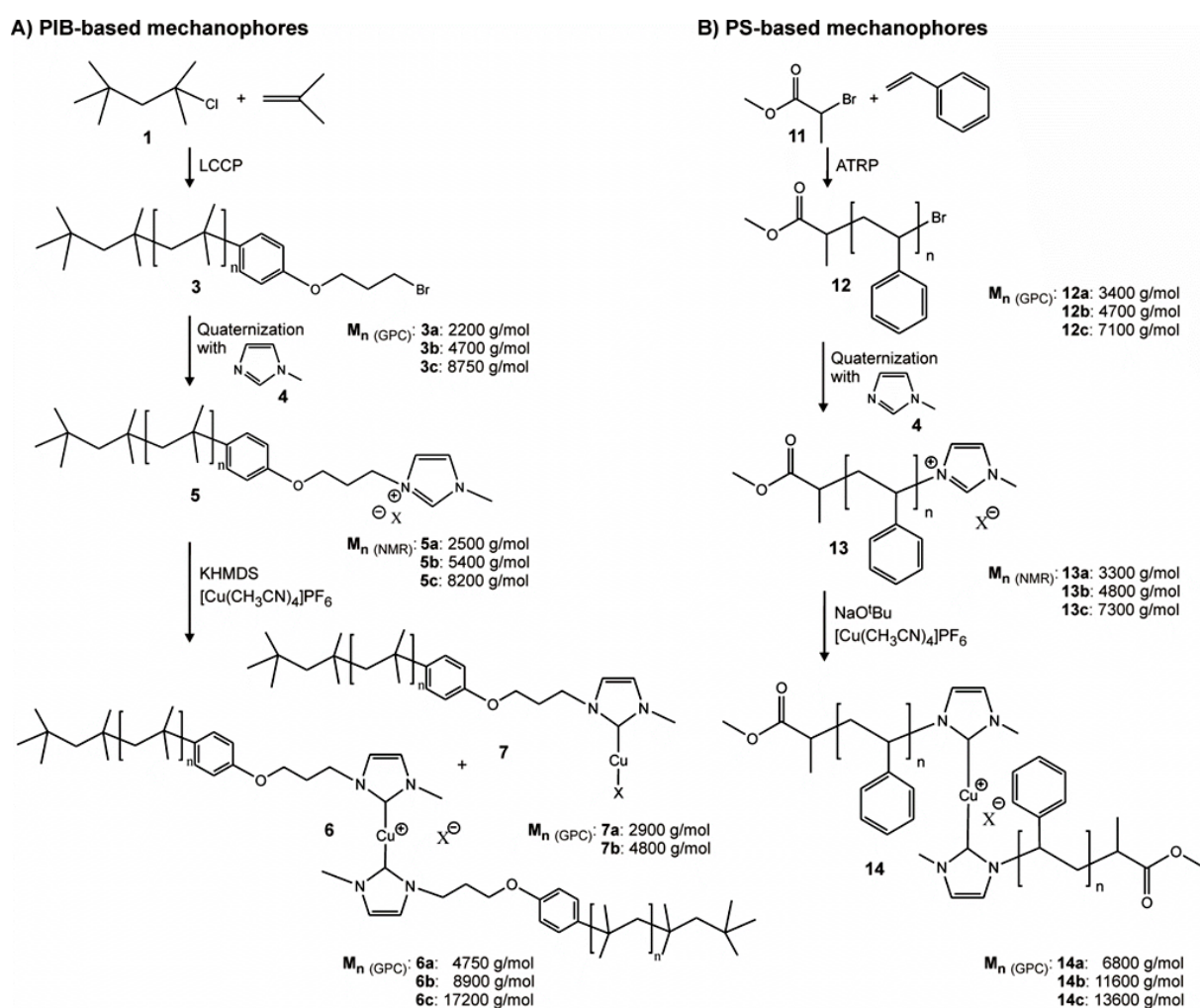


Figure 78. Synthetic pathway for the polymeric bis(*N*)-heterocyclic carbene copper(I)X mechanocatalysts (**6** and **14**): A) Bromo-telechelic poly(isobutylene) (PIB) (**3**) was synthesized through LCCP techniques and subsequently quaternized with *N*-methylimidazole (**4**) obtaining the *N*-methylimidazolium telechelic PIB (**5**). The final mechanoresponsive PIB-based bis(*N*-methylimidazol-2-ylidene)copper(I)X complex (**6**) as well as the corresponding copper(I) monocarbene complexes (**7**) were received by deprotonation of **5** with KHMDS forming thus the free carbene and coordination to the free copper(I) salt. B) The bromo-telechelic poly(styrene) (PS) (**12**) was polymerized by ATRP and transformed by quaternization with **4** to the *N*-methylimidazolium telechelic PIB (**13**). Deprotonation by NaO^tBu and subsequent coordination of the NHC-macroligand to the copper(I) salt yielded the latent PS-based bis(*N*-methylimidazol-2-ylidene)copper(I)X complex (**14**).

In a second step the bromo-telechelic polymers (**3** and **12**) were transformed into their *N*-methylimidazolium-telechelic counterparts (**5** and **13**) by an *in situ* nucleophilic substitution to the iodine-telechelic polymers and subsequent quaternization with *N*-methylimidazole yielding the NHC-macroligand precursors **5** and **13**. Finally, the biscarbene mechanocatalysts **6** and **14** were obtained after deprotonation of **5** and **13** forming the free carbene and subsequent coordination to the Cu(I) salt. The obtained molecular weights ranged from 4750 g/mol to 17200 g/mol in case of the PIB-based biscarbene complexes (**6**) as well as from 6800 g/mol to 13600 g/mol in case of the PS-based mechanocatalysts (**14**). Moreover, the PIB-based monocarbene copper(I) complexes (**7**) bearing solely one polymeric-NHC ligand were synthesized, while no PS-based monocarbene complexes (**15**) could be isolated. The structural proof of the synthesized polymers was accomplished by ¹H- and ¹³C-NMR spectroscopy as well as by GPC and MALDI-TOF-MS.

The activation of the synthesized latent polymeric copper(I)X bis(*N*-heterocyclic carbene) catalysts **6** and **14** were accomplished subjecting them to external mechanical force, which led in turns to a cleavage of one sterically shielding NHC-ligand generating thus the corresponding catalytic active copper(I)X monocarbene complexes **7** and **15** (Figure 79) which was proven in solution by *in situ* GPC as well as ¹H-NMR spectroscopic investigations. First of all, the true latent nature of the PIB- (**6**) and PS-based (**14**) mechanocatalysts could be demonstrated probing their stability under silent ambient conditions in GPC as well as ¹H-NMR spectroscopic investigations: The constancy of molecular weight in GPC as well as the unshifted characteristic resonances within the ¹H-NMR spectroscopy proved the persistence of the desired structure. Subjecting solutions of the mechanophores **6** and **14** in THF/MeOH 30:1 mixtures to ultrasonication led to a significant reduction of the molecular weight during the sonication process, whereat prolonged sonication led to a stronger molecular weight decrease. Quantifying the cleavage efficiencies revealed a more efficient chain scission using mechanocatalysts with higher initial molecular weights. Thus, 84% of the PIB-based biscarbene catalysts **6c** with an initial molecular weight of 17200 g/mol could be cleaved after 20 sonication cycles (50 h), while mechanophores with shorter attended PIB chains offered cleavage efficiencies of only 55% for **6b** (8900 g/mol) respectively 45% for **6a** (4750 g/mol). In case of the PS-based mechanocatalysts **14**, 80% of the catalyst with the longest attached PS chains (**14c**) of 13600 g/mol could be cleaved, while for the shortest catalyst **14a** (6800 g/mol) only 46% of the chains were cleaved. Hence, almost the same cleavage efficiencies were determined for PS- (**14**) as for PIB-based (**6**) mechanophores, but for **14** even at lower molecular weights indicating a more efficient scission for the PS-based mechanophores due to their higher polarity (compared to **6**). Thus, better solvent-polymer interactions with THF which enabled a faster coil-to-stretch transformation of the attendant polymer chains and consequently a more efficient force transmission. Moreover, it could be proven, that the addition of MeOH increased the amount of cleaved mechanophore significantly from e.g. only 11% for **6c** (17200 g/mol) in pure THF compared to 84% when THF/MeOH 30:1 mixtures were used as solvent. ¹H-NMR spectroscopic investigations had shown that MeOH is able to protonate the cleaved free NHC-ligand preventing thus the back reaction with the monocarbene complexes (**7** and **15**) to the initial biscarbene catalysts.

Additional *in situ* ¹H-NMR spectroscopic investigation supported this observation revealing under ultrasonication of **6** the appearance of the corresponding monocarbene complex **7** as well as the cleaved and protonated *N*-methylimidazolium-telechelic PIB (**5**). Moreover, the decomposition of the monocarbene species by elimination of the *N*-methylimidazolium end group could be detected via the performed ¹H-NMR spectroscopic investigations. Comparable experiments with the PS-based complexes were not possible due to the overlay of the crucial resonances.

Moreover, the thermal treatment of the polymeric mechanocatalysts revealed also a decomposition determined in GPC as well as ¹H-NMR spectroscopic investigations. However, no formation of the catalytic active monocarbene complexes could be observed indicating a direct elimination of the *N*-methylimidazolium end groups from the polymer chain.

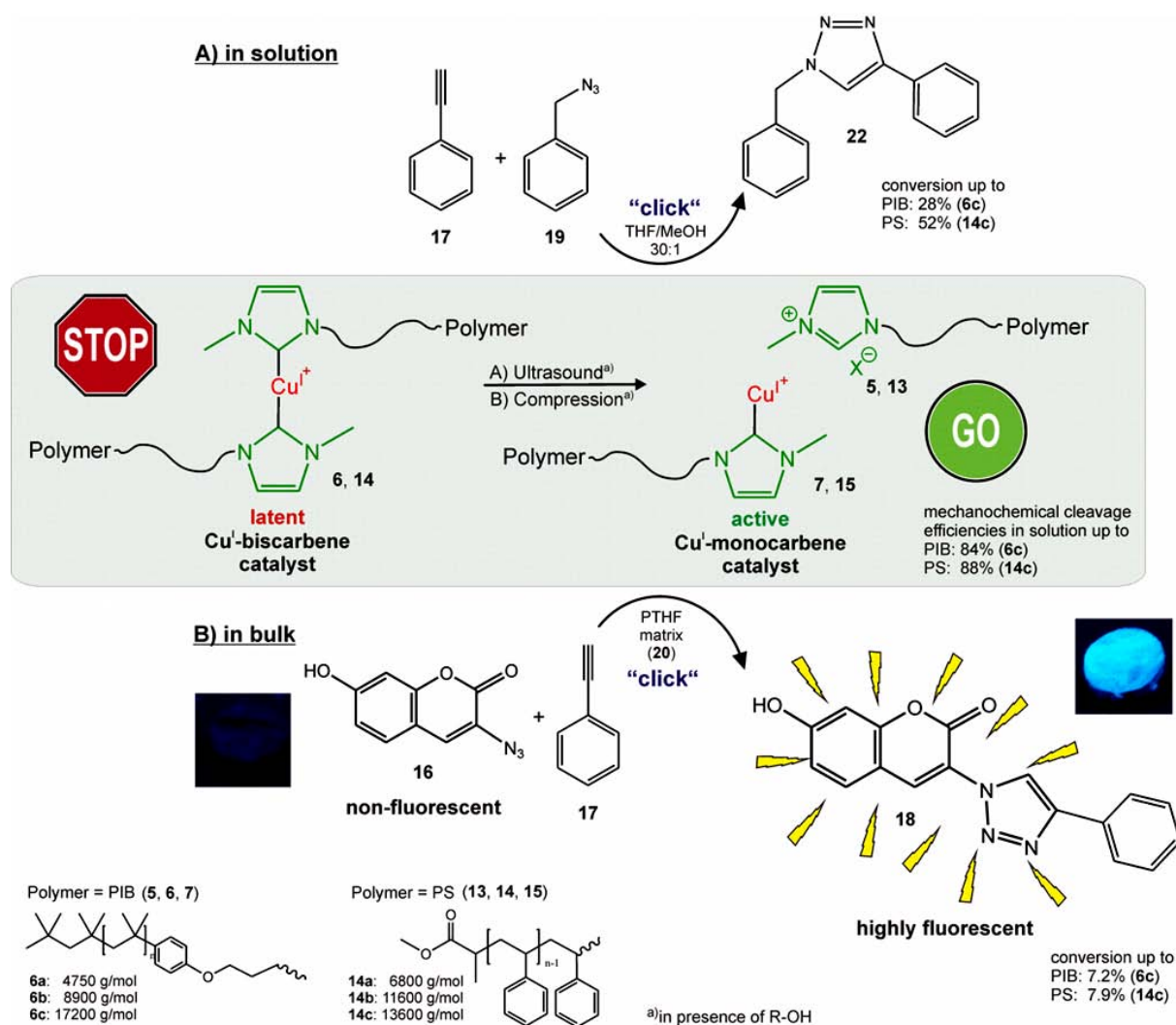


Figure 79. The force-induced activation of the latent mechanolabile PIB- (**6**) and PS-based (**14**) bis(*N*-heterocyclic carbene) copper(I)X complexes by ultrasound in solution or by compression in the bulk state cleaved off one shielding NHC-ligand and generated thus the catalytic active monocarbene complexes (**7** and **15**) and in the presence of alcohols the *N*-methylimidazolium-telechelic polymers (**5** and **13**). A) The model “click” reaction of phenylacetylene (**17**) and benzyl azide (**19**) was chosen in order to investigate the catalytic activity of **6** and **14** in solution via ¹H-NMR spectroscopy, while B) the fluorogenic “click” reaction of non-fluorescent 3-azido-7-hydroxy-coumarin dye (**16**) with phenylacetylene (**17**) forming the highly fluorescent 7-hydroxy-3-(4-phenyl-1*H*-[1,2,3]triazole-1-yl)-coumarin dye (**18**) was selected to probe the mechanochemical activation of the latent **6** and **14** in the solid state by fluorescence spectroscopy.

Furthermore, the catalytic activity of the synthesized mechanocatalyst (**6** and **14**) as well as the monocarbene catalysts (**7**) was tested in solution applying the mechanical force by ultrasonication or in the solid state using compression force. A model CuAAC “click” reaction of phenylacetylene (**17**) and benzyl azide (**19**) was selected to investigate the catalytic activity in the liquid state (Figure 79A) and was monitored through *in situ* ¹H-NMR spectroscopy in THF-*d*₈/MeOH 30:1 solutions proving the latency of the biscarbene mechanocatalysts **6** and **14** by the absence of any “click” product **22** under silent conditions at room temperature. Ultrasonication introduced in compliance with the GPC and ¹H-NMR spectroscopy monitored scission experiments a catalytic activity with increased conversion of the CuAAC “click” reaction from **17** and **19** by increasing the chain length of the attached polymer handle. Subjecting the highest molecular weight PIB-based mechanophore **6c** (17200 g/mol) to 10 cycles of ultrasonication (25 h) yielded a “click” conversion of 28%, while in case of the lower molecular weight catalysts **6b** (8900 g/mol) only 19% and for **6a** (4750 g/mol) just 11%

“click” conversion could be determined. The PS-based mechanocatalysts **14** showed in general a higher activity towards the model “click” reaction yielding the “click” product **22** in conversions of 52% applying the highest molecular weight PS-catalyst **14c** (13600 g/mol). Similar to **6** the “click” conversion decreased to 23% with decreasing initial molecular weight to 6800 g/mol in case of **14a**.

Moreover, the PIB-based monocarbene complexes **7** were tested within the CuAAC of **17** and **19** revealing a catalytic active even without applied ultrasound, as no shielding second ligand blocks the catalytic active site of the copper. Thus, the monocarbene catalyst **7a** (2900 g/mol) showed without applied ultrasound a “click” conversion of 11%, which is exactly the same as obtained subjecting the corresponding biscarbene mechanophore **6a** (4750 g/mol) to 10 ultrasonication cycles.

Finally, the mechanochemical activation was probed within a solid polymer matrix, devoid of any solvent proving their mechanochemical activability also in the bulk state. The catalytic activity of the designed mechanophores **6** and **14** was demonstrated using the fluorogenic “click”-reaction of the non-fluorescent 3-azido-7-hydroxy-coumarin dye (**16**) with phenylacetylene (**17**) generating the highly fluorescent 7-hydroxy-3-(4-phenyl-*IH*-[1,2,3]triazole-1-yl)-coumarin dye (**18**) (Figure 79B). Applying mechanical force was accomplished by an automated hydraulic press within several compression cycles with a pressure of 10 tons and subsequent stress release, which activated in turns the mechanolabile catalysts. The progress of the CuAAC “click” reaction was monitored by fluorescence spectroscopy revealing an increased “click” conversion with increased initial chain length of the implemented copper(I) mechanophore. 7.2% conversion could be achieved using the highest molecular weight PIB-based biscarbene complex **6c** (17200 g/mol), while a conversion of 7.9% was determined for **14c** (13600 g/mol). The lower molecular weight catalyst for PS (**14**) and PIB (**6**) showed significant less respectively no catalytic activity as their attended polymer chains were too short to enable an efficient entanglement with the matrix material preventing thus the transmission of the external force to the labile Cu-NHC bond. However, no significant differences between the PIB- (**6**) and PS-based (**14**) biscarbene complexes towards the conversion of the catalyzed “click” reaction could be observed in the bulk state as a decomposition of the mechanocatalysts is favored, likewise to the behavior in solution.

Moreover, it could be verified that the fluorogenic “click” reaction using **6** and **14** as catalyst is truly latent and could solely be triggered by mechanical compression force, but not due to thermal treatment at 60°C even for several days. A well suitable quantifiability has been demonstrated enabling thus the potential application of the designed mechanocatalytical system within autonomous stress- reporting or damage-sensing materials.

6 References

- [1] Li, J.; Nagamani, C.; Moore, J. S.; Polymer Mechanochemistry: From Destructive to Productive; *Acc. Chem. Res.*; **2015**, *48* (8), 2181-2190.
- [2] Boulatov, R., *Polymer Mechanochemistry*. Springer International Publishing: Heidelberg, 2015; Vol. 369.
- [3] Binder, W. H., *Self-Healing Polymers. From Principles to Applications*. Wiley-VCH: Weinheim, 2013; p 440.
- [4] Caruso, M. M.; Davis, D. A.; Shen, Q.; Odom, S. A.; Sottos, N. R.; White, S. R.; Moore, J. S.; Mechanically-Induced Chemical Changes in Polymeric Materials; *Chem. Rev.*; **2009**, *109* (11), 5755-5798.
- [5] Groote, R.; Jakobs, R. T. M.; Sijbesma, R. P.; Mechanocatalysis: forcing latent catalysts into action; *Polym. Chem.*; **2013**, *4* (18), 4846-4859.
- [6] Beyer, M. K.; Clausen-Schaumann, H.; Mechanochemistry: The Mechanical Activation of Covalent Bonds; *Chem. Rev.*; **2005**, *105* (8), 2921-2948.
- [7] Brantley, J. N.; Wiggins, K. M.; Bielawski, C. W.; Polymer mechanochemistry: the design and study of mechanophores; *Polym. Int.*; **2013**, *62*, 2–12.
- [8] Paulusse, J. M. J.; Sijbesma, R. P.; Reversible Mechanochemistry of a Pd^{II} Coordination Polymer; *Angew. Chem. Int. Ed.*; **2004**, *43* (34), 4460-4462.
- [9] Paulusse, J. M. J.; Huijbers, J. P. J.; Sijbesma, R. P.; Reversible, High Molecular Weight Palladium and Platinum Coordination Polymers Based on Phosphorus Ligands; *Macromolecules*; **2005**, *38* (15), 6290-6298.
- [10] Paulusse, J. M. J.; Huijbers, J. P. J.; Sijbesma, R. P.; Quantification of Ultrasound-Induced Chain Scission in Pd^{II}-Phosphine Coordination Polymers; *Chem. Eur. J.*; **2006**, *12* (18), 4928-4934.
- [11] Paulusse, J. M. J.; Sijbesma, R. P.; Selectivity of mechanochemical chain scission in mixed palladium(ii) and platinum(ii) coordination polymers; *Chem. Commun.*; **2008**, (37), 4416-4418.
- [12] Karthikeyan, S.; Potisek, S. L.; Piermattei, A.; Sijbesma, R. P.; Highly Efficient Mechanochemical Scission of Silver-Carbene Coordination Polymers; *J. Am. Chem. Soc.*; **2008**, *130* (45), 14968-14969.
- [13] Groote, R.; Szyja, B. M.; Pidko, E. A.; Hensen, E. J. M.; Sijbesma, R. P.; Unfolding and Mechanochemical Scission of Supramolecular Polymers Containing a Metal-Ligand Coordination Bond; *Macromolecules*; **2011**, *44* (23), 9187-9195.
- [14] Rooze, J.; Groote, R.; Jakobs, R. T. M.; Sijbesma, R. P.; van Iersel, M. M.; Rebrov, E. V.; Schouten, J. C.; Keurentjes, J. T. F.; Mechanism of Ultrasound Scission of a Silver-Carbene Coordination Polymer; *J. Phys. Chem. B*; **2011**, *115* (38), 11038-11043.
- [15] Groote, R.; van Haandel, L.; Sijbesma, R. P.; The effect of molecular weight and catalyst concentration on catalytic activity in mechanochemically activated transesterification using silver(I)-N-heterocyclic carbene latent catalysts; *J. Polym. Sci., Part A: Polym. Chem.*; **2012**, *50* (23), 4929-4935.
- [16] Groote, R.; Jakobs, R. T. M.; Sijbesma, R. P.; Performance of Mechanochemically Activated Catalysts Is Enhanced by Suppression of the Thermal Effects of Ultrasound; *ACS Macro Lett.*; **2012**, *1* (8), 1012-1015.
- [17] Piermattei, A.; Karthikeyan, S.; Sijbesma, R. P.; Activating catalysts with mechanical force; *Nature Chem.*; **2009**, *1* (2), 133-137.
- [18] Jakobs, R. T. M.; Sijbesma, R. P.; Mechanical Activation of a Latent Olefin Metathesis Catalyst and Persistence of its Active Species in ROMP; *Organometallics*; **2012**, *31* (6), 2476-2481.
- [19] Jakobs, R. T. M.; Ma, S.; Sijbesma, R. P.; Mechanocatalytic Polymerization and Cross-Linking in a Polymeric Matrix; *ACS Macro Lett.*; **2013**, *2* (7), 613-616.
- [20] Tennyson, A. G.; Wiggins, K. M.; Bielawski, C. W.; Mechanical Activation of Catalysts for C-C Bond Forming and Anionic Polymerization Reactions from a Single Macromolecular Reagent; *J. Am. Chem. Soc.*; **2010**, *132* (46), 16631-16636.
- [21] Kersey, F. R.; Yount, W. C.; Craig, S. L.; Single-Molecule Force Spectroscopy of Bimolecular Reactions: System Homology in the Mechanical Activation of Ligand Substitution Reactions; *J. Am. Chem. Soc.*; **2006**, *128* (12), 3886-3887.
- [22] Wiggins, K. M.; Hudnall, T. W.; Tennyson, A. G.; Bielawski, C. W.; Selective scission of pyridine-boronium complexes: mechanical generation of Bronsted bases and polymerization catalysts; *J. Mater. Chem.*; **2011**, *21* (23), 8355-8359.
- [23] Lenhardt, J. M.; Ong, M. T.; Choe, R.; Evenhuis, C. R.; Martinez, T. J.; Craig, S. L.; Trapping a Diradical Transition State by Mechanochemical Polymer Extension; *Science*; **2010**, *329* (5995), 1057-1060.
- [24] Klukovich, H. M.; Kouznetsova, T. B.; Kean, Z. S.; Lenhardt, J. M.; Craig, S. L.; A backbone lever-arm effect enhances polymer mechanochemistry; *Nature Chem.*; **2013**, *5* (2), 110-114.

- [25] Ramirez, A. L. B.; Kean, Z. S.; Orlicki, J. A.; Champhekar, M.; Elsagr, S. M.; Krause, W. E.; Craig, S. L.; Mechanochemical strengthening of a synthetic polymer in response to typically destructive shear forces; *Nature Chem.*; **2013**, *5* (9), 757-761.
- [26] Lenhardt, J. M.; Ogle, J. W.; Ong, M. T.; Choe, R.; Martinez, T. J.; Craig, S. L.; Reactive Cross-Talk between Adjacent Tension-Trapped Transition States; *J. Am. Chem. Soc.*; **2011**, *133* (10), 3222-3225.
- [27] Black, A. L.; Orlicki, J. A.; Craig, S. L.; Mechanochemically triggered bond formation in solid-state polymers; *J. Mater. Chem.*; **2011**, *21* (23), 8460-8465.
- [28] Lenhardt, J. M.; Black, A. L.; Craig, S. L.; gem-Dichlorocyclopropanes as Abundant and Efficient Mechanophores in Polybutadiene Copolymers under Mechanical Stress; *J. Am. Chem. Soc.*; **2009**, *131* (31), 10818-10819.
- [29] Lenhardt, J. M.; Black, A. L.; Beiermann, B. A.; Steinberg, B. D.; Rahman, F.; Samborski, T.; Elsagr, J.; Moore, J. S.; Sottos, N. R.; Craig, S. L.; Characterizing the mechanochemically active domains in gem-dihalocyclopropanated polybutadiene under compression and tension; *J. Mater. Chem.*; **2011**, *21* (23), 8454-8459.
- [30] Black Ramirez, A. L.; Ogle, J. W.; Schmitt, A. L.; Lenhardt, J. M.; Cashion, M. P.; Mahanthappa, M. K.; Craig, S. L.; Microstructure of Copolymers Formed by the Reagentless, Mechanochemical Remodeling of Homopolymers via Pulsed Ultrasound; *ACS Macro Lett.*; **2012**, *1* (1), 23-27.
- [31] Kean, Z. S.; Ramirez, A. L. B.; Craig, S. L.; High mechanophore content polyester-acrylate ABA block copolymers: Synthesis and sonochemical activation; *J. Polym. Sci., Part A: Polym. Chem.*; **2012**, *50* (17), 3481-3484.
- [32] Wang, J.; Kouznetsova, T. B.; Kean, Z. S.; Fan, L.; Mar, B. D.; Martínez, T. J.; Craig, S. L.; A Remote Stereochemical Lever Arm Effect in Polymer Mechanochemistry; *J. Am. Chem. Soc.*; **2014**, *136* (43), 15162-15165.
- [33] Lenhardt, J. M.; Black Ramirez, A. L.; Lee, B.; Kouznetsova, T. B.; Craig, S. L.; Mechanistic Insights into the Sonochemical Activation of Multimechanophore Cyclopropanated Polybutadiene Polymers; *Macromolecules*; **2015**, *48* (18), 6396-6403.
- [34] Lee, B.; Niu, Z.; Wang, J.; Sledobnick, C.; Craig, S. L.; Relative Mechanical Strengths of Weak Bonds in Sonochemical Polymer Mechanochemistry; *J. Am. Chem. Soc.*; **2015**, *137* (33), 10826-10832.
- [35] Wang, J.; Kouznetsova, T. B.; Niu, Z.; Ong, M. T.; Klukovich, H. M.; Rheingold, A. L.; Martinez, T. J.; Craig, S. L.; Inducing and quantifying forbidden reactivity with single-molecule polymer mechanochemistry; *Nature Chem.*; **2015**, *7* (4), 323-327.
- [36] Diesendruck, C. E.; Steinberg, B. D.; Sugai, N.; Silberstein, M. N.; Sottos, N. R.; White, S. R.; Braun, P. V.; Moore, J. S.; Proton-Coupled Mechanochemical Transduction: A Mechanogenerated Acid; *J. Am. Chem. Soc.*; **2012**, *134* (30), 12446-12449.
- [37] Klukovich, H. M.; Kean, Z. S.; Ramirez, A. L. B.; Lenhardt, J. M.; Lin, J.; Hu, X.; Craig, S. L.; Tension Trapping of Carbonyl Ylides Facilitated by a Change in Polymer Backbone; *J. Am. Chem. Soc.*; **2012**, *134* (23), 9577-9580.
- [38] Hickenboth, C. R.; Moore, J. S.; White, S. R.; Sottos, N. R.; Baudry, J.; Wilson, S. R.; Biasing reaction pathways with mechanical force; *Nature*; **2007**, *446*, 423-427.
- [39] Potisek, S. L.; Davis, D. A.; Sottos, N. R.; White, S. R.; Moore, J. S.; Mechanophore-Linked Addition Polymers; *J. Am. Chem. Soc.*; **2007**, *129* (45), 13808-13809.
- [40] Kean, Z. S.; Black Ramirez, A. L.; Yan, Y.; Craig, S. L.; Bicyclo[3.2.0]heptane Mechanophores for the Non-scissile and Photochemically Reversible Generation of Reactive Bis-enones; *J. Am. Chem. Soc.*; **2012**, *134* (31), 12939-12942.
- [41] Kean, Z. S.; Niu, Z.; Hewage, G. B.; Rheingold, A. L.; Craig, S. L.; Stress-Responsive Polymers Containing Cyclobutane Core Mechanophores: Reactivity and Mechanistic Insights; *J. Am. Chem. Soc.*; **2013**, *135* (36), 13598-13604.
- [42] Kryger, M. J.; Munaretto, A. M.; Moore, J. S.; Structure-Mechanochemical Activity Relationships for Cyclobutane Mechanophores; *J. Am. Chem. Soc.*; **2011**, *133* (46), 18992-18998.
- [43] Kryger, M. J.; Ong, M. T.; Odom, S. A.; Sottos, N. R.; White, S. R.; Martinez, T. J.; Moore, J. S.; Masked Cyanoacrylates Unveiled by Mechanical Force; *J. Am. Chem. Soc.*; **2010**, *132* (13), 4558-4559.
- [44] Robb, M. J.; Moore, J. S.; A Retro-Staudinger Cycloaddition: Mechanochemical Cycloelimination of a β -Lactam Mechanophore; *J. Am. Chem. Soc.*; **2015**, *137* (34), 10946-10949.
- [45] Hickenboth, C. R.; Rule, J. D.; Moore, J. S.; Preparation of enediyne-crosslinked networks and their reactivity under thermal and mechanical conditions; *Tetrahedron*; **2008**, *64* (36), 8435-8448.
- [46] Rule, J. D.; Wilson, S. R.; Moore, J. S.; Radical Polymerization Initiated by Bergman Cyclization; *J. Am. Chem. Soc.*; **2003**, *125* (43), 12992-12993.
- [47] Krupička, M.; Sander, W.; Marx, D.; Mechanical Manipulation of Chemical Reactions: Reactivity Switching of Bergman Cyclizations; *J. Phys. Chem. Lett.*; **2014**, *5* (5), 905-909.
- [48] Nagamani, C.; Liu, H.; Moore, J. S.; Mechanogeneration of Acid from Oxime Sulfonates; *J. Am. Chem. Soc.*; **2016**, *138* (8), 2540-2543.

- [49] Shiraki, T.; Diesendruck, C. E.; Moore, J. S.; The mechanochemical production of phenyl cations through heterolytic bond scission; *Faraday Discuss.*; **2014**, *170* (0), 385-394.
- [50] Diesendruck, C. E.; Peterson, G. I.; Kulik, H. J.; Kaitz, J. A.; Mar, B. D.; May, P. A.; White, S. R.; Martínez, T. J.; Boydston, A. J.; Moore, J. S.; Mechanically triggered heterolytic unzipping of a low-temperature polymer; *Nature Chem.*; **2014**, *6* (7), 623-628.
- [51] Diesendruck, C. E.; Zhu, L.; Moore, J. S.; Alkyne mechanochemistry: putative activation by transoidal bending; *Chem. Commun.*; **2014**, *50* (87), 13235-13238.
- [52] Wang, J.; Kouznetsova, T. B.; Niu, Z.; Rheingold, A. L.; Craig, S. L.; Accelerating a Mechanically Driven anti-Woodward–Hoffmann Ring Opening with a Polymer Lever Arm Effect; *J. Org. Chem.*; **2015**, *80* (23), 11895-11898.
- [53] Brown, C. L.; Craig, S. L.; Molecular engineering of mechanophore activity for stress-responsive polymeric materials; *Chemical Science*; **2015**, *6* (4), 2158-2165.
- [54] Wang, J.; Kouznetsova, T. B.; Craig, S. L.; Reactivity and Mechanism of a Mechanically Activated anti-Woodward–Hoffmann–DePuy Reaction; *J. Am. Chem. Soc.*; **2015**, *137* (36), 11554-11557.
- [55] Beiermann, B. A.; Davis, D. A.; Kramer, S. L. B.; Moore, J. S.; Sottos, N. R.; White, S. R.; Environmental effects on mechanochemical activation of spiropyran in linear PMMA; *J. Mater. Chem.*; **2011**, *21* (23), 8443-8447.
- [56] Beiermann, B. A.; Kramer, S. L. B.; Moore, J. S.; White, S. R.; Sottos, N. R.; Role of Mechanophore Orientation in Mechanochemical Reactions; *ACS Macro Lett.*; **2012**, *1* (1), 163-166.
- [57] Beiermann, B. A.; Kramer, S. L. B.; May, P. A.; Moore, J. S.; White, S. R.; Sottos, N. R.; The Effect of Polymer Chain Alignment and Relaxation on Force-Induced Chemical Reactions in an Elastomer; *Adv. Funct. Mater.*; **2013**, *24* (11), 1529–1537.
- [58] Davis, D. A.; Hamilton, A.; Yang, J.; Cremer, L. D.; Van Gough, D.; Potisek, S. L.; Ong, M. T.; Braun, P. V.; Martinez, T. J.; White, S. R.; Moore, J. S.; Sottos, N. R.; Force-induced activation of covalent bonds in mechanoresponsive polymeric materials; *Nature*; **2009**, *459* (7243), 68-72.
- [59] Lee, C. K.; Davis, D. A.; White, S. R.; Moore, J. S.; Sottos, N. R.; Braun, P. V.; Force-Induced Redistribution of a Chemical Equilibrium; *J. Am. Chem. Soc.*; **2010**, *132* (45), 16107-16111.
- [60] Gossweiler, G. R.; Hewage, G. B.; Soriano, G.; Wang, Q.; Welshofer, G. W.; Zhao, X.; Craig, S. L.; Mechanochemical Activation of Covalent Bonds in Polymers with Full and Repeatable Macroscopic Shape Recovery; *ACS Macro Lett.*; **2014**, *3* (3), 216-219.
- [61] Gossweiler, G. R.; Kouznetsova, T. B.; Craig, S. L.; Force-Rate Characterization of Two Spiropyran-Based Molecular Force Probes; *J. Am. Chem. Soc.*; **2015**, *137* (19), 6148–6151.
- [62] Zhang, H.; Chen, Y.; Lin, Y.; Fang, X.; Xu, Y.; Ruan, Y.; Weng, W.; Spiropyran as a Mechanochromic Probe in Dual Cross-Linked Elastomers; *Macromolecules*; **2014**, *47* (19), 6783–6790.
- [63] Chen, Y.; Zhang, H.; Fang, X.; Lin, Y.; Xu, Y.; Weng, W.; Mechanical Activation of Mechanophore Enhanced by Strong Hydrogen Bonding Interactions; *ACS Macro Lett.*; **2014**, *3*, 141-145.
- [64] Fang, X.; Zhang, H.; Chen, Y.; Lin, Y.; Xu, Y.; Weng, W.; Biomimetic Modular Polymer with Tough and Stress Sensing Properties; *Macromolecules*; **2013**, *46* (16), 6566-6574.
- [65] Hong, G.; Zhang, H.; Lin, Y.; Chen, Y.; Xu, Y.; Weng, W.; Xia, H.; Mechanoresponsive Healable Metallosupramolecular Polymers; *Macromolecules*; **2013**, *46* (21), 8649-8656.
- [66] Lee, C. K.; Diesendruck, C. E.; Lu, E.; Pickett, A. N.; May, P. A.; Moore, J. S.; Braun, P. V.; Solvent Swelling Activation of a Mechanophore in a Polymer Network; *Macromolecules*; **2014**, *47* (8), 2690-2694.
- [67] Lee, C. K.; Beiermann, B. A.; Silberstein, M. N.; Wang, J.; Moore, J. S.; Sottos, N. R.; Braun, P. V.; Exploiting Force Sensitive Spiroyrans as Molecular Level Probes; *Macromolecules*; **2013**, *46* (10), 3746-3752.
- [68] Kingsbury, C. M.; May, P. A.; Davis, D. A.; White, S. R.; Moore, J. S.; Sottos, N. R.; Shear activation of mechanophore-crosslinked polymers; *J. Compos. Mater.*; **2011**, *21* (23), 8381-8388.
- [69] Degen, C. M.; May, P. A.; Moore, J. S.; White, S. R.; Sottos, N. R.; Time-Dependent Mechanochemical Response of SP-Cross-Linked PMMA; *Macromolecules*; **2013**, *46* (22), 8917-8921.
- [70] Celestine, A.-D. N.; Beiermann, B. A.; May, P. A.; Moore, J. S.; Sottos, N. R.; White, S. R.; Fracture-induced activation in mechanophore-linked, rubber toughened PMMA; *Polymer*; **2014**, *55* (16), 4164-4171.
- [71] Grady, M. E.; Beiermann, B. A.; Moore, J. S.; Sottos, N. R.; Shockwave Loading of Mechanochemically Active Polymer Coatings; *ACS Appl. Mater. Interfaces*; **2014**, *6* (8), 5350-5355.
- [72] Beiermann, B. A.; Kramer, S. L. B.; May, P. A.; Moore, J. S.; White, S. R.; Sottos, N. R.; The Effect of Polymer Chain Alignment and Relaxation on Force-Induced Chemical Reactions in an Elastomer; *Adv. Funct. Mater.*; **2014**, *24* (11), 1529–1537.
- [73] Zhang, H.; Gao, F.; Cao, X.; Li, Y.; Xu, Y.; Weng, W.; Boulatov, R.; Mechanochromism and Mechanical-Force-Triggered Cross-Linking from a Single Reactive Moiety Incorporated into Polymer Chains; *Angew. Chem.*; **2016**, *128* (9), 3092-3096.

- [74] Kean, Z. S.; Gossweiler, G. R.; Kouznetsova, T. B.; Hewage, G. B.; Craig, S. L.; A Coumarin Dimer Probe of Mechanochemical Scission Efficiency in the Sonochemical Activation of Chain-Centered Mechanophore Polymers; *Chem. Commun.*; **2015**, *51*, 9157-9160.
- [75] Song, Y.-K.; Lee, K.-H.; Hong, W.-S.; Cho, S.-Y.; Yu, H.-C.; Chung, C.-M.; Fluorescence sensing of microcracks based on cycloreversion of a dimeric anthracene moiety; *J. Mater. Chem.*; **2012**, *22* (4), 1380-1386.
- [76] Gostl, R.; Sijbesma, R. P.; π -extended anthracenes as sensitive probes for mechanical stress; *Chemical Science*; **2016**, *7* (1), 370-375.
- [77] Church, D. C.; Peterson, G. I.; Boydston, A. J.; Comparison of Mechanochemical Chain Scission Rates for Linear versus Three-Arm Star Polymers in Strong Acoustic Fields; *ACS Macro Lett.*; **2014**, *3* (7), 648-651.
- [78] Konda, S. S. M.; Brantley, J. N.; Varghese, B. T.; Wiggins, K. M.; Bielawski, C. W.; Makarov, D. E.; Molecular Catch Bonds and the Anti-Hammond Effect in Polymer Mechanochemistry; *J. Am. Chem. Soc.*; **2013**, *135* (34), 12722-12729.
- [79] Wiggins, K. M.; Syrett, J. A.; Haddleton, D. M.; Bielawski, C. W.; Mechanically Facilitated Retro [4 + 2] Cycloadditions; *J. Am. Chem. Soc.*; **2011**, *133* (18), 7180-7189.
- [80] Li, J.; Shiraki, T.; Hu, B.; Wright, R. A. E.; Zhao, B.; Moore, J. S.; Mechanophore Activation at Heterointerfaces; *J. Am. Chem. Soc.*; **2014**, *136* (45), 15925-15928.
- [81] Chen, Y.; Spiering, A. J. H.; Karthikeyan, S.; Peters, G. W. M.; Meijer, E. W.; Sijbesma, R. P.; Mechanically induced chemiluminescence from polymers incorporating a 1,2-dioxetane unit in the main chain; *Nature Chem.*; **2012**, *4* (7), 559-562.
- [82] Chen, Y.; Sijbesma, R. P.; Dioxetanes as Mechanoluminescent Probes in Thermoplastic Elastomers; *Macromolecules*; **2014**, *47* (12), 3797-3805.
- [83] Clough, J. M.; Sijbesma, R. P.; Dioxetane Scission Products Unchanged by Mechanical Force; *ChemPhysChem*; **2014**, *15* (16), 3565-3571.
- [84] Ducrot, E.; Chen, Y.; Bulters, M.; Sijbesma, R. P.; Creton, C.; Toughening Elastomers with Sacrificial Bonds and Watching Them Break; *Science*; **2014**, *344* (6180), 186-189.
- [85] Groote, R.; Szyja, B. M.; Leibfarth, F. A.; Hawker, C. J.; Doltsinis, N. L.; Sijbesma, R. P.; Strain-Induced Strengthening of the Weakest Link: The Importance of Intermediate Geometry for the Outcome of Mechanochemical Reactions; *Macromolecules*; **2014**, *47* (3), 1187-1192.
- [86] Kean, Z. S.; Hawk, J. L.; Lin, S.; Zhao, X.; Sijbesma, R. P.; Craig, S. L.; Increasing the Maximum Achievable Strain of a Covalent Polymer Gel Through the Addition of Mechanically Invisible Cross-Links; *Adv. Mater.*; **2014**, *26* (34), 6013-6018.
- [87] Clough, J. M.; Balan, A.; van Daal, T. L. J.; Sijbesma, R. P.; Probing Force with Mechanobase-Induced Chemiluminescence; *Angew. Chem. Int. Ed.*; **2016**, *55* (4), 1445-1449.
- [88] Wiggins, K. M.; Bielawski, C. W.; A Mechanochemical Approach to Deracemization; *Angew. Chem. Int. Ed.*; **2012**, *51* (7), 1640-1643.
- [89] Staudinger, H.; Bondy, H. F.; Über Isopren und Kautschuk, 19. Mitteil.: Über die Molekülgröße des Kautschuks und der Balata; *Ber. Dtsch. Chem. Ges.*; **1930**, *63* (3), 734-736.
- [90] Staudinger, H.; Heuer, W.; Über hochpolymere Verbindungen, 93. Mitteil.: Über das Zerreißen der Faden-Moleküle des Poly-styrols; *Ber. Dtsch. Chem. Ges.*; **1934**, *67* (7), 1159-1164.
- [91] Staudinger, H.; Leupold, E. O.; Über Isopren und Kautschuk, 18. Mitteil.: Viscositäts-Untersuchungen an Balata; *Ber. Dtsch. Chem. Ges.*; **1930**, *63* (3), 730-733.
- [92] Berkowski, K. L.; Potisek, S. L.; Hickenboth, C. R.; Moore, J. S.; Ultrasound-Induced Site-Specific Cleavage of Azo-Functionalized Poly(ethylene glycol); *Macromolecules*; **2005**, *38* (22), 8975-8978.
- [93] Encina, M. V.; Lissi, E.; Sarasúa, M.; Gargallo, L.; Radic, D.; Ultrasonic degradation of polyvinylpyrrolidone: Effect of peroxide linkages; *J. Polym. Sci., Polym. Lett. Ed.*; **1980**, *18* (12), 757-760.
- [94] Ong, M. T.; Leiding, J.; Tao, H.; Virshup, A. M.; Martínez, T. J.; First Principles Dynamics and Minimum Energy Pathways for Mechanochemical Ring Opening of Cyclobutene; *J. Am. Chem. Soc.*; **2009**, *131* (18), 6377-6379.
- [95] Ribas-Arino, J.; Shiga, M.; Marx, D.; Unravelling the Mechanism of Force-Induced Ring-Opening of Benzocyclobutenes; *Chem. Eur. J.*; **2009**, *15* (48), 13331-13335.
- [96] Beyer, M. K.; The mechanical strength of a covalent bond calculated by density functional theory; *J. Chem. Phys.*; **2000**, *112* (17), 7307-7312.
- [97] Michael, P.; Binder, W. H.; A Mechanochemically Triggered "Click" Catalyst; *Angew. Chem. Int. Ed.*; **2015**, *54* (47), 13918-13922.
- [98] Basedow, A.; Ebert, K.; Ultrasonic degradation of polymers in solution; *Adv. Polym. Sci.*; **1977**, *22*, 83-148.
- [99] Price, G. J.; The use of ultrasound for the controlled degradation of polymer solutions; *Advances in Sonochemistry*; **1990**, *1*, 231-287.

- [100] Suslick, K. S.; Price, G. J.; Application of ultrasound to materials chemistry; *Annu. Rev. Mater. Sci.*; **1999**, *29* (1), 295-326.
- [101] Paulusse, J. M. J.; Sijbesma, R. P.; Ultrasound in polymer chemistry: Revival of an established technique; *J. Polym. Sci., Part A: Polym. Chem.*; **2006**, *44* (19), 5445-5453.
- [102] Wiggins, K. M.; Brantley, J. N.; Bielawski, C. W.; Methods for activating and characterizing mechanically responsive polymers; *Chem. Soc. Rev.*; **2013**, *42* (17), 7130-7147.
- [103] May, P. A.; Moore, J. S.; Polymer mechanochemistry: techniques to generate molecular force via elongational flows; *Chem. Soc. Rev.*; **2013**, *42* (18), 7497-7506.
- [104] Buchholz, B. A.; Zahn, J. M.; Kenward, M.; Slater, G. W.; Barron, A. E.; Flow-induced chain scission as a physical route to narrowly distributed, high molar mass polymers; *Polymer*; **2004**, *45* (4), 1223-1234.
- [105] Horn, A. F.; Merrill, E. W.; Midpoint scission of macromolecules in dilute solution in turbulent flow; *Nature*; **1984**, *312* (5990), 140-141.
- [106] Zysman, V.; Nguyen, T. Q.; Kausch, H.-H.; Degradation on freezing dilute polystyrene solutions in p-xylene; *J. Polym. Sci., Part B: Polym. Phys.*; **1994**, *32* (7), 1257-1269.
- [107] Wang, S.; Yan, X.; Ding, J.; Liu, M.; Cheng, R.; Wu, C.; Qian, R.; On the cryogenic “degradation” of polystyrene in dilute solution; *Journal of Macromolecular Science, Part B*; **1997**, *36* (2), 187-194.
- [108] Imato, K.; Irie, A.; Kosuge, T.; Ohishi, T.; Nishihara, M.; Takahara, A.; Otsuka, H.; Mechanophores with a Reversible Radical System and Freezing-Induced Mechanochemistry in Polymer Solutions and Gels; *Angew. Chem. Int. Ed.*; **2015**, *54* (21), 6168–6172.
- [109] Imato, K.; Nishihara, M.; Kanehara, T.; Amamoto, Y.; Takahara, A.; Otsuka, H.; Self-Healing of Chemical Gels Cross-Linked by Diarylbibenzofuranone-Based Trigger-Free Dynamic Covalent Bonds at Room Temperature; *Angew. Chem. Int. Ed.*; **2012**, *51* (5), 1138-1142.
- [110] Sohma, J.; Mechanochemistry of polymers; *Prog. Polym. Sci.*; **1989**, *14* (4), 451-596.
- [111] Rinaldi, L.; Martina, K.; Baricco, F.; Rotolo, L.; Cravotto, G.; Solvent-Free Copper-Catalyzed Azide-Alkyne Cycloaddition under Mechanochemical Activation; *Molecules*; **2015**, *20* (2), 2837-2849.
- [112] Moses, D.; Feldblum, A.; Ehrenfreund, E.; Heeger, A. J.; Chung, T. C.; MacDiarmid, A. G.; Pressure dependence of the photoabsorption of polyacetylene; *Physical Review B*; **1982**, *26* (6), 3361-3369.
- [113] Muramatsu, Y.; Yamamoto, T.; Hasegawa, M.; Yagi, T.; Koinuma, H.; Piezochromic behaviour of regioregular poly(3-hexylthiophene-2,5-diyl) and poly(5,8-dihexadecyloxyanthraquinone-1,4-diyl); *Polymer*; **2001**, *42* (15), 6673-6675.
- [114] Schütze, D.; Holz, K.; Müller, J.; Beyer, M. K.; Lüning, U.; Hartke, B.; Pinpointing Mechanochemical Bond Rupture by Embedding the Mechanophore into a Macrocyclic; *Angew. Chem. Int. Ed.*; **2015**, *54* (8), 2556-2559.
- [115] Schmidt, S. W.; Kersch, A.; Beyer, M. K.; Clausen-Schaumann, H.; Mechanically activated rupture of single covalent bonds: evidence of force induced bond hydrolysis; *Phys. Chem. Chem. Phys.*; **2011**, *13* (13), 5994-5999.
- [116] Grandbois, M.; Beyer, M.; Rief, M.; Clausen-Schaumann, H.; Gaub, H. E.; How Strong Is a Covalent Bond?; *Science*; **1999**, *283* (5408), 1727-1730.
- [117] Schmidt, S. W.; Filippov, P.; Kersch, A.; Beyer, M. K.; Clausen-Schaumann, H.; Single-Molecule Force-Clamp Experiments Reveal Kinetics of Mechanically Activated Silyl Ester Hydrolysis; *ACS Nano*; **2012**, *6* (2), 1314-1321.
- [118] Suslick, K. S.; Mechanochemistry and sonochemistry: concluding remarks; *Faraday Discuss.*; **2014**, *170* (0), 411-422.
- [119] Florea, M.; New use of size exclusion chromatography in kinetics of mechanical degradation of polymers in solution; *J. Appl. Polym. Sci.*; **1993**, *50* (12), 2039-2045.
- [120] Price, G. J.; Smith, P. F.; Ultrasonic degradation of polymer solutions—III. The effect of changing solvent and solution concentration; *Eur. Polym. J.*; **1993**, *29* (2–3), 419-424.
- [121] Vijayalakshmi, S. P.; Madras, G.; Effect of initial molecular weight and solvents on the ultrasonic degradation of poly(ethylene oxide); *Polym. Degrad. Stab.*; **2005**, *90* (1), 116-122.
- [122] Price, G. J.; Smith, P. F.; Ultrasonic degradation of polymer solutions: 2. The effect of temperature, ultrasound intensity and dissolved gases on polystyrene in toluene; *Polymer*; **1993**, *34* (19), 4111-4117.
- [123] Jiang, S.; Zhang, L.; Xie, T.; Lin, Y.; Zhang, H.; Xu, Y.; Weng, W.; Dai, L.; Mechanoresponsive PS-PnBA-PS Triblock Copolymers via Covalently Embedding Mechanophore; *ACS Macro Lett.*; **2013**, *2* (8), 705-709.
- [124] Gragert, M.; Schunack, M.; Binder, W. H.; Azide/Alkyne-“Click”-Reactions of Encapsulated Reagents: Toward Self-Healing Materials; *Macromol. Rapid Commun.*; **2011**, *32* (5), 419-425.
- [125] Osswald, T.; Menges, G.; Failure and damage of polymers. In *Materials science of polymers for engineers* 2nd ed.; Hanser: Munich: 2003; pp 447-519.
- [126] Hillewaere, X. K. D.; Du Prez, F. E.; Fifteen chemistries for autonomous external self-healing polymers and composites; *Prog. Polym. Sci.*; **2015**, *49–50*, 121-153.

- [127] Herbst, F.; Döhler, D.; Michael, P.; Binder, W. H.; Self-Healing Polymers via Supramolecular Forces; *Macromol. Rapid Commun.*; **2013**, *34* (3), 203-220.
- [128] Michael, P.; Döhler, D.; Binder, W. H.; Improving autonomous self healing via combined chemical/physical principles; *Polymer*; **2015**, *69*, 216-227.
- [129] Guimard, N. K.; Oehlenschlaeger, K. K.; Zhou, J.; Hilf, S.; Schmidt, F. G.; Barner-Kowollik, C.; Current Trends in the Field of Self-Healing Materials; *Macromol. Chem. Phys.*; **2012**, *213* (2), 131-143.
- [130] Döhler, D.; Michael, P.; Binder, W. H., Principles of Self-Healing Polymers. In *Self-Healing Polymers. From Principles to Applications.*, Binder, W. H., Ed. Wiley-VCH: Weinheim, 2013; pp 7-60.
- [131] Esser-Kahn, A. P.; Odom, S. A.; Sottos, N. R.; White, S. R.; Moore, J. S.; Triggered Release from Polymer Capsules; *Macromolecules*; **2011**, *44* (14), 5539-5553.
- [132] Samadzadeh, M.; Boura, S. H.; Peikari, M.; Kasiriha, S. M.; Ashrafi, A.; A review on self-healing coatings based on micro/nanocapsules; *Prog. Org. Coat.*; **2010**, *68* (3), 159-164.
- [133] Blaiszik, B. J.; Kramer, S. L. B.; Olugebefola, S. C.; Moore, J. S.; Sottos, N. R.; S.R.White; Self-Healing Polymers and Composites; *Annu. Rev. Mater. Res.*; **2010**, *40*, 179-211.
- [134] Shchukin, D. G.; Container-based multifunctional self-healing polymer coatings; *Polym. Chem.*; **2013**, *4* (18), 4871-4877.
- [135] Zhu, D. Y.; Rong, M. Z.; Zhang, M. Q.; Self-healing polymeric materials based on microencapsulated healing agents: From design to preparation; *Prog. Polym. Sci.*; **2015**, *49-50*, 175-220.
- [136] Zhang, P.; Li, G.; Advances in healing-on-demand polymers and polymer composites; *Prog. Polym. Sci.*; **2016**.
- [137] Reutenauer, P.; Buhler, E.; Boul, P. J.; Candau, S. J.; Lehn, J. M.; Room Temperature Dynamic Polymers Based on Diels–Alder Chemistry; *Chem. Eur. J.*; **2009**, *15* (8), 1893-1900.
- [138] Peterson, A. M.; Jensen, R. E.; Palmese, G. R.; Room-Temperature Healing of a Thermosetting Polymer Using the Diels–Alder Reaction; *ACS Appl. Mater. Interfaces*; **2010**, *2* (4), 1141-1149.
- [139] Pratama, P. A.; Sharifi, M.; Peterson, A. M.; Palmese, G. R.; Room Temperature Self-Healing Thermoset Based on the Diels–Alder Reaction; *ACS Appl. Mater. Interfaces*; **2013**, *5* (23), 12425-12431.
- [140] Oehlenschlaeger, K. K.; Mueller, J. O.; Brandt, J.; Hilf, S.; Lederer, A.; Wilhelm, M.; Graf, R.; Coote, M. L.; Schmidt, F. G.; Barner-Kowollik, C.; Adaptable Hetero Diels–Alder Networks for Fast Self-Healing under Mild Conditions; *Adv. Mater.*; **2014**, 3561–3566.
- [141] Zhong, Y.; Wang, X.; Zheng, Z.; Du, P.; Polyether–maleimide-based crosslinked self-healing polyurethane with Diels–Alder bonds; *J. Appl. Polym. Sci.*; **2015**, *132* (19), 41944.
- [142] Murphy, E. B.; Bolanos, E.; Schaffner-Hamann, C.; Wudl, F.; Nutt, S. R.; Auad, M. L.; Synthesis and Characterization of a Single-Component Thermally Remendable Polymer Network: Staudinger and Stille Revisited; *Macromolecules*; **2008**, *41* (14), 5203-5209.
- [143] Oehlenschlaeger, K. K.; Guimard, N. K.; Brandt, J.; Mueller, J. O.; Lin, C. Y.; Hilf, S.; Lederer, A.; Coote, M. L.; Schmidt, F. G.; Barner-Kowollik, C.; Fast and catalyst-free hetero-Diels-Alder chemistry for on demand cyclable bonding/debonding materials; *Polym. Chem.*; **2013**, *4* (16), 4348-4355.
- [144] Kötteritzsch, J.; Stumpf, S.; Hoeppener, S.; Vitz, J.; Hager, M. D.; Schubert, U. S.; One-Component Intrinsic Self-Healing Coatings Based on Reversible Crosslinking by Diels–Alder Cycloadditions; *Macromol. Chem. Phys.*; **2013**, *214* (14), 1636-1649.
- [145] Zhang, B.; Digby, Z. A.; Flum, J. A.; Foster, E. M.; Sparks, J. L.; Konkolewicz, D.; Self-healing, malleable and creep limiting materials using both supramolecular and reversible covalent linkages; *Polym. Chem.*; **2015**, *6* (42), 7368-7372.
- [146] Bergman, S. D.; Wudl, F.; Mendable polymers; *J. Mater. Chem.*; **2008**, *18* (1), 41-62.
- [147] Chen, X.; Wudl, F.; Mal, A. K.; Shen, H.; Nutt, S. R.; New Thermally Remendable Highly Cross-Linked Polymeric Materials; *Macromolecules*; **2003**, *36* (6), 1802-1807.
- [148] Chen, X.; Dam, M. A.; Ono, K.; Mal, A.; Shen, H.; Nutt, S. R.; Sheran, K.; Wudl, F.; A Thermally Remendable Cross-Linked Polymeric Material; *Science*; **2002**, *295* (5560), 1698-1702.
- [149] Delaittre, G.; Guimard, N. K.; Barner-Kowollik, C.; Cycloadditions in Modern Polymer Chemistry; *Acc. Chem. Res.*; **2015**, *48* (5), 1296-1307.
- [150] Haehnel, A.; Sagara, Y.; Simon, Y.; Weder, C., Mechanochemistry in Polymers with Supramolecular Mechanophores. Springer Berlin Heidelberg: 2015; pp 1-31.
- [151] Bode, S.; Sandmann, B.; Hager, M. D.; Schubert, U. S., Metal-Complex-Based Self-Healing Polymers. In *Self-Healing Polymers*, Wiley-VCH Verlag GmbH & Co. KGaA: 2013; pp 301-314.
- [152] Mark, J. E., *Polymer Data Handbook*. Oxford University Press, Inc.: 1999.
- [153] Carey, F.; Sundberg, R.; *Advanced Organic Chemistry - Part A: Structure and Mechanisms*; 5th ed.; Springer New York, **2007**.
- [154] Blanksby, S. J.; Ellison, G. B.; Bond Dissociation Energies of Organic Molecules; *Acc. Chem. Res.*; **2003**, *36* (4), 255-263.

- [155] Grubbs, R. H.; Wenzel, A. G., *Handbook of Metathesis, Volume 1: Catalyst Development and Mechanism*. 2nd ed.; Wiley-VCH: Weinheim, 2015; Vol. 1.
- [156] Vougioukalakis, G. C.; Grubbs, R. H.; Ruthenium-Based Heterocyclic Carbene-Coordinated Olefin Metathesis Catalysts; *Chem. Rev.*; **2010**, *110* (3), 1746-1787.
- [157] Schaper, L.-A.; Hock, S. J.; Herrmann, W. A.; Kühn, F. E.; Synthese und Anwendung wasserlöslicher NHC-Übergangsmetall-Komplexe; *Angew. Chem.*; **2013**, *125* (1), 284-304.
- [158] Cazin, C. S. J., *N-Heterocyclic Carbenes in Transition Metal Catalysis and Organocatalysis*. Springer: Dordrecht Heidelberg London New York, 2011; Vol. 32.
- [159] Díez-González, S.; Nolan, S. P.; [(NHC)₂Cu]X Complexes as Efficient Catalysts for Azide-Alkyne Click Chemistry at Low Catalyst Loadings; *Angew. Chem. Int. Ed.*; **2008**, *47* (46), 8881-8884.
- [160] Díez-González, S.; Stevens, E. D.; Scott, N. M.; Petersen, J. L.; Nolan, S. P.; Synthesis and Characterization of [Cu(NHC)₂]X Complexes: Catalytic and Mechanistic Studies of Hydrosilylation Reactions; *Chem. Eur. J.*; **2008**, *14* (1), 158-168.
- [161] Lazreg, F.; Slawin, A. M. Z.; Cazin, C. S. J.; Heteroleptic Bis(N-heterocyclic carbene)Copper(I) Complexes: Highly Efficient Systems for the [3+2] Cycloaddition of Azides and Alkynes; *Organometallics*; **2012**, *31* (22), 7969-7975.
- [162] Hawk, J.; Craig, S., Physical and Materials Applications of Pincer Complexes. In *Organometallic Pincer Chemistry*, van Koten, G.; Milstein, D., Eds. Springer Berlin Heidelberg: 2013; Vol. 40, pp 319-352.
- [163] Koten, G. v.; Gossage, R. A., *The Privileged Pincer-Metal Platform: Coordination Chemistry & Applications*. Springer International Publishing: Cham Heidelberg New York Dordrecht London, 2016; Vol. 54.
- [164] Koten, G. v.; Milstein, D., *Organometallic Pincer Chemistry*. Springer Berlin Heidelberg: 2013; Vol. 40.
- [165] Yount, W. C.; Loveless, D. M.; Craig, S. L.; Strong Means Slow: Dynamic Contributions to the Bulk Mechanical Properties of Supramolecular Networks; *Angew. Chem. Int. Ed.*; **2005**, *44* (18), 2746-2748.
- [166] Yount, W. C.; Loveless, D. M.; Craig, S. L.; Small-Molecule Dynamics and Mechanisms Underlying the Macroscopic Mechanical Properties of Coordinatively Cross-Linked Polymer Networks; *J. Am. Chem. Soc.*; **2005**, *127* (41), 14488-14496.
- [167] Loveless, D. M.; Jeon, S. L.; Craig, S. L.; Chemoresponsive viscosity switching of a metallo-supramolecular polymer network near the percolation threshold; *J. Mater. Chem.*; **2007**, *17* (1), 56-61.
- [168] Larsen, M. B.; Boydston, A. J.; "Flex-Activated" Mechanophores: Using Polymer Mechanochemistry To Direct Bond Bending Activation; *J. Am. Chem. Soc.*; **2013**, *135* (22), 8189-8192.
- [169] Simons, S. S.; Johnson, D. F.; Reaction of o-phthalaldehyde and thiols with primary amines: formation of 1-alkyl(and aryl)thio-2-alkylisoindoles; *J. Org. Chem.*; **1978**, *43* (14), 2886-2891.
- [170] Döhler, D.; Michael, P.; Neumann, S.; Binder, W. H.; Selbstheilende Polymere; *Chemie in unserer Zeit*; **2016**, *50* (2), 90-101.
- [171] Lechtken, P.; Anwendung nicht-isothermer Kinetik auf chemilumineszente Systeme. Thermolyse von 1,2-Dioxetanen; *Chem. Ber.*; **1976**, *109* (8), 2862-2870.
- [172] Binder, W. H.; Sachsenhofer, R.; 'Click' Chemistry in Polymer and Materials Science; *Macromol. Rapid Commun.*; **2007**, *28* (1), 15-54.
- [173] Meldal, M.; Tornøe, C. W.; Cu-Catalyzed Azide-Alkyne Cycloaddition; *Chem. Rev.*; **2008**, *108* (8), 2952-3015.
- [174] Tornøe, C. W.; Christensen, C.; Meldal, M.; Peptidotriazoles on Solid Phase: [1,2,3]-Triazoles by Regiospecific Copper(I)-Catalyzed 1,3-Dipolar Cycloadditions of Terminal Alkynes to Azides; *J. Org. Chem.*; **2002**, *67* (9), 3057-3064.
- [175] Rostovtsev, V. V.; Green, L. G.; Fokin, V. V.; Sharpless, K. B.; A Stepwise Huisgen Cycloaddition Process: Copper(I)-Catalyzed Regioselective "Ligation" of Azides and Terminal Alkynes; *Angew. Chem. Int. Ed.*; **2002**, *41* (14), 2596-2599.
- [176] Haldon, E.; Nicasio, M. C.; Perez, P. J.; Copper-catalysed azide-alkyne cycloadditions (CuAAC): an update; *Org. Biomol. Chem.*; **2015**, *13* (37), 9528-9550.
- [177] Huisgen, R.; 1.3-Dipolare Cycloadditionen Rückschau und Ausblick; *Angew. Chem.*; **1963**, *75* (13), 604-637.
- [178] Huisgen, R.; Cycloadditionen — Begriff, Einteilung und Kennzeichnung; *Angew. Chem.*; **1968**, *80* (9), 329-337.
- [179] Gothelf, K. V.; Jorgensen, K. A.; Asymmetric 1,3-Dipolar Cycloaddition Reactions; *Chem. Rev.*; **1998**, *98* (2), 863-910.
- [180] Kolb, H. C.; Finn, M. G.; Sharpless, K. B.; Click Chemistry: Diverse Chemical Function from a Few Good Reactions; *Angew. Chem. Int. Ed.*; **2001**, *40* (11), 2004-2021.

- [181] van Dijk, M.; Rijkers, D. T. S.; Liskamp, R. M. J.; van Nostrum, C. F.; Hennink, W. E.; Synthesis and Applications of Biomedical and Pharmaceutical Polymers via Click Chemistry Methodologies; *Bioconjugate Chem.*; **2009**, *20* (11), 2001-2016.
- [182] Díaz, D. D.; Punna, S.; Holzer, P.; McPherson, A. K.; Sharpless, K. B.; Fokin, V. V.; Finn, M. G.; Click chemistry in materials synthesis. I. Adhesive polymers from copper-catalyzed azide-alkyne cycloaddition; *J. Polym. Sci., Part A: Polym. Chem.*; **2004**, *42* (17), 4392-4403.
- [183] Iha, R. K.; Wooley, K. L.; Nystrom, A. M.; Burke, D. J.; Kade, M. J.; Hawker, C. J.; Applications of Orthogonal "Click" Chemistries in the Synthesis of Functional Soft Materials; *Chem. Rev.*; **2009**, *109* (11), 5620-5686.
- [184] Binder, W. H.; Sachsenhofer, R.; 'Click' Chemistry in Polymer and Material Science: An Update; *Macromol. Rapid Commun.*; **2008**, *29* (12-13), 952-981.
- [185] Sumerlin, B. S.; Vogt, A. P.; Macromolecular Engineering through Click Chemistry and Other Efficient Transformations; *Macromolecules*; **2009**, *43* (1), 1-13.
- [186] Jeremias, A. J.; Finn, M. G.; Jeffrey, T. K.; Nicholas, J. T.; Construction of Linear Polymers, Dendrimers, Networks, and Other Polymeric Architectures by Copper-Catalyzed Azide-Alkyne Cycloaddition "Click" Chemistry; *Macromol. Rapid Commun.*; **2008**, *29* (12-13), 1052-1072.
- [187] Espeel, P.; Du Prez, F. E.; "Click"-Inspired Chemistry in Macromolecular Science: Matching Recent Progress and User Expectations; *Macromolecules*; **2015**, *48* (1), 2-14.
- [188] Tiwari, V. K.; Mishra, B. B.; Mishra, K. B.; Mishra, N.; Singh, A. S.; Chen, X.; Cu-Catalyzed Click Reaction in Carbohydrate Chemistry; *Chem. Rev.*; **2016**, *116* (5), 3086-3240.
- [189] Chassaing, S.; Beneteau, V.; Pale, P.; When CuAAC 'Click Chemistry' goes heterogeneous; *Catal. Sci. Technol.*; **2016**, *6* (4), 923-957.
- [190] Lazreg, F.; Nahra, F.; Cazin, C. S. J.; Copper-NHC complexes in catalysis; *Coord. Chem. Rev.*; **2015**, *293-294* (0), 48-79.
- [191] Golas, P. L.; Tsarevsky, N. V.; Sumerlin, B. S.; Matyjaszewski, K.; Catalyst Performance in "Click" Coupling Reactions of Polymers Prepared by ATRP: Ligand and Metal Effects; *Macromolecules*; **2006**, *39* (19), 6451-6457.
- [192] Chan, T. R.; Hilgraf, R.; Sharpless, K. B.; Fokin, V. V.; Polytriazoles as Copper(I)-Stabilizing Ligands in Catalysis; *Org. Lett.*; **2004**, *6* (17), 2853-2855.
- [193] Wu, P.; Feldman, A. K.; Nugent, A. K.; Hawker, C. J.; Scheel, A.; Voit, B.; Pyun, J.; Fréchet, J. M. J.; Sharpless, K. B.; Fokin, V. V.; Efficiency and Fidelity in a Click-Chemistry Route to Triazole Dendrimers by the Copper(I)-Catalyzed Ligation of Azides and Alkynes; *Angew. Chem., Int. Ed.*; **2004**, *43* (30), 3928-3932.
- [194] Liu, Y.; Díaz, D. D.; Accurso, A. A.; Sharpless, K. B.; Fokin, V. V.; Finn, M. G.; Click chemistry in materials synthesis. III. Metal-adhesive polymers from Cu(I)-catalyzed azide-alkyne cycloaddition; *J. Polym. Sci., Part A: Polym. Chem.*; **2007**, *45* (22), 5182-5189.
- [195] Kaur, H.; Zinn, F. K.; Stevens, E. D.; Nolan, S. P.; (NHC)CuI (NHC = N-Heterocyclic Carbene) Complexes as Efficient Catalysts for the Reduction of Carbonyl Compounds; *Organometallics*; **2004**, *23* (5), 1157-1160.
- [196] Díez-González, S.; Correa, A.; Cavallo, L.; Nolan, S. P.; (NHC)Copper(I)-Catalyzed [3+2] Cycloaddition of Azides and Mono- or Disubstituted Alkynes; *Chem. Eur. J.*; **2006**, *12* (29), 7558-7564.
- [197] Marion, N.; Díez-González, S.; Nolan, S. P.; N-Heterocyclic Carbenes as Organocatalysts; *Angew. Chem. Int. Ed.*; **2007**, *46* (17), 2988-3000.
- [198] Díez-González, S.; Stevens, E. D.; Nolan, S. P.; A [(NHC)CuCl] complex as a latent Click catalyst; *Chem. Commun.*; **2008**, *0* (39), 4747-4749.
- [199] Díez-González, S.; Escudero-Adán, E. C.; Benet-Buchholz, J.; Stevens, E. D.; Slawin, A. M. Z.; Nolan, S. P.; [(NHC)CuX] complexes: Synthesis, characterization and catalytic activities in reduction reactions and Click Chemistry. On the advantage of using well-defined catalytic systems; *Dalton Trans.*; **2010**, *39* (32), 7595-7606.
- [200] Egbert, J. D.; Cazin, C. S. J.; Nolan, S. P.; Copper N-heterocyclic carbene complexes in catalysis; *Catal. Sci. Technol.*; **2013**, *3* (4), 912-926.
- [201] Díez-González, S.; Scott, N. M.; Nolan, S. P.; Cationic Copper(I) Complexes as Efficient Precatalysts for the Hydrosilylation of Carbonyl Compounds; *Organometallics*; **2006**, *25* (9), 2355-2358.
- [202] Díez-González, S.; Nolan, S. P.; Copper, Silver, and Gold Complexes in Hydrosilylation Reactions; *Acc. Chem. Res.*; **2008**, *41* (2), 349-358.
- [203] Dröge, T.; Glorius, F.; Das Maß aller Ringe – N-heterocyclische Carbene; *Angew. Chem.*; **2010**, *122* (39), 7094-7107.
- [204] Nakamura, T.; Terashima, T.; Ogata, K.; Fukuzawa, S.-i.; Copper(I) 1,2,3-Triazol-5-ylidene Complexes as Efficient Catalysts for Click Reactions of Azides with Alkynes; *Org. Lett.*; **2011**, *13* (4), 620-623.
- [205] Nolte, C.; Mayer, P.; Straub, B. F.; Isolation of a Copper(I) Triazolide: A "Click" Intermediate; *Angew. Chem. Int. Ed.*; **2007**, *46* (12), 2101-2103.

- [206] Rodionov, V. O.; Fokin, V. V.; Finn, M. G.; Mechanism of the Ligand-Free CuI-Catalyzed Azide–Alkyne Cycloaddition Reaction; *Angew. Chem. Int. Ed.*; **2005**, *117* (15), 2250-2255.
- [207] Meldal, M.; Polymer “Clicking” by CuAAC Reactions; *Macromol. Rapid Commun.*; **2008**, *29* (12-13), 1016-1051.
- [208] Michael, P. Synthesis of copolymers containing terminal alkyne groups for self-healing materials. Martin Luther University Halle-Wittenberg, Halle (Saale), 2011.
- [209] Döhler, D.; Michael, P.; Binder, W. H.; Autocatalysis in the Room Temperature Copper(I)-Catalyzed Alkyne–Azide “Click” Cycloaddition of Multivalent Poly(acrylate)s and Poly(isobutylene)s; *Macromolecules*; **2012**, *45* (8), 3335–3345.
- [210] Schunack, M.; Gragert, M.; Döhler, D.; Michael, P.; Binder, W. H.; Low-Temperature Cu(I)-Catalyzed “Click” Reactions for Self-Healing Polymers; *Macromol. Chem. Phys.*; **2012**, *213* (2), 205-214.
- [211] Michael, P.; Binder, W. H.; A Mechanochemically Triggered “Click” Catalyst; *Angew. Chem.*; **2015**, *127* (47), 14124–14128.
- [212] He, H.; Zhong, M.; Adzima, B.; Luebke, D.; Nulwala, H.; Matyjaszewski, K.; A Simple and Universal Gel Permeation Chromatography Technique for Precise Molecular Weight Characterization of Well-Defined Poly(ionic liquid)s; *J. Am. Chem. Soc.*; **2013**, *135* (11), 4227-4230.
- [213] Dröge, T.; Glorius, F.; The Measure of All Rings—N-Heterocyclic Carbenes; *Angew. Chem. Int. Ed.*; **2010**, *49* (39), 6940-6952.
- [214] Fevre, M.; Pinaud, J.; Gnanou, Y.; Vignolle, J.; Taton, D.; N-Heterocyclic carbenes (NHCs) as organocatalysts and structural components in metal-free polymer synthesis; *Chem. Soc. Rev.*; **2013**, *42* (5), 2142-2172.
- [215] Clayden, J.; Greeves, N.; Warren, S.; Wothers, P.; *Organic Chemistry*; 1st ed.; Oxford University Press: Oxford, **2006**.
- [216] Fraser, R. R.; Mansour, T. S.; Savard, S.; Acidity measurements on pyridines in tetrahydrofuran using lithiated silylamines; *J. Org. Chem.*; **1985**, *50* (17), 3232-3234.
- [217] Benhamou, L.; Vujkovic, N.; César, V.; Gornitzka, H.; Lugan, N. I.; Lavigne, G.; Facile Derivatization of a “Chemo-active” NHC Incorporating an Enolate Backbone and Relevant Tuning of Its Electronic Properties; *Organometallics*; **2010**, *29* (11), 2616-2630.
- [218] Chun, J.; Lee, H. S.; Jung, I. G.; Lee, S. W.; Kim, H. J.; Son, S. U.; Cu₂O: A Versatile Reagent for Base-Free Direct Synthesis of NHC-Copper Complexes and Decoration of 3D-MOF with Coordinatively Unsaturated NHC-Copper Species; *Organometallics*; **2010**, *29* (7), 1518-1521.
- [219] Lazreg, F.; Cordes, D. B.; Slawin, A. M. Z.; Cazin, C. S. J.; Synthesis of Homoleptic and Heteroleptic Bis-N-heterocyclic Carbene Group 11 Complexes; *Organometallics*; **2015**, *34* (2), 419-425.
- [220] Mehr, S. K. S. Synthesis of bis[N-heterocyclic carbene-telechelic poly(tetrahydrofuran)] copper (I) complex as a mechanocatalyst. Martin Luther University Halle-Wittenberg, Halle 2016.
- [221] Brotherton, W. S.; Michaels, H. A.; Simmons, J. T.; Clark, R. J.; Dalal, N. S.; Zhu, L.; Apparent Copper(II)-Accelerated Azide–Alkyne Cycloaddition; *Org. Lett.*; **2009**, *11* (21), 4954-4957.
- [222] Kirai, N.; Yamamoto, Y.; Homocoupling of Arylboronic Acids Catalyzed by 1,10-Phenanthroline-Ligated Copper Complexes in Air; *European Journal of Organic Chemistry*; **2009**, *2009* (12), 1864-1867.
- [223] Kuang, G.-C.; Guha, P. M.; Brotherton, W. S.; Simmons, J. T.; Stanke, L. A.; Nguyen, B. T.; Clark, R. J.; Zhu, L.; Experimental Investigation on the Mechanism of Chelation-Assisted, Copper(II) Acetate-Accelerated Azide–Alkyne Cycloaddition; *J. Am. Chem. Soc.*; **2011**, *133* (35), 13984-14001.
- [224] Le Droumaguet, C.; Wang, C.; Wang, Q.; Fluorogenic click reaction; *Chem. Soc. Rev.*; **2010**, *39*, 1233-1239.
- [225] Sivakumar, K.; Xie, F.; Cash, B. M.; Long, S.; Barnhill, H. N.; Wang, Q.; A Fluorogenic 1,3-Dipolar Cycloaddition Reaction of 3-Azidocoumarins and Acetylenes; *Org. Lett.*; **2004**, *6* (24), 4603-4606.
- [226] Zhou, Z.; Fahrni, C. J.; A Fluorogenic Probe for the Copper(I)-Catalyzed Azide–Alkyne Ligation Reaction: Modulation of the Fluorescence Emission via ³(n,π*)–¹(π,π*) Inversion; *J. Am. Chem. Soc.*; **2004**, *126* (29), 8862-8863.
- [227] Gottlieb, H. E.; Kotlyar, V.; Nudelman, A.; NMR Chemical Shifts of Common Laboratory Solvents as Trace Impurities; *J. Org. Chem.*; **1997**, *62* (21), 7512-7515.
- [228] Fulmer, G. R.; Miller, A. J. M.; Sherden, N. H.; Gottlieb, H. E.; Nudelman, A.; Stoltz, B. M.; Bercaw, J. E.; Goldberg, K. I.; NMR Chemical Shifts of Trace Impurities: Common Laboratory Solvents, Organics, and Gases in Deuterated Solvents Relevant to the Organometallic Chemist; *Organometallics*; **2010**, *29* (9), 2176-2179.
- [229] Storey, R. F.; Lee, Y.; Sulfonation of tert-alkyl chlorides: Application to the tert-chloride-terminated polyisobutylene system; *J. Polym. Sci. Part A: Polym. Chem.*; **1991**, *29* (3), 317-325.
- [230] Morgan, D. L.; Martinez-Castro, N.; Storey, R. F.; End-Quenching of TiCl₄-Catalyzed Quasilinging Polyisobutylene with Alkoxybenzenes for Direct Chain End Functionalization; *Macromolecules*; **2010**, *43* (21), 8724-8740.

- [231] Morgan, D. L.; Storey, R. F.; End-Quenching of Quasi-Living Isobutylene Polymerizations with Alkoxybenzene Compounds; *Macromolecules*; **2009**, *42* (18), 6844-6847.
- [232] Dervaux, B.; Meyer, F.; Raquez, J.-M.; Olivier, A.; Du Prez, F. E.; Dubois, P.; Imidazolium End-Functionalized ATRP Polymers as Directing Agents for CNT Dispersion and Confinement; *Macromol. Chem. Phys.*; **2012**, *213* (12), 1259-1265.
- [233] Alvarez, S. G.; Alvarez, M. T.; A Practical Procedure for the Synthesis of Alkyl Azides at Ambient Temperature in Dimethyl Sulfoxide in High Purity and Yield; *Synthesis*; **1997**, *1997* (04), 413,414.
- [234] Yoshida, S.; Suga, H.; Seki, S.; Thermodynamic Studies of Solid Polyethers. III. Poly(tetrahydrofuran), $-\text{[(CH}_2\text{)}_4\text{O]}_n-$; *Polym J*; **1973**, *5* (1), 25-32.

7 Appendix

7.1 NMR-spectra of bromo-telechelic PIB (3)

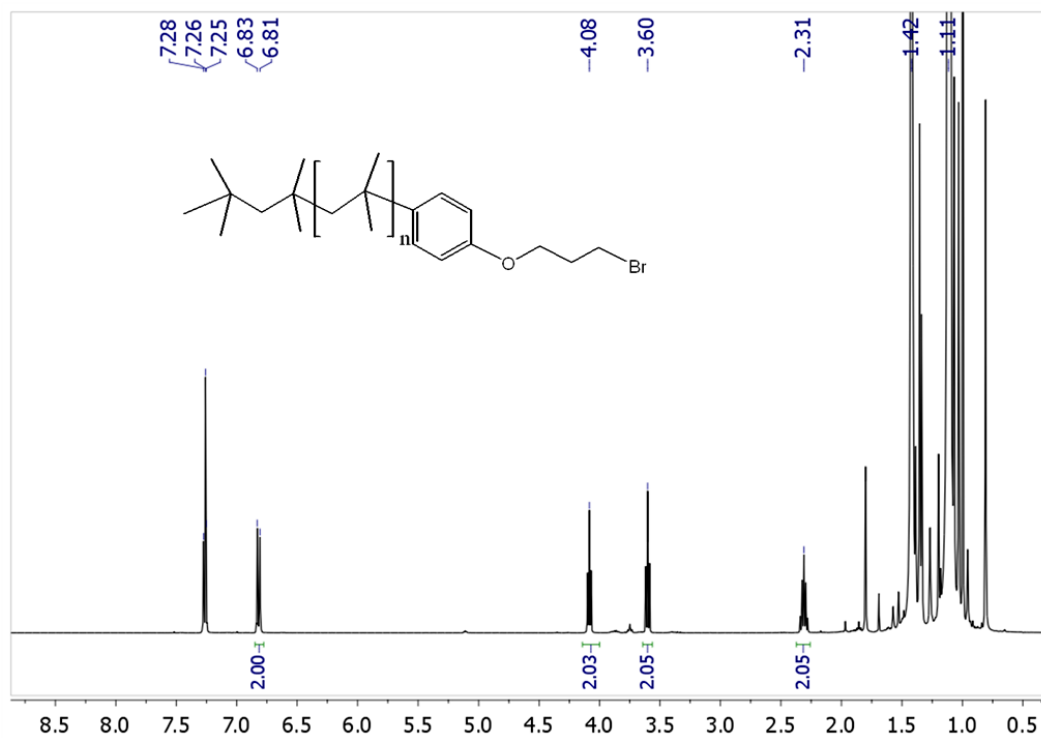


Figure A1. ¹H-NMR spectrum of bromo-telechelic PIB **3a** in CDCl₃. (Reprinted from ref⁹⁷ with permission of Wiley and Sons)

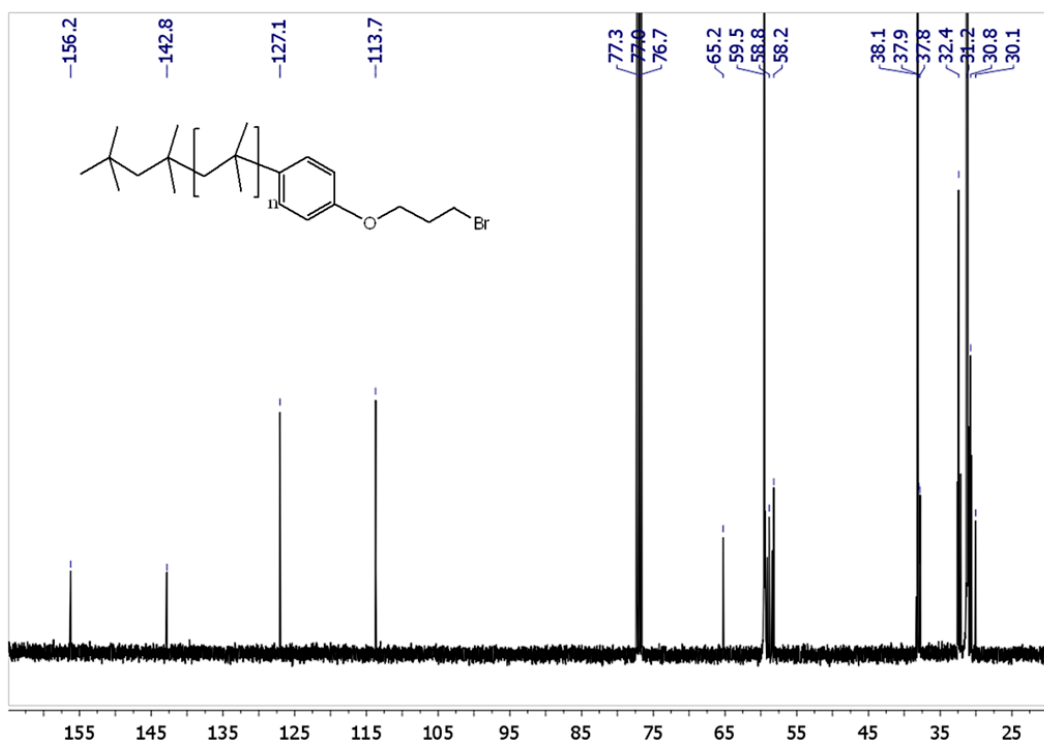


Figure A2. ¹³C-NMR spectrum of bromo-telechelic PIB **3a** in CDCl₃. (Reprinted from ref⁹⁷ with permission of Wiley and Sons)

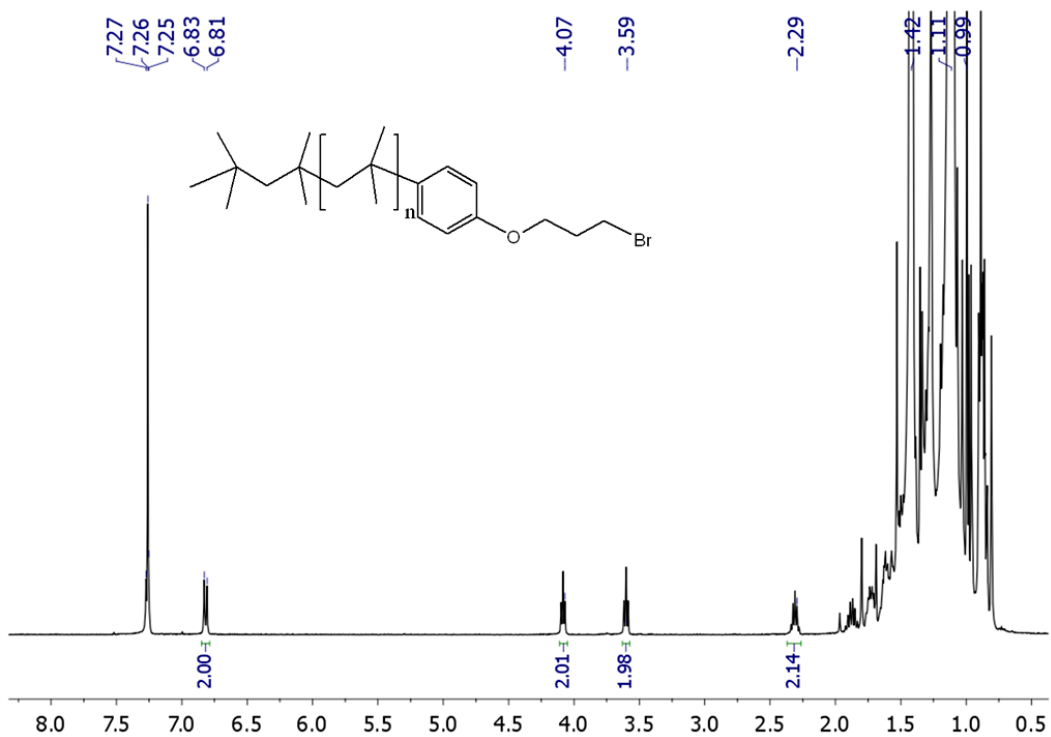


Figure A3. ¹H-NMR spectrum of bromo-telechelic PIB **3b** in CDCl₃. (Reprinted from ref⁹⁷ with permission of Wiley and Sons)

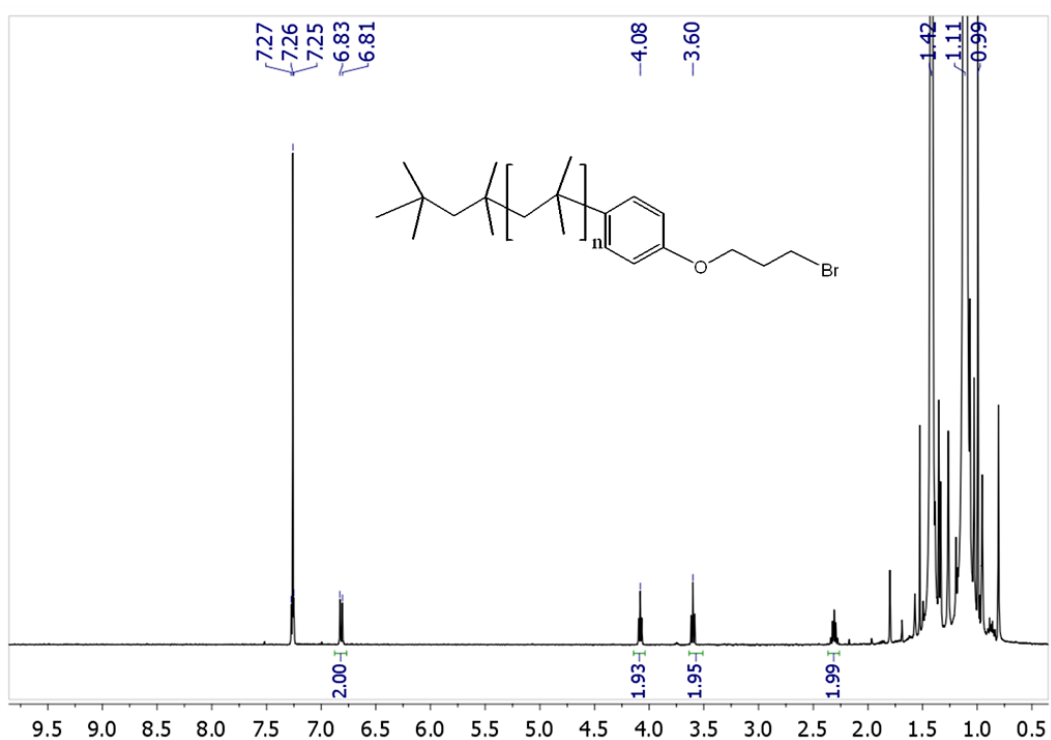


Figure A4. ¹H-NMR spectrum of bromo-telechelic PIB **3c** in CDCl₃. (Reprinted from ref⁹⁷ with permission of Wiley and Sons)

7.2 NMR-spectra and MALDI-TOF-MS of *N*-methylimidazolium-telechelic PIB (5)

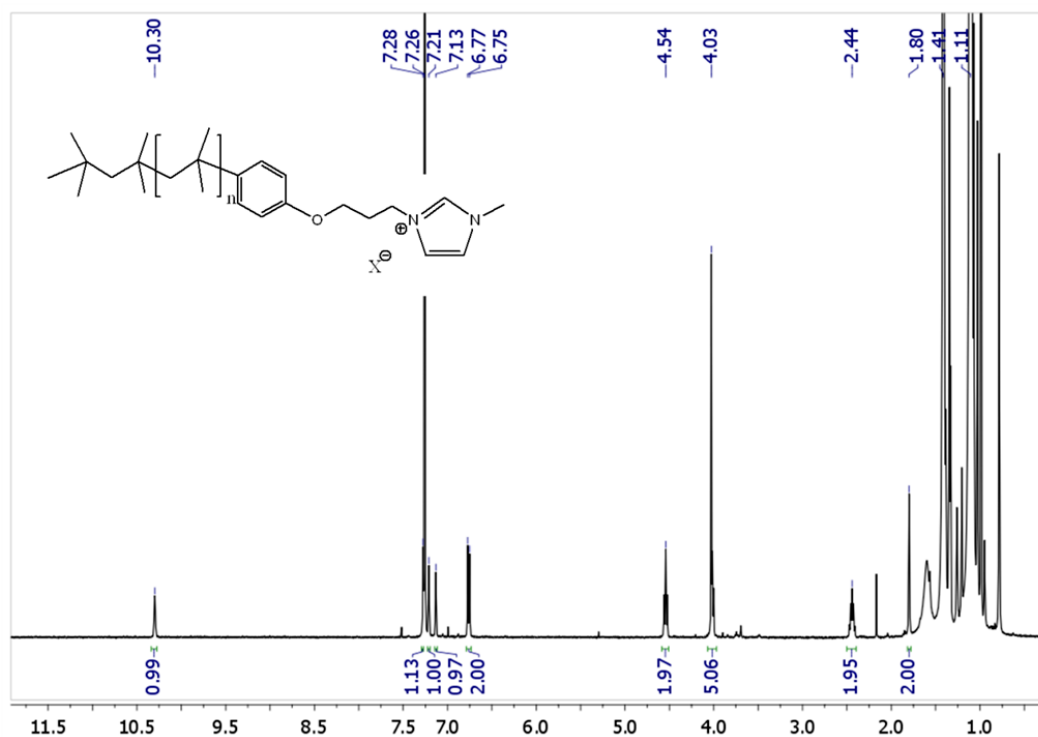


Figure A5. ¹H-NMR spectrum of *N*-methylimidazolium-telechelic PIB **5a** in CDCl₃. (Reprinted from ref⁹⁷ with permission of Wiley and Sons)

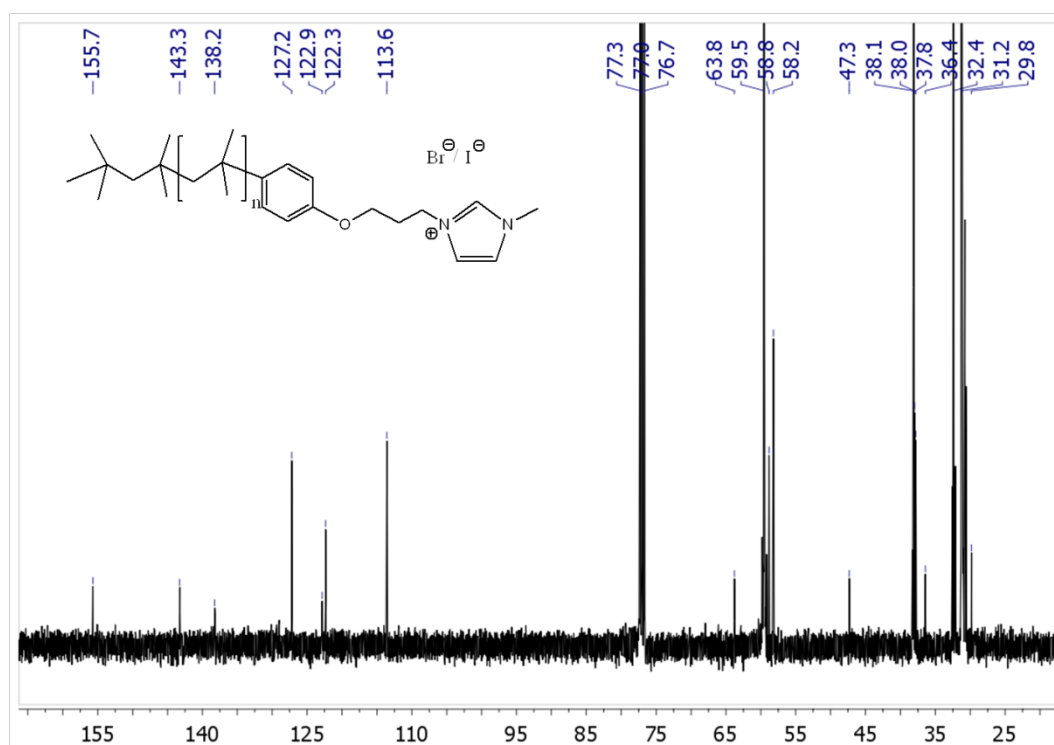


Figure A6. ¹³C-NMR spectrum of *N*-methylimidazolium-telechelic PIB **5a** in CDCl₃. (Reprinted from ref⁹⁷ with permission of Wiley and Sons)

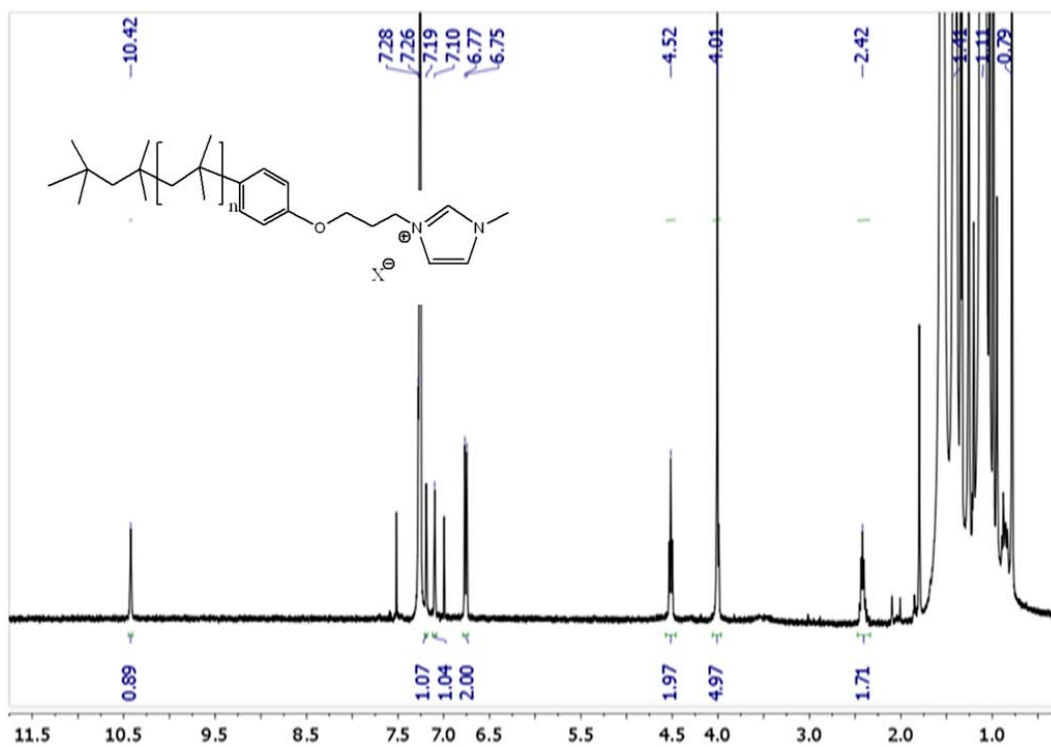


Figure A7. $^1\text{H-NMR}$ spectrum of *N*-methylimidazolium-telechelic PIB **5b** in CDCl_3 . (Reprinted from ref⁹⁷ with permission of Wiley and Sons)

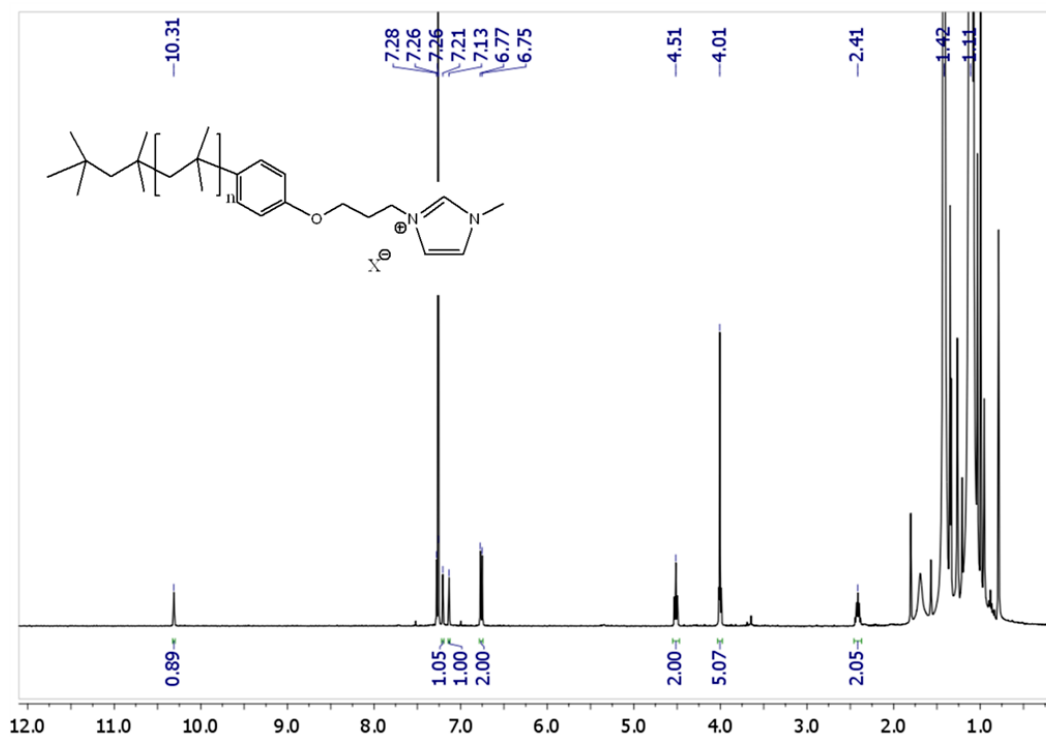


Figure A8. $^1\text{H-NMR}$ spectrum of *N*-methylimidazolium-telechelic PIB **5c** in CDCl_3 . (Reprinted from ref⁹⁷ with permission of Wiley and Sons)

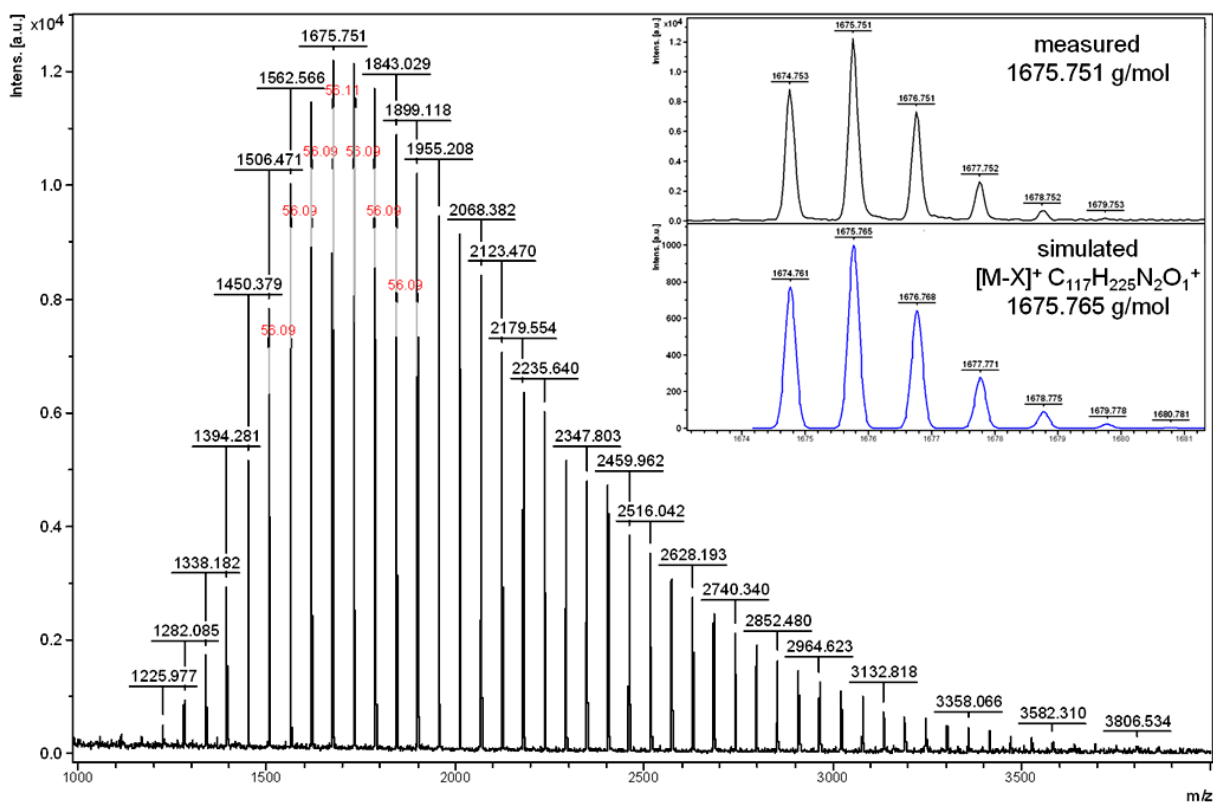


Figure A9. MALDI-TOF-mass spectrum of *N*-methylimidazolium-telechelic PIB **5a** using dithranol as matrix and NaTFA as salt. **5a** was found without counterion or addition cation. Enlargement shows isotopic pattern as well as simulation of **5a**. (Reprinted from ref⁹⁷ with permission of Wiley and Sons)

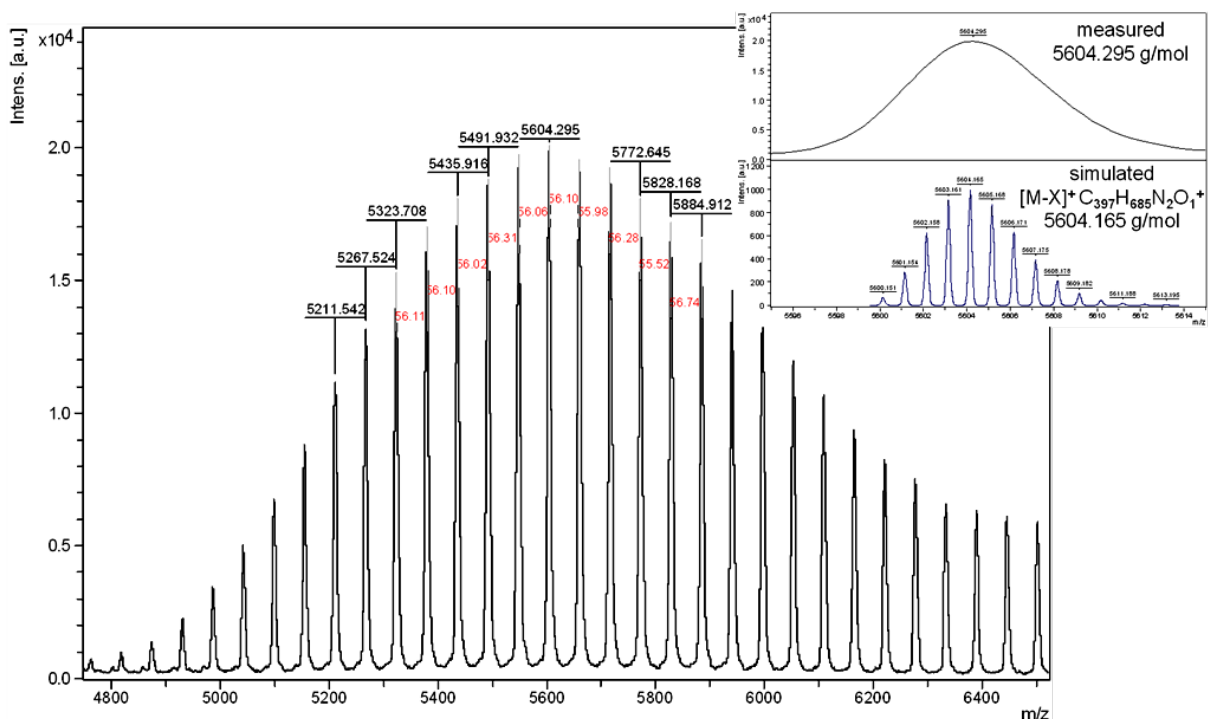


Figure A10. MALDI-TOF-mass spectrum of *N*-methylimidazolium-telechelic PIB **5b** using dithranol as matrix and NaTFA as salt. **5b** was found without counterion or addition cation. Enlargement shows a proper matching of measured and simulation peak of **5b**, albeit no isotopic pattern is visible.

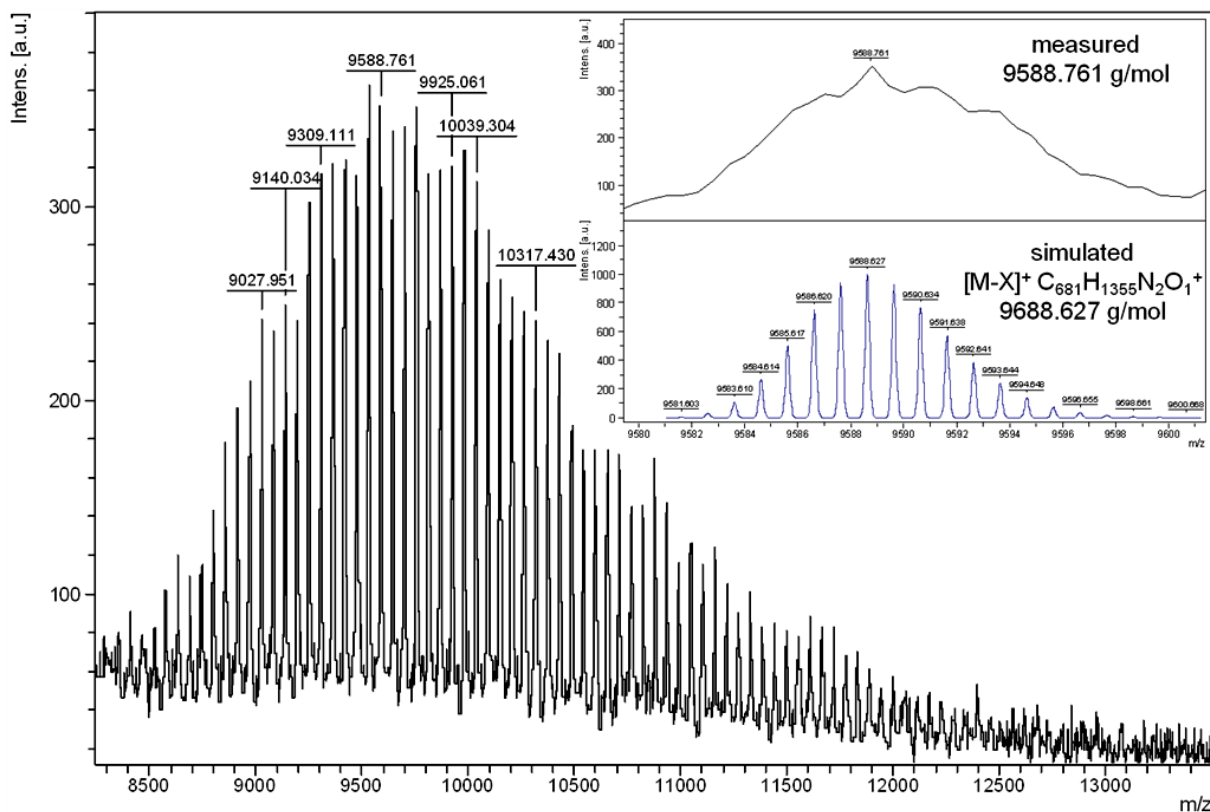


Figure A11. MALDI-TOF-mass spectrum of *N*-methylimidazolium-telechelic PIB **5c** using dithranol as matrix and NaTFA as salt. **5c** was found without counterion or addition cation. Enlargement shows a proper matching of measured and simulation peak of **5c**, albeit no isotopic pattern is visible.

7.3 GPC, NMR-spectra and MALDI-TOF-MS of bis(*N*-methylimidazol-2-ylidene-telechelic poly(isobutylene) copper(I)X [Cu(PIB-NHC)₂]X (**6**)

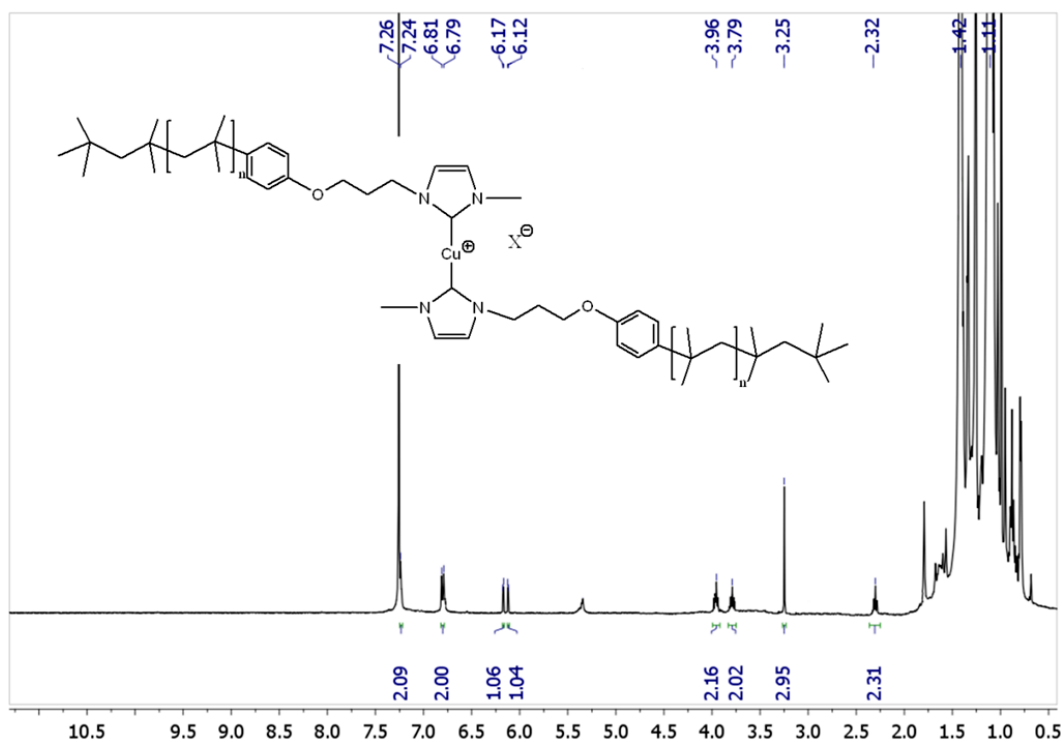


Figure A12. ¹H-NMR spectrum of bis(*N*-methylimidazol-2-ylidene-telechelic poly(isobutylene) copper(I)X [Cu(PIB-NHC)₂]X **6a** in CDCl₃. (Reprinted from ref⁹⁷ with permission of Wiley and Sons)

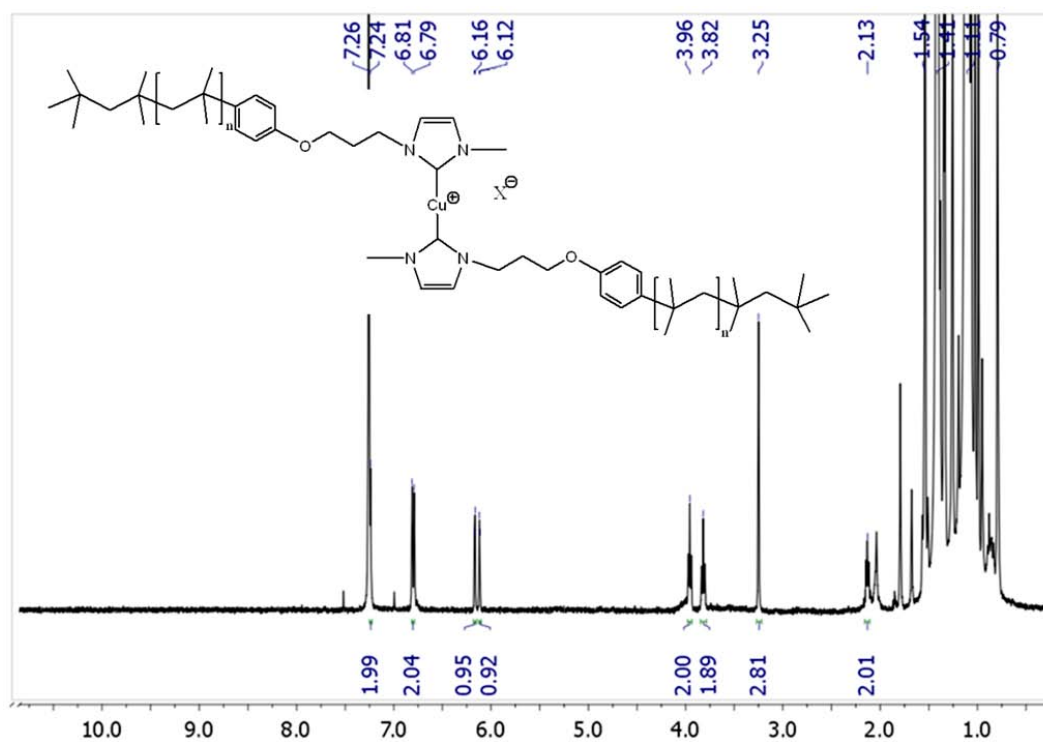


Figure A13. ¹H-NMR spectrum of bis(*N*-methylimidazol-2-ylidene-telechelic poly(isobutylene) copper(I)X [Cu(PIB-NHC)₂]X **6b** in CDCl₃. (Reprinted from ref⁹⁷ with permission of Wiley and Sons)

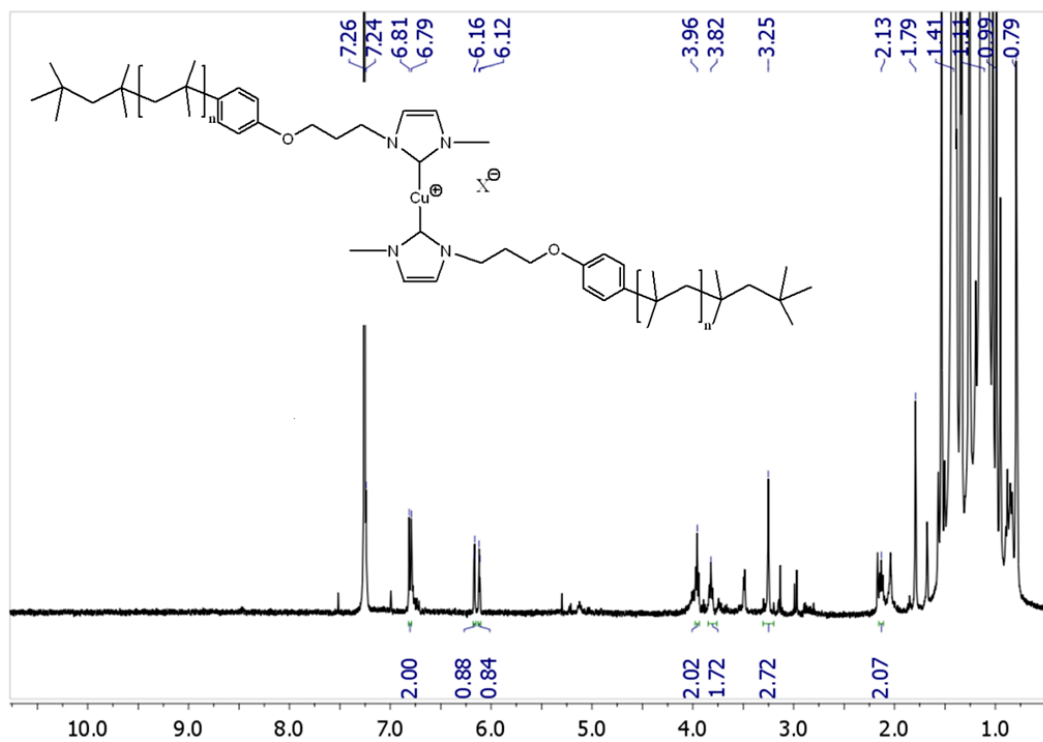


Figure A14. ¹H-NMR spectrum of bis(*N*-methylimidazol-2-ylidene-telechelic poly(isobutylene) copper(I)X [Cu(PIB-NHC)₂]X **6c** in CDCl₃. (Reprinted from ref⁹⁷ with permission of Wiley and Sons)

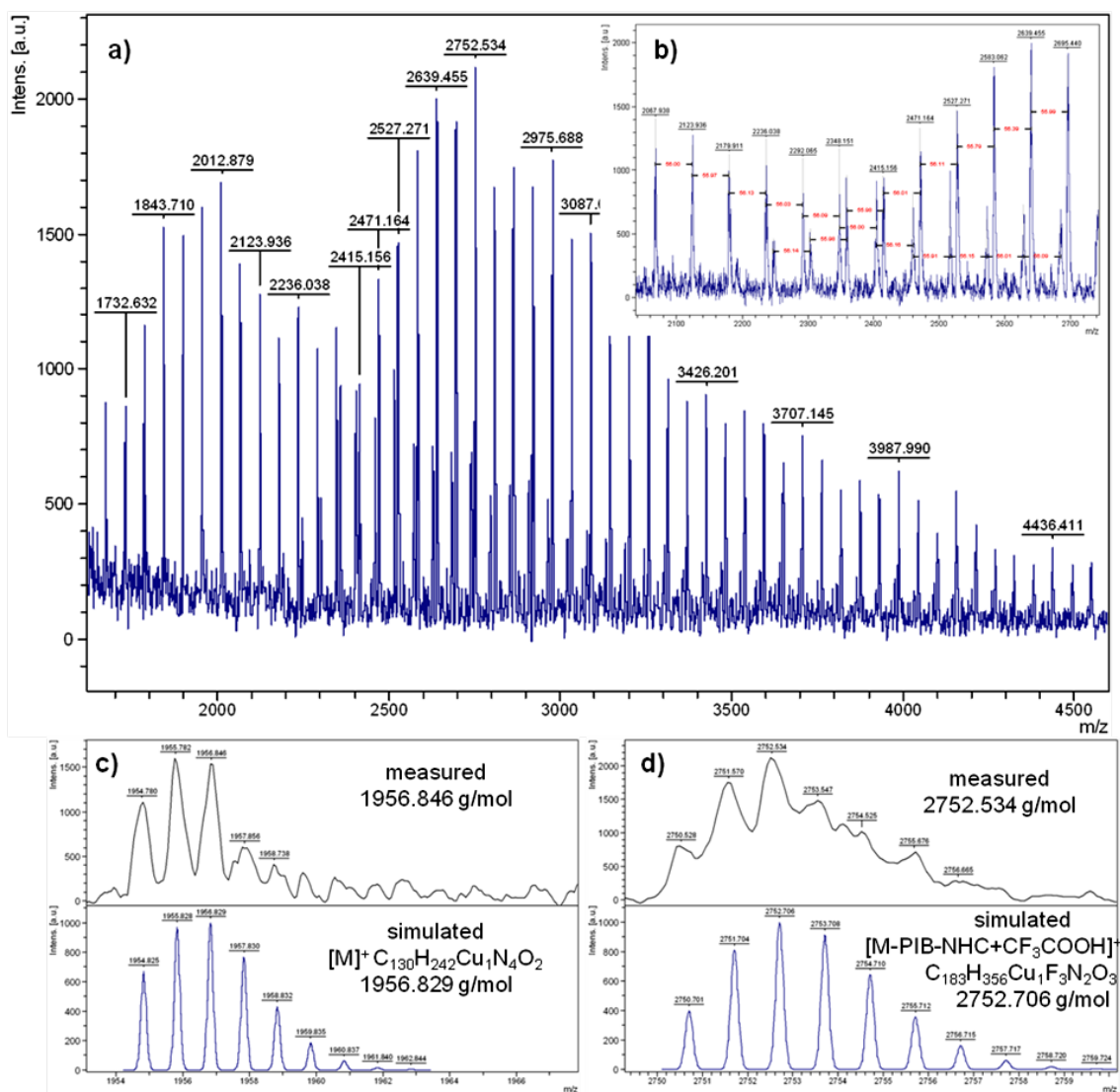


Figure A15. MALDI-TOF-mass spectrum of bis(*N*-methylimidazol-2-ylidene-telechelic poly(isobutylene)copper(I)X [Cu(PIB-NHC)₂]X (**6a**) using DCTB as matrix and LiTFA as salt. **a**) Full spectrum of **6a** showing two series, **b**) enlargement of overlay area of both series, **c**) isotopic pattern as well as simulation of 1st series assigned to the polymeric bis-carbene complex **6a** without counterion and **d**) isotopic pattern as well as simulation of 2nd series assigned to decomposed **6a** (without counterion and one cleaved-off polymeric ligand flying together with CF₃COOH). (Reprinted from ref⁹⁷ with permission of Wiley and Sons)

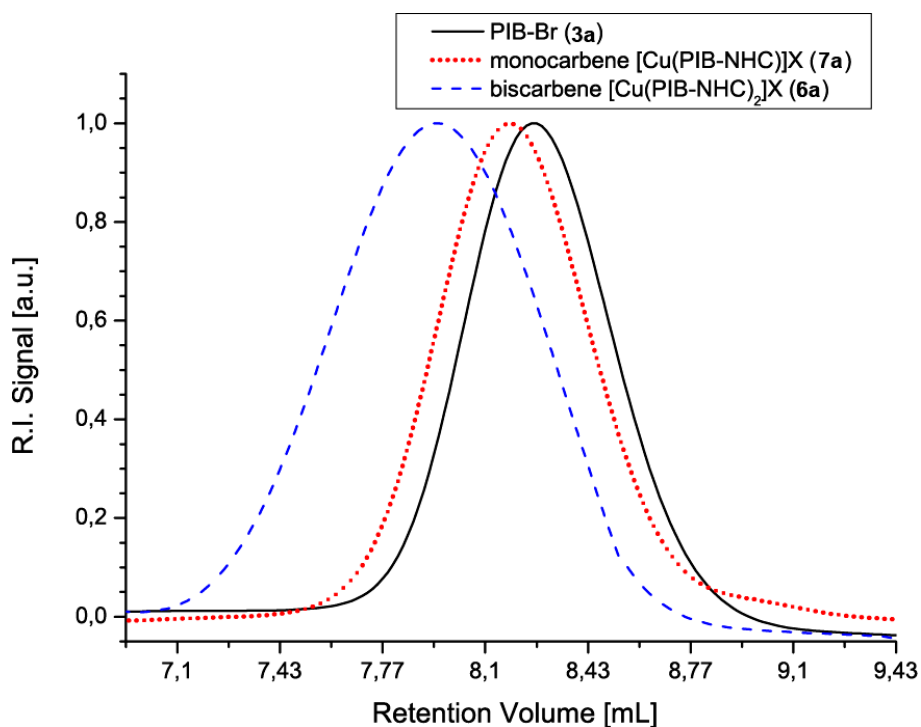


Figure A16. GPC traces of bromo-telechelic PIB (**3a**; PIB-Br; M_n (GPC) = 2200 g/mol) as well as corresponding mono- (**7a**; [Cu(PIB-NHC)]Br; M_n (GPC) = 2900 g/mol) and biscarbene complexes (**6a**; [Cu(PIB-NHC)₂]Br; M_n (GPC) = 4750 g/mol) indicating the doubling of molecular weight during the mechanocatalyst formation. (Reprinted from ref⁹⁷ with permission of Wiley and Sons)

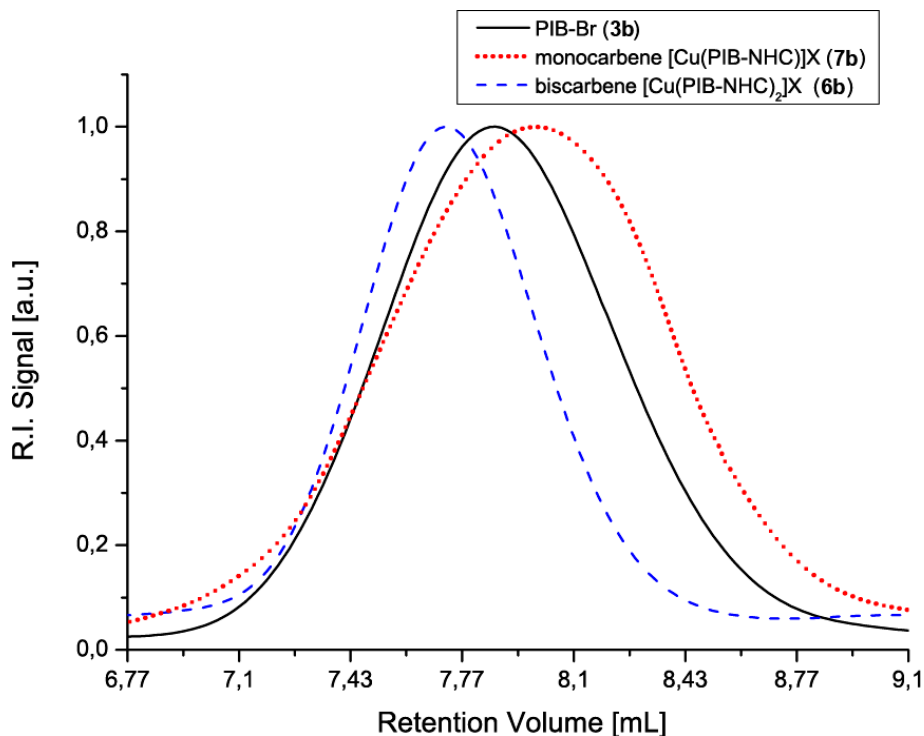


Figure A17. GPC traces of bromo-telechelic PIB (**3b**; PIB-Br; M_n (GPC) = 4700 g/mol) as well as corresponding mono- (**7b**; [Cu(PIB-NHC)]Br; M_n (GPC) = 4800 g/mol) and biscarbene complexes (**6b**; [Cu(PIB-NHC)₂]Br; M_n (GPC) = 8900 g/mol) indicating the doubling of molecular weight during the mechanocatalyst formation. (Reprinted from ref⁹⁷ with permission of Wiley and Sons)

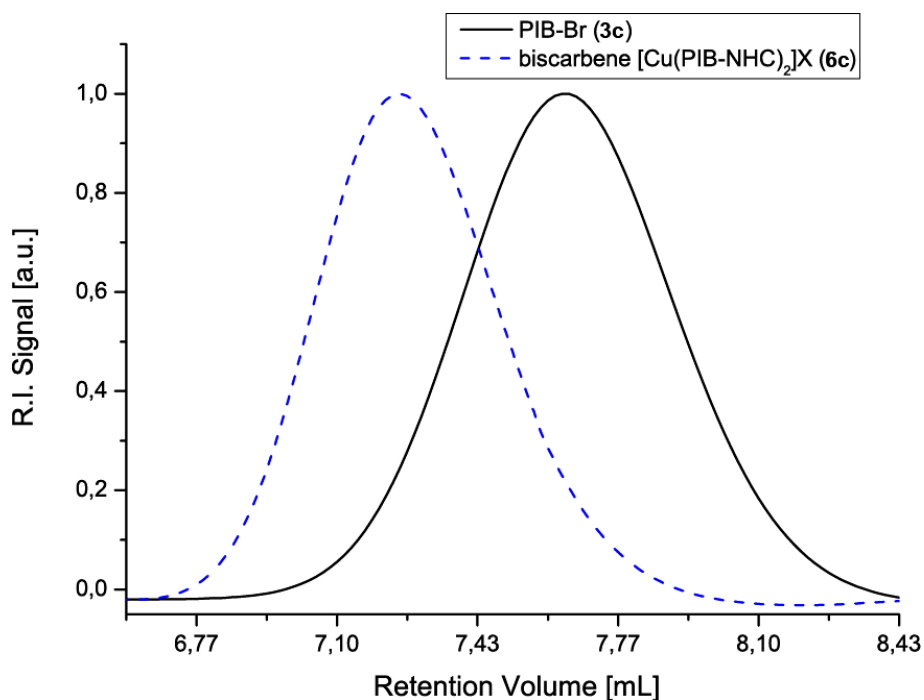


Figure A18. GPC traces of bromo-telechelic PIB (**3c**; PIB-Br; M_n (GPC) = 8750 g/mol) as well as corresponding biscarbene complexes (**6c**; [Cu(PIB-NHC)₂]Br; M_n (GPC) = 17200 g/mol) indicating the doubling of molecular weight during the mechanocatalyst formation. (Reprinted from ref⁹⁷ with permission of Wiley and Sons)

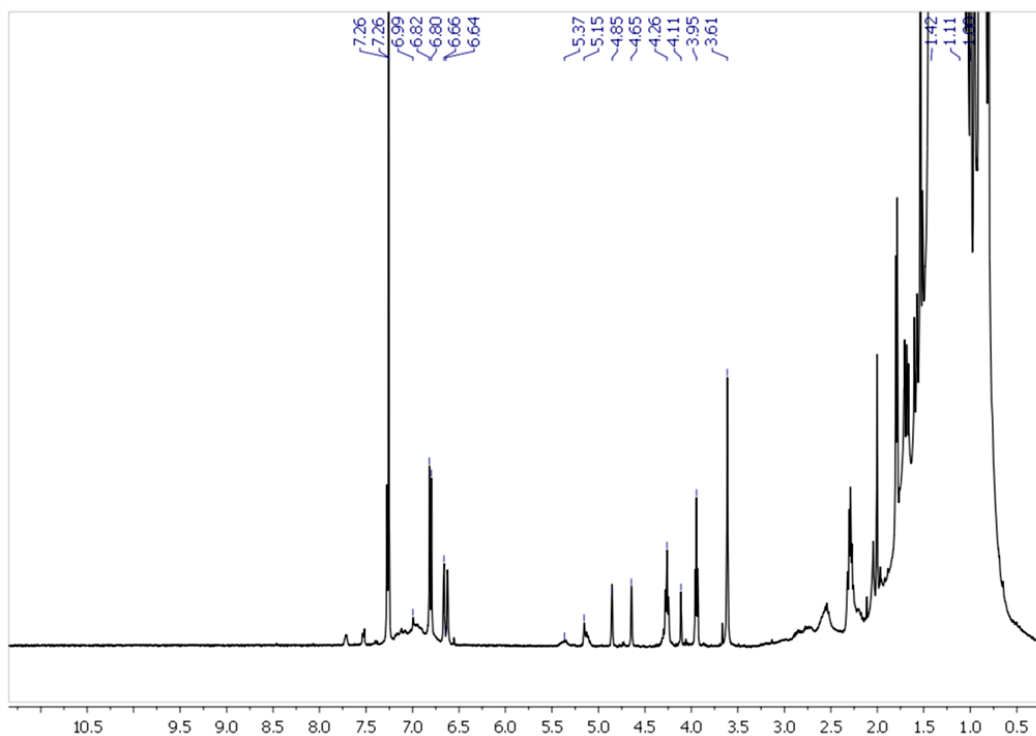


Figure A19. Example for ¹H-NMR spectrum of **21** in CDCl₃.

7.4 NMR-spectra and ESI-TOF-MS of 1-(3-phenoxypropyl)-3-methylimidazolium bromide (**8**)

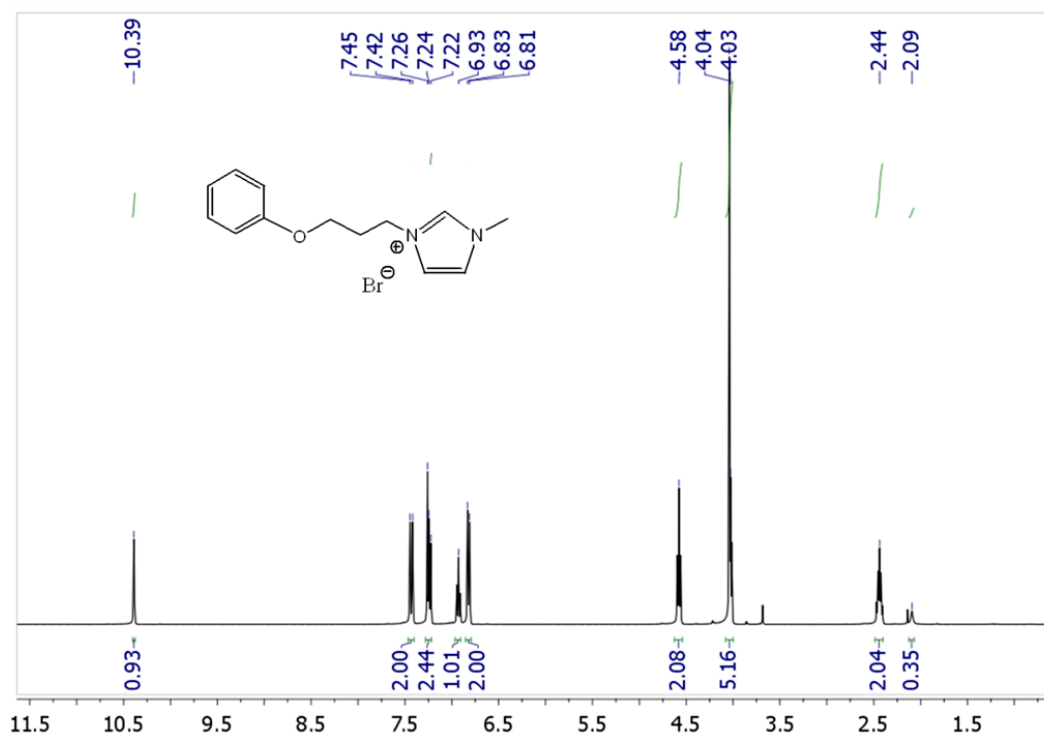


Figure A20. ¹H-NMR spectrum of 1-(3-phenoxypropyl)-3-methylimidazolium bromide (**8**) in CDCl₃.

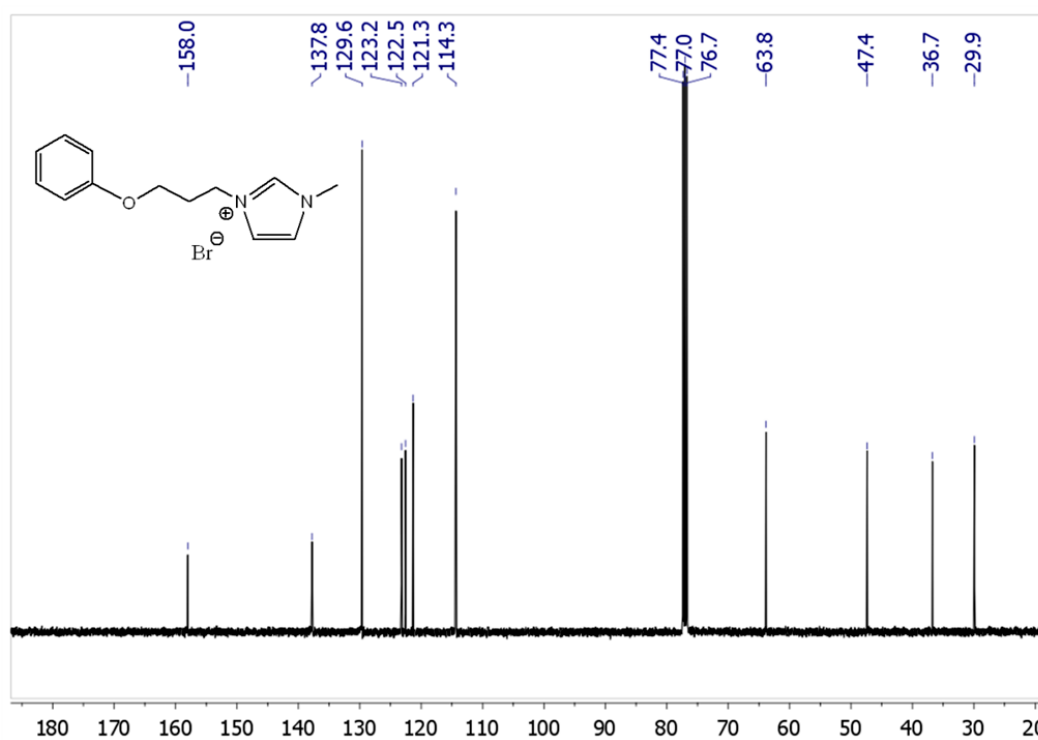


Figure A21. ¹³C-NMR spectrum of 1-(3-phenoxypropyl)-3-methylimidazolium bromide (**8**) in CDCl₃.

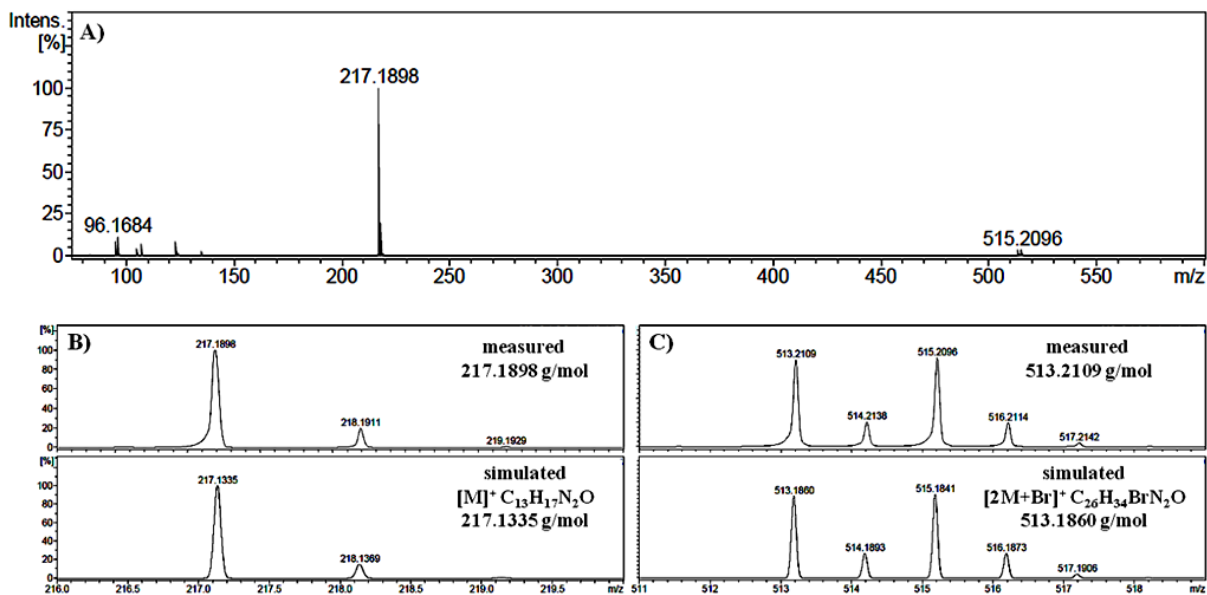


Figure A22. A) ESI-TOF-mass spectrum of 1-(3-phenoxypropyl)-3-methylimidazolium bromide (**8**) showing two species $[M]^+$ and $[2M+Br]^+$. B) **8** was found without counterion or additional cation $[M]^+$ as well as C) bromo-bridged dimer $[2M+Br]^+$. Isotopic pattern of the measured and simulated peak match very well.

7.5 NMR-spectra of bis(1-(3-phenoxypropyl)-3-methylimidazol-2-ylidene) copper (I) bromide (**10**)

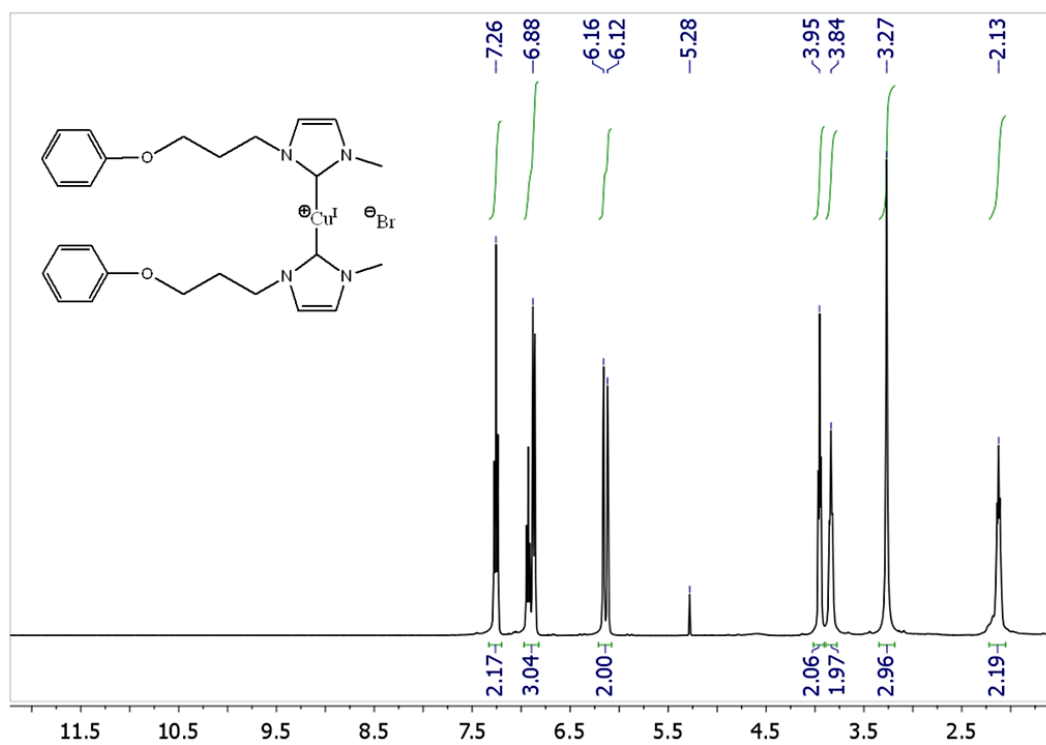


Figure A23. 1H -NMR spectrum of bis(1-(3-phenoxypropyl)-3-methylimidazol-2-ylidene) copper (I) bromide (**10**) in $CDCl_3$.

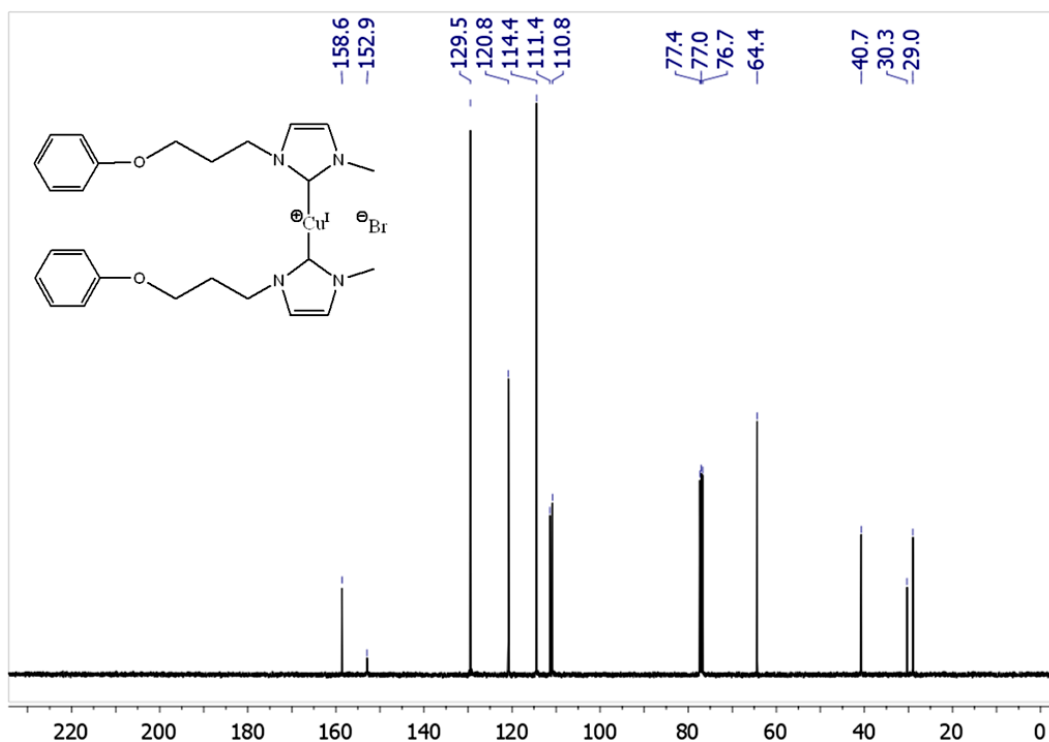


Figure A24. ^{13}C -NMR spectrum of bis(1-(3-phenoxypropyl)-3-methylimidazol-2-ylidene) copper (I) bromide (**10**) in CDCl_3 .

7.6 NMR-spectra of bromo-telechelic poly(styrene)s (**12**)

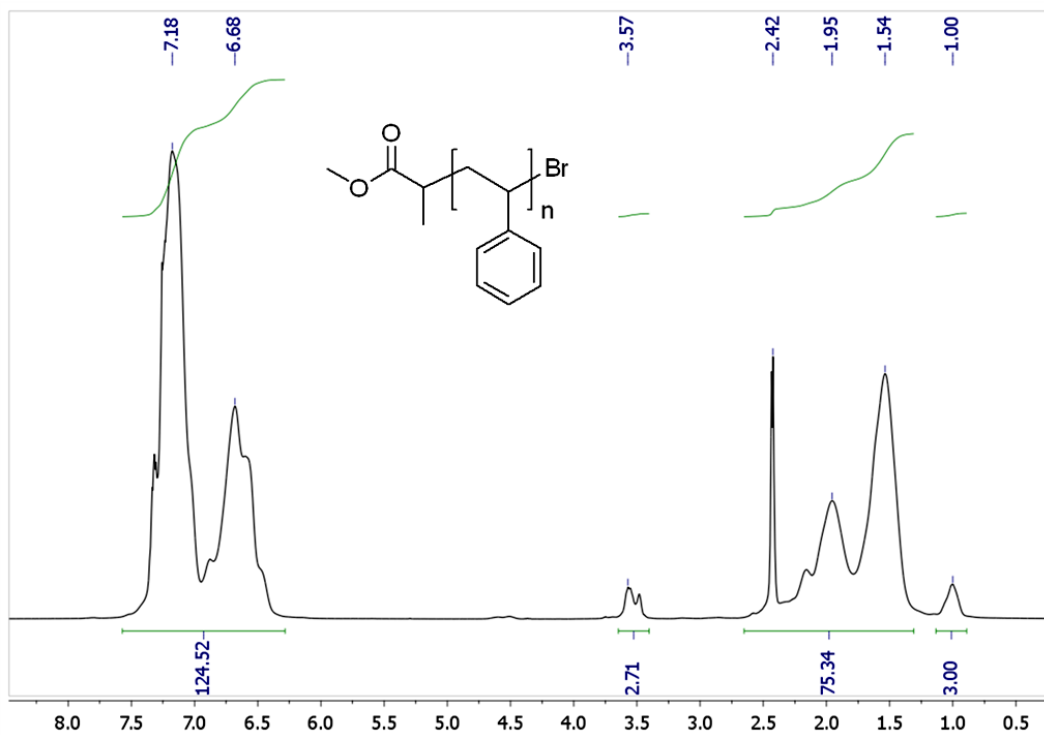


Figure A25. ^1H -NMR spectrum of bromo-telechelic poly(styrene)s (**12a**) in CDCl_3 .

7.7 NMR-spectra and MALDI-TOF-MS of *N*-methylimidazolium-telechelic PS (13)

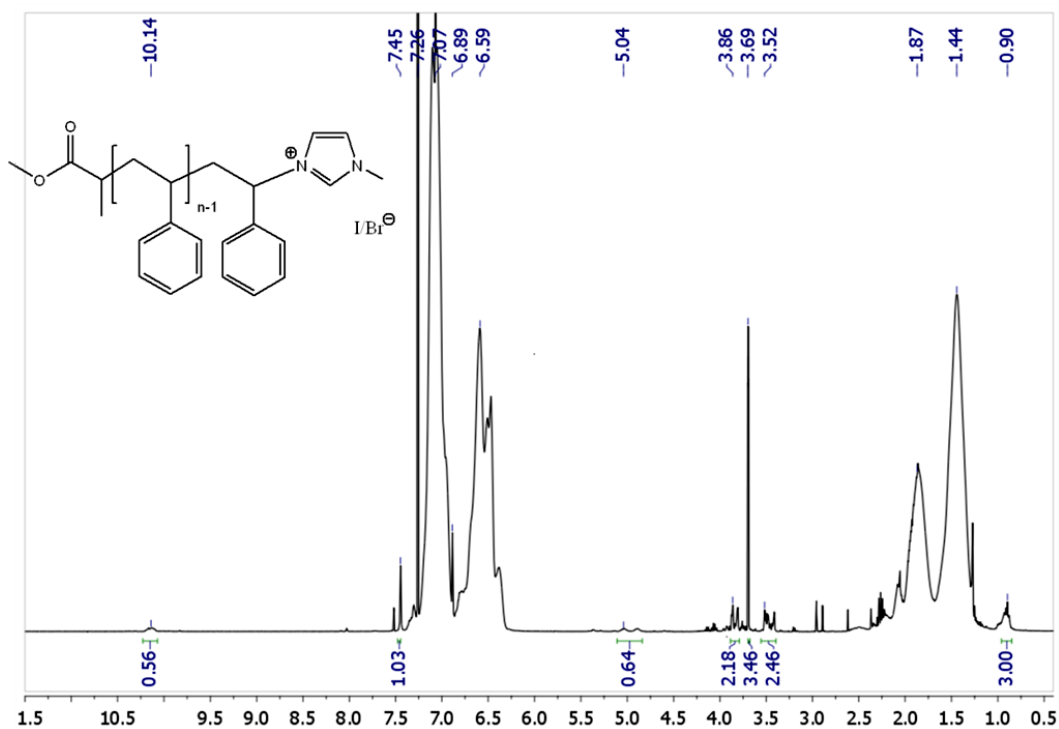
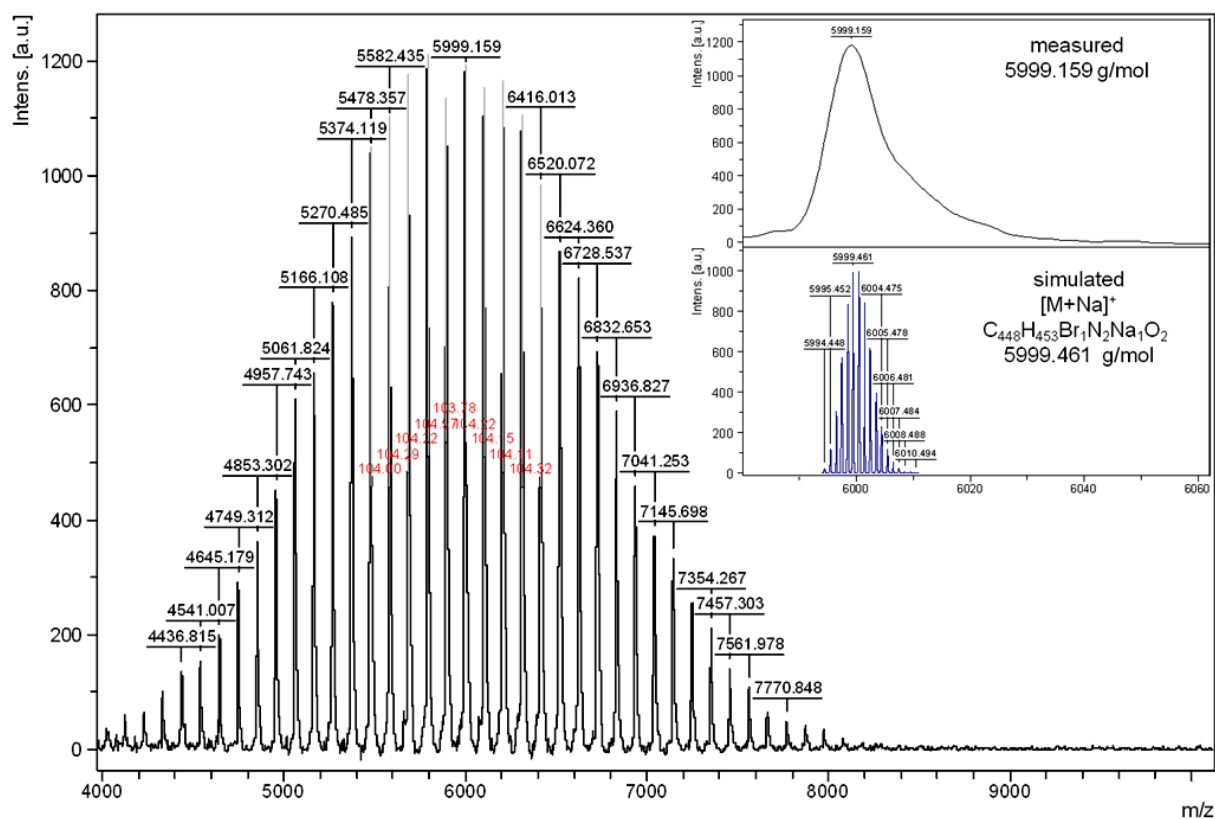


Figure A26. ¹H-NMR spectrum of *N*-methylimidazolium-telechelic PS (13a) in CDCl₃.



7.8 GPC and NMR-spectra of bis(*N*-methylimidazol-2-ylidene-telechelic poly(styrene) copper(I)X complex [Cu(PS-NHC)₂]X (14)

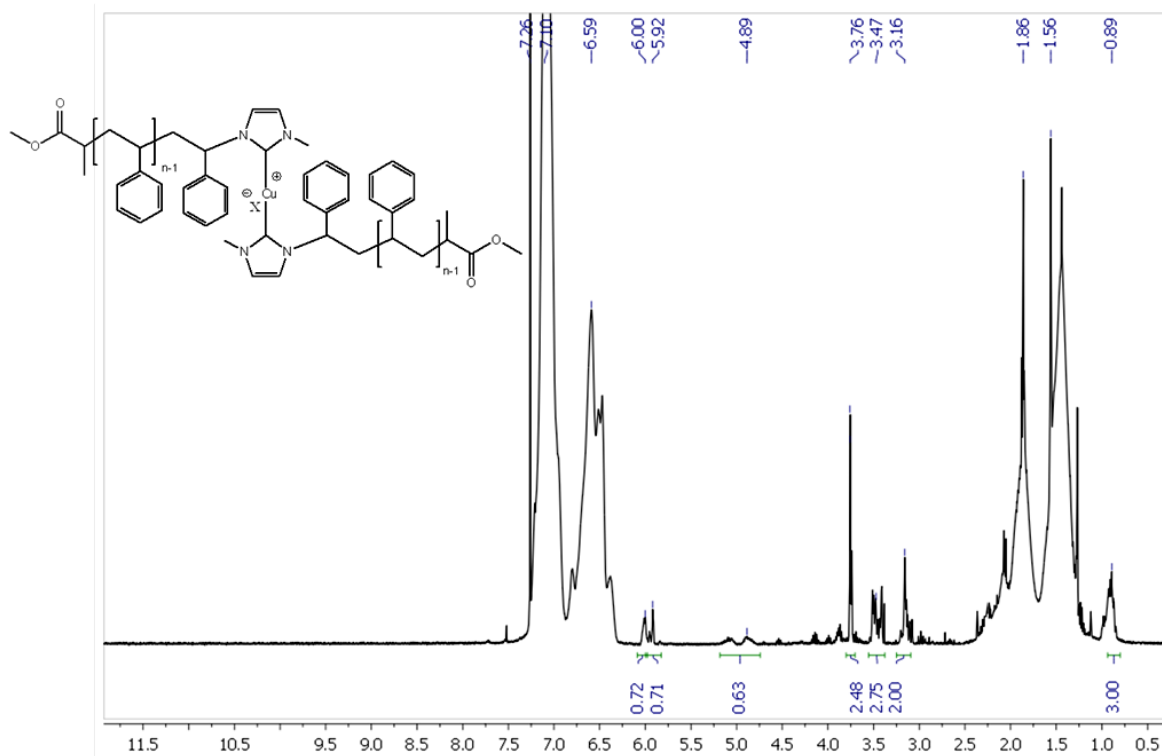


Figure A28. ¹H-NMR spectrum of bis(*N*-methylimidazol-2-ylidene-telechelic poly(styrene) copper(I)X complex [Cu(PS-NHC)₂]X (14a).

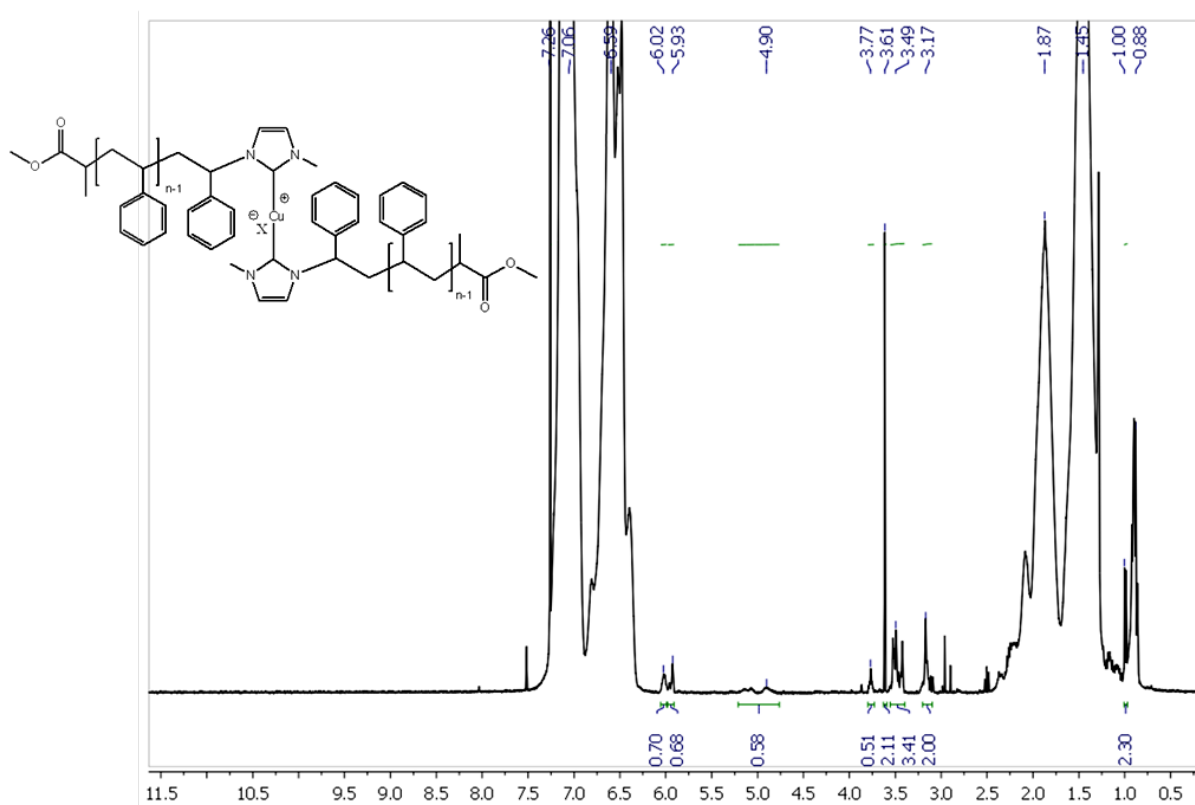


Figure A29. ¹H-NMR spectrum of bis(*N*-methylimidazol-2-ylidene-telechelic poly(styrene) copper(I)X complex [Cu(PS-NHC)₂]X (14c).

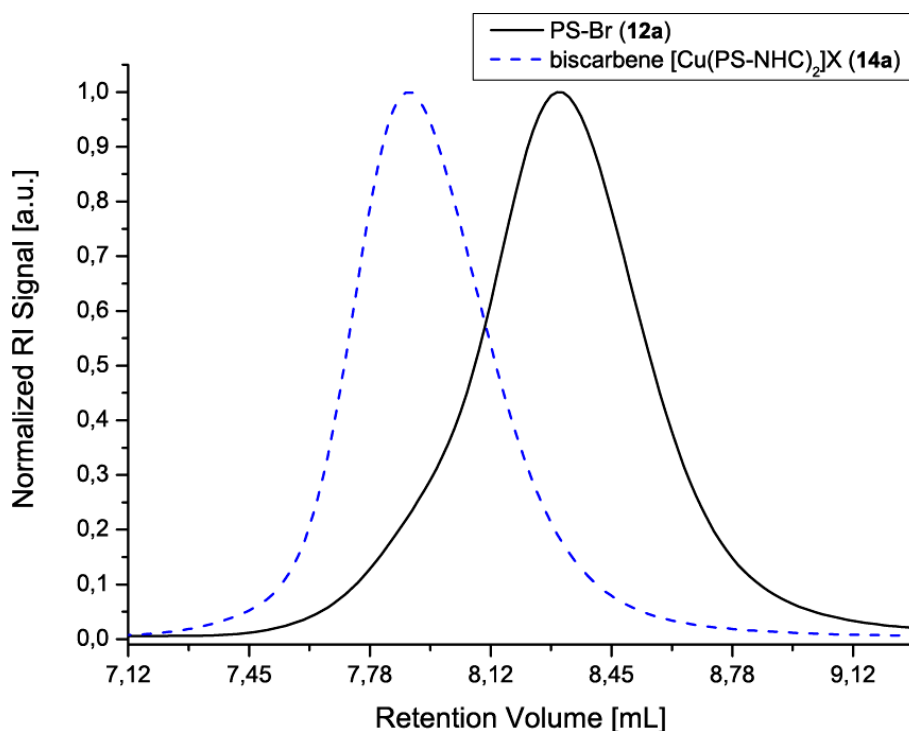


Figure A30. GPC traces of bromo-telechelic PS (**12a**; PS-Br; M_n (GPC) = 3400 g/mol) as well as corresponding biscarbene complexes (**14a**; $[\text{Cu}(\text{PS-NHC})_2]\text{X}$; M_n (GPC) = 6800 g/mol) indicating the doubling of molecular weight during the mechanocatalyst formation.

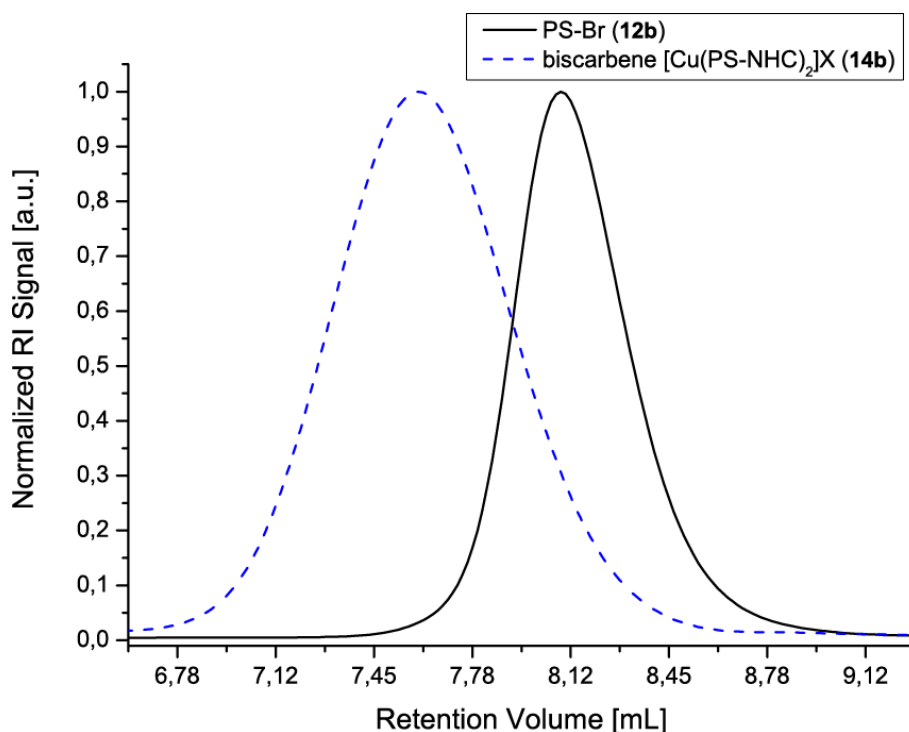


Figure A31. GPC traces of bromo-telechelic PS (**12b**; PS-Br; M_n (GPC) = 4700 g/mol) as well as corresponding biscarbene complexes (**14b**; $[\text{Cu}(\text{PS-NHC})_2]\text{X}$; M_n (GPC) = 11600 g/mol) indicating the doubling of molecular weight during the mechanocatalyst formation.

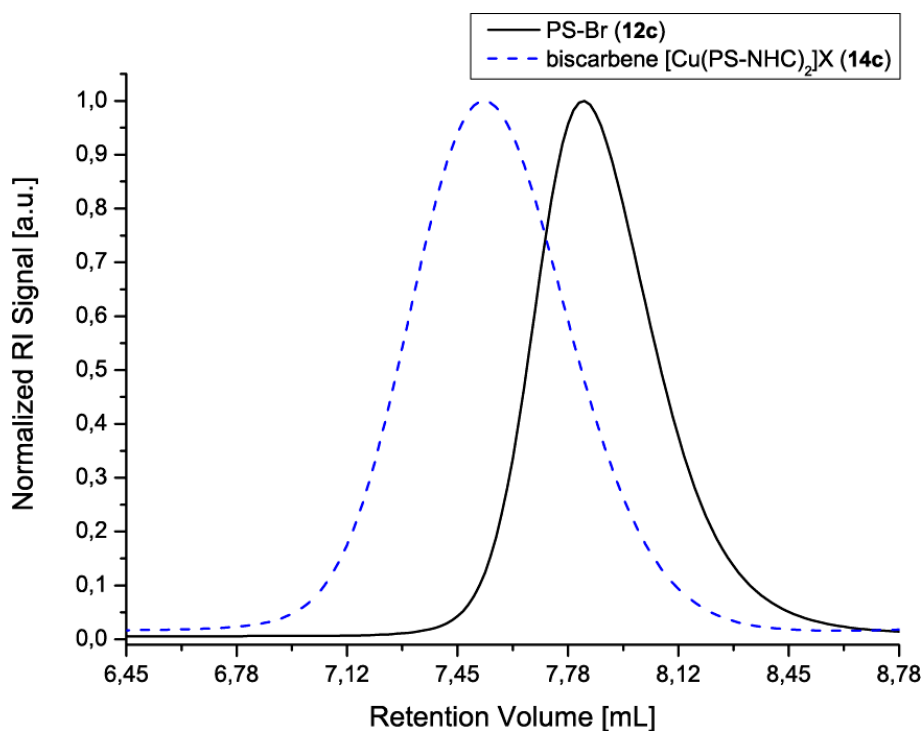


Figure A32. GPC traces of bromo-telechelic PS (**12c**; PS-Br; M_n (GPC) = 7100 g/mol) as well as corresponding biscarbene complexes (**14c**; $[\text{Cu}(\text{PS-NHC})_2]\text{X}$; M_n (GPC) = 13600 g/mol) indicating the doubling of molecular weight during the mechanocatalyst formation.

7.9 NMR-spectra and ESI-TOF-MS of 3-azido-7-hydroxycoumarin (**15**)

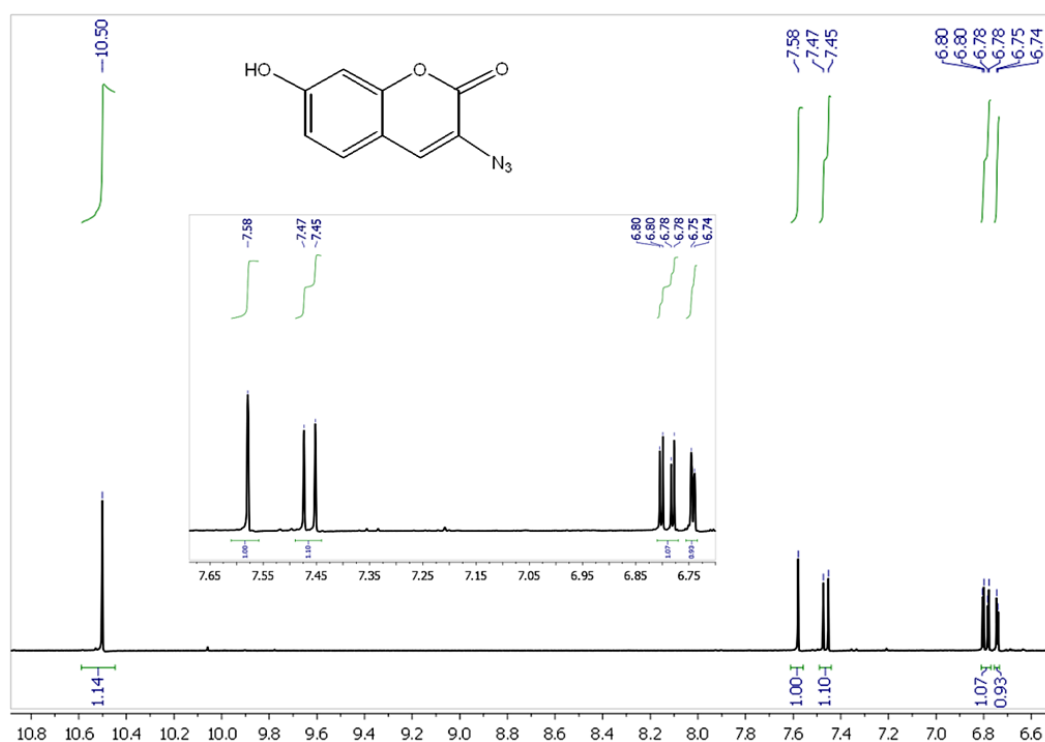


Figure A33. $^1\text{H-NMR}$ spectrum of 3-azido-7-hydroxycoumarin (**15**) in DMSO-d_6 .

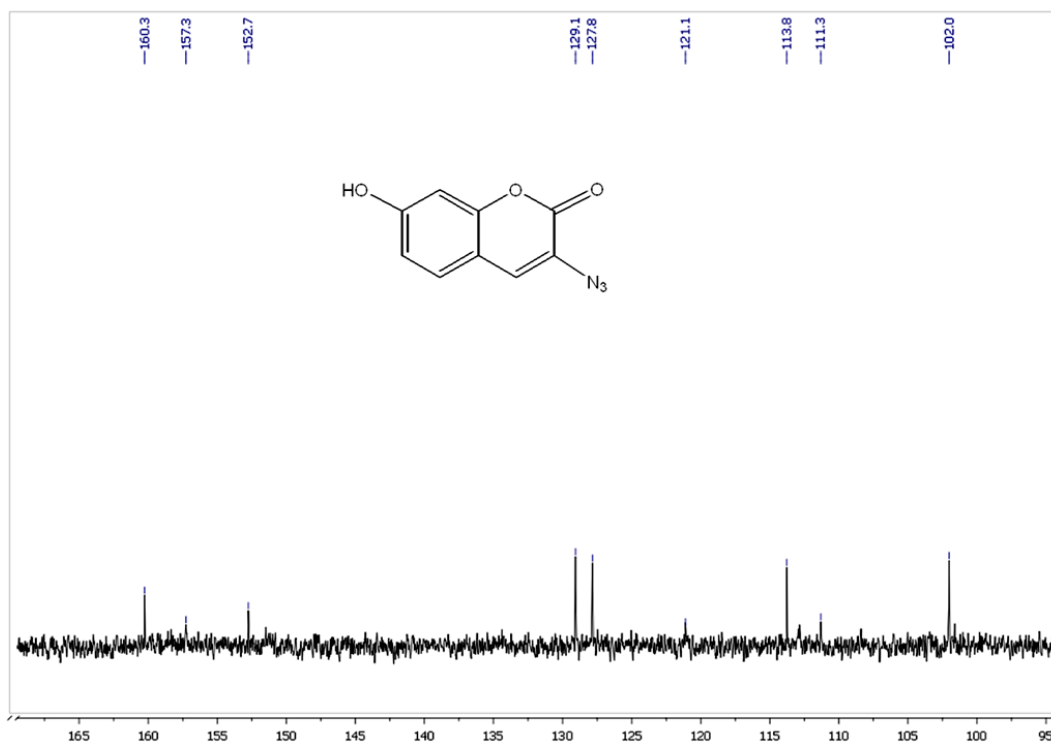


Figure A34. ¹³C-NMR spectrum of 3-azido-7-hydroxycoumarin (**15**) in DMSO-d₆.

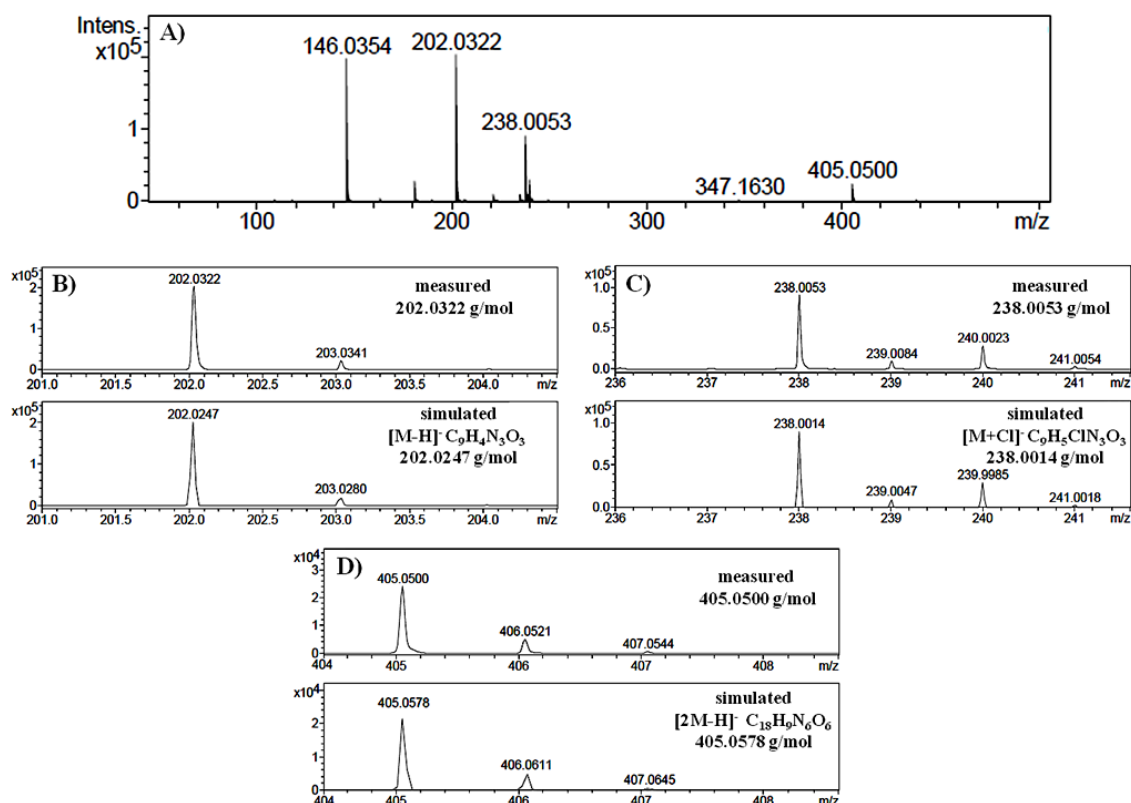


Figure A35. A) ESI-TOF-MS of 3-azido-7-hydroxycoumarin (**15**) with three identified species (B-D), B) [M-H]⁻ C₉H₄N₃O₃: simulated 202.0247 g/mol, found 202.0322 g/mol; C) [M+Cl]⁻ C₉H₅ClN₃O₃: simulated 238.0014 g/mol, found 238.0053 g/mol; D) [2M-H]⁻ C₁₈H₉N₆O₆: simulated 405.0578 g/mol, found 405.0500 g/mol.

7.10 NMR-spectra and ESI-TOF-MS 7-hydroxy-3-(4-phenyl-1*H*-[1,2,3]triazole-1-yl)-coumarin (17)

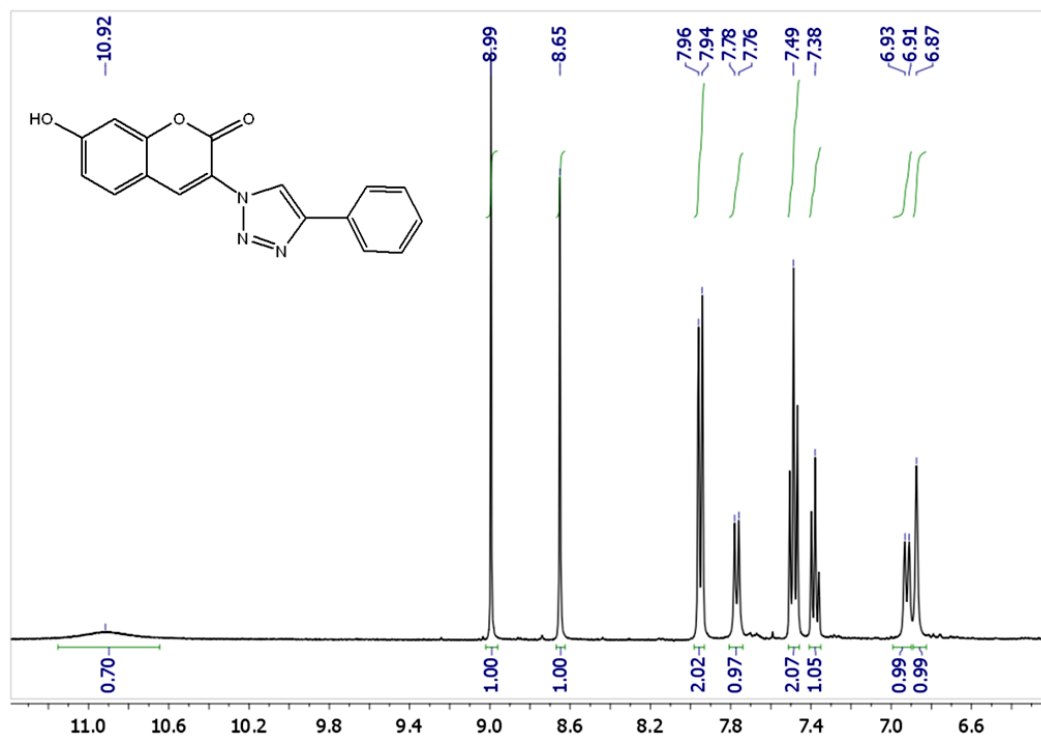


Figure A36. ¹H-NMR spectrum of 7-hydroxy-3-(4-phenyl-1*H*-[1,2,3]triazole-1-yl)-coumarin (17).

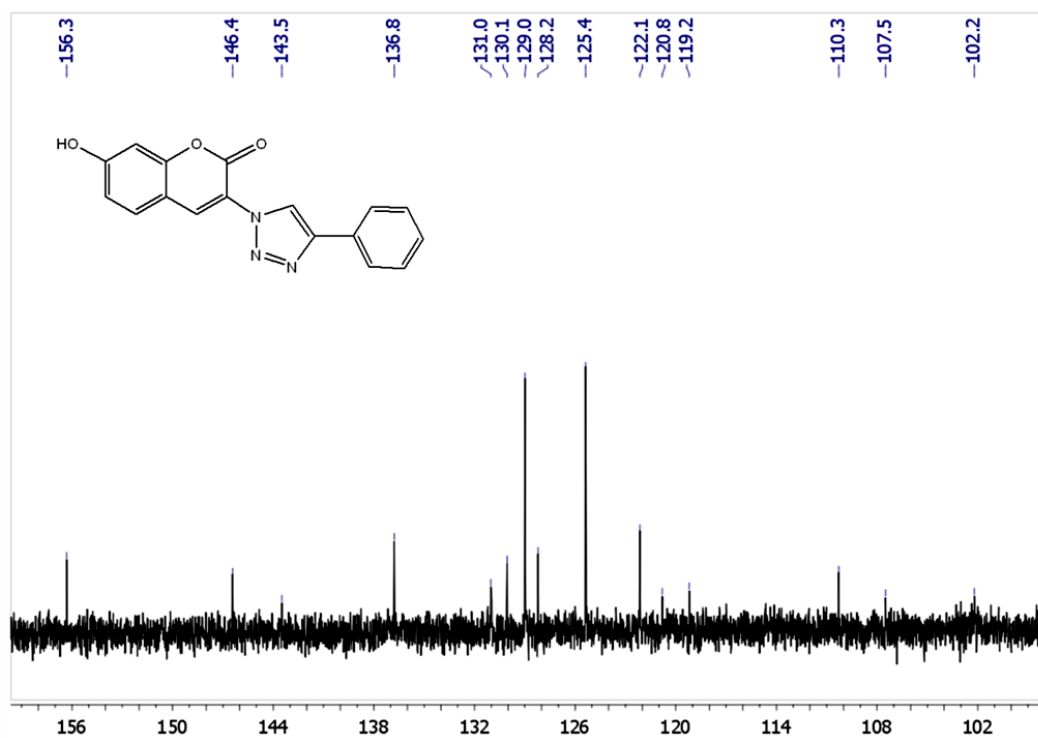


Figure A37. ¹³C-NMR spectrum of 7-hydroxy-3-(4-phenyl-1*H*-[1,2,3]triazole-1-yl)-coumarin (17).

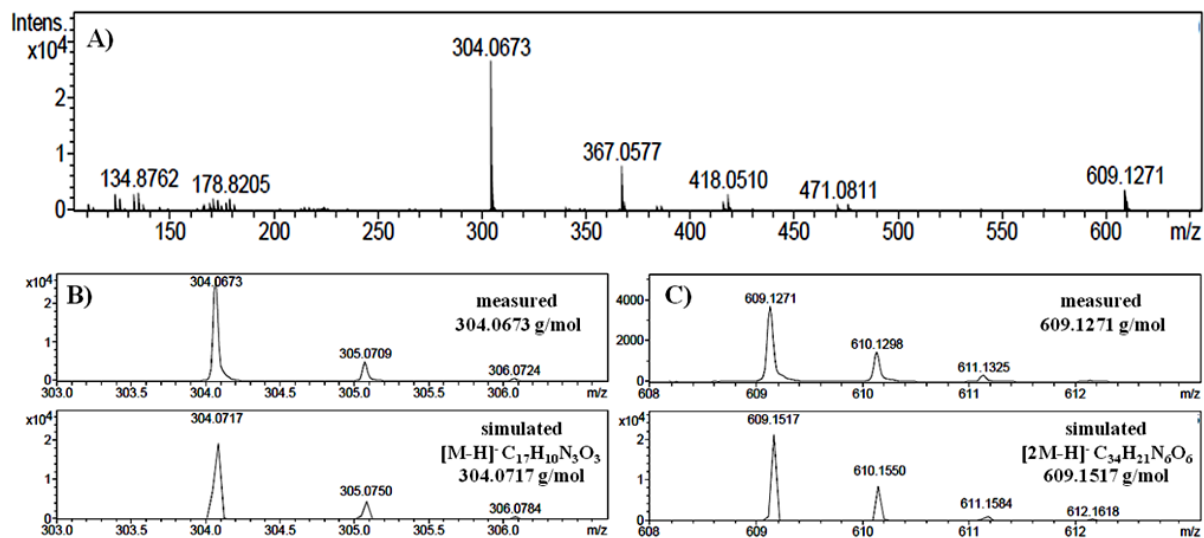


Figure A38. A) ESI-TOF-MS of 7-hydroxy-3-(4-phenyl-1H-[1,2,3]triazole-1-yl)-coumarin (**17**) with two identified species (B-C), B) [M-H]⁻ C₁₇H₁₀N₃O₃: simulated 304.0717 g/mol, found 304.0673 g/mol and C) [2M-H]⁻ C₃₄H₂₁N₆O₆: simulated 609.1517 g/mol, found 609.1271 g/mol.

7.11 Calibration of GPC traces

Table A1. GPC calibration of RI-signal intensity in dependency of the concentration of the appropriate bis- (I) and monovalent (II) species of the Cu(I) mechanophores (**6** and **14**).

Ent.				for PIB-based Cu(I) mechanophores (6)					
	V			6a		6b		6c	
	c [mg/mL]	Polymer [μL]	THF [μL]	c (I) [mol/L]	c (II) [mol/L]	c (I) [mol/L]	c (II) [mol/L]	c (I) [mol/L]	c (II) [mol/L]
1	10	1000	0	$2.11 \cdot 10^{-3}$	$4.00 \cdot 10^{-3}$	$1.12 \cdot 10^{-3}$	$2.13 \cdot 10^{-3}$	$5.81 \cdot 10^{-4}$	$1.16 \cdot 10^{-3}$
2	8	800	200	$1.68 \cdot 10^{-3}$	$3.20 \cdot 10^{-3}$	$8.99 \cdot 10^{-4}$	$1.70 \cdot 10^{-3}$	$4.65 \cdot 10^{-4}$	$9.30 \cdot 10^{-4}$
3	6	600	400	$1.26 \cdot 10^{-3}$	$2.40 \cdot 10^{-3}$	$6.74 \cdot 10^{-4}$	$1.28 \cdot 10^{-3}$	$3.49 \cdot 10^{-4}$	$6.98 \cdot 10^{-4}$
4	4	400	600	$8.42 \cdot 10^{-4}$	$1.60 \cdot 10^{-3}$	$4.49 \cdot 10^{-4}$	$8.51 \cdot 10^{-4}$	$2.33 \cdot 10^{-4}$	$4.65 \cdot 10^{-4}$
5	3	300	700	$6.32 \cdot 10^{-4}$	$1.20 \cdot 10^{-3}$	$3.37 \cdot 10^{-4}$	$6.38 \cdot 10^{-4}$	$1.74 \cdot 10^{-4}$	$3.49 \cdot 10^{-4}$
6	2	200	800	$4.21 \cdot 10^{-4}$	$8.00 \cdot 10^{-4}$	$2.25 \cdot 10^{-4}$	$4.26 \cdot 10^{-4}$	$1.16 \cdot 10^{-4}$	$2.33 \cdot 10^{-4}$
7	1	100	900	$2.11 \cdot 10^{-4}$	$4.00 \cdot 10^{-4}$	$1.12 \cdot 10^{-4}$	$2.13 \cdot 10^{-4}$	$5.81 \cdot 10^{-5}$	$1.16 \cdot 10^{-4}$
8	0	0	1000	0	0	0	0	0	0
Ent.				for PS-based Cu(I) mechanophores (14)					
	V			14a		14b		14c	
	c [mg/mL]	Polymer [μL]	THF [μL]	c (I) [mol/L]	c (II) [mol/L]	c (I) [mol/L]	c (II) [mol/L]	c (I) [mol/L]	c (II) [mol/L]
1	10	1000	0	$1.47 \cdot 10^{-3}$	$3.23 \cdot 10^{-3}$	$8.62 \cdot 10^{-4}$	$2.00 \cdot 10^{-3}$	$7.35 \cdot 10^{-4}$	$1.27 \cdot 10^{-3}$
2	8	800	200	$1.18 \cdot 10^{-3}$	$2.58 \cdot 10^{-3}$	$6.89 \cdot 10^{-4}$	$1.60 \cdot 10^{-3}$	$5.88 \cdot 10^{-4}$	$1.01 \cdot 10^{-3}$
3	6	600	400	$8.82 \cdot 10^{-4}$	$1.94 \cdot 10^{-3}$	$5.17 \cdot 10^{-4}$	$1.20 \cdot 10^{-3}$	$4.41 \cdot 10^{-4}$	$7.59 \cdot 10^{-4}$
4	4	400	600	$5.88 \cdot 10^{-4}$	$1.29 \cdot 10^{-3}$	$3.45 \cdot 10^{-4}$	$8.00 \cdot 10^{-4}$	$2.94 \cdot 10^{-4}$	$5.06 \cdot 10^{-4}$
5	3	300	700	$4.41 \cdot 10^{-4}$	$9.68 \cdot 10^{-4}$	$2.59 \cdot 10^{-4}$	$6.00 \cdot 10^{-4}$	$2.21 \cdot 10^{-4}$	$3.79 \cdot 10^{-4}$
6	2	200	800	$2.94 \cdot 10^{-4}$	$6.45 \cdot 10^{-4}$	$1.72 \cdot 10^{-4}$	$4.00 \cdot 10^{-4}$	$1.47 \cdot 10^{-4}$	$2.53 \cdot 10^{-4}$
7	1	100	900	$1.47 \cdot 10^{-4}$	$3.23 \cdot 10^{-4}$	$8.62 \cdot 10^{-5}$	$2.00 \cdot 10^{-4}$	$7.35 \cdot 10^{-5}$	$1.27 \cdot 10^{-4}$
8	0	0	1000	0	0	0	0	0	0

Derivation of eq1 and eq2

1st scenario for PIB-based mechanophores:

Ultrasound induced scission of biscarbene mechanocatalyst **6** lead to the formation of two polymeric species with the half molecular weight, whereat the concentration/RI-response calibrations of the GPC revealed solely the half RI-response for the lower molecular weight scission product (protonated/deprotonated **5** and **7**) at the same concentrations as the ratio of the slopes of I/II is 2. Thus only one of the two cleaved molecules can be detected, leading to a “virtually” cleavage of one mechanophore into one scission product. Accordingly the following derivation can be accomplished:

$$n \cdot M_n(\mathbf{6}) + m \cdot M_n(\mathbf{7}) = (n+m) \cdot M_n(\text{determined}) \quad \text{Aeq1}$$

If activation takes place and the **6** is cleaved and n is reduced by X (amount of cleaved mechanophores), while m increased by 1X (as only one scission product can be seen).

$$n = 1-X$$

$$m = X$$

Together with **Aeq1** it holds:

$$(1-X) \cdot M_n(6) + X \cdot M_n(7) = (1-X+X) \cdot M_n(determined) \quad \mathbf{Aeq2}$$

Combination and reordering resulted in **eq1**.

$$X = \frac{M_n(determined) - M_n(6)}{M_n(7) - M_n(6)} \quad \mathbf{eq1}$$

2nd scenario for PS-based mechanophores:

Ultrasound induced scission of **14** lead to the formation of two polymeric species, which lead according to the concentration/RI-response calibrations of the GPC to a doubling of the obtained RI-response at the same concentrations as the ratio of the slopes of I/II is 1. Thus, in this case also “virtually” both scission products can be detected by GPC enabling the following derivation of **eq2**:

$$n \cdot M_n(14) + m \cdot M_n(15) = (n+m) \cdot M_n(determined) \quad \mathbf{Aeq3}$$

If activation takes place and the **14** is cleaved and n is reduced by X (amount of cleaved mechanophores), while m increased by 2X (as both products can be seen).

$$n = 1-X$$

$$m = 2X$$

Together with **Aeq3** it holds:

$$(1-X) \cdot M_n(14) + 2X \cdot M_n(15) = (1-X+2X) \cdot M_n(determined) \quad \mathbf{Aeq4}$$

Combination and reordering resulted in **eq2**.

$$X = \frac{M_n(determined) - M_n(14)}{M_n(determined)} \quad \mathbf{eq2}$$

GPC RI-signal intensity calibrations in dependency of the mechanophore concentration

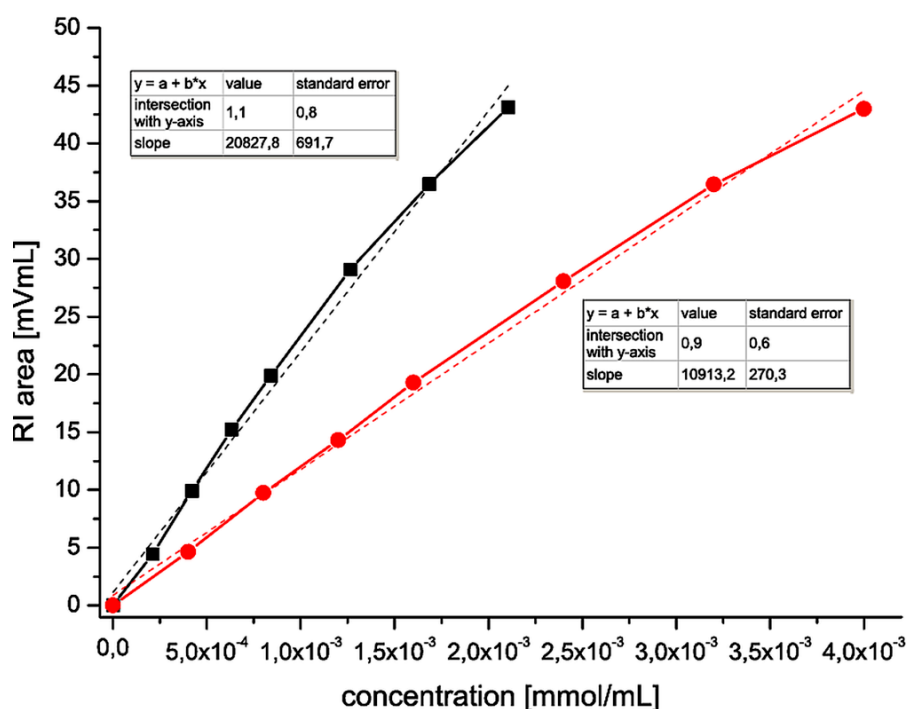


Figure A39. Concentration dependent RI-signal intensity in GPC measurements of bis(*N*-methylimidazol-2-ylidene-telechelic poly(isobutylene) copper(I)X complex [Cu(PIB-NHC)₂]X (**6a**) and linear regression to determine the slopes (black squares (■) corresponding bivalent species I; red circles (●) monovalent moieties II.

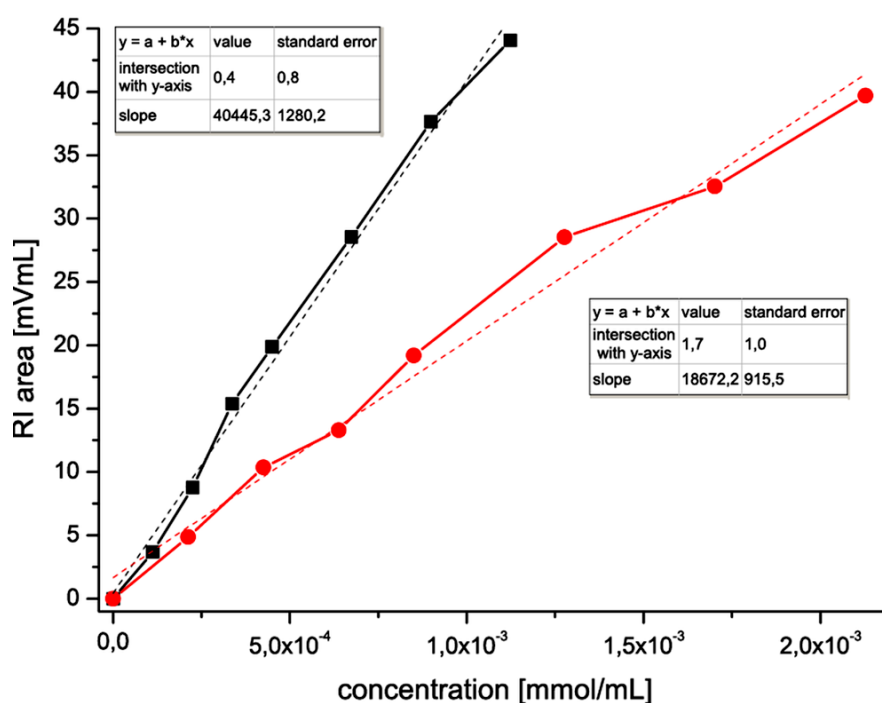


Figure A40. Concentration dependent RI-signal intensity in GPC measurements of bis(*N*-methylimidazol-2-ylidene-telechelic poly(isobutylene) copper(I)X complex [Cu(PIB-NHC)₂]X (**6b**) and linear regression to determine the slopes (black squares (■) corresponding bivalent species I; red circles (●) monovalent moiety II.

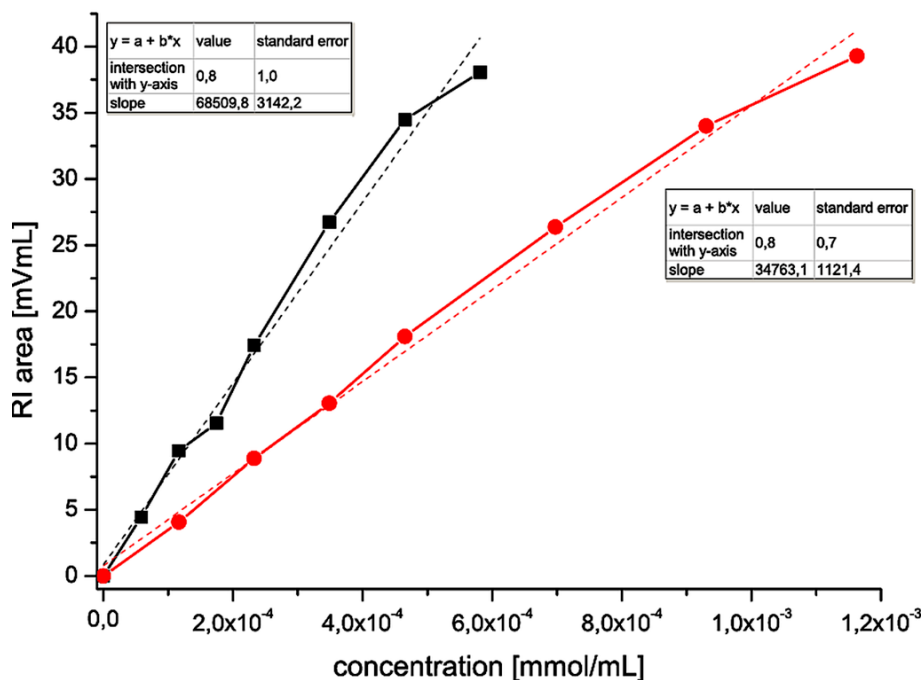


Figure A41. Concentration dependent RI-signal intensity in GPC measurements of bis(*N*-methylimidazol-2-ylidene-telechelic poly(isobutylene) copper(I)X complex [Cu(PIB-NHC)₂]X (**6c**) and linear regression to determine the slopes (black squares (■) corresponding bivalent species I; red circles (●) monovalent moiety II.

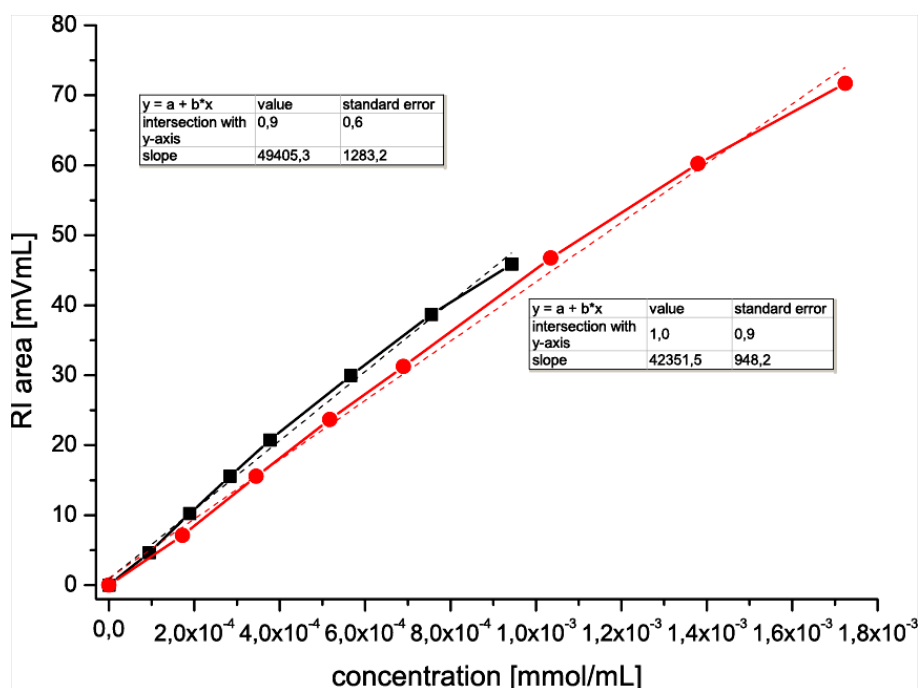


Figure A42. Concentration dependent RI-signal intensity in GPC measurements of bis(*N*-methylimidazol-2-ylidene-telechelic poly(styrene) copper(I)X complex [Cu(PS-NHC)₂]X (**14b**) and linear regression to determine the slopes (black squares (■) corresponding bivalent species I; red circles (●) monovalent moiety II.

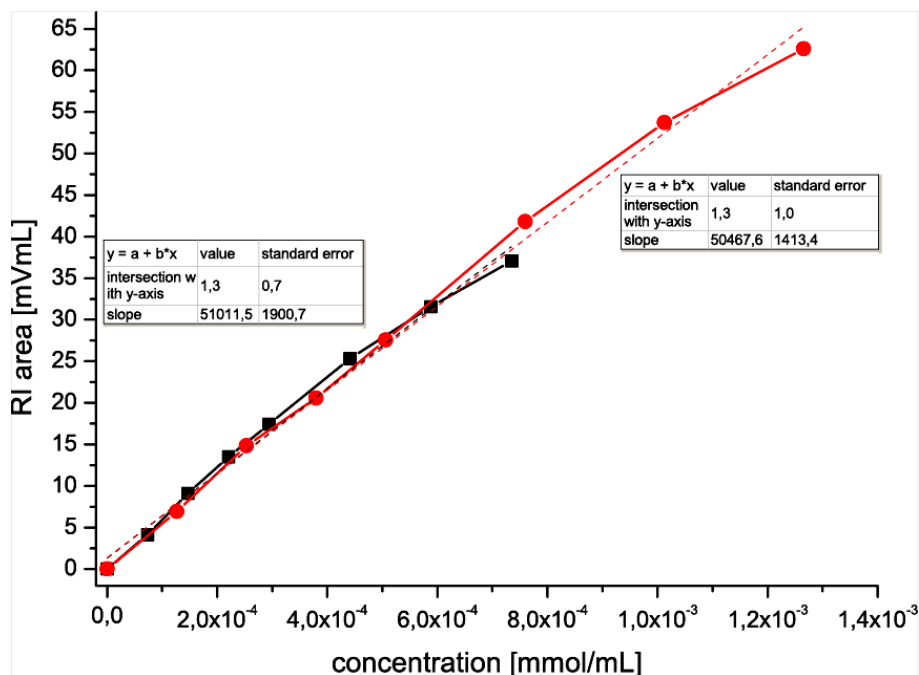


Figure A43. Concentration dependent RI-signal intensity in GPC measurements of bis(*N*-methylimidazol-2-ylidene-telechelic poly(styrene) copper(I)X complex [Cu(PS-NHC)₂]X (**14c**) and linear regression to determine the slopes (black squares (■) corresponding bivalent species I; red circles (●) monovalent moiety II.

7.12 GPC traces of ultrasound-induced cleavage of mechanocatalyst in solution

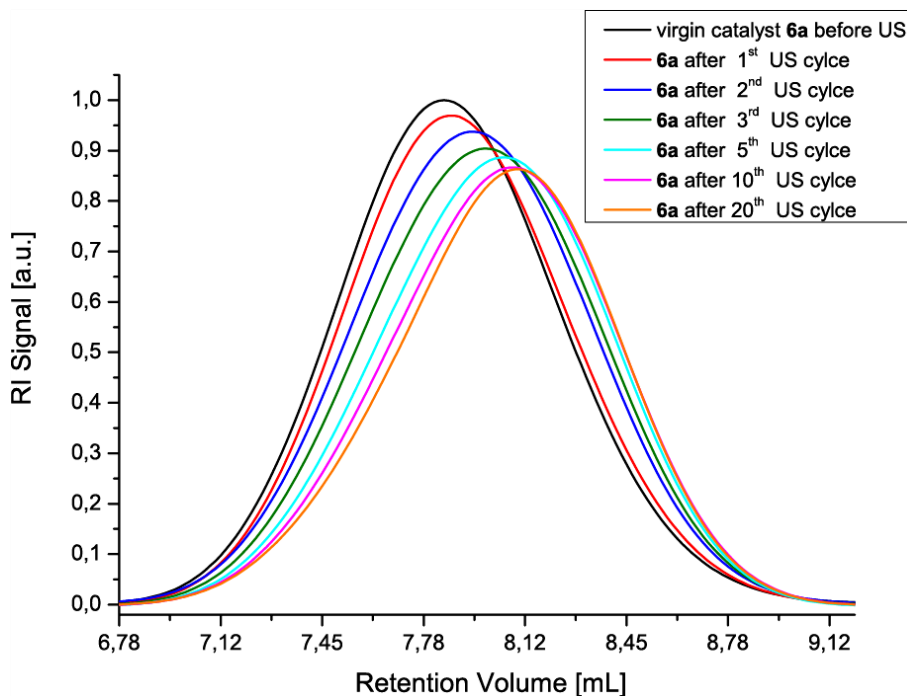


Figure A44. GPC traces of mechanocatalyst **6a** before ultrasonication and decreasing molecular weight indicated by increased retention volume after multiple sonication cycles at 20°C in THF/MeOH 30:1.

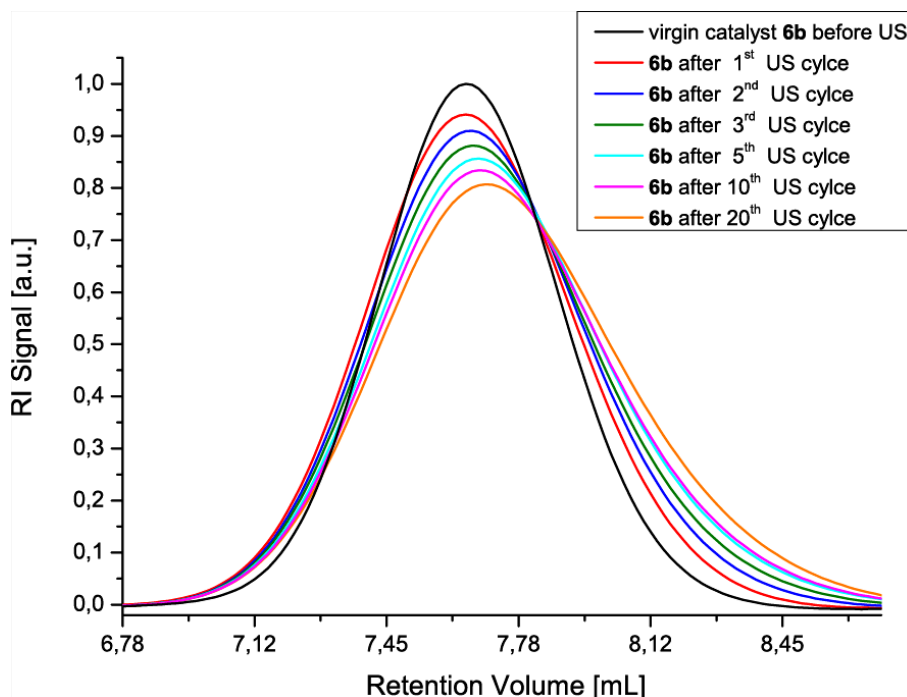


Figure A45. GPC traces of mechanocatalyst **6b** before ultrasonication and decreasing molecular weight indicated by increased retention volume after multiple sonication cycles at 20°C in THF/MeOH 30:1.

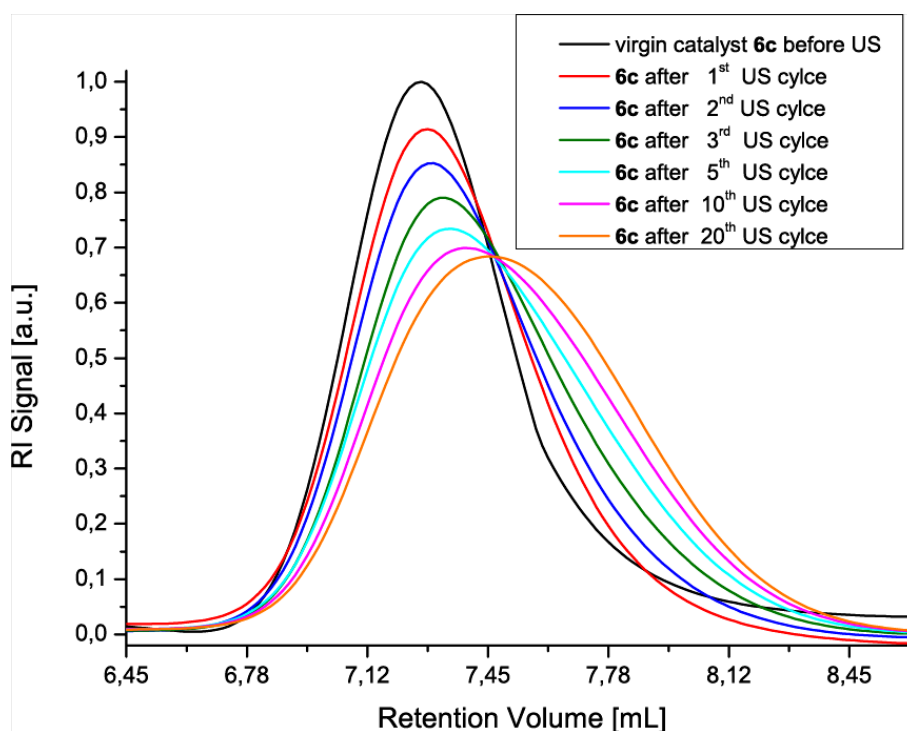


Figure A46. GPC traces of mechanocatalyst **6c** before ultrasonication and decreasing molecular weight indicated by increased retention volume after multiple sonication cycles at 20°C in THF/MeOH 30:1.

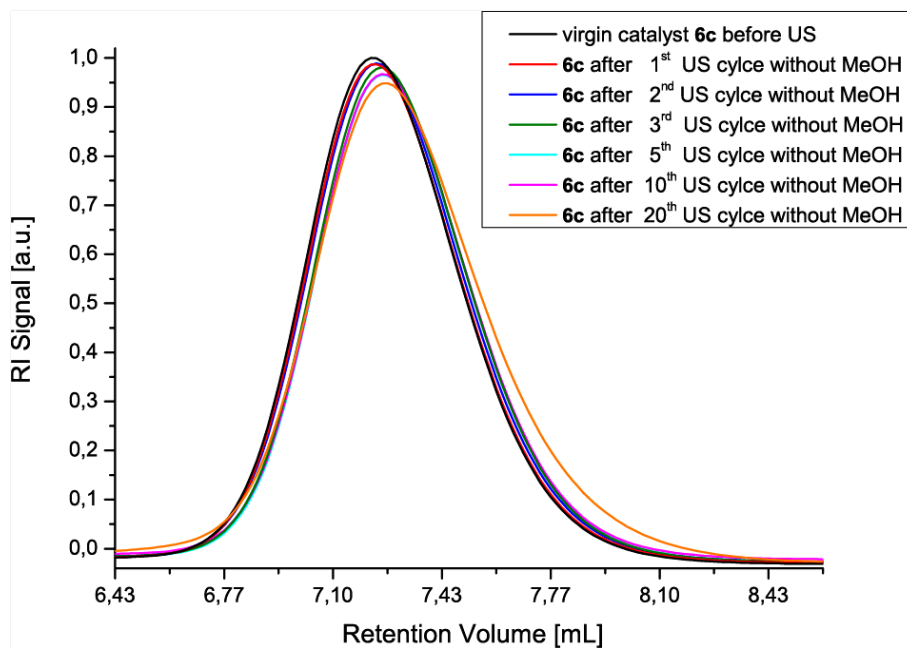


Figure A47. GPC traces of mechanocatalyst **6c** before ultrasonication and decreasing molecular weight indicated by increased retention volume after multiple sonication cycles at 20°C in pure THF without adding MeOH.

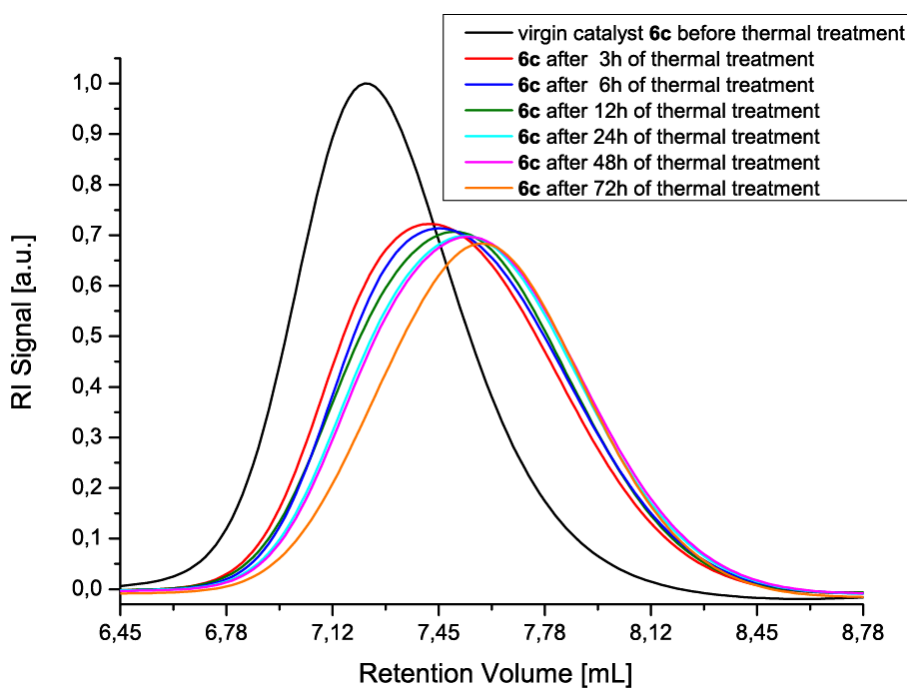


Figure A48. GPC traces of mechanocatalyst **6c** without ultrasonication under thermal treatment at 65°C in THF/MeOH 30:1.

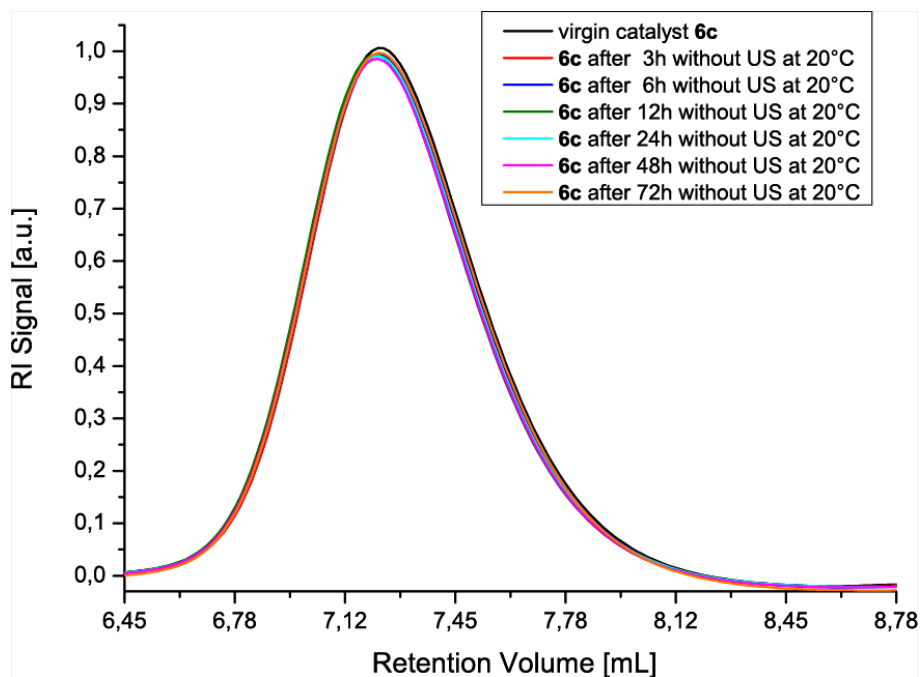


Figure A49. GPC traces of control experiment for mechanocatalyst **6c** without ultrasonication at 20°C in THF/MeOH 30:1.

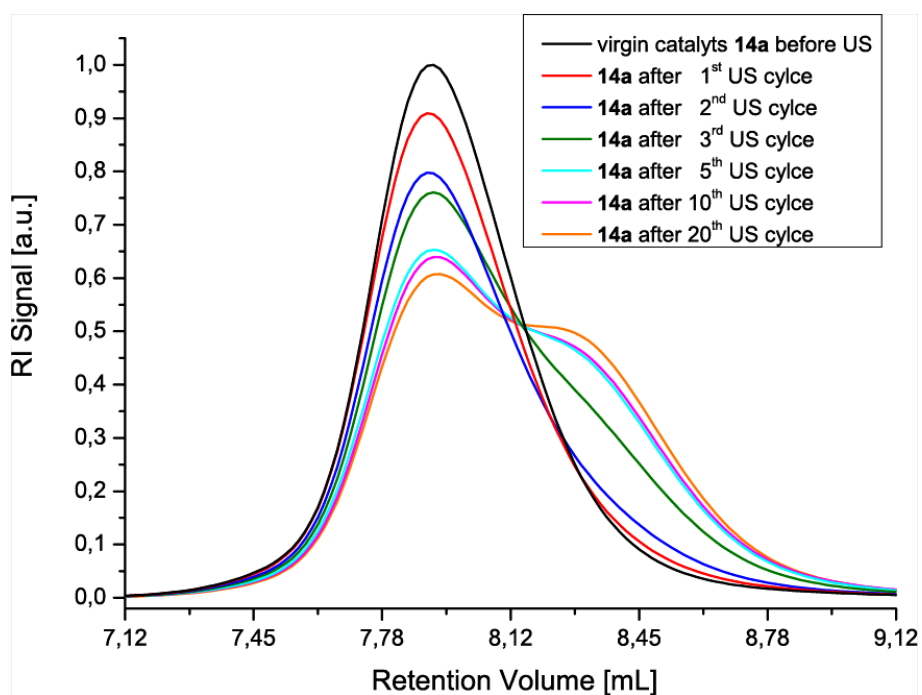


Figure A50. GPC traces of mechanocatalyst **14a** before ultrasonication and decreasing molecular weight indicated by increased retention volume after multiple sonication cycles at 20°C in THF/MeOH 30:1.

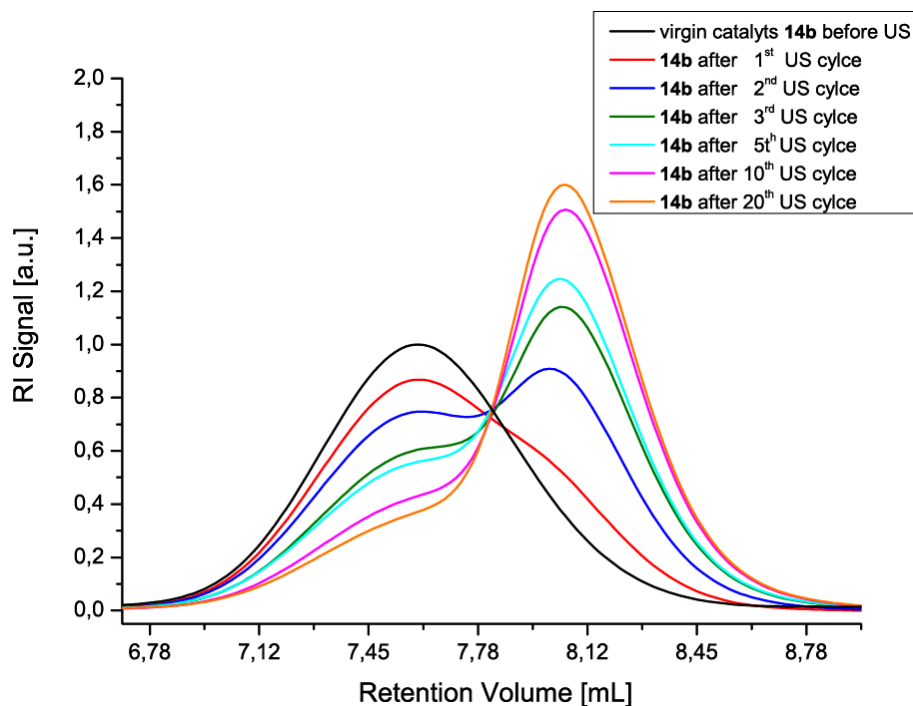


Figure A51. GPC traces of mechanocatalyst **14b** before ultrasonication and decreasing molecular weight indicated by increased retention volume after multiple sonication cycles at 20°C in THF/MeOH 30:1.

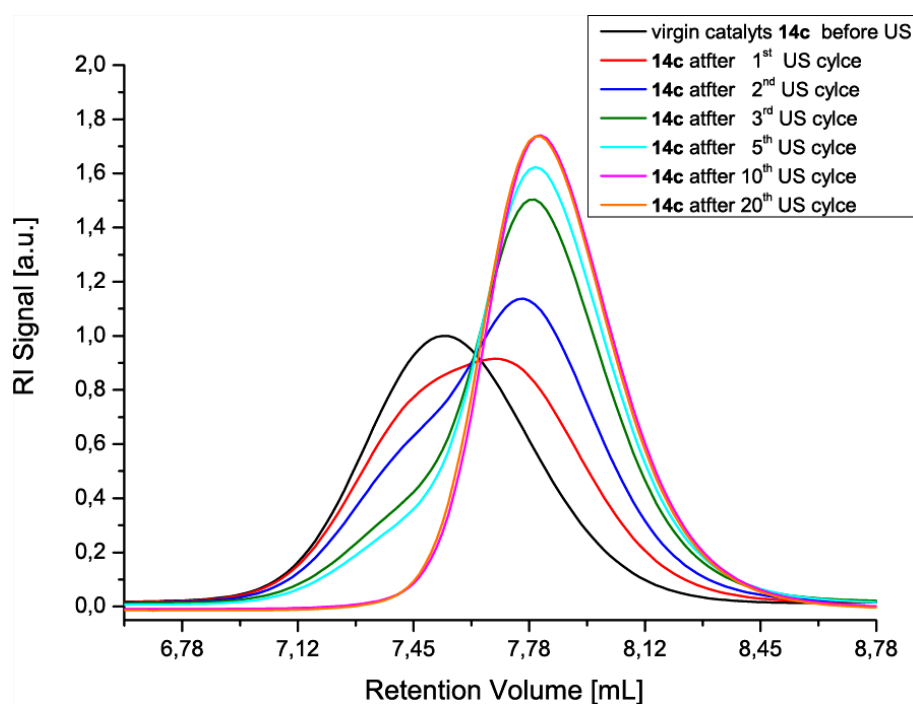


Figure A52. GPC traces of mechanocatalyst **14c** before ultrasonication and decreasing molecular weight indicated by increased retention volume after multiple sonication cycles at 20°C in THF/MeOH 30:1.

7.13 $^1\text{H-NMR}$ spectra of CuAAC “click” kinetic of **17** and **19** using mechanocatalysts

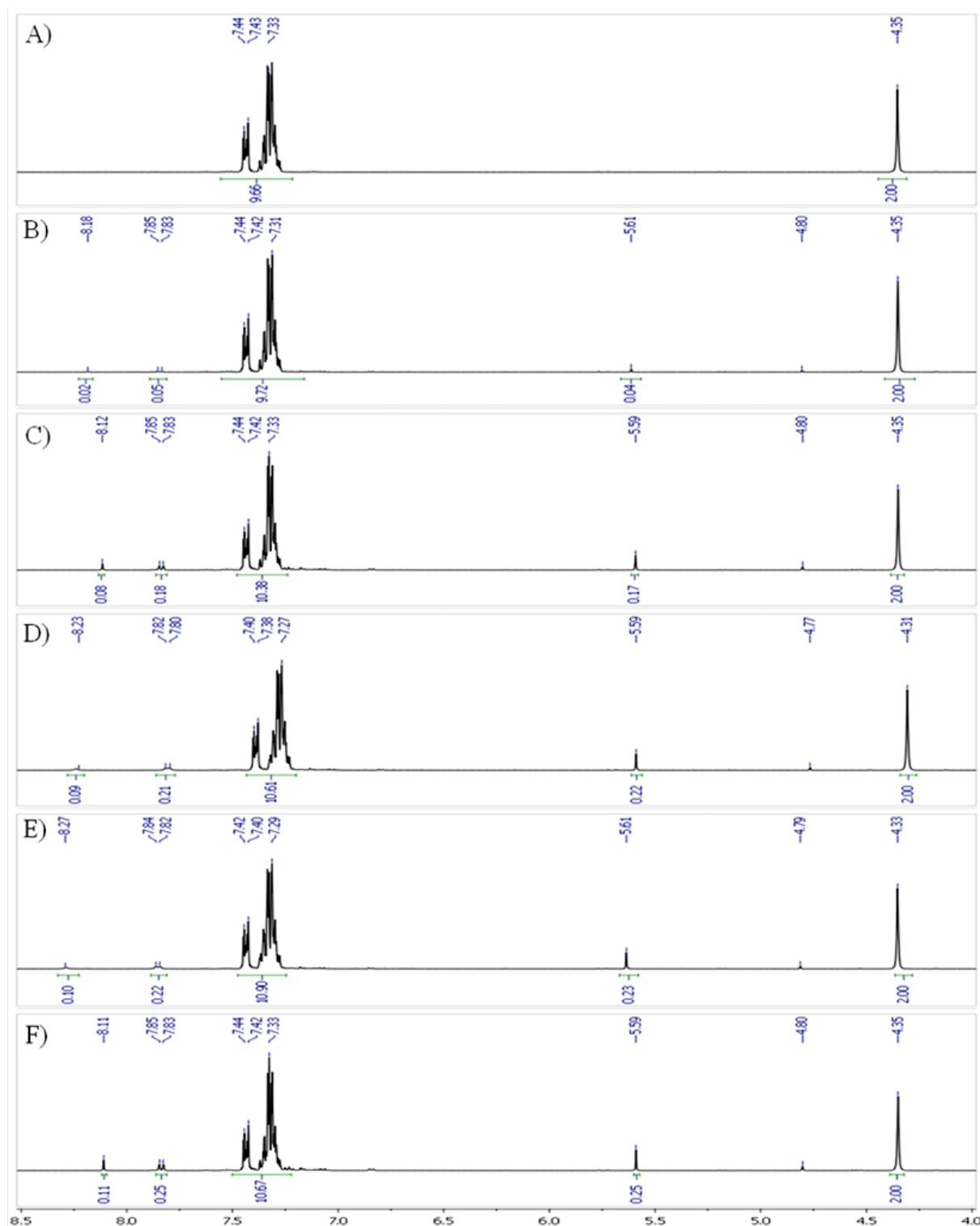


Figure A53. $^1\text{H-NMR}$ spectra of CuAAC kinetic from **17** and **19** subjected to several ultrasonication cycles at room temperature in THF- d_8 /MeOH (30:1): (A) before 1st sonication cycle (0% “click” conversion^a), (B) after 1st sonication cycle (150 min) (2% conversion^a), (C) after 2nd sonication cycle (300 min) (8% conversion^a), (D) after 3rd sonication cycle (450 min) (10% conversion^a), (E) after 5th sonication cycle (750 min) (10% conversion^a) and (F) after 10th sonication cycle (1500 min) (11% conversion^a).

^adetermined through the increasing triazole resonance at 8.12 ppm as well as the shift of the CH_2 resonance from 4.34 to 5.58 ppm

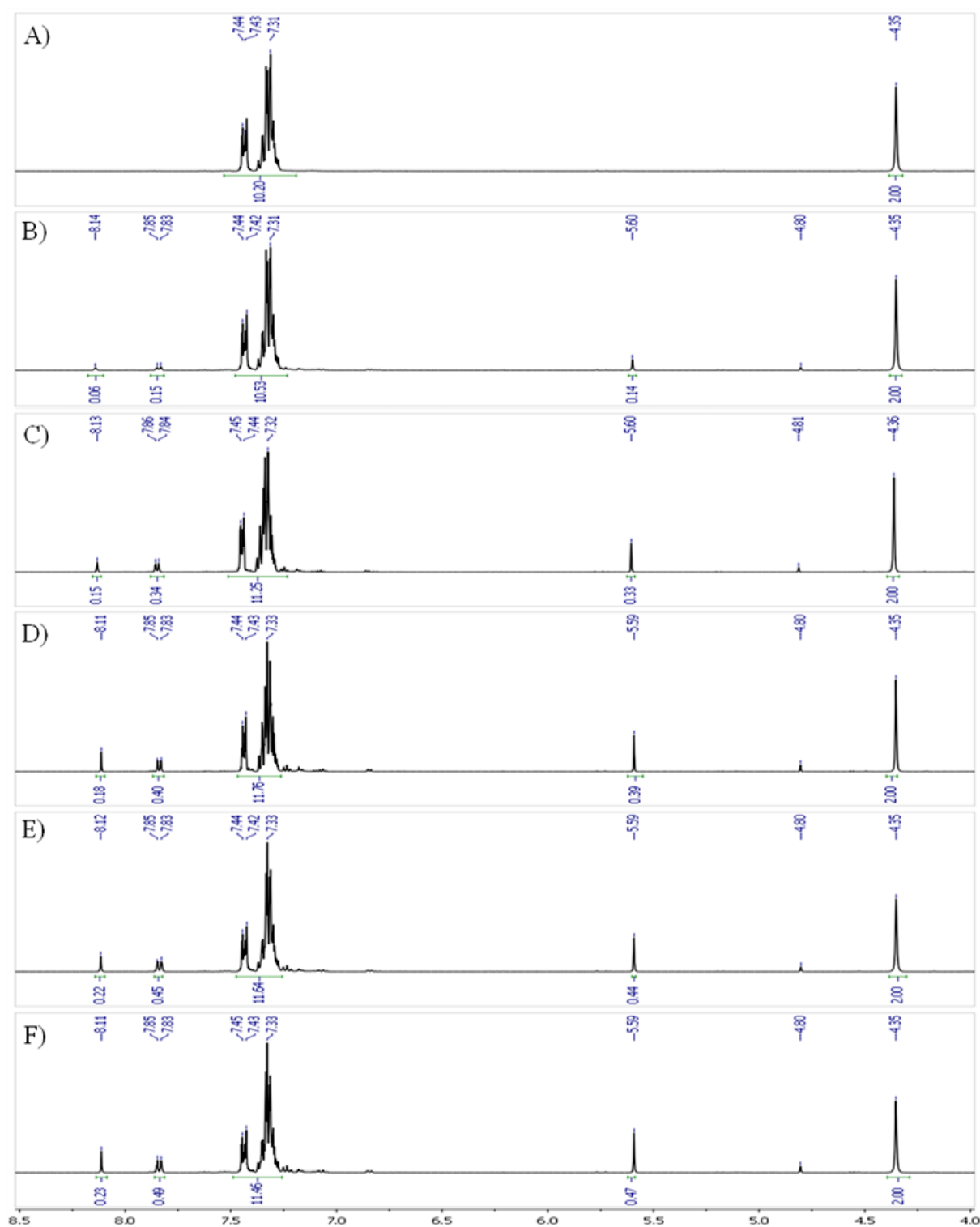


Figure A54. $^1\text{H-NMR}$ spectra of CuAAC kinetic from **17** and **19** subjecting PIB-based mechanocatalyst **6b** to several ultrasonication cycles at room temperature in THF- d_8 /MeOH (30:1): (A) before 1st sonication cycle 0% “click” conversion^{a)}, (B) after 1st sonication cycle (150 min) 6% conversion^{a)}, (C) after 2nd sonication cycle (300 min) 14% conversion^{a)}, (D) after 3rd sonication cycle (450 min) 16% conversion^{a)}, (E) after 5th sonication cycle (750 min) 18% conversion^{a)} and (F) after 10th sonication cycle (1500 min) 19% conversion^{a)}.

^{a)}determined through the increasing triazole resonance at 8.12 ppm as well as the shift of the CH_2 resonance from 4.34 to 5.58 ppm

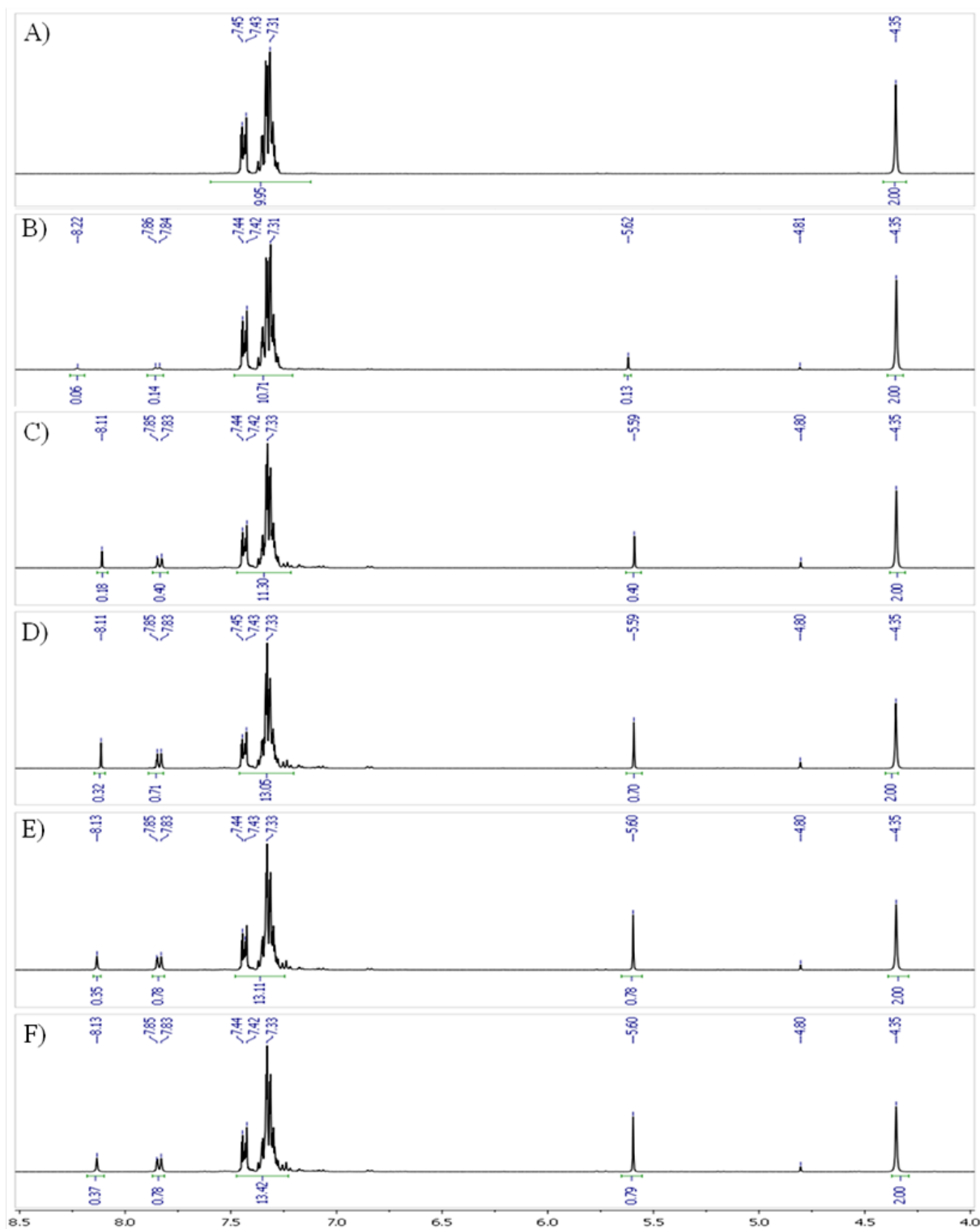


Figure A55. ¹H-NMR spectra of CuAAC kinetic from **17** and **19** subjecting PIB-based mechanocatalyst **6c** to several ultrasonication cycles at room temperature in THF-d₈/MeOH (30:1): (A) before 1st sonication cycle 0% “click” conversion^{a)}, (B) after 1st sonication cycle (150 min) 6% conversion^{a)}, (C) after 2nd sonication cycle (300 min) 17% conversion^{a)}, (D) after 3rd sonication cycle (450 min) 26% conversion^{a)}, (E) after 5th sonication cycle (750 min) 28% conversion^{a)} and (F) after 10th sonication cycle (1500 min) 28% conversion^{a)}.

^{a)}determined through the increasing triazole resonance at 8.12 ppm as well as the shift of the CH₂ resonance from 4.34 to 5.58 ppm

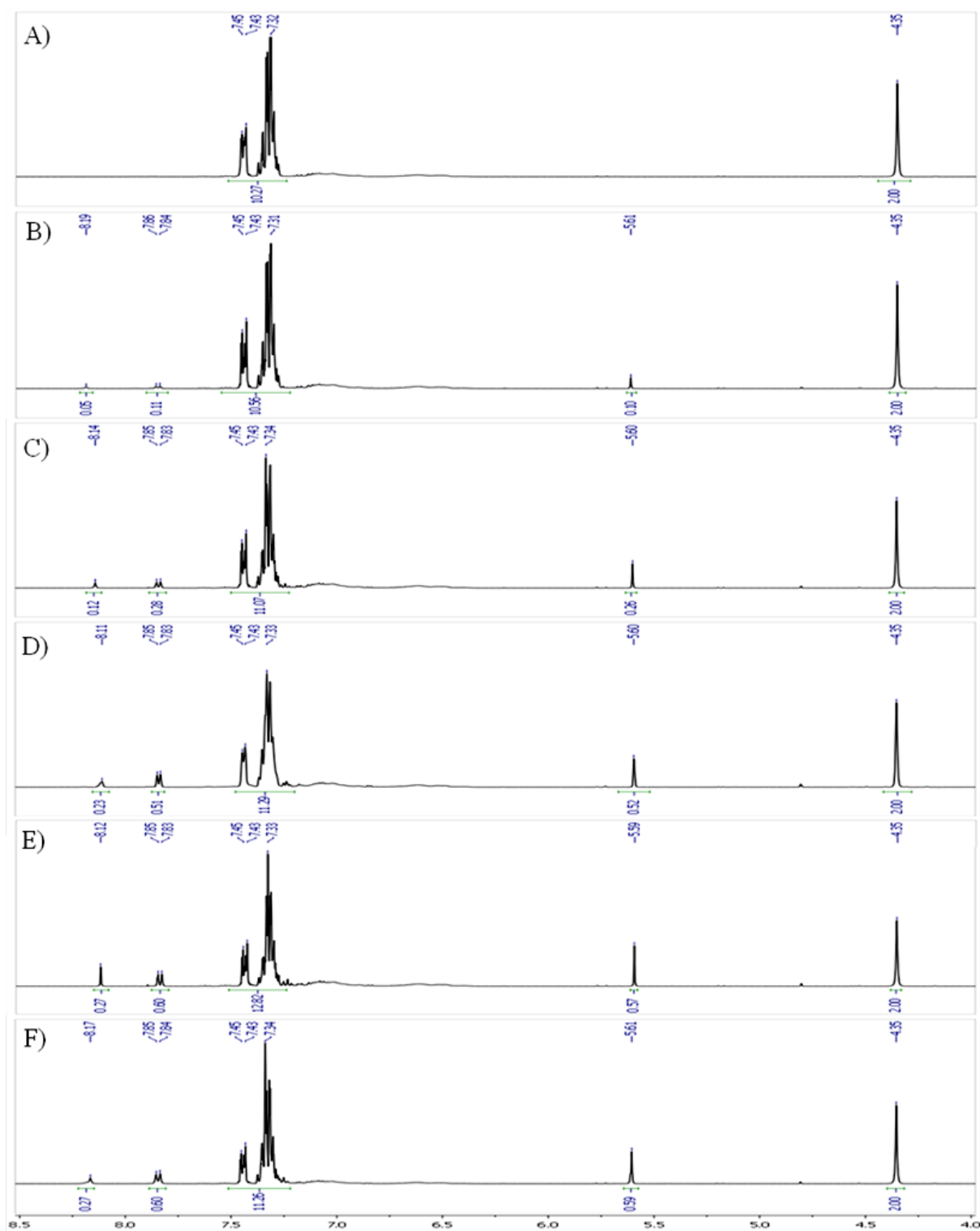


Figure A56. $^1\text{H-NMR}$ spectra of CuAAC kinetic from **17** and **19** subjecting PS-based mechanocatalyst **14a** to several ultrasonication cycles at room temperature in THF- d_8 /MeOH (30:1): (A) before 1st sonication cycle 0% “click” conversion^{a)}, (B) after 1st sonication cycle (150 min) 5% conversion^{a)}, (C) after 2nd sonication cycle (300 min) 12% conversion^{a)}, (D) after 3rd sonication cycle (450 min) 21% conversion^{a)}, (E) after 5th sonication cycle (750 min) 22% conversion^{a)} and (F) after 10th sonication cycle (1500 min) 23% conversion^{a)}.

^{a)}determined through the increasing triazole resonance at 8.12 ppm as well as the shift of the CH_2 resonance from 4.34 to 5.58 ppm

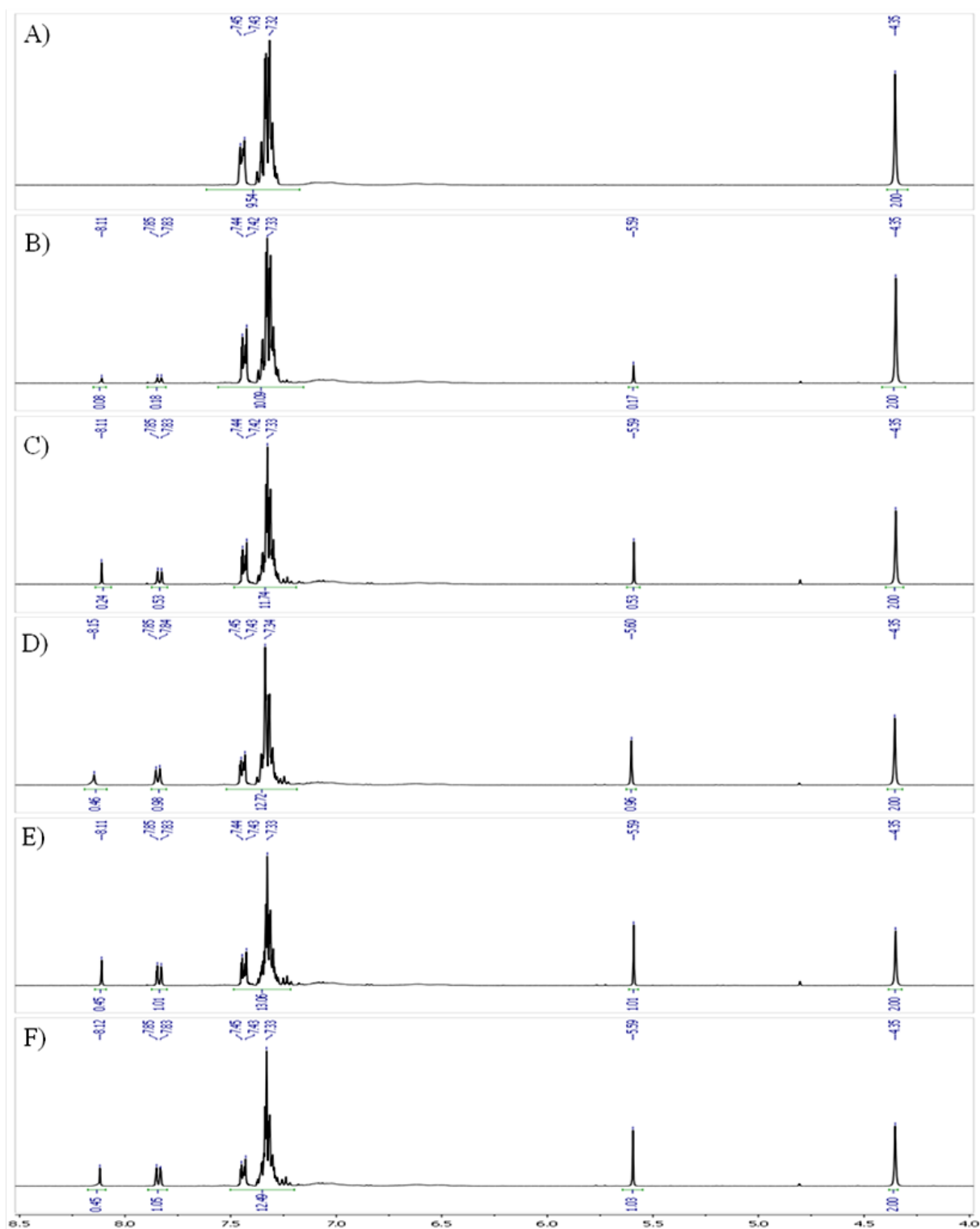


Figure A57. $^1\text{H-NMR}$ spectra of CuAAC kinetic from **17** and **19** subjecting PS-based mechanocatalyst **14b** to several ultrasonication cycles at room temperature in THF- d_8 /MeOH (30:1): (A) before 1st sonication cycle 0% “click” conversion^{a)}, (B) after 1st sonication cycle (150 min) 8% conversion^{a)}, (C) after 2nd sonication cycle (300 min) 21% conversion^{a)}, (D) after 3rd sonication cycle (450 min) 32% conversion^{a)}, (E) after 5th sonication cycle (750 min) 34% conversion^{a)} and (F) after 10th sonication cycle (1500 min) 34% conversion^{a)}.

^{a)}determined through the increasing triazole resonance at 8.12 ppm as well as the shift of the CH_2 resonance from 4.34 to 5.58 ppm

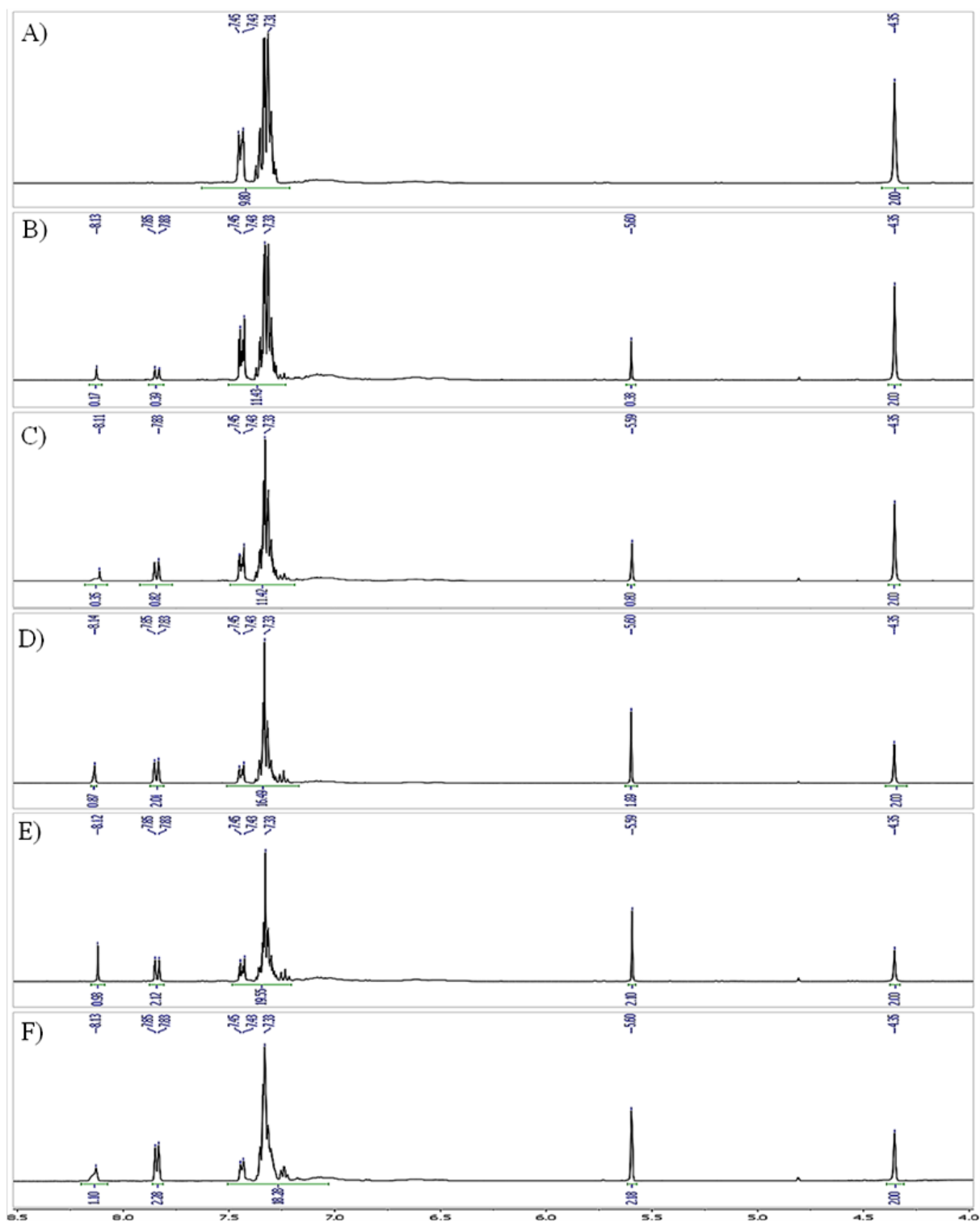


Figure A58. $^1\text{H-NMR}$ spectra of CuAAC kinetic from **17** and **19** subjecting PS-based mechanocatalyst **14c** to several ultrasonication cycles at room temperature in THF- d_8 /MeOH (30:1): (A) before 1st sonication cycle 0% “click” conversion^{a)}, (B) after 1st sonication cycle (150 min) 16% conversion^{a)}, (C) after 2nd sonication cycle (300 min) 28% conversion^{a)}, (D) after 3rd sonication cycle (450 min) 49% conversion^{a)}, (E) after 5th sonication cycle (750 min) 51% conversion^{a)} and (F) after 10th sonication cycle (1500 min) 52% conversion^{a)}.

^{a)}determined through the increasing triazole resonance at 8.12 ppm as well as the shift of the CH_2 resonance from 4.34 to 5.58 ppm

7.14. Mechanochemical activation of latent catalysts in solid state by compression

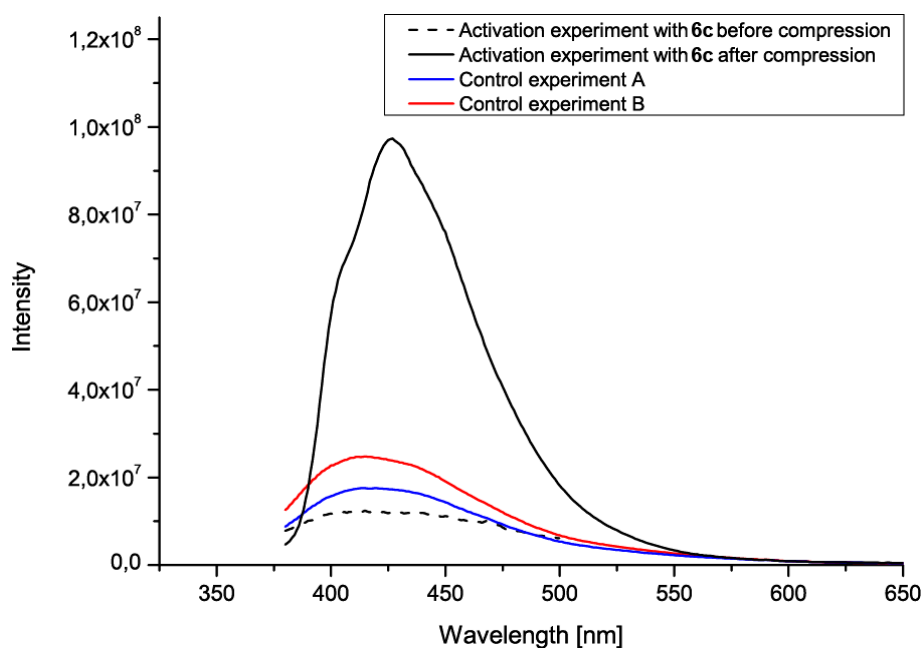


Figure A59. Fluorescence measurements of fluorogenic “click” reaction of 3-azido-7-hydroxy-coumarin (**16**) with phenylacetylene (**17**) using $[\text{Cu}(\text{PIB-NHC})_2]\text{X}$ (**6c**) ($M_{n(\text{GPC})} = 17200$ g/mol) within the high molecular weight PTHF matrix when excited at 360 nm; solid black line mechanochemical triggered reaction of **16** and **17** using **6c** as catalyst after three applied pressure cycles; dashed black line mixture of **16** and **17** with **6c** before applied pressure; blue line control experiment A mixture of **16** and **17** without **6c** in PTHF after three applied pressure cycles; red line control experiment B mixture of **16** and **17** with **6c** in PTHF matrix after thermal treatment at 60°C for 72 h.

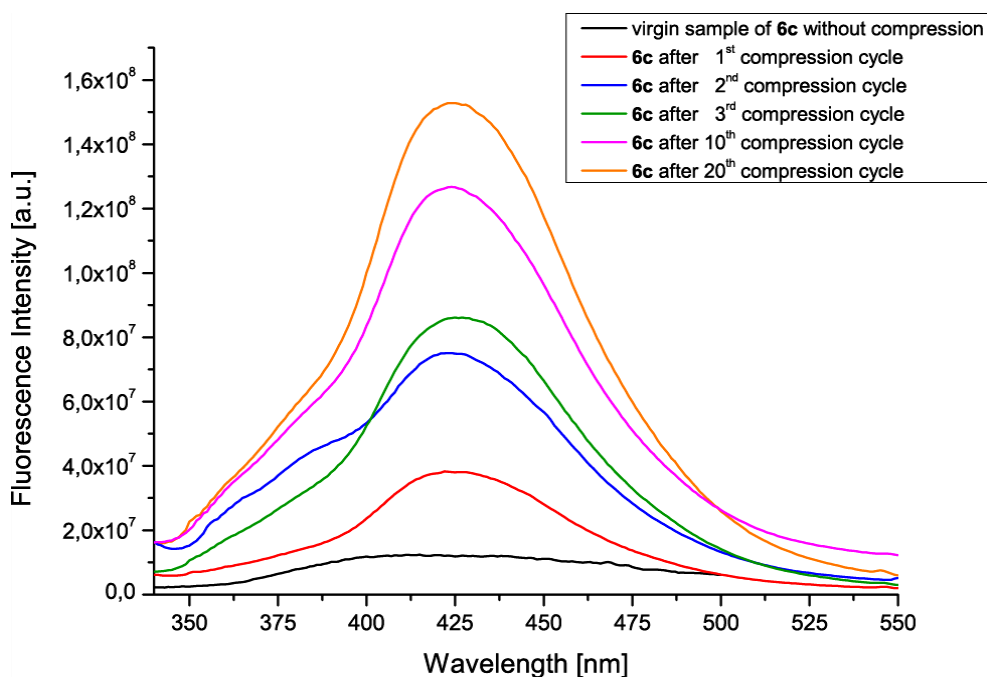


Figure A60. Compression cycle dependent fluorescence spectra of the fluorogenic “click” reaction of 3-azido-7-hydroxy-coumarin (**16**) with phenylacetylene (**17**) using the PIB-based mechanocatalyst $[\text{Cu}(\text{PIB-NHC})_2]\text{X}$ (**6c**) ($M_{n(\text{GPC})} = 17200$ g/mol) within the high molecular weight PTHF matrix when excited at 360 nm. Increased numbers of compression cycles led to an increased fluorescence.

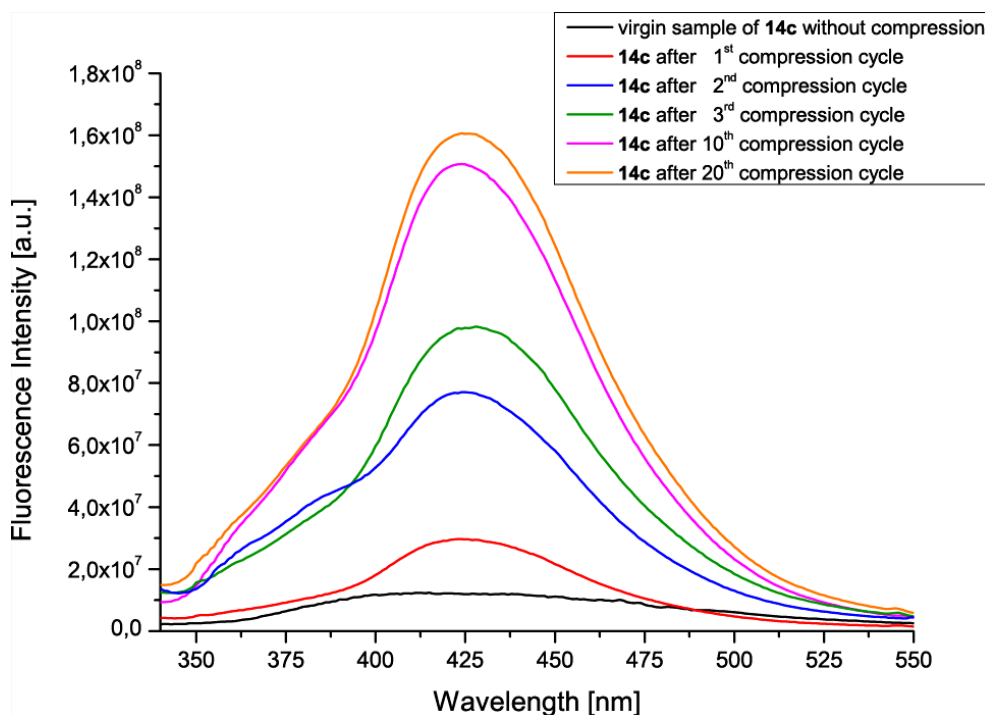


Figure A61. Compression cycle dependent fluorescence spectra of the fluorogenic “click” reaction of 3-azido-7-hydroxy-coumarin (**16**) with phenylacetylene (**17**) using the PS-based mechanocatalyst $[\text{Cu}(\text{PS-NHC})_2]\text{X}$ (**14c**) ($M_{n(\text{GPC})} = 13600 \text{ g/mol}$) within the high molecular weight PTHF matrix when excited at 360 nm. Increased numbers of compression cycles led to an increased fluorescence.

8 Curriculum Vitae

Philipp Michael (M. Sc.)

Geburtsdatum: 02.09.1986
Geburtsort: Halle (Saale)
Staatangehörigkeit: Deutsch
Familienstand: ledig
Adresse: 06110 Halle (Saale)
Wegscheiderstraße 9
Telefonnummer: 0345/5226929
0151/15368686
Email: philipp.michael@chemie.uni-halle.de

Zeitraum	Schul Ausbildung/Studium	Abschluss
02.09.1986	geboren in Halle/Saale	
1992 - 1996	Besuch der Grundschule Neumarkt Halle	
1996 - 2006	Besuch des Elisabeth-Gymnasiums Halle	Abitur Note: 1,7
2006 - 2009	Bachelor-Studium an der Martin-Luther-Universität Halle-Wittenberg im Bereich der Makromolekularen Chemie: Synthese von Block-Copolymeren mit freien Radikalen über ROMP	Bachelor of Science Note: 1,6
2009 - 2011	Master-Studium an der Martin-Luther-Universität Halle-Wittenberg im Bereich der Makromolekularen Chemie: Synthese und Charakterisierung selbstheilender Polymere auf Basis von Acrylaten	Master of Science Note: 1,3
seit Dez. 2011	Wissenschaftlicher Mitarbeiter der Martin-Luther-Universität Halle-Wittenberg im Bereich der Makromolekularen Chemie	

Sprachkenntnisse

Deutsch (Muttersprache)

Englisch (Fließend in Wort und Schrift)

Publikationen

Döhler, D.; Michael, P.; Neumann, S.; Binder, W. H.; Selbstheilende Polymere; *Chemie in unserer Zeit*; **2016**, *50* (2), 90-101.

Michael, P.; Binder, W. H.; A Mechanochemically Triggered “Click” Catalyst; *Angew. Chem.*; **2015**, *127* (47), 14124-14128.

Michael, P.; Binder, W. H.; A Mechanochemically Triggered “Click” Catalyst; *Angew. Chem. Int. Ed.*; **2015**, *54* (47), 13918-13922.

Michael, P.; Döhler, D.; Binder, W. H.; Improving autonomous self healing via combined chemical/physical principles; *Polymer*; **2015**, *69*, 216-227.

Vasiliu, S.; Kampe, B.; Theil, F.; Dietzek, B.; Döhler, D.; Michael, P.; Binder, W. H.; Popp, J.; Insights into the Mechanism of Polymer Coating Self-Healing Using Raman Spectroscopy; *Appl. Spectrosc.*; **2014**, *68* (5), 541-548.

Herbst, F.; Döhler, D.; Michael, P.; Binder, W. H.; Self-Healing Polymers via Supramolecular Forces; *Macromol. Rapid Commun.*; **2013**, *34* (3), 203-220.

Döhler, D.; Michael, P.; Binder, W. H., Principles of Self-Healing Polymers. In *Self-Healing Polymers. From Principles to Applications.*, Binder, W. H., Ed. Wiley-VCH: Weinheim, 2013; pp 7-60.

Döhler, D.; Michael, P.; Binder, W. H.; Autocatalysis in the Room Temperature Copper(I)-Catalyzed Alkyne-Azide “Click” Cycloaddition of Multivalent Poly(acrylate)s and Poly(isobutylene)s; *Macromolecules*; **2012**, *45* (8), 3335–3345.

Schunack, M.; Gragert, M.; Döhler, D.; Michael, P.; Binder, W. H.; Low-Temperature Cu(I)-Catalyzed “Click” Reactions for Self-Healing Polymers; *Macromol. Chem. Phys.*; **2012**, *213* (2), 205-214.

Präsentationen auf Konferenzen

Philipp Michael, Diana Döhler, Wolfgang H. Binder; Mechanochemical and Supramolecular Self-Healing Polymers; Meeting of Priority Programme SPP 1568 “Design and Generic Principles of Self-Healing Materials”, Dezember 15-16. 2015, Jena, Deutschland; Vortrag.

Philipp Michael, Wolfgang H. Binder; Development of latent mechanocatalyst for copper(I)-catalyzed azide/alkyne “click” reactions; ICSHM 2015, Juni 22-24. 2015 Durham, NC, USA, Vortrag.

Philipp Michael, Wolfgang H. Binder; WP2: Choice of chemical reactions related to self-healing function; IASS (Improving aircraft safety by self healing structures and protecting nanofillers) Webex meeting, Februar 27. 2015, Halle, Deutschland; Vortrag.

Diana Döhler, Philipp Michael, Wolfgang H. Binder; Mechanochemical and Supramolecular Self-Healing Polymers; Meeting of Priority Programme SPP 1568 “Design and Generic Principles of Self-Healing Materials”, Dezember 11-12. 2014, Jena, Deutschland; Vortrag.

Philipp Michael, Wolfgang H. Binder; WP2: Choice of chemical reactions related to self-healing function; IASS (Improving aircraft safety by self healing structures and protecting nanofillers) meeting, September 22-23. 2014, Salerno, Italien; Vortrag.

Philipp Michael, Diana Döhler, Marlen Malke, Wolfgang H. Binder; Investigation of novel crosslinking reactions as versatile tool for designing self-healing polymers; ICSHM 2013, Juni 16-20. 2013, Ghent, Belgien, Poster.

Wolfgang H. Binder, Florian Herbst, Philipp Michael, Diana Döhler, Parvin Zare, Anja Stojanovic; Self-healing by hydrogen bonding and click reactions; Dutch German symposium on Self Healing Materials, September 30. - Oktober 1. 2013; Gouda, Niederlande; Vortrag.

Wolfgang H. Binder, Florian Herbst, Philipp Michael, Diana Döhler, Parvin Zare, Anja Stojanovic; Self-healing by hydrogen bonding and click reactions; Dutch German symposium on Self Healing Materials, September 30. - Oktober 1. 2013; Gouda, Niederlande; Poster.

Philipp Michael, Diana Döhler, Wolfgang H. Binder; Autocatalytic Effects in Copper(I)-catalyzed Alkyne-azide-click Reactions (CuAAC); Meeting of Priority Programme SPP 1568 "Design and Generic Principles of Self-Healing Materials", August 1-2. 2012, Jena, Deutschland; Vortrag.

Philipp Michael, Diana Döhler, Marlen Malke, Maria Gragert, Wolfgang H. Binder; Development of self-healing polymeric material using copper(I) catalyzed azide-alkyne click chemistry; Polymeric Materials 2012 (P2012), September 12-14. 2012, Halle (Saale), Deutschland; Vortrag.

Wolfgang H. Binder, Philipp Michael, Diana Döhler; Liquid Polyisobutylenes as Polymers for Self-Healing Materials and their Investigation via *in situ* Rheology; Kick-off Meeting of Priority Programme SPP 1568 "Design and Generic Principles of Self-Healing Materials", Oktober 13-14. 2011, Jena, Deutschland; Vortrag.

Halle (Saale),

Philipp Michael

9 Eigenständigkeitserklärung

Hiermit erkläre ich an Eides statt, dass ich die vorliegende Arbeit selbstständig und ohne fremde Hilfe verfasst habe. Andere als die angegebenen Quellen und Hilfsmittel wurden nicht benutzt und die den benutzten Werken wörtlich oder inhaltlich entnommenen Stellen wurden als solche kenntlich gemacht.

Außerdem erkläre ich, dass ich die vorliegende Dissertation an keiner anderen wissenschaftlichen Einrichtung zur Erlangung eines akademischen Grades eingereicht zu haben.

Halle (Saale), den

Philipp Michael